Ferromanganese crusts from the seamounts north of the Madeira Island: composition, origin and paleoceanographic conditions

DISSERTATION

zur Erlangung des Doktorgrades

Dr. rer. nat.

an der Mathematisch-Naturwissenschaftlichen Fakultät der Christian-Albrechts-Universität zu Kiel

vorgelegt von

Susana Bolhão Muiños

Kiel, 2015

Referent:	Prof. Dr. Martin Frank
Koreferent:	Prof. Dr. Anton Eisenhauer
Tag der Disputation:	18. März 2015
Zum Druck genehmigt:	Kiel, 18 März, 2015

gez., Der Dekan

Hiermit erkläre ich, dass ich die vorliegende Doktorarbeit selbständig und ohne Zuhilfenahme unerlaubter Hilfsmittel erstellt habe. Weiterhin versichere ich, dass der Inhalt dieser Arbeit weder in dieser, noch in veränderter Form, einer weiteren Prüfungsbehörde vorliegt. Ferner versichere ich, dass die Arbeit unter Einhaltung der Regeln guter wissenschaftlicher Praxis der Deutschen Forschungsgemeinschaft entstanden ist.

Susana Bolhão Muiños

"(....)

A imensidade imensa do mar imenso!

(....)"

In Ode Marítima, Álvaro de Campos

"(....)

The immense immensity of the immense sea!

(....)"

In Maritime Ode, Álvaro de Campos

To my Father,

Acknowledgements

First, I would like to express my gratitude to my supervisor Prof. Dr. Martin Frank for accepting me as PhD student and for all his guidance, teaching, incentive, friendship, and enormous patience throughout all these years. Vielen herzlichen Dank!

I also want to sincerely thank my co-supervisors: Dr. James Hein and Dr. Fátima Abrantes. Jim, thank you very much for your support, teachings, friendship, and the amazing time I spent in sunny California. Doutora Fátima, muito obrigada por me ter "adoptado" e por me ter dado todo o seu apoio, amizade e compreensão ao longo destes anos.

Un agradecimiento especial también para Dr. Susana Martín Lebreiro por su apoyo y supervisión durante el primer par de años de la tesis doctoral. Muchas Gracias!

I acknowledge the chief-scientists, the onboard scientific teams, and the funding agencies of Meteor M51/1, Tore-Madeira and TTR-11 cruises for kindly providing me with the samples that made this study possible.

To those that directly helped in the analytical work: Brian Haley, Claudia Ehlert, Roland Stumpf, Jutta Heinz, Rachel Dunham, Tracey Conrad, thank you very much!

I express my gratitude to Dr. José Hipólito Monteiro and Dr. Luís Gaspar: You are responsible for my beginning in the marine authigenic minerals' field. Thank you for always being available and for believing in me.

To Dr. Antje Voelker I would like to express my sincere thanks for the readiness, availability, support, and help every time needed.

I must also thank the scientists who helped me and with whom I had fruitful discussions during my PhD work: Dr. Jürgen Fischer, Dr. Lothar Stramma, Prof. Dr. Francis E. Grousset, Prof. Dr. Michael Staubwasser. Prof. Luís M. Pinheiro, Prof. Dr. Luísa Duarte, Engº Luís Martins, Engº Silva Lopes, and Dr. Vieira Silva are also acknowledged.

I acknowledge the financial support from the Portuguese Foundation for Science and Technology (FCT) through fellowship grant SFRH/BD/22263/2005 (co-financed by POCI 2010/EU), project PDCT/MAR/56823/2004-CROSTAS, and travel support through the bilateral cooperation program (GRICES/DAAD).

Additional financial support was provided by Laboratório Nacional de Energia e Geologia (LNEG) and by Instituto Português do Mar e da Atmosfera (IPMA) fellowships. I thank Dr. Nuno Lourenço and Dr. Pedro Terrinha for their support during the final months while completing my thesis.

Thanks go to my colleagues from GEOMAR for the welcoming environment and for help, especially to Rina, Helena, Joana, Nabil, Karen, and Basak for their companionship, help and support during my stays in Kiel.

I also highly appreciate the support, incentive and friendship throughout all these years of my colleagues from the DivGM (and formerly DGM/UGM), in particular to Mário, Pedro, Margarida, Vasco, and Cristina.

To all my friends thank you for always being present and available and making my life full of joy. Thanks for the friendship, companionship, listening, good laughs, and for the not so good moments also. Obrigada!

Last but not least: To my family, thank you very much for all. You are amazing! To my sweet niece thank you very much for the overwhelming hugs and for making me notice the simplicity of life. A special word goes to my parents and Ricardo: Thank you for all your infinite love, support, strength, understanding, patience ... There are not enough words to express my gratitude. I would never have reached this far without you. I dedicate this work to my father, who sadly could not physically accompany me until the end of this journey, but who always has been and will be present in my days.

To you my beloved baby, thank you for enduring these last hectic days and for giving me the strength needed to finish this chapter of my(our) life(s). I am wishful for having you in my arms!

Abstract

Ferromanganese oxyhydroxides in the oceans occur as nodules, crusts, and massive beds. They can be classified as diagenetic, hydrogenetic, hydrothermal, and mixed-type deposits. Studies carried out on northeast Atlantic seamounts indicate the prevailing presence of ferromanganese deposits of hydrogenetic origin. Hydrogenetic ferromanganese crusts (Fe-Mn crusts) form by the direct precipitation, on hard-rock substrates, of colloidal hydrated metal oxides that are scavenged from the water column. The hydrogenetic precipitation promotes the enrichment of Fe-Mn crusts in trace metals, most of which are of economic interest, such as Co, Ni, Te, rare earth elements, and platinum-group elements, among others. Beyond their economic potential Fe-Mn crusts are considered condensed stratigraphic sections and proxy records obtained from crusts can be used as indicators of the oceanic and climatic history of the past 75 Ma.

The present work aims to study ferromanganese deposits from the northeast Atlantic Ocean in an integrated way, considering them both as paleoceanographic archives and as potentially economic resources.

Chapter III deals with the reconstruction of the isotopic composition of water masses from the northeast Atlantic. In this study three Fe-Mn crusts, distributed over a water depth profile comprising the present-day depths of Mediterranean Outflow Water (MOW) and North East Atlantic Deep Water (NEADW), were analyzed and new time series of the lead (Pb) and neodymium (Nd) isotope evolution of northeast Atlantic water masses over the past 15 Ma are presented. The similarity between the Pb and Nd time series patterns of the studied crusts of the northeastern with those of the northwestern Atlantic over the past 4 Ma shows that there has been efficient mixing between the two basins. However, the changes occurred 1-3 Ma earlier in the eastern basin indicating that the northeastern Atlantic led the major change in Pb and Nd isotope composition, probably due to an efficient export of Labrador Sea Water to the eastern Atlantic *via* a northern route such as across the Charlie-Gibbs Fracture Zone rather than through the equatorial fractures zones. The Pb

isotope evolution during the Pliocene-Pleistocene can be explained by a mixture between two principal end-members corresponding to MOW and NEADW. The invariant Pb isotope composition of the shallowest crust, which grew within the present-day MOW, however, indicates that external sources such as Saharan dust are likely to have played a role as well.

In order to obtain information on the external sources and the climatic changes in weathering inputs contributing to the study area over the past ~12 Ma, the findings of Chapter III are revisited in Chapter IV but considering the radiogenic isotope composition of Pb, Nd and Sr in the detrital fraction of 31 crust surfaces scrapings, 15 samples from depth profiles of 3 selected crusts for time-series studies, and 6 accompanying sediment samples. These data provided information on the detrital inputs showing that the sources of detrital material contributing to the northeast Atlantic over the last ~12 Ma comprise essentially North African sources. More importantly, the data reveal that the prevailing climatic conditions have not changed significantly over the past ~12 Ma.

The study of the composition and considerations of the resource potential of the deposits from the study area is the subject of Chapter V. Eighteen deep-sea Fe-Mn crusts from 10 seamounts in the northeast Atlantic were studied. Based on the mineralogical and chemical compositions, the studied crusts are typical hydrogenetic crusts adjacent to continental margins and exhibit a Co+Cu+Ni maximum of 0.96 wt%. Platinum-group element contents analyzed for five samples showed Pt contents from 153 to 512 ppb. The study of the enrichment of trace metals of economic interest in Fe-Mn crusts is of specific interest for the evaluation of the resource potential of these deposits. Tonnages for specific metals in chosen areas, in and adjacent to the Portuguese Exclusive Economic Zone, were calculated. The results indicate that the study area is comparable to parts of the central Pacific Ocean indicating that these Atlantic deposits may be an important future resource.

This integrated study demonstrates the potential of Fe-Mn crusts for the study of paleoclimatic and paleoceanographic changes in the northeast Atlantic over the last ~15 Ma, and the importance that these deposits might represent in the future as potential sources of critical metals.

Kurzfassung

Eisen-Mangan-Oxyhydroxide kommen im Weltmeer als Knollen, Krusten und massive Ablagerungen in Sedimenten vor. Sie werden als diagenetische, hydrogenetische oder Mischtyp-Ablagerungen klassifiziert. Studien an Tiefseebergen im Nordostatlantik belegen überwiegend Eisenmanganablagerungen hydrogenetischen Ursprungs. Hydrogenetische Eisen-Mangan-(Fe-Mn)-Krusten bilden sich auf harten Untergründen als direkte Ausfällungen kolloidaler, hydratisierter Metalloxide aus der Wassersäule. Hydrogenetische Bildungsmechanismen fördern die Anreicherung von Spurenelementen in den Fe-Mn-Krusten, von denen Co, Ni, Ti, seltene Erden oder Elemente der Platingruppe, von wirtschaftlichem Interesse sind. Zusätzlich zu ihrem wirtschaftlichen Potenzial stellen Fe-Mn-Krusten kondensierte, stratigraphische Aufzeichnungen dar und Zeitserien von Parametern, die in den Krusten archiviert wurden, sind Anzeiger der ozeanischen und klimatischen Geschichte der letzten 75 Millionen Jahre.

Die vorliegende Studie basiert auf Eisen-Manganablagerungen aus dem nordöstlichen Atlantik und integriert paläoozeanographische Aufzeichnungen und potentielle wirtschaftliche Ressourcen.

Das dritte Kapitel behandelt die Rekonstruktion der isotopischen Zusammensetzung der Wassermassen im Nordostatlantik. In dieser Studie wurden drei Fe-Mn-Krusten, die ein Tiefenprofil durch die heutige Ausdehnung des Mittelmeeraustromwasser (MOW) und des nordostatlantischen Tiefenwassers (NEADW) bilden, untersucht und neue Zeitserien der Blei-(Pb)- und Neodym (Nd)-Isotopie nordostatlantischer Wassermassen während der letzten 15 Millionenjahre präsentiert. Die Ähnlichkeiten zwischen den Pb- und Nd-Zeitserien der untersuchten Krusten aus dem Nordostatlantik und aus dem Nordwestatlantik belegen eine effektive Mischung der Wassermassen beider Becken während der letzten 4 Millionen Jahre. Allerdings traten signifikante Änderungen im östlichen Becken 1-3 Millionen Jahre früher ein, was nahelegt, daß sich die Ursachen einschneidender Änderungen der Pb und Nd-Isotopenzusammensetzung im Nordostatlantik

unmittelbarer auswirkten, wahrscheinlich aufgrund eines effizienten Exports von Labradorseewasser in den Ostatlantik über eine direkte nördliche Route wie die Charlie-Gibbs Störungszone anstatt über die äquatoriale Bruchzonen. Die Pb-Isotopenentwicklung während des Plio-Pleistozäns läßt sich durch die Mischung zweierEndglieder, dem MOW und dem NEADW, erklären. Die stabile, unveränderte Pb-Isotopenzeitserie der Kruste aus der niedrigsten Wassertiefe, die im heutigen Tiefenbereich des MOW wuchs, zeigt allerdings, daß externe Quellen wie Saharastaub wahrscheinlich ebenfalls eine Rolle spielten.

Die Ergebnisse des dritten Kapitels werden im vierten wieder aufgegriffen, um Informationen über die externen Quellen und klimabedingte Änderungen im Erosionseintrag in das Untersuchungsgebiet während der letzten 12 Millionen Jahre zu erhalten. Dafür wurden die Verhältnisse der radiogenen Isotope Pb, Nd und Sr in der detritischen Fraktion der Oberflächen von 31 Krusten, die durch Abkratzen der Krustenoberfläche gewonnen wurden, in 15 Proben aus Tiefenprofilen der drei für Zeitserienanalysen ausgewählten Krusten und in 6 benachbarten Sedimentproben bestimmt. Die Daten zum Detrituseintrag zeigen, daß die Quellen des detritischen Materials, das während der letzten ca. 12 Millionen Jahre in den Nordostatlantik eingetragen wurde, überwiegend in Nordafrika lagen. Als wichtiges Ergebnis belegen die Daten, daß sich die vorherrschenden Klimabedingungen während der letzten ca. 12 Millionen Jahre nicht signifikant geändert haben.

Kapitel V behandelt die geochemische Zusammensetzung der Ablagerungen im Untersuchungsgebiet im Hinblick auf ihr Lagerstättenpotenzial. Achtzehn Tiefsee-Fe-Mn-Krusten von 10 submarinen Bergen des Nordostatlantiks wurden untersucht. Aufgrund ihrer mineralogischen und geochemischen Zusammensetzungen sind die untersuchten Krusten typische hydrogenetische Krusten wie sie auf Kontinentalhängen gefunden werden und haben Co+Cu+Ni-Maximalkonzentrationen von 0.96 Gewichtsprozent. Elemente der Platingruppe, die für fünf Proben bestimmt wurden, zeigen Pt-Gehalte von 153 bis 512 ppb. Die Studie zur Anreicherung von Spurenelementen in den Fe-Mn-Krusten, die von wirtschaftlichem Interesse sind, ist von direkter Bedeutung für die Einschätzung des Ressourcenpotenzials dieser Ablagerungen. Förderleistungen für bestimmte Metalle wurden für ausgewählte Gebiete innerhalb und in Nachbarschaft zur exklusiven portugiesischen Wirtschaftszone berechnet. Die Ergebnisse zeigen, daß das

Untersuchungsgebiet vergleichbar zu Bereichen des zentralen Pazifiks ist und daß diese atlantischen Ablagerungen wichtige, zukünftige Ressourcen darstellen könnten.

Diese integrierte Studie veranschaulicht das Potenzial von Fe-Mn-Krusten als Archive von paläoklimatischen und paläoozeanographischen Änderungen im Nordostatlantik während der letzten ca. 15 Millionen Jahre und die Bedeutung dieser Ablagerungen als zukünftige, mögliche Quellen für wirtschaftlich bedeutende Metalle.

Table of contents

II. MATERIAL AND METHODS

IV. RADIOGENIC Pb, Nd, AND Sr ISOTOPE COMPOSITION OF THE DETRITAL FRACTION OF Fe-Mn CRUSTS FROM NE ATLANTIC SEAMOUNTS: TRACERS OF DETRITAL INPUTS OVER THE PAST 12 MILLION YEARS

General Introduction

I.1. Hydrographic and climatic evolution of the Northeast Atlantic Ocean over the past ~15 million years

Integrated knowledge of the factors controlling the oceans represents nowadays one of the biggest challenges for reliable and realistic prediction of man-made climate change; the oceans play a crucial role for the redistribution of heat around the globe, through ocean circulation, and for the regulation of atmospheric CO_2 levels, through deep water formation.

As a result of the surface circulation and the Global Thermohaline Conveyor Belt, the ocean contributes to the stabilization of the climatic system (Broecker, 1991). In fact, the strength of the present-day Meridional Overturning Circulation (Figure I.1.), which controls deep ventilation and meridional heat transport around the globe, has to a large extent been controlled by the strength of North Atlantic Deep Water (NADW) production. NADW is formed by the contribution of three principal water masses at high northern latitudes: Labrador Seawater (LSW), Denmark Strait Overflow Water (DSOW), and Iceland-Scotland Overflow Water (ISOW), with variable amounts of Subpolar Mode Water admixed (Schmitz and McCartney, 1993). Moreover, it has been suggested that the contribution of highly saline and warm Mediterranean Outflow Water (MOW) is important for the thermohaline boundary conditions of the North Atlantic, thus preconditioning water masses that contribute to the formation of NADW (cf. Reid, 1978; Voelker et al., 2006). The NADW is exported from the western north Atlantic flowing south within the Western Boundary Undercurrent and reaching the eastern North Atlantic basin through gaps in the Mid-Atlantic Ridge such as the Romanche or Vema Fracture Zones (cf. Broecker et al., 1985). North East Atlantic Deep Water (NEADW) is formed by mixing of a branch of ISOW that does not flow into the northwestern basin, with LSW, Lower Deep Water (LDW, modified Antarctic Bottom Water (AABW)), and modified NADW (Lacan and Jeandel, 2005a).

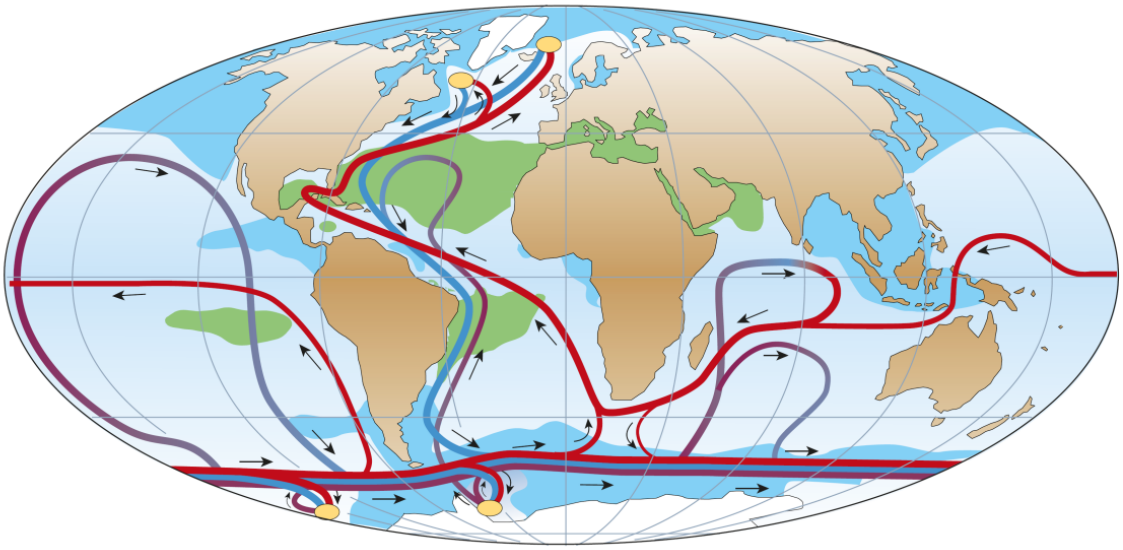

Figure I.1. Schematic picture of global ocean circulation with illustration of the Meridional Overturning Circulation, with the northward movement of warm and salty surface waters in the Atlantic Ocean (in red) and the southward return flow of cold, deep waters (in blue). The bottom currents are represented in purple. The yellow circles correspond to the locations of deep water formation. The black arrows indicate the direction of the currents (from Rahmstorf, 2002).

During the Middle and Late Miocene two major paleoceanographic events, affecting the heat and salt budget of the oceans, have caused major changes of climate and of the thermohaline circulation: i) the gradual closure of the Isthmus of Panama, culminating in the cut-off of water exchange between the Atlantic and the Pacific around 4-3 million years (Ma) and ii) the Messinian Salinity Crisis (MSC). During the MSC (5.96-5.33 Ma; Krijgsmann et al., 1999) the Mediterranean Sea became, at least periodically, isolated from the world's oceans, which resulted in the evaporation of the basin and the deposition of vast evaporite formations. The gradual closure of the Panama gateway had major impacts on intermediate and deep water circulation leading to increased NADW export at ~4.6 Ma (Driscoll and Haug, 1998; Frank et al., 1999a; Reynolds et al., 1999). However the impact these major changes had on the onset of Northern Hemisphere Glaciation (NHG) are still under debate (e.g. Schneider and Schmittner, 2006). In the case of the Mediterranean Sea, Khélifi et al. (2009) for example suggested that a major aridification of the Mediterranean caused an intensification of the

Mediterranean outflow 3.5-3.3 Ma ago which, in turn, could have led to climate changes in the NW Atlantic.

I.2. Radiogenic isotopes as proxies

Radiogenic isotopes are produced by the decay of a radioactive parent isotope (e.g. Faure, 1986). As the result of Earth's mantle partial melting processes rocks of the continental crust and the mantle have acquired significant isotope differences as a function of the ratios between daughter and parent isotope abundances, and thus the variability of the parent/daughter element and isotopic ratios in nature is a function of age (radioactive decay; half-life) and chemical differences between those two elements (DePaolo, 1988); The weathering and erosion products of the continental rocks from the surrounding continents are ultimately delivered to seawater, as dissolved or particulate matter, resulting in the different isotopic signatures of water masses found in the oceans. These isotopic signatures can be extracted from marine archives and used as proxies to study geochemical processes, such as continental weathering and water mass mixing in the oceans (e.g. Frank, 2002; Frank, 2011), as is the case for the radiogenic isotope systems of Pb, Nd, and Sr (Table I.1). Moreover, radiogenic isotopes are not influenced by biological fractionation processes and changes in their seawater values are a function of water mass mixing and/or by addition of external sources such as riverine, aeolian or, in the particular case of Pb, hydrothermal inputs (cf. Frank, 2002; van de Flierdt et al., 2004).

Lead and Nd have residence times on the order or shorter than the global mixing time of the ocean (~1,500 yr; Broecker and Peng, 1982) resulting in distinct isotopic signatures of water masses, which can thus be used as proxies for water mass mixing and weathering inputs (Frank, 2002).

Strontium, in contrast, has a residence time longer than the global mixing of the ocean and is thus efficiently mixed on a global scale. For this reason the Sr isotope composition of seawater only changes as a function of plate tectonics and major orogenies and provides information about long term changes in weathering inputs (e.g. Frank, 2011). The combined use of different radiogenic isotope systems (e.g. different sources to the oceans, different

behavior during weathering, and different residence times) enables us to identify changes in continental weathering flux to the oceans (cf. Burton, 2006).

Table I.1. Radiogenic isotope systems (Frank, 2002)

Element	Radiogenic Isotope	Parent Isotope	Residence Time	Half-Life
Nd	^{143}Nd	^{147}Sm	~400*[1] to ~700*[2] yrs	106 Gyrs
Pb	^{206}Pb	^{238}U	~50 yrs (Atlantic) / ~200-400 yrs (Pacific)	4.47 Gyrs
	^{207}Pb	^{235}U		704 Myrs
	^{208}Pb	^{232}Th		14 Gyrs
Sr	^{87}Sr	^{87}Rb	several Myrs	48.8 Gyrs

*[1] Arsouze et al., 2009
*[2] Rempfer et al., 2011

One of the major challenges concerning the use of the radiogenic isotopes has been the identification of reliable archives and methods to extract the significant isotopic variations of past seawater. Changes in radiogenic isotope signatures providing information on past circulation and weathering inputs at different time scales have been successfully extracted from chemical sediments or seawater-derived chemical components of sediments (e.g. Frank, 2002; 2011). Hydrogenetic ferromanganese crusts (Fe-Mn crusts) are seawater precipitates which record the chemistry of the seawater at the time of their formation. Due to their slow growth rates (<10 mm/Ma) Fe-Mn crusts record changes in the radiogenic isotope composition of past seawater on long time scales (Burton et al., 1997; Abouchami et al., 1999; Burton et al., 1999; Frank et al., 1999b; Reynolds et al., 1999; Claude-Ivanaj et al., 2001; Frank et al., 2002; 2003), as far back as 75 Ma (Klemm et al., 2005). In order to increase the time resolution of these archives, Laser-Ablation measurements of Pb and Nd isotopes in Fe-Mn crusts have been performed (Christensen et al., 1997; Foster et al., 2007).

Nonetheless, the achieved resolution is still barely high enough to allow for glacial/interglacial reconstructions. Efforts have been made to identify archives enabling higher resolution reconstructions (decadal, centennial and millennial), and so far, the most commonly used sedimentary archives are foraminifera shells (Vance and Burton, 1999; Burton and Vance, 2000; Vance et al., 2004; Klevenz et al., 2008; Osborne et al., 2008), fossil fish teeth (Martin and Haley, 2000; Scher and Martin, 2006; Martin et al., 2010), deep sea corals (van de Flierdt et al., 2006; Colin et al., 2010; Copard et al., 2010; van de Flierdt et al., 2010), and thin ferromanganese coatings on foraminifera or other sediment particles (Rutberg et al., 2000; Bayon et al., 2002; Gutjahr et al., 2007; Pahnke et al., 2008; Piotrowski et al., 2009). Despite the fact that there is still some debate concerning the reliability of some of the extraction procedures (e.g. Wilson et al., 2013), efforts are being made to improve the use of these high resolution archives which contribute important new information for paleoceanographic and paleoclimatic studies.

I.2.1. Neodymium isotopes

The radiogenic ^{143}Nd is the result of the alpha-decay of its parent isotope ^{147}Sm, meaning that the ratio between ^{143}Nd and the primordial ^{144}Nd, to which ^{143}Nd is commonly normalized to, is variable. The production of stable ^{143}Nd occurs at very slow rates due to the long half-life of ^{147}Sm (106 Gyrs; Table I.1.).

The differences between the measured ^{143}Nd/^{144}Nd ratios are quite small and for this reason, the radiogenic isotope compositions of Nd are presented in the ε-notation ("epsilon parameter"; DePaolo and Wasserburg, 1976):

$$\varepsilon Nd = \left[\frac{\left(^{143}Nd/^{144}Nd\right)sample}{\left(^{143}Nd/^{144}Nd\right)CHUR} - 1\right] x\ 10^4$$

As from equation, the ε_{Nd} values represent the deviation (in parts per 10,000) of the measured ^{143}Nd/^{144}Nd ratio in a sample from that of CHUR (**Ch**rondritic **U**niform **R**eservoir),

assuming that the hypothetical Nd isotopic evolution of the Earth has been similar in age and in its Sm/Nd ratios to that of the isotope evolution of chondritic meteorites (e.g. Goldstein and Hemming, 2003). The present-day value of CHUR is 0.512638 (Jacobsen and Wasserburg, 1980).

Despite the fact that Sm^{3+} and Nd^{3+} have similar chemical and physical characteristics (e.g. similar ionic radii) Nd is slightly more incompatible than Sm and for this reason Nd is, in general, concentrated relative to Sm during fractional crystallization of magmas and therefore enriched in crustal rocks (which have lower Sm/Nd ratios and lower $^{143}Nd/^{144}Nd$) when compared to rocks derived from the upper mantle (Faure, 1986). For this reason continents have lower $^{143}Nd/^{144}Nd$ ratios and therefore more negative ε_{Nd} values. On the other hand, Mid-ocean basalts (MORBs) as well as Oceanic island basalts (OIBs) have higher $^{143}Nd/^{144}Nd$ ratios (positive ε_{Nd} values).

The main source of Nd to the oceans is continental weathering, such as dissolved and particulate riverine and aeolian inputs (e.g. Goldstein and Jacobsen, 1987; Goldstein and Hemming, 2003). Also "boundary exchange" processes at the boundaries of the oceans, such as shelf areas, are considered important contributors of these elements to seawater and thus may alter the isotopic composition of seawater (Lacan and Jeandel, 2005b). In fact, there is recent modeling evidence suggesting that the major contribution of Nd to seawater occurs across the sediment-water interface at continental margins (Tachikawa et al., 2003; Arsouze et al., 2009; Rempfer et al., 2011). In the particular case of Nd, it has also been suggested that submarine groundwater discharge may contribute to the isotopic signature of Nd in seawater (Johanneston and Burdige, 2007).

As the difference between the isotopic ratios increases with age, and as the ages of the continental terrains (which are the main source of Nd to seawater) surrounding the different ocean basins varies, one can use these isotopic heterogeneities to trace the provenance of the dissolved and particulate Nd isotope signatures in the ocean on a global scale (e.g. Goldstein and Hemming, 2003). In fact, the general present-day isotopic distribution of Nd in the world ocean water masses is characteristic and distinctive for each ocean basin, reflecting the isotopic composition of the surrounding rocks, and in more detail within the basins the isotopic signatures of particular water masses reflects the path of thermohaline circulation (e.g. Frank, 2002): The least radiogenic ε_{Nd} values (up to -26) are

found in the North Atlantic in sites surrounded by old continental rocks of Proterozoic and Archean age (cf. Frank, 2002) and the most radiogenic ε_{Nd} values (-5 to +2) are found in the North Pacific reflecting the input from young volcanic island arc rocks along its rim. The Indian Ocean has intermediate ε_{Nd} values (-10 to -7) (e.g. Piepgras et al., 1979; Piepgras and Wasserburg, 1980; Goldstein and O'Nions, 1981; Frank, 2002; Goldstein and Hemming, 2003).

Due to its intermediate residence time (RT) in the ocean (~400 to ~700 yrs; Arsouze et al., 2009; Rempfer et al., 2011), Nd isotopes exhibit a quasi-conservative behavior in the open ocean, in particular if far from any lithogenic input (von Blanckenburg, 1999), and are thus an important tracer for water mass mixing and ocean circulation (e.g. Jones et al., 2008; Jeandel et al., 2013).

I.2.2. Lead isotopes

The stable radiogenic isotopes of lead (Table I.1.) are the final products of the radioactive decay-series with the parent isotopes uranium (U) and thorium (Th): the decay of ^{238}U produces ^{206}Pb (half-life is 4.47Gyrs), ^{235}U produces ^{207}Pb (half-life is 704 Myrs), and ^{232}Th produces ^{208}Pb (half-life is 14Gyrs) (e.g. Frank, 2002). Additionally there is primordial ^{204}Pb, to which the radiogenic Pb isotopes are commonly normalized. This normalization to ^{204}Pb gives the largest variability between reservoirs (Komárek et al., 2008) and is thus important for discriminatory studies. Radiogenic Pb isotopes can also be expressed as ratios between each other (e.g. $^{206}Pb/^{207}Pb$; $^{208}Pb/^{206}Pb$) which can be determined very precisely.

The differences in Pb isotope ratios found in nature are a function of the age of the rocks and the fractionation of the parent-daughter ratios (U/Pb and Th/Pb) during the formation of continental crust. Uranium and Th have similar chemical and physical characteristics (e.g. similar ionic radii) and geochemical coherence (they substitute for each other extensively) and in the course of partial melting and fractional crystallization of magmas both elements are concentrated in silicate melts when compared to Pb (e.g. Faure, 1986). Consequently, crustal rocks have higher U/Pb and Th/Pb ratios than mantle-derived rocks.

Additionally, Pb isotopes are fractionated during weathering of the continental rocks. In the course of the radioactive decay of the U- and Th-decay series, minerals hosting U and Th

suffer damages in their crystal structure due to radiation and thus the radiogenic isotopes of Pb are more mobile during weathering processes than primordial ^{204}Pb, which leads to the fractionation of the Pb isotopes (Erel et al., 1994; Jones et al., 2000). This effect known as "incongruent weathering" (von Blanckenburg and Nägler, 2001) results in the fact that the dissolved Pb isotopic compositions may not necessarily reflect the isotopic composition of the source rocks (cf. Frank, 2002).

The main source of Pb to the oceans is riverine input but aeolian and hydrothermal inputs may be of local importance for the dissolved Pb isotopic signal (e.g. Frank, 2002). As a consequence of the atmospheric input of Pb with anthropogenically modified composition, originating from leaded fuel, the present-day Pb (natural) isotope distribution on seawater is completely overprinted by anthropogenic Pb (Schaule and Patterson, 1981; Shen and Boyle, 1988; Weiss et al., 2003). In fact, the preanthropogenic Pb isotope distribution can only be recovered in deep waters from Fe-Mn crust surfaces (Abouchami and Goldstein, 1995; von Blanckenburg et al., 1996) and from the hydrogenetic Fe-Mn coatings of marine sediments (cf. Gutjahr et al., 2009).

Similar to Nd, the Pb isotope variations in deep waters also roughly reflect the path of thermohaline circulation (Abouchami and Goldstein, 1995) and show a general provinciality which results from the different weathering inputs of the surrounding continental rocks. However and as previously mentioned, the isotope composition of Pb resulting from the weathering of the continental rocks and the isotope composition of dissolved Pb in the ocean may be different from the isotopic composition of the source rocks. This is due to incongruent weathering and is the cause for the more radiogenic Pb values found in the North Atlantic, which has been particularly pronounced since the onset of the NHG due to the enhanced exposure of fresh erosional surfaces as a consequence of glacial erosion (von Blanckenburg and Nägler, 2001). In fact, the general present-day isotopic distribution of Pb in the ocean is characterized by high $^{206}Pb/^{204}Pb$ ratios around 19.3 for present NADW and in less radiogenic $^{206}Pb/^{204}Pb$ ratios between 18.5 and 18.8 for deep Pacific water masses. The Indian Ocean and the Southern Ocean water masses show intermediate $^{206}Pb/^{204}Pb$ ratios between those values (cf. Frank, 2002).

Moreover, Pb is a highly particle reactive element being rapidly removed throughout the water column by adsorption onto particles (scavenging) (e.g. Chester, 1990) and

consequently, the RT of Pb in seawater is very short: around 50 years in the Atlantic Ocean, and up to 200 years in the deep Pacific Ocean (Schaule and Patterson, 1981; von Blanckenburg and Igel, 1999). Due to its short RT (which is much shorter than the global mixing time of the ocean) the isotopic composition of Pb (as extracted from Fe-Mn crusts and coatings) varies within each ocean basin and is a valuable tracer for local variations in weathering inputs and for short distance, local water mass mixing (e.g. Abouchami and Goldstein, 1995; Frank, 2011).

I.2.3. Strontium isotopes

Strontium has four naturally occurring stable isotopes: ^{84}Sr, ^{86}Sr, ^{87}Sr, and ^{88}Sr but only ^{87}Sr is radiogenic. The radiogenic ^{87}Sr is the result of the radioactive beta-decay of its parent isotope ^{87}Rb, (half-life: 48.8 Gyrs; Table I.1.). Variations in the relative abundances of ^{87}Sr are commonly normalized to stable ^{86}Sr and expressed as $^{87}Sr/^{86}Sr$ ratios (e.g. Faure, 1986).

The differences in the Sr isotope ratios found in rocks and minerals are a function of the age and of the parent-daughter ratio (Rb/Sr). The geochemical behavior of Rb and Sr differs: Rb is an alkali metal occurring as Rb^{+} in solution, whereas Sr is an alkali earth and occurs in solution as Sr^{2+}. Also, as a result of their largely different ionic radii, they are incorporated in different minerals: Sr substitutes for Ca in the lattice of Ca-bearing minerals whereas Rb substitutes for K. Thus, during fractional crystallization Sr is concentrated in Ca-bearing minerals (e.g. plagioclase) and concentrated in the liquid phase whereas Rb remains in the residual magma (e.g. Faure, 1986). This results in higher Rb/Sr in continental crust than in the mantle. Consequently, continental rocks have high $^{87}Sr/^{86}Sr$ ratios whereas mantle-derived rocks show depleted $^{87}Sr/^{86}Sr$ ratios (Faure, 1986; Veizer, 1989; Wilson, 1989; Banner, 2004). Moreover, the $^{87}Sr/^{86}Sr$ ratios vary with grain size of the weathered continental products: due to the chemical substitution of K by Rb, Rb tends to be enriched in K-rich minerals, such as clay minerals. Additionally, during chemical weathering Sr is more easily released into solution than Rb and thus finer-grained weathering products tend to be enriched in Rb-bearing weathering products (such as clays). This results in strongly increased $^{87}Sr/^{86}Sr$ ratios in the finer fraction of sediments (Dasch, 1969; Faure, 1986; Blum and Erel, 1997; Meyer et al., 2011).

The main source of Sr to the oceans is riverine input but hydrothermal inputs and (diagenetic) alteration of (Sr-rich) marine carbonates in the drainage areas and/or in ocean basins may also play a role (e.g. Frank, 2002; Banner, 2004). The oceans are the final repository of the weathering products of continental material, and thus, the Sr isotopic composition of seawater is controlled by mixing of continent-derived fluxes, as well as of fluxes derived from the alteration of oceanic basalts and sediments (Banner, 2004). The difference between continent- and mantle-derived $^{87}Sr/^{86}Sr$ ratios, and mixing of multiple sources with distinct isotopic composition, has controlled the Sr isotopic evolution of seawater. Despite the fact that the various fluxes of Sr to the oceans have distinct isotopic signatures, the Sr isotopic composition of seawater is homogenously distributed at any moment of geologic time as a consequence of its conservative behavior and very long RT in seawater ($\sim 2x10^6$ yrs) compared to the global mixing time of the ocean, which promotes its effective mixing (e.g. Veizer, 1989; Frank, 2002; Banner, 2004). However, the $^{87}Sr/^{86}Sr$ ratio of the oceans varied in the course of geologic time as a function of changes in the kinds of rocks exposed to weathering (Faure, 1986), and is the most commonly used proxy of the geologic history of chemical weathering (e.g. Veizer et al., 1999; Ravizza and Zachos, 2003). Major changes on the slope of the Sr isotope evolution of seawater, such as periods of significantly increased $^{87}Sr/^{86}Sr$, are the reflection of intense continental weathering caused by major orogenies such as the uplift of the Himalayas (Raymo and Ruddiman, 1992; Richter et al., 1992), or by major glaciations such as the first major Oligocene glaciation (Armstrong, 1971; Capo and DePaolo, 1990). Contrarily, periods of decreasing $^{87}Sr/^{86}Sr$ in seawater are related to increased hydrothermal activity resulting from major continental breakup (e.g. Frank, 2002; Ravizza and Zachos, 2003; Burton, 2006). At present the seawater $^{87}Sr/^{86}Sr$ value is 0.70916 (Palmer and Edmond, 1989).

In what concerns marine sediments, their Sr isotopic composition reflects the contribution from both authigenic and allogenic (detrital) components (Faure, 1986). The Sr isotopic composition of the authigenic fraction is identical to that of the seawater present at the time of its formation while the isotopic composition of the detrital fraction depends on the ages and Rb/Sr ratios of the mineral particles that originate from weathering of (old sialic) continent-derived rocks and/or (young volcanic) mantle-derived rocks (Faure, 1986). Moreover, and based in recent studies (Jung et al., 2004; Colin et al., 2006) it has ben suggested that the variations in the Sr isotopic composition of marine sediments reflect

changes in the degree of physical *versus* chemical weathering of the continental rocks. In this way, the variation in the $^{87}Sr/^{86}Sr$ ratios of the silicate fraction of marine sediments can be used as a recorder of sediment provenance, as well as of the relative importance of physical *versus* chemical weathering regimes of the continental terrains surrounding the different ocean basins (Faure, 1986 and references therein; Jung et al., 2004; Colin et al., 2006).

I.3. Ferromanganese crusts as recorders of past ocean circulation and weathering inputs

Hydrogenetic Fe-Mn crusts are considered condensed stratigraphic sections recording the oceanic and climatic history of the past 75 Ma (Klemm et al., 2005). Due to their slow growth, they have the capacity to record the chemical conditions of the seawater from which they formed and are considered reliable archives for past ocean circulation and weathering on long time scales (cf. Frank, 2002).

The area of study, in the NE Atlantic, is influenced by the MOW, which is characterized by high salinity and temperature and low oxygen content. As manganese is soluble in low-oxygen conditions, this water mass is enriched in dissolved Mn^{2+} between 800 to 1,200 m water depth (the core of MOW) (e.g. Ambar et al., 1999).

Given the sampling location, influenced by the connection of the Atlantic and the Mediterranean Sea, these deposits may have experienced environmental fluctuations as Koschinsky et al. (1996) pointed out for the Lion Seamount. Fluctuations in the intensity of the Oxygen Minimum Zone (OMZ) may have interrupted crust growth at certain times and the strong influence of the MOW in this area has influenced the composition of these crusts.

Based on the study of the records of the radiogenic isotope composition of Nd, Pb and Sr obtained from dated Fe-Mn crusts, from their detrital fraction, and from accompanying sediments we are able to identify the origin and mixing of water masses, and the sources and evolution of weathering inputs into the northeast Atlantic over the past 15 Ma. In fact, Pb and Nd isotopic changes can be attributed to changes in deep-water circulation patterns and weathering inputs (e.g. Abouchami et al., 1999; Frank et al., 1999; 2002).

Radiogenic isotope time series, obtained from dated ($^{10}Be/^{9}Be$ dating) crusts can complement other high resolution paleoceanographic studies (centennial/decadal), by providing a record of the long-term average evolution of the proxies.

I.4. Ferromanganese crusts as potential metal resources

Manganese and ferromanganese oxides in the oceans occur as nodules, crusts, and massive beds. They can be classified as diagenetic, hydrogenetic, hydrothermal, and mixed-type deposits (Halbach, 1986; Hein et al., 1997; Wen et al., 1997).

The first occurrences of ferromanganese nodules or concretions in the oceans were reported by the Challenger Expedition of 1873-1876 (Murray and Renard, 1891) and since then various discoveries and studies were performed. During the 1960's and 1970's there was an increasing interest in the commercial exploitation of seabed minerals, in particular concerning the deposits in the Pacific Ocean (Mero, 1962; Manheim, 1965; Bonatti and Nayudu, 1965; Price, 1967; Cronan, 1977) and it was noted that the Fe-Mn deposits with the highest cobalt content occurred in topographic highs (seamounts and ridges) (e.g. Mero, 1962; 1965; Hein, 2000). It was by this time that Fe-Mn crusts began to be distinguished from abyssal manganese nodules and that their economic interest was recognized (Cronan, 1977; Halbach et al., 1982). However, after the big interest in the exploitation of ferromanganese nodules and crusts during the 1970's and 1980's the low metal prices and technological limitations delayed the enthusiasm for mining seabed minerals up to the 2000's.

The high concentrations of trace elements in crusts is due, in part, to their supply via the oxygen minimum layers in the water column, which are then scavenged under oxic conditions resulting from turbulent mixing of water masses around seamounts. In fact, seamounts act as obstructions to oceanic water mass flow, creating seamount-generated currents of generally enhanced energy relative to the flow at distance from the seamounts. These currents, which are strongest along the outer rim of the summit region of seamounts, promote the formation of thick crusts, enhanced turbulent mixing, and produce upwelling,

leading to increased primary productivity and maintenance of the OMZ above the seamounts (Hein, 2000).

Hydrogenetic metal precipitation is characterized by very slow growth rates, on the order of 1 to 7 mm/Ma, which together with their extremely high specific-surface area for adsorption (average 325 m^2/g of crusts) and high porosity (average 60%) (Hein et al., 1997; Hein, 2000) promotes the enrichment of Fe-Mn crusts in many trace metals. Most of these metals are of economic interest and essential for green- and high-tech applications (Hein et al., 2013), such as Co, Ni, Te, rare earth elements (REEs), and platinum-group elements (PGEs) and thus Fe-Mn crusts are considered an important metal resource.

With the fast growing markets for metals, such as in Asia, the demand for rare metals will continue to increase drastically in the future (Hein et al., 2010); this and the continuous increase in metal prices will increase the potential for marine mining in the near future.

The areas which have the greatest economic potential for nodules and crusts are the Clarion-Cliperton Fe-Mn Nodule Zone (CCZ) and the prime Fe-Mn crust zone (PCZ), both in the central Pacific Ocean (e.g. Hein et al., 2013). These zones and their Fe-Mn nodule and crust occurrences are located in the international seabed Area (the *Area*), which represents the areas of the ocean floor and subsoil beyond national jurisdictions and that are instead regulated by the International Seabed Authority (ISA). The Regulations on Prospecting and Exploration for Polymetallic Nodules in the *Area* were already adopted in 2000 and as interest in crusts is accelerating, the ISA has prepared draft regulations for exploration for Fe-Mn crusts, which have been discussed and approved during its 18th session in July 2012. To date, ISA has entered twelve contracts for exploration of polymetallic nodules in the CCZ and two contracts for exploration of cobalt-rich ferromanganese crusts in the western Pacific Ocean.

The required parameters for hydrogenetic Fe-Mn crust formation, such as the existence of isolated seamounts with steep slopes, which are free of sediment, strong currents, and the existence of an OMZ are also found in the Atlantic (Koschinsky et al., 1995). Indeed, studies already done in the NE Atlantic seamounts (e.g. Koschinsky et al., 1995, 1996; Gaspar, 2001; Muiños et al., 2002; Muiños, 2005) indicate the general presence of Fe-Mn deposits of hydrogenetic origin. Despite that, studies on the occurrences of Fe-Mn nodules and crusts in

the Atlantic Ocean are still in their infancy and there is a clear need for investigation concerning the origin, distribution, and resource potential assessment of these deposits.

I.5. Objectives and thesis outline

The objective of this study is to better understand and determine the paleoceanographic, geological and chemical conditions responsible for the formation of hydrogenetic ferromanganese deposits in northeast Atlantic seamounts (in particular those within the Portuguese Exclusive Economic Zone), their concentration in trace metals of economic interest and in which way the chemical and isotopic composition of the crusts reflects the paleoclimatic and paleoceanographic conditions of the northeast Atlantic Ocean. To accomplish this objective, it was considered: i) to characterize the distribution of crust deposits in the study area; ii) determining changes in composition of crusts taking into account their mineralogical composition, major and minor elements distribution, REE patterns, ages and growth rates, spatial and temporal variations in isotopic composition and their association with crust thickness, water depth, and geographic location; iii) to determine their origin, taking into account the oceanographic conditions, such as water mass characteristics and their effect on crust chemistry and isotopic composition, and the geological conditions controlling the formation of the deposits.

In Chapter II the material and methods used in the thesis work are described.

Chapters III, IV and V represent the manuscripts produced during thesis work and that have either already been published in scientific journals or that are to be submitted soon. These articles/chapters cover the objectives of the thesis:

> The subject of Chapter III is the reconstruction of the Pb and Nd isotopic composition of water masses from the NE Atlantic, as extracted from dated Fe-Mn crusts. In this study three Fe-Mn crusts, distributed over a water depth profile comprising the present-day depths of MOW and NEADW, were analyzed. The time series of Pb and Nd have recorded the evolution of changes in the mixing of NE Atlantic water masses and of the weathering inputs into the NE Atlantic over the past 15 Ma.

In Chapter IV we revisited the findings of Chapter III but considering the detrital fraction of Fe-Mn crusts. Based on the results obtained from the study described in Chapter III, it was concluded that it was important to reconstruct changes in weathering inputs, mainly aeolian dust, during the same time interval by analyzing the radiogenic isotope composition of the detrital fraction in the crusts and accompanying sediments. These data provide independent information on the sources of the detrital inputs and their climatically driven changes and augment the results obtained from the Nd and Pb isotope data of the hydrogenetic fraction of the crusts.

Chapter V covers the study of the composition and considerations of the resource potential of the deposits from the study area. Despite that a detailed evaluation of the potential resources is not possible in the frame of a study like this, it was possible to obtain a qualitative evaluation of the concentrations of some potential economic metals and their resource potential.

Finally, Chapter VI consists of a summary and conclusions of the overall results obtained in the individual articles/chapters, as well as a short outlook into future work.

I.6. Manuscripts

Declaration of my own contribution to the following thesis chapters:

Chapter III: New constraints on the Pb and Nd isotopic evolution of NE Atlantic water masses

Statement:

The samples were collected during cruise M51/1, in which I participated. The samples were impregnated by me at the Department of Soils from the Portuguese National Agronomic Station, Oeiras (now INIAV). I performed the computer controlled microdrilling and the chemical preparation for Pb and Nd isotopes and attended the measurements carried out by M. Frank. I also performed the sub-sampling for $^{10}Be/^{9}Be$ dating at ETH –Zurich. The $^{10}Be/^{9}Be$ ratios were measured at the Zurich AMS Facility (jointly operated by the Swiss

Federal Institute of Technology, Zurich and Paul Scherrer Institute, Villigen, Switzerland) by C. Maden (ETH-Zurich). I interpreted the data and wrote the manuscript. All co-authors contributed to the discussion and helped improving and revising the manuscript.

Chapter IV: Radiogenic Pb, Nd, and Sr isotope composition of the detrital fraction of Fe-Mn crusts from NE Atlantic seamounts: Tracers of detrital inputs over the past 12 million years

Statement:

The samples were collected during the Trident 86, TTR-11, M51/1, and Tore-Madeira cruises, of which I participated in TTR-11 and M51/1. Samples from the Tore-Madeira cruise were kindly provided for this work by J. Girardeau (CNRS, France) through L.M. Pinheiro (Univ. Aveiro, Portugal). J.H. Monteiro was the PI of the project, through which part of the work was financially supported. The re-sampling was performed by me at LNEG, Portugal. I also performed the oxide leaching and freeze drying of the samples at LNEG, Portugal and at GEOMAR, Kiel. The total dissolutions and chromatographic separation and purification of Pb, Nd and Sr were performed by me at Geomar, Kiel. The Pb, Nd, and Sr isotope compositions were measured by me together with B. Haley, C. Ehlert, and R. Stumpf at GEOMAR, Kiel. I also performed the sub-sampling and chemical preparation of the samples for dating by radioactive cosmogenic ^{10}Be and stable ^{9}Be at GEOMAR, Kiel. I discussed and interpreted the data with the help of Martin Frank, James R. Hein, Antje Voelker and Fátima Abrantes and wrote the chapter.

Chapter V: Deep-Sea Fe-Mn crusts from the Northeast Atlantic Ocean: Composition and resource considerations

Statement:

The samples were collected during the Trident 86, TTR-11, M51/1, and Tore-Madeira cruises, of which I participated in TTR-11 and M51/1. Samples from Tore-Madeira cruise were kindly made available for this work by J. Girardeau (CNRS, France) through L.M. Pinheiro (Univ. Aveiro, Portugal). J.H. Monteiro was the PI of the project, through which part of the work was financially supported. I prepared the samples at LNEG, Portugal. The

mounting of the slides for XRD was performed by me at USGS, Menlo Park, USA, under guidance of James R. Hein. The Q-Mode factor analysis and CCM were performed by T. Conrad. I interpreted the data with the help of James R. Hein and I wrote the manuscript. All co-authors contributed to the discussion and helped improving and revising the manuscript.

References

Abouchami W., Galer S. J. G., and Koschinsky A. (1999), Pb and Nd isotopes in NE Atlantic Fe-Mn crusts: proxies for metal paleosources and paleocean circulation. *Geochimica et Cosmochimica Acta* 63(10), 1489-1505.

Abouchami W. and Goldstein S. L. (1995), A lead isotopic study of Circum-Antarctic manganese nodules. *Geochimica et Cosmochimica Acta* 59(9), 1809-1820.

Ambar I., Armi L., Bower A., and Ferreira T. (1999), Some aspects of time variability of the Mediterranean Water off south Portugal. *Deep-Sea Research I* 46, 1109-1136.

Armstrong R. L. (1971), Glacial Erosion and the Variable Isotopic Composition of Strontium in Sea Water. *Nature* 230, 132-133. doi:10.1038/physci230132a0.

Arsouze T., Dutay J.-C., Lacan F., and Jeandel C. (2009), Reconstructing the Nd oceanic cycle using a coupled dynamical –biogeochemical model. *Biogeosciences* 6, 2829–2846.

Banner J. L. (2004), Radiogenic isotopes: systematics and applications to earth surface processes and chemical stratigraphy. *Earth-Science Reviews* 65(3-4), 141-194.

Bayon G., German C. R., Boella R. M., Milton J. A., Taylor R. N., and Nesbitt R. W. (2002), An improved method for extracting marine sediment fractions and its application to Sr and Nd isotopic analysis. *Chemical Geology* 187(3-4), 179-199.

Blum J. D. and Erel Y. (1997), Rb-Sr isotope systematics of a granitic soil chronosequence: The importance of biotite weathering. *Geochimica et Cosmochimica Acta* 61(15), 3193-3204.

Bonatti E. and Nayudu Y. R. (1965), The origin of manganese nodules on the ocean floor. *Am. J. Sci* 263, 17-39.

Broecker W. S. (1991), The Great Ocean Conveyor. *Oceanography* 4(2), 79-89.

Broecker W. S. and Peng T.-H. (1982), *Tracers in the Sea*. Lamont-Doherty Geological Observatory, Columbia University.

Broecker W. S., Rooth C., and Peng T.-H. (1985), Ventilation of the deep northeastern Atlantic. *Journal of Geophysical Research* 90, 6940-6944.

Burke W. H., Denison R. E., Hetherington E. A., Koepnick R. B., Nelson H. F., and Otto J. B. (1982), Variation of seawater 87Sr/86Sr throughout Phanerozoic time. *Geology* 10(10), 516-519.

Burton K. W. (2006), Global weathering variations inferred from marine radiogenic isotope records. *Journal of Geochemical Exploration* 88(1-3), 262-265.

Burton K. W., Lee D.-C., Christensen J. N., Halliday A. N., and Hein J. R. (1999), Actual timing of neodymium isotopic variations recorded by Fe-Mn crusts in the western North Atlantic. *Earth and Planetary Science Letters* 171, 149-156.

Burton K. W., Ling H.-F., and O'Nions R. K. (1997), Closure of the Central American Isthmus and its effect on deep-water formation in the North Atlantic. *Nature* 386, 382-385.

Burton K. W. and Vance D. (2000), Glacial-interglacial variations in the neodymium isotope composition of seawater in the Bay of Bengal recorded by planktonic foraminifera. *Earth and Planetary Science Letters* 176(3-4), 425-441.

Capo R. C. and DePaolo D. J. (1990), Seawater Strontium Isotopic Variations from 2.5 Million Years Ago to the Present. *Science* 249(4964), 51-55. doi:10.1126/science.249.4964.51.

Chester R. (1990), *Marine Geochemistry*. Unwin Hyman.

Christensen J. N., Halliday A. N., Godfrey L. V., Hein J. R., and Rea D. K. (1997), Climate and ocean dynamics and the lead isotopic records in Pacific ferromanganese crusts. *Science* 277, 913-918.

Claude-Ivanaj C., Hofmann A. W., Vlastelic I., and Koschinsky A. (2001), Recording changes in ENADW composition over the last 340 ka using high-precision lead isotopes in a Fe-Mn crust. *Earth and Planetary Science Letters* 188(1-2), 73-89.

Colin C., Frank N., Copard K. v., and Douville E. (2010), Neodymium isotopic composition of deep-sea corals from the NE Atlantic: implications for past hydrological changes during the Holocene. *Quaternary Science Reviews* 29(19-20), 2509-2517.

Colin C., Turpin L., Blamart D., Frank N., Kissel C., and Duchamp S. (2006), Evolution of weathering patterns in the Indo-Burman Ranges over the last 280 kyr: effects of sediment provenance on $^{87}Sr/^{86}Sr$ ratios tracer. *Geochemistry, Geophysics, Geosystems* 7, Q03007. doi:10.1029/2005GC000962.

Copard K., Colin C., Douville E., Freiwald A., Gudmundsson G., De Mol B., and Frank N. (2010), Nd isotopes in deep-sea corals in the North-eastern Atlantic. *Quaternary Science Reviews* 29(19-20), 2499-2508.

Cronan D. S. (1977), Deep- sea nodules: distribution and geochemistry. In *Marine Manganese Deposits* (ed. G. P. Glasby), pp. 11-44. Elsevier Scientific Publishing Company.

Dasch E. J. (1969), Strontium isotopes in weathering profiles, deep-sea sediments, and sedimentary rocks. *Geochimica et Cosmochimica Acta* 33(12), 1521-1552.

DePaolo D. J. (1988), *Neodymium Isotope Geochemistry: An Introduction*. Springer-Verlag.

DePaolo D. J. and Wasserburg G. J. (1976), Nd isotopic variations and petrogenetic models. *Geophysical Research Letters* 3(5), 249-252.

Driscoll N. W. and Haug G. H. (1998), A short circuit in thermohaline circulation: A cause for Northern Hemisphere Glaciation. *Science* 282(5388), 436-438.

Erel Y., Harlavan Y., and Blum J. D. (1994), Lead isotope systematics of granitoid weathering. *Geochimica et Cosmochimica Acta* 58(23), 5299-5306.

Faure G. (1986), *Principles of isotope Geology*. John Wiley and Sons.

Foster G. L., Vance D., and Prytulak J. (2007), No change in the neodymium isotope composition of deep water exported from the North Atlantic on glacial-interglacial scales. *Geology* 35(1), 37-40.

Frank M. (2002), Radiogenic isotopes:tracers of past ocean circulation and erosional input. *Reviews of Geophysics* 40(1), 1-38.

Frank M. (2011), Geochemical proxies of ocean circulation and weathering inputs: Radiogenic isotopes of Nd, Pb, Sr, Hf, and Os. *IOP Conference Series: Earth and Environmental Science*, 012010. doi: 10.1088/1755-1315/14/1/012010.

Frank M., Flierdt T. v. d., Halliday A. N., Kubik P. W., Hattendorf B., and Gunther D. (2003), Evolution of deepwater mixing and weathering inputs in the central Atlantic Ocean over the past 33 Myr. *Paleoceanography* 18(4), 17.

Frank M., Reynolds B. C., and O'Nions R. K. (1999a), Nd and Pb isotopes in Atlantic and Pacific water masses before and after the closure of the Panama gateway. *Geology* 27(12), 1147-1150.

Frank M., O'Nions R. K., Hein J. R., and Banakar V. K. (1999b), 60Myr records of major elements and Pb-nd isotopes from hydrogenous ferromanganese crusts: Reconstruction of seawater paleochemistry. *Geochimica et Cosmochimica Acta* 63(11/12), 1689-1708.

Frank M., Whiteley N., Kasten S., Hein J. R., and O'Nions K. (2002), North Atlantic Deep Water export to the Southern Ocean over the past 14Myr: Evidence from Nd and Pb isotopes in ferromanganese crusts. *Paleoceanography* 17(NO.2), 12-1 a 12-9.

Gaspar L. (2001), Química e mineralogia de depósitos de ferromanganês da montanha submarina Lion, ZEE da Madeira, Portugal. *Actas do VI Congresso de Geoquímica dos Países de Língua Portuguesa/XII Semana da Geoquímica*, 604-608.

Goldstein S. J. and Jacobsen S. B. (1987), The Nd and Sr isotopic systematics of river-water dissolved material: Implications for the sources of Nd and Sr in seawater. *Chemical Geology: Isotope Geoscience section* 66(3-4), 245-272.

Goldstein S. L. and Hemming S. R. (2003), 6.17-Long-lived Isotopic Tracers in Oceanography, Paleoceanography, and Ice-sheet Dynamics. In *Treatise on Geochemistry* (eds. H. D. Holland and K. K. Turekian), pp. 453-489. Pergamon.

Goldstein S. L. and O'Nions R. K. (1981), Nd and Sr isotopic relationships in pelagic clays and ferromanganese deposits. *Nature* 292, 324-327.

Gutjahr M., Frank M., Halliday A. N., and Keigwin L. D. (2009), Retreat of the Laurentide ice sheet tracked by the isotopic composition of Pb in western North Atlantic seawater during termination 1. *Earth and Planetary Science Letters* 286, 546-555.

Gutjahr M., Frank M., Stirling C. H., Klemm V., Flierdt T. v. d., and Halliday A. N. (2007), Reliable extraction of a deepwater trace metal isotope signal from Fe-Mn oxyhydroxide coatings of marine sediments. *Chemical Geology* 242, 351-370.

Halbach P. (1986), Process controlling the heavy metal distribution in Pacific ferromanganese nodules and crusts. *Geologische Rundschau* 75/1, 235-247.

Halbach P., Manhein F. T., and Otten P. (1982), Co-rich ferromanganese deposits in the marginal seamount regions of the central pacific basin: results of the Midpac'81. *Erzmetall* 35, 447-453.

Hein J. R. (2000), Polymetallic massive sulphides and cobalt-rich ferromanganese crusts: status and prospects. In *ISA Technical Study: No.2*, pp. 36-100. International Seabed Authority.

Hein J. R., Conrad T. A., and Staudigel H. (2010), Seamount Mineral Deposits, a source of rare metals for high-technology industries. *Oceanography* 23(No.1), 184-189.

Hein J. R., Koschinsky A., Halbach P., Manheim F. T., Bau M., Kang J.-K., and Lubick N. (1997), Iron and manganese oxide mineralization in the Pacific. In *Manganese Mineralization: Geochemistry and mineralogy of terrestial and marine deposits*, Geological Society Special Publication No. 119 (eds. K. Nicholson, J. R. Hein, J. R. Buhn, and S. Dasgupta), pp. 123-138.

Hein J. R., Mizell K., Koschinsky A., and Conrad T. A. (2013), Deep-ocean mineral deposits as a source of critical metals for high- and green-technology applications: Comparison with land-based resources. *Ore Geology Reviews* 51(0), 1-14.

Jacobsen S. B. and Wasserburg G. J. (1980), Sm-Nd isotopic evolution of chondrites. *Earth and Planetary Science Letters* 50(1), 139-155.

Jeandel C., Delattre H., Grenier M., Pradoux C., and Lacan F. (2013), Rare earth element concentrations and Nd isotopes in the Southeast Pacific Ocean. *Geochemistry, Geophysics, Geosystems* 14(2), 328-341.

Johannesson K. H. and Burdige D. J. (2007), Balancing the global oceanic neodymium budget: Evaluating the role of groundwater. *Earth and Planetary Science Letters* 253(1-2), 129-142.

Jones C. E., Halliday A. N., Rea D. K., and Owen R. M. (2000) Eolian inputs of lead to the North Pacific. *Geochimica et Cosmochimica Acta* 64(8), 1405-1416.

Jones K. M., Khatiwala S. P., Goldstein S. L., Hemming S. R., and van de Flierdt T. (2008), Modeling the distribution of Nd isotopes in the oceans using an ocean general circulation model. *Earth and Planetary Science Letters* 272(3-4), 610-619.

Jung S. J. A., Davies G. R., Ganssen G. M., and Kroon D. (2004), Stepwise Holocene aridification in NE Africa deduced from dust-borne radiogenic isotope records. *Earth and Planetary Science Letters* 221, 27–37.

Khélifi N., Sarnthein M., Andersen N., Blanz T., Frank M., Garbe-Schönberg D., Haley B. A., Stumpf R., and Weinelt M. (2009), A major and long-term Pliocene intensification of the Mediterranean Outflow, 3.5-3.3 Ma ago. *Geology* 37, 811-814.

Klemm V., Levasseur S., Frank M., Hein J. R., and Halliday A. N. (2005), Osmium isotope stratigraphy of a marine ferromanganese crust. *Earth and Planetary Science Letters* 238(1-2), 42-48.

Klevenz V., Vance D., Schmidt D. N., and Mezger K. (2008), Neodymium isotopes in benthic foraminifera: Core-top systematics and a down-core record from the Neogene south Atlantic. *Earth and Planetary Science Letters* 265(3-4), 571-587.

Komárek M., Ettler V., Chrastny V., and Mihaljevic M. (2008), Lead isotopes in environmental sciences: A review. *Environment International* 34(4), 562-577.

Koschinsky A., Gerven M. v., and Halbach P. (1995), First investigations of massive ferromanganese crusts in the NE Atlantic in comparison with hydrogenetic Pacific occurrences. 13, 375-391.

Koschinsky A., Halbach P., Hein J. R., and Mangini A. (1996), Ferromanganese crusts as indicators for paleoceanographic events in the NE Atlantic. *Geol Rudsch* 85, 567-576.

Krijgsman W., Hilgen F. J., Raffi I., Sierro F. J., and Wilson D. S. (1999), Chronology, causes and progression of the Messinian salinity crisis. *Nature* 400, 652-655.

Lacan F. and Jeandel C. (2005a), Acquisition of the neodymium isotopic composition of the North Atlantic Deep water. *Geochemistry, Geophysics, Geosystems* 6, Q12008.

Lacan F. and Jeandel C. (2005b), Neodymium isotopes as a new tool for quantifying exchange fluxes at the continent-ocean interface. *Earth and Planetary Science Letters* 232(3-4), 245-257.

Manheim F. T. (1965), Manganese-iron accumulations in the shallow marine environment. *Symposium on Marine Geochemistry*, 217-276.

Martin E. E., Blair S. W., Kamenov G. D., Scher H. D., Bourbon E., Basak C., and Newkirk D. N. (2010), Extraction of Nd isotopes from bulk deep sea sediments for paleoceanographic studies on Cenozoic time scales. *Chemical Geology* 269(3-4), 414-431.

Martin E. E. and Haley B. A. (2000), Fossil fish teeth as proxies for seawater Sr and Nd isotopes. *Geochimica et Cosmochimica Acta* 64(5), 835-847.

Mero J. L. (1962), Ocean-Floor Manganese Nodules. *Economic Geology* 57, 747-767.

Mero J. L. (1965), *The Mineral Resources of the Sea*. Elsevier.

Meyer I., Davies G. R., and Stuut J.-B. W. (2011), Grain size control on Sr-Nd isotope provenance studies and impact on paleoclimate reconstructions: An example from deep-sea sediments offshore NW Africa. *Geochemistry, Geophysics, Geosystems* 12(3), Q03005.

Muiños S. B. (2005), Contribuição da análise multivariada para o estudo de crostas submarinas de ferro e manganês do Atlântico Nordeste. Master, Universidade Técnica de Lisboa.

Muiños S. B., Gaspar L., Monteiro J. H., Salgueiro R., Ramos J. F., Magalhães V. H., and Rodrigues T. (2002), Ferromanganese deposits from the Nameless Seamount: Preliminary results. *IOC Workshop Report* 183, 27-30.

Murray J. and Renard A. F. (1891,) Report on the deep-sea deposits. *"Scientific results, HMS Challenger"*, 391-400.

Osborne A. H., Vance D., Rohling E. J., Barton N., Rogerson M., and Fello N. (2008), A humid corridor across the Sahara for the migration of early modern humans out of Africa 120,000 years ago. *Proceedings of the National Academy of Sciences of the United States of America* 105(43), 16444-16447.

Pahnke K., Goldstein S. L., and Hemming S. R. (2008), Abrupt changes in Antarctic Intermediate Water circulation over the past 25,000 years. *Nature Geoscience* 1(12), 870-874.

Palmer M. R. and Edmond J. M. (1989), The strontium isotope budget of the modern ocean. *Earth and Planetary Science Letters* 92(1), 11-26.

Piepgras D. J. and Wasserburg G. J. (1980), Neodymium isotopic variations in seawater. *Earth and Planetary Science Letters* 50(1), 128-138.

Piepgras D. J., Wasserburg G. J., and Dasch E. J. (1979), The isotopic composition of Nd in different ocean masses. *Earth and Planetary Science Letters* 45(2), 223-236.

Piotrowski A. M., Banakar V. K., Scrivner A. E., Elderfield H., Galy A., and Dennis A. (2009), Indian Ocean circulation and productivity during the last glacial cycle. *Earth and Planetary Science Letters* 285(1-2), 179-189.

Price N. B. (1967), Some geochemical observations on manganese-iron oxide nodules from different depth environments. *Marine Geology* 5(5-6), 511-538.

Rahmstorf, S. (2002), Ocean circulation and climate during the past 120 000 years. *Nature,* 419, 207-214, doi:10.1038/nature01090.

Ravizza G. E. and Zachos J. C. (2003), 6.20-Records of Cenozoic Ocean Chemistry. In *Treatise on Geochemistry* (eds. H. D. Holland and K. K. Turekian), pp. 551-581. Pergamon.

Raymo M. E. and Ruddiman W. F. (1992), Tectonic forcing of late Cenozoic climate. *Nature* 359, 117-122.

Reid J. L. (1978), On the middepth circulation and salinity field in the North Atlantic Ocean. *Journal of Geophysical Research: Oceans* 83(C10), 5063-5067.

Rempfer J., Stocker T. F., Joos F., Dutay J.-C., and Siddall M. (2011), Modelling Nd-isotopes with a coarse resolution ocean circulation model: Sensitivities to model parameters and source/sink distributions. *Geochimica et Cosmochimica Acta* 75(20), 5927-5950.

Reynolds B. C., Frank M., and O'Nions R. K. (1999), Nd- and Pb-isotope time series from Atlantic ferromanganese crusts: implications for changes in provenance and paleocirculation over the last 8 Myr. *Earth and Planetary Science Letters* 173, 381-396.

Richter F. M., Rowley D. B., and DePaolo D. J. (1992), Sr isotope evolution of seawater: the role of tectonics. *Earth and Planetary Science Letters* 109(1-2), 11-23.

Rutberg R. L., Hemming S. R., and Goldstein S. L. (2000), Reduced North Atlantic Deep Water flux to the glacial Southern Ocean inferred from neodymium isotope ratios. 405(6789), 935-938.

Schaule B. K. and Patterson C. C. (1981), Lead concentrations in the northeast Pacific: evidence for global anthropogenic perturbations. *Earth and Planetary Science Letters* 54(1), 97-116.

Scher H. D. and Martin E. E. (2006), Timing and Climatic Consequences of the Opening of Drake Passage. *Science* 312 (5772), 428-430, doi 10.1126/science.1120044

Schmitz J., W.J and McCartney M. S. (1993), On the North Atlantic circulation. *Reviews of Geophysics* 31(1), 29-49.

Schneider B. and Schmittner A. (2006), Simulating the impact of the Panamanian seaway closure on ocean circulation, marine productivity and nutrient cycling. *Earth and Planetary Science Letters* 246(3-4), 367-380.

Shen G. T. and Boyle E. A. (1988), Thermocline ventilatiion of preanthropogenic lead in the western north Atlantic. *Journal of Geophysical Research* 93(C12), 15,715-15,732.

Tachikawa K., Athias V., and Jeandel C. (2003), Neodymium budget in the modern ocean and paleo-oceanographic implications. *Journal of Geophysical Research: Oceans* 108(C8), 3254.

van de Flierdt T., Frank M., Halliday A. N., Hein J. R., Hattendorf B., Gunther D., and Kubik P. W. (2004), Deep and bottom water export from the Southern Ocean to the Pacific over the past 38 million years. *Paleoceanography* 19(PA1020 doi: 10,1029/2003PA000923).

van de Flierdt T., Robinson L. F., and Adkins J. F. (2010), Deep-sea coral aragonite as a recorder for the neodymium isotopic composition of seawater. *Geochimica et Cosmochimica Acta* 74(21), 6014-6032.

van de Flierdt T., Robinson L. F., Adkins J. F., Hemming S. R., and Goldstein S. L. (2006), Temporal stability of the neodymium isotope signature of the Holocene to glacial North Atlantic. *Paleoceanography* 21(4), PA4102.

Vance D. and Burton K. (1999), Neodymium isotopes in planktonic foraminifera: a record of the response of continental weathering and ocean circulation rates to climate change. *Earth and Planetary Science Letters* 173(4), 365-379.

Vance D., Scrivner A. E., Beney P., Staubwasser M., Henderson G. M., and Slowey N. C. (2004), The use of foraminifera as a record of the past neodymium isotope composition of seawater. *Paleoceanography* 19, PA2009, 10.1029/2003PA000957.

Veizer J. (1989), Strontium Isotopes in Seawater through Time. *Annual Review of Earth and Planetary Sciences* 17(1), 141-167. doi:10.1146/annurev.ea.17.050189.001041.

Veizer J., Ala D., Azmy K., Bruckschen P., Buhl D., Bruhn F., Carden G.A.F., Diener A., Ebneth S., Godderis Y., Jasper T., Korte C., Pawellek F., Podlaha O.G., and Strauss H. (1999), $^{87}Sr/^{86}Sr$, $\delta^{13}C$ and $\delta^{18}O$ evolution of Phanerozoic seawater. *Chemical Geology*, 161(1–3), 59-88. doi: 10.1016/S0009-2541(99)00081-9.

Voelker A. H. L., Lebreiro S. M., Schonfeld J., Cacho I., Erlenkeuser H., and Abrantes F. (2006), Mediterranean outflow strengthening during northern hemisphere coolings: A salt source for the glacial Atlantic? *Earth and Planetary Science Letters* 245, 39-55.

von Blanckenburg F. (1999), Perspectives: paleoceanography-tracing past ocean circulation? *Science* 286(5446), 1862-1863.

von Blanckenburg F. and Igel H. (1999), Lateral mixing and advection of reactive isotope tracers in ocean basins: observations and mechanisms. *Earth and Planetary Science Letters* 169, 113-128.

von Blanckenburg F. and Nagler F. (2001), Weathering versus circulation-controlled changes in radiogenic isotope tracer composition of the Labrador Sea and North Atlantic Deep Water. *Paleoceanography* 16(4), 424-434.

von Blanckenburg F., O'Nions R. K., and Hein J. R. (1996), Distribution and sources of pre-anthropogenic lead isotopes in deep ocean water from Fe-Mn crusts. *Geochimica et Cosmochimica Acta* 60(24), 4957-4963.

Weiss D., Boyle E. A., Wu J., Chavagnac V. r., Michel A., and Reuer M. K. (2003), Spatial and temporal evolution of lead isotope ratios in the North Atlantic Ocean between 1981 and 1989. *Journal of Geophysical Research: Oceans* 108(C10), 3306.

Wen X., De Carlo E. H., and Li Y. H. (1997), Interelement relationships in ferromanganese crusts from the central Pacific ocean: Their implications for crust genesis. *Marine Geology* 136(3-4), 277-297.

Wilson D. J., Piotrowski A. M., Galy A., and Clegg J. A. (2013), Reactivity of neodymium carriers in deep sea sediments: Implications for boundary exchange and paleoceanography. *Geochimica et Cosmochimica Acta* 109, 197-221.

Wilson M. (1989), *Igneous Petrogenesis: A global tectonic approach*. Chapman & Hall.

Material and Methods

II.1. Sample selection and preparation for isotope geochemistry, geochemistry and mineralogy

Samples of ferromanganese (Fe-Mn) crusts for this study were collected at different sites (Figure II.1.) during the following cruises: Trident, TTR-11 (I.O.C., 2002), M51/1 (Hoernle and Scientific Party, 2003), and Tore-Madeira (Merle, 2006). The sampling area covers the NE Atlantic seamounts, including seamounts within the Portuguese EEZ, the Canary Islands area, and the Mediterranean Sea and are distributed over a large depth range and correspondingly over a range of different chemical and oceanographic environments, such as the well oxygenated deep waters, MOW, and the waters of the OMZ. The sample set available for this thesis project (with a depth range of ~ 813m to ~ 4,595 m) is ideally suited to develop knowledge on the paleoceanographic, geological and chemical conditions under which these crusts grew.

Three sample sets were considered:

- **Sample Set 1**- Samples used in the study of the radiogenic isotope composition of Pb and Nd in Fe-Mn crusts in order to identify the origin and mixing of water masses and the evolution of weathering inputs into the northeast Atlantic over the past 15 million years. The results of this study are presented in Chapter III;
- **Sample Set 2**- Samples used in the study of the radiogenic isotope composition of Pb, Nd, and Sr in the detrital fraction of Fe-Mn crusts and some associated sediments in order to reconstruct changes in weathering inputs, mainly aeolian dust, during the same time interval as studied for Sample Set 1. Strontium isotopes are considered in order to complement the information obtained from the other radiogenic isotopes and are needed for further interpretations, such as the source areas of the detrital inputs. The results of this study are presented in Chapter IV;

- **Sample Set 3**- Samples used for geochemical and mineralogical studies in order to determine variations in the composition of crust deposits and to evaluate the resource potential of these deposits within the Portuguese Exclusive Economic Zone (EEZ). The results of this study are presented in Chapter V.

Some samples were used in results for all three chapters.

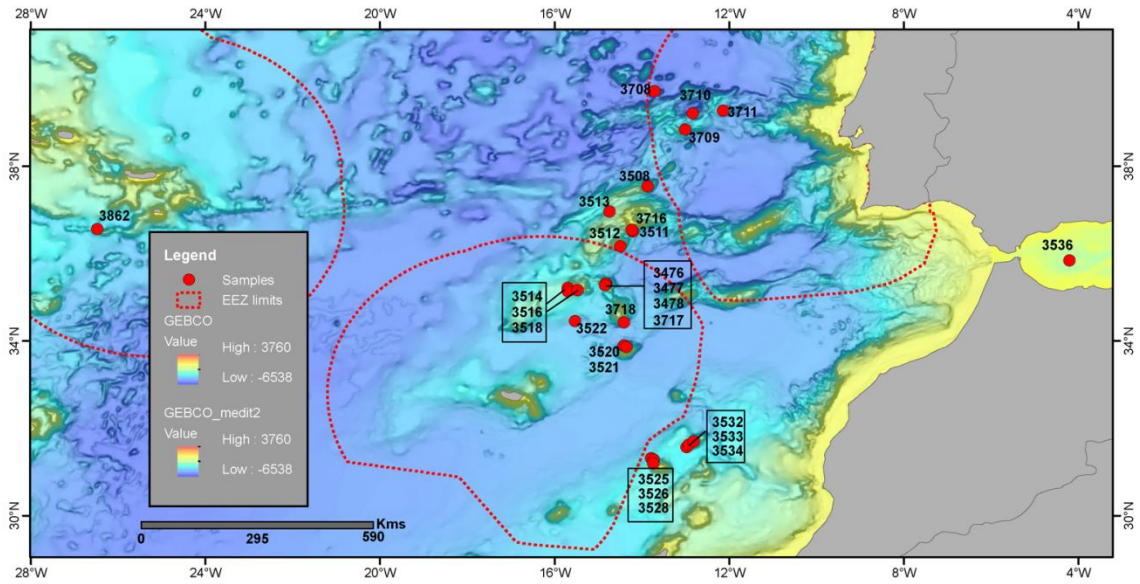

Figure II.1. Study area with locations of the sample set.

II.1.1. Sample Set 1: Study of the radiogenic isotopes of Pb and Nd in Fe-Mn crusts

Three Fe-Mn crust samples, distributed through a water depth profile (~813 m to ~4,600m) representing the present-day depths of MOW and NADW were chosen (Table II.1.). These crusts were prepared (sawed, dried, epoxy impregnated) and sub-sampled. The sub-sampling was performed perpendicular to the macroscopic growth laminations using a computer-controlled drill with 10 mm diameter, in steps of 0.5 mm for the top centimeter of the crust and in steps of 1 mm for the remaining depths (Figure II.2.).

Table II.1. List of samples used in the study of the radiogenic isotope composition of Pb and Nd of Fe-Mn crusts

Sample ID	Field ID	Latitude (N)*[1]	Longitude (W)*[1]	Water depth (m)*[1]	Seamount	Geographic Area
3511-1	M51/1-410DR	35.5100	-14.2127	~2300	Josephine	Madeira
3513-14	M51/1-414DR	36.9700	-14.7475	~4600	MTR	Madeira
3514-6	M51/1-417DR	35.2142	-15.7032	~800	Lion	Madeira

*[1] Coordinates and water depths correspond to intermediate values of the beginning and end of bottom dredge stations. MTR means Madeira-Tore Rise.

Figure II.2. Selected samples for the study of the radiogenic isotopes of Pb and Nd, with detail of the computer-controlled drill sampling and the hand-drilled sampling for dating.

II.1.2. Sample Set 2: Study of the radiogenic isotopes of Pb, Nd and Sr in the detrital fraction of Fe-Mn crusts and some accompanying sediments

Thirty one Fe-Mn crusts were selected, prepared (sawed, dried) and sub-sampled (Table II.2a.). The sub-sampling process consisted in filing the crusts surfaces in order to obtain about 1g of crust surface scrapings to perform the Pb, Nd and Sr isotopic work of the detrital fraction.

Sediment samples representative of the study area were also considered in order to compare their compositions with the signatures of the detrital fractions extracted from the Fe-Mn crusts (Table II.2b.). This allowed for the integration of the results and confirmation of the reliability of the ferromanganese crust-derived data in terms of complete purification.

A total of fifty-seven sub-samples comprising 31 crust surfaces scrapings, 15 samples from depth profiles of 3 selected crusts for time-series studies, 6 sediment samples, and five duplicate samples were prepared.

Additionally, two Fe-Mn crust samples (3478-B.3.5. and 3516-1) were selected for $^{10}Be/^{9}Be$ dating.

Table II.2a. List of Fe-Mn crust samples used in the study of the radiogenic isotope composition of Pb, Nd and Sr of the detrital (allogenic) fraction

Sample ID	Field ID	Latitude (N)*[1]	Longitude (W)*[1]	Water depth (m)*[1]	Seamount	Geographic Area
3476-B.3.2.	TTR11-352GR	35.3150	-14.8317	1855	Nameless	Madeira
3476- B.3.3	TTR11-352GR	35.3150	-14.8317	1855	Nameless	Madeira
3477-B.3.4 (+Dpl)	TTR11-353GR	35.3117	-14.8300	1853	Nameless	Madeira
3478-B.2.2.	TTR11-354GR	35.3167	-14.8350	1839	Nameless	Madeira
3478-B.3.5.	TTR11-354GR	35.3167	-14.8350	1839	Nameless	Madeira
3508-6	M51/1-404DR	37.5417	-13.8725	1800	Teresa	Madeira
3512-42	M51/1-412DR	36.1725	-14.4962	2018	Josephine	Madeira
3513-14	M51/1-414DR	36.9700	-14.7475	4594	MTR	Madeira
3514-6	M51/1-417DR	35.2142	-15.7032	813	Lion	Madeira

Sample ID	Field ID	Latitude (N)*[1]	Longitude (W)*[1]	Water depth (m)*[1]	Seamount	Geographic Area
3516-1	M51/1-419DR	35.1442	-15.7046	1859	Lion	Madeira
3518-2	M51/1-421DR	35.1725	-15.4882	1955	Lion	Madeira
3520-9 (+Dpl)	M51/1-425DR	33.9008	-14..4222	2685	Seine	Madeira
3521-6	M51/1-426DR	33.8683	-14.3680	1362	Seine	Madeira
3708-1	TM-D3B	39.7217	-13.7152	4140	Tore	Madeira
3709-1	TM-D5	38.8442	-13.0147	2803	Tore	Madeira
3711-2	TM-D9	39.2775	-12.1486	3110	Tore	Madeira
3716-3	TM-D17B	36.5517	-14.2388	1620	Josephine	Madeira
3717-12	TM-D19	35.2767	-14.8500	2198	Nameless	Madeira
3718-1	TM-D20	34.4258	-14.4173	3756	Unicorn	Madeira
3525-9	M51/1-448DR	31.3216	-13.8009	3043	Dacia	Canaries
3526-4	M51/1-449DR	31.2875	-13.7456	2622	Dacia	Canaries
3528-7	M51/1-451DR	31.2058	-13.7498	1845	Dacia	Canaries
3528-9	M51/1-451DR	31.2058	-13.7498	1845	Dacia	Canaries
3532-3	M51/1-456DR	31.5725	-12.9845	2637	Annika	Canaries
3533-7	M51/1-457DR	31.6267	-12.9382	1602	Annika	Canaries
3534-11	M51/1-458DR	31.7083	-12.8156	2128	Annika	Canaries
3534-14	M51/1-458DR	31.7083	-12.8156	2128	Annika	Canaries
3536-3	M51/1-462DR	35.8450	-4.2125	1221	Ibn Batouta	Mediterranean
3862	TR86-8D	36.5667	-26.4833	2575	Azores	Azores

*[1] except for samples from the TTR-11 cruise that were collected by TV-Grab, all the other coordinates and water depths (M51/1- Meteor 51/1, TM-Tore-Madeira and TR-Trident 86) correspond to intermediate values of the beginning and end of bottom dredge stations. MTR means Madeira-Tore Rise. Dpl means duplicate. Samples in bold font have been sub-sampled in profiles of five depths (each) for time series measurements.

Table II.2b. List of sediment samples used in the study of the radiogenic isotope composition of Pb, Nd and Sr (Dpl means duplicate)

Sample ID	Field ID	Latitude (N)	Longitude (W)	Water depth (m)	Seamount	Geographic Area
3476-A1	TTR11-352GR	35.3150	-14.8317	1855	Nameless	Madeira
3476-A2	TTR11-352GR	35.3150	-14.8317	1855	Nameless	Madeira
3477-A1 (+Dpl)	TTR11-353GR	35.3117	-14.8300	1853	Nameless	Madeira
3477-A2 (+Dpl)	TTR11-353GR	35.3117	-14.8300	1853	Nameless	Madeira
3478-A1	TTR11-354GR	35.3167	-14.8350	1839	Nameless	Madeira
3478-A2	TTR11-354GR	35.3167	-14.8350	1839	Nameless	Madeira

II.1.3. Sample Set 3: Study of the geochemical and mineralogical composition of Fe-Mn crusts

Detailed geochemical and mineralogical studies were performed on eighteen samples (Table II.3.). These 18 samples were sawed perpendicularly to crust growth in order to obtain slabs representative of the bulk crust, dried and milled. The powders were then homogenized and used for geochemical studies (major and minor elements, REEs, and five of these samples were also analyzed for PGEs).

The preparation of the samples for the determination of the mineralogical composition by X-ray diffraction (XRD) consisted in a first step of the grinding of the sample (to fit through 100-mesh sieve) using a mortar and pestle and in a second step of the mounting of packed slides.

Table II.3. List of Fe-Mn crust samples used for mineralogical and element geochemical analyses

Sample ID	Field ID	Latitude (N)*[1]	Longitude (W)*[1]	Water depth (m)*[1]	Seamount	Geographic Area
3477-B.3.4.	TTR11-353GR	35.3117	-14.8300	1853	Nameless	Madeira
3478-B.3.5.	TTR11-354GR	35.3167	-14.8350	1839	Nameless	Madeira
3717-12	TM-D19	35.2767	-14.8500	2198	Nameless	Madeira

Sample ID	Field ID	Latitude (N)*[1]	Longitude (W)*[1]	Water depth (m)*[1]	Seamount	Geographic Area
3521-6	M51/1-426DR	33.8683	-14.3680	1362	Seine	Madeira
3522-4	M51/1-428DR	34.4567	-15.5387	2946	Godzilla	Madeira
3718-1	TM-D20	34.4258	-14.4173	3756	Unicorn	Madeira
3513-13	M51/1-414DR	36.9700	-14.7475	4594	MTR	Madeira
3513-14	M51/1-414DR	36.9700	-14.7475	4594	MTR	Madeira
3513-16	M51/1-414DR	36.9700	-14.7475	4594	MTR	Madeira
3708-1	TM-D3B	39.7217	-13.7152	4140	Tore	Madeira
3709-1	TM-D5	38.8442	-13.0147	2803	Tore	Madeira
3710-1	TM-D6B	39.2158	-12.8464	4245	Tore	Madeira
3711-2	TM-D9	39.2775	-12.1486	3110	Tore	Madeira
3525-9	M51/1-448DR	31.3216	-13.8009	3043	Dacia	Canaries
3533-7	M51/1-457DR	31.6267	-12.9382	1602	Annika	Canaries
3534-14.1	M51/1-458DR	31.7083	-12.8156	2128	Annika	Canaries
3536-3	M51/1-462DR	35.8450	-4.2125	1221	Ibn Batouta	Mediterranean
3862	TR86-8D	36.5667	-26.4833	2575	Azores	Azores

*[1] except for samples from the TTR-11 cruise that were collected by TV-Grab, all the other coordinates and water depths (M51/1- Meteor 51/1, TM-Tore-Madeira and TR-Trident 86) correspond to intermediate values from on- and off-bottom dredge locations. MTR means Madeira-Tore Rise. Bold font samples have been analyzed for PGEs.

II.2. Laboratory procedures for the isotope geochemical studies

The complete work included chemical leaching to extract the hydrogenetic/detrital fractions followed by the chromatographic separation and purification of the elements of interest and their measurements. The chemical preparation includes in a first step the dissolution of the hydrogenetic fraction followed by the total dissolution of the detrital fraction. The second step is ion chromatographic column chemistry in order to separate and purify Pb, Nd, and Sr for isotopic measurements and the third step consists in isotope measurements (Figure II.3.). The chemical leaching was performed at GEOMAR and at LNEG, I.P. The total

dissolutions, the ion chromatographic separation and purification, and the measurements were performed under Clean Lab conditions at GEOMAR, Kiel.

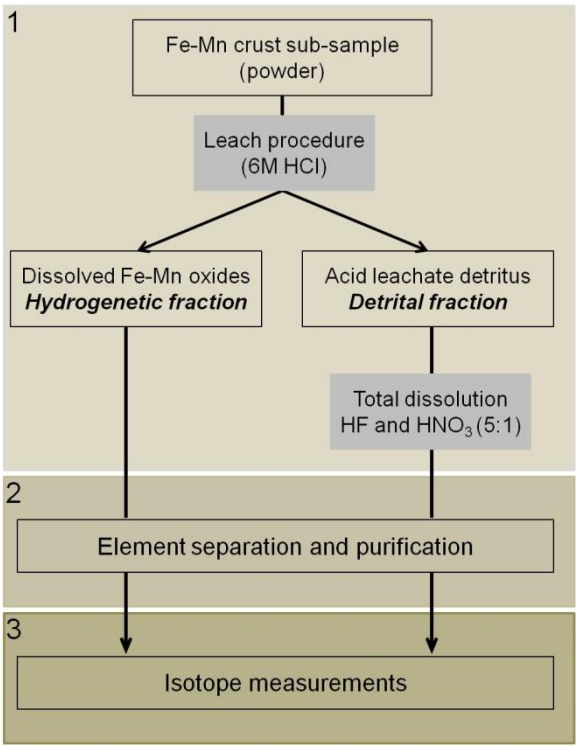

Figure II.3. Schematic overview of the sample preparation procedure. 1) Leaching procedures for isotopic studies; 2) Chromatographic column chemistry for element separation and purification; 3) measurements.

II.2.1. Leaching procedures for radiogenic isotope studies

Past seawater dissolved radiogenic isotope compositions were extracted from the hydrogenetic Fe-Mn oxyhydroxide (authigenic) fraction of Fe-Mn crust samples whereas the detrital radiogenic isotope signal can be achieved from the residual fraction, both from Fe-Mn crust samples and accompanying sediments.

Hydrogenetic Fe-Mn oxyhydroxide fraction

For the extraction of the hydrogenetic Fe-Mn oxyhydroxide fraction (Sample Set 1), 5-8 mg of powdered sample was leached in 1 mL of 6M HCl on a hotplate (~110°C) until dissolution

(around 10 minutes). After dissolution the samples were centrifuged (5' at 10,000 rpm) in order to separate the residue (e.g. epoxy resin, detrital particles) from the supernatant in preparation for the ion-chromatographic column chemistry.

For the study of the detrital fraction (Sample Set 2) ~ 1g of sample powder from the scraped surface samples of the crusts or the sediment samples were leached in 10 mL of 6N HCl (4N HCl for sediment samples) on a hotplate (80-90^{o}C) for around 12 hours. After complete dissolution of the oxide-oxyhydroxide fraction, the supernatant solution was separated through centrifugation (5' at 4,000 rpm).

Detrital fraction

The residual detrital fraction, which remained after removal of the Fe oxyhydroxide ($O_x(OH)_y$) and Mn oxide, was triple rinsed (washed/centrifuged) with Milli-Q water and was then freeze-dried.

The detrital particles were inspected under the binocular to confirm that the entire Fe and Mn fractions were leached and removed. In those cases where the particles still had visible oxide-oxyhydroxide coatings, the leaching procedure was repeated until complete removal was achieved.

The resulting dried (pure) detrital fractions were transferred to 15 mL acid cleaned Teflon vials for further processing under Clean Lab conditions. The total dissolution procedure was achieved in a mixture of 5 mL of concentrated HF/1 mL of concentrated HNO3 (5:1), at 150^{o}C on a hotplate for 3 to 4 days, in tightly closed vials. After ~4 days the samples were cooled and the vials were transferred into an ultrasonic bath for 1 hour and were then evaporated over night. If the samples did not completely dissolve they went through the total dissolution procedure again. When the samples were totally dissolved they were transferred (refluxing and drying) into the HCl form in two steps: first in 5 mL 12N HCl, secondly in 1 mL 6M HCl.

In order to perform the further chemical procedures (chromatographic column chemistry for element separation and purification) the samples were dried and converted into nitric form by refluxing and drying in 3 M HNO_3.

II.2.2. Ion-chromatographic column chemistry for element separation and purification

Prior to the ion chromatographic procedures all samples were centrifuged in order to avoid loading of undissolved particles into the chromatographic columns.

For the separation and purification of Pb, Nd, and Sr previously published methods were adopted: Galer and O'Nions (1989) for Pb, Cohen et al. (1988) for Nd, and Bayon et al. (2002) for Sr.

In order to separate and purify Pb, anion exchange columns (50 µL AG1-X8 resin, mesh size 100-200; Table II.4.) were used. For Nd and Sr, the samples went through a first separation step on cation exchange columns (0.8mL AG50W-X12 resin, mesh size 200-400; Table II.5.) in order to separate the alkaline earth metals from the REEs. Subsequent separation of Nd from the other REEs was achieved on columns containing 2mL Ln Spec resin (mesh 50-100; Table II.6.). Strontium purification was carried on columns loaded with 50 µL Sr Spec resin (mesh 50-100; Table II.7.)(Figure II.4.).

Table II.4. Chromatographic procedure for the purification of Pb (50 µL BioRad® AG1-X8 resin, mesh size 100-200 µm)

Step	Stage	Acid	Volume
1	Clean column	1M HNO_3	1 x 1 reservoir
		Milli-Q water	2 x 1 reservoir
2	Load resin	Resin	50 µL
3	Clean resin	0.25M HNO_3	3x 1mL
4	Condition resin	Solution A*[1]	2 x 100 µL
5	**Load sample**	**Sample (in Solution A)**	**1 x 300 µL**
6	Collect matrix (Nd+Sr)	Solution A	2 x 10 0µL
			1 x 150 µL
		Solution B*[2]	1 x 200 µL
7	**Collect Pb**	**Solution B**	**1 x 300 µL**
8	Waste resin	Milli-Q water	Backwash

*[1] Solution A: 10 mL 1 M HNO_3 + 1mL 2 M HBr + 4 mL Milli-Q water
*[2] Solution B: 5 mL 1 M HNO_3 + 0.15 mL 2 M HBr + 4.85 mL Milli-Q water

Table II.5. Chromatographic procedure for separation of the REEs, including Nd, from the alkaline elements, including Sr (0.8 mL BioRad® AG50W-X12 resin, mesh size 200-400 μm)

Step	Stage	Acid	Volume
1	Clean resin	6M HCl	1 x 8 mL
2	Condition resin	1M HCl	1 x 0.5 mL 1 x 1 mL
3	**Load sample**	**Sample (in 1M HCl)**	**1 x 0.5 mL**
4	wash-in sample	0.25M HNO_3	3x 0.6 mL
5	Elute matrix	3 M HCl	1 x 5 mL
6	**Collect matrix (Sr)**	**3 M HCl**	**1 x 5 mL**
7	Change acid	Milli-Q water	2 x 1 mL
8	Elute matrix (Ba)	2.5M HNO_3	1 x 8 mL
9	**Collect matrix (REE, Nd)**	**6M HNO_3**	**1 x 6 mL**
10	Clean resin	6M HNO_3	1 x 6 mL
11	Change acid	Milli-Q water	2 x 1 mL
12	Store column	1M HCl	1 x 1 mL

Table II.6. Chromatographic procedure for the purification of Sr (50 μL Eichrom® Sr-Spec resin, mesh size 50-100 μm)

Step	Stage	Acid	Volume
1	Clean column	Milli-Q water	1 x 1 reservoir 2 x 1 reservoir
2	Load resin	Resin	50 μL
3	Clean resin	Milli-Q water	1 x 1 mL
4	Condition resin	3M HNO_3	2 x 50 μL 2 x 75 μL
5	**Load sample**	**Sample (in 3M HNO_3)**	**1 x 50 μL**
6	Elute matrix	3M HNO_3	2 x 50 μL 1 x 300 μL
7	**Collect Sr**	**Milli-Q water**	**1 x 500 μL**
8	Waste resin	Milli-Q water	backwash

Table II.7. Chromatographic procedure for the purification of Nd (2 mL Eichrom® Ln-Spec resin, mesh size 50-100 µm)

Step	Stage	Acid	Volume
1	Clean resin	6M HCl	1 x 8 mL
2	Condition resin	0.1M HCl	1 x 0.5 mL 1 x 1 mL
3	**Load sample**	**Sample (in 0.1M HCl)**	**1 x 0.5 mL**
4	wash-in sample/elute Ba	0.1M HCl	1x 0.5 mL
5	Elute matrix (LREE)	0.25M HCl	1 x 7.5 mL
6	**Collect Nd**	**0.25M HCl**	**1 x 5 mL**
7	Clean resin	6M HCl	1 x 8 mL
8	Pass and store column	0.3M HCl	1 + 1 mL

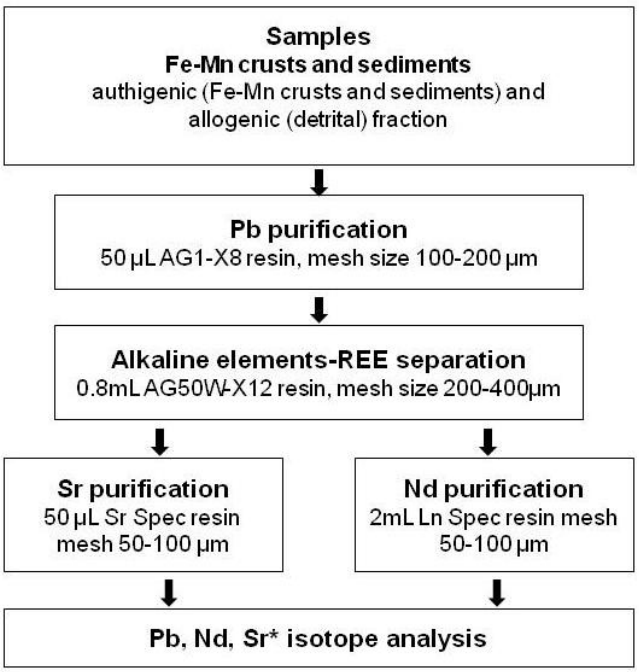

Figure II.4. Schematic overview of the successive element separation and purification procedure applied.*Sr isotope analysis were only performed on the detrital fractions.

II.2.3. Dating with $^{10}Be/^{9}Be$

Two selected Fe-Mn crusts were sub-sampled to cover the entire thicknesses of the crusts and dated by profiles of the radioactive cosmogenic ^{10}Be and stable ^{9}Be. The chemical preparation of the sub-samples was carried out at GEOMAR, Kiel, and followed closely the method described by Henken-Mellies et al. (1990). For this procedure ~10 mg of homogenized sample was precisely weighted and dissolved in 6M HCl on a hotplate for at least 1 hour. After dissolution, the sample was centrifuged and an aliquot (of ~10% of the solution) for ^{9}Be measurement was taken and precisely weighted. A precise amount (between 0.5-1 ml) of ^{9}Be-carrier was added (AAS-1000 ppm Be-standard solution). The remaining solution was used for the extraction of ^{10}Be from marine Fe-Mn crusts. The method consists in various precipitation and re-dissolution steps at controlled pH values. These precipitation and re-dissolution steps are needed in order to separate the alkali metals (under acid conditions Be precipitates as a hydroxide together with Fe whereas the aluminum and other alkali metals stay in solution), the iron (under basic conditions the Fe precipitates as hydroxide whereas Be stays in solution), and the boron (to avoid isobaric interference during the Accelerator Mass Spectrometry (AMS) measurements) from the beryllium in order to have just Be in the final solution.

II.3. Methods

II.3.1. Radiogenic isotope measurements

The radiogenic isotope measurements were performed on a *Nu Plasma* High Resolution Multicollector- Inductively Coupled Plasma- Mass Spectrometer (HR MC-ICP-MS, *Nu Instruments*).

Sample Set 1

The measurements of Sample Set 1 were performed at ETH Zurich.

Measured $^{143}Nd/^{144}Nd$ ratios were corrected for instrumental mass bias using a $^{146}Nd/^{144}Nd$ of 0.7219 and normalized to the JMC-Nd standard ($^{143}Nd/^{144}Nd$ ratio of 0.511833) cross-calibrated to the La Jolla standard (0.511858). The calculation of the age-corrected $\varepsilon_{Nd(T)}$

values used a $^{147}Sm/^{144}Nd$ of 0.115. For the Nd isotope measurements of different sessions, the 2σ external precision varied between 30 ppm and 33 ppm.

For the Pb isotope measurements, a Tl-doping procedure (e.g., Belshaw et al., 1998) was applied. All Pb isotope ratios were normalized to the NIST SRM981 standard and the ratios used for external normalization are those given by Abouchami et al. (1999). For the Pb isotope measurements of different sessions, the 2σ external precision was 116, 144, 172, 46, and 74 ppm for $^{206}Pb/^{204}Pb$, $^{207}Pb/^{204}Pb$, $^{208}Pb/^{204}Pb$, $^{207}Pb/^{206}Pb$, and $^{208}Pb/^{206}Pb$, respectively.

Sample Set 2

The measurements for Sample Set 2 were also performed on a HR MC-ICP-MS (*Nu instruments*) at GEOMAR, Kiel.

All purified Nd, Pb and Sr samples followed a concentration test prior to isotope analysis in order to achieve comparable beam sizes by adjusting their concentrations to a similar value.

Measured $^{143}Nd/^{144}Nd$ ratios were corrected for instrumental mass bias using a $^{146}Nd/^{144}Nd$ of 0.7219 and normalized to the accepted value of the JNdi-1 standard of 0.512115 (Tanaka et al., 2000). For the Nd isotope measurements of different sessions, the 2σ external precision was 46 and 47 ppm.

For the determination of Pb isotope ratios a standard bracketing method was used (Albarède et al., 2004) and all Pb isotope ratios were normalized to the accepted values for NBS981 given by Abouchami et al. (1999). The 2σ external reproducibility of this standard, during repeated sessions on the mass spectrometer, was ±0.003, ±0.004, ±0.012, ±0.0008, and ±0.0001 for $^{206}Pb/^{204}Pb$, $^{207}Pb/^{204}Pb$, $^{208}Pb/^{204}Pb$, $^{208}Pb/^{206}Pb$, and $^{207}Pb/^{206}Pb$, respectively.

The measured $^{87}Sr/^{86}Sr$ isotope ratios were corrected for instrumental mass bias and interferences (^{86}Kr, ^{87}Rb) by using $^{86}Sr/^{88}Sr$ = 0.1194 (Steiger and Jäger, 1977), and normalized to the widely accepted value of 0.710245 for the NIST NBS987 standard. The 2σ external reproducibility of this standard, measured during different sessions, varied between 23 and 48 ppm.

II.3.2. Bulk element chemistry

Sample Set 3 was analyzed for bulk element chemistry. The analyses were performed at SGS Canada Inc. Five selected samples were also analyzed for PGE and Au contents, at Genalysis Laboratory Services, Ltd (Australia). The methods used for the determination of each element are described in Table II.8.

Table II.8. Applied methods for bulk chemistry analyses

Method	Element/ion
Fused-disk XRF	Fe, Mn, Si, Al, Ca, Mg, Na, K, Ti, P
4-acid digestion + ICP-OES	S, Ba, Cr, Cu, Li, Ni, Sr, V, Zn, Zr
4-acid digestion + ICP-MS	Ag, As, Be, Bi, Cd, Co, Ga, Ge, Hf, In, Mo, Nb, Pb, Rb, Sb, Sc, Sn, Ta, Tl, W, Cs
Lithium-metaborate fusion + ICP-MS	Th, U, Y, REEs
4-acid digestion, hydride generation + AAS	Se, Te
Cold vapor AAS	Hg
Specific-ion electrode	Cl^-
Fire assay + ICP-MS	PGEs, Au

XRF: X-ray fluorescence; ICP-OES: Inductively coupled plasma-optical emission spectrometry; ICP-MS: Inductively coupled plasma- mass spectrometry; AAS: Atomic absorption spectrometry.

The precision (based on duplicate analyses of 10% of the samples) was better than 5% for S, As, Ba, Be, Bi, Cd, Co, Cr, Cu, Ga, Ge, In, Li, Mo, Ni, Pb, Rb, Sc, Se, Sr, Te, Th, Tl, U, V, Zn, REEs, Cl^-, and Cs, and better than 10% for Sb, Sn, W, and Hg. For some elements the precision shows a wider range of variation of 10-30% for Ag, 11-28% for Hf, 15-24% for Nb, 13-24% for Ta, and 5-16% for Zr. For the PGE and Au contents the analytical accuracy, which was calculated using repeated measurements of the international standards AMIS0056 and

HGMNEW, is better than 5% for Os and Ru, and better than 10% for Ir, Pd, and Pt. For Au the analytical accuracy is 13% and for Rh it varies from 5-17%.

II.3.3. Mineralogy

The mounting of the XRD slides and the determination of the mineralogical composition of all 18 crusts was performed at the United States Geological Survey (USGS), on a Philips diffractometer using Cu-Kα radiation and carbon curved-crystal monochromator.

The interpretation of the diffractograms and identification of the mineralogical phases was also performed at USGS using the program X'Pert High Score from Philips Analytical B.V. (PANalytical) v. SET48-1.0. For the determination of mineral contents a semi-quantitative determination, considering the relative intensity of the peaks and previously determined weighing factors (Cook et al., 1975; Hein et al., 1988), was used and the nomenclature used for the manganese minerals was that of Usui et al. (1989).

II.3.4. Dating with $^{10}Be/^{9}Be$

The measurements of ^{10}Be were performed at the Zürich AMS Facility of the Paul Scherrer Institute and the ETH Zürich, Switzerland. For the normalization of the measured $^{10}Be/^{9}Be$ ratios, the secondary ETH Zürich S2007N standard material with a nominal value of $^{10}Be/^{9}Be = 28.1 \times 10^{-12}$ (Kubik and Christl, 2010) was used. The concentrations of stable ^{9}Be (and of Sr, Ba, REEs, and Pb) were measured by ICP-MS at the Geosciences Institute at the University of Kiel on aliquots of the same solutions as those used for the ^{10}Be measurements, and on Fe-Mn nodule reference material NOD A1 (Garbe-Schönberg, 1993). The measurement of the natural authigenic ^{9}Be is needed in order to guarantee that the determined natural $^{10}Be/^{9}Be$ represents a true seawater ratio, which should be consistent with the modern seawater ratio for the surface sample.

References

Abouchami W., Galer S. J. G., and Koschinsky A. (1999), Pb and Nd isotopes in NE Atlantic Fe-Mn crusts: proxies for metal paleosources and paleocean circulation. *Geochimica et Cosmochimica Acta* 63(10), 1489-1505.

Albarède F., Telouk P., Blichert-Toft J., Boyet M., Agranier A., and Nelson B. (2004), Precise and accurate isotopic measurements using multiple-collector ICPMS. *Geochimica et Cosmochimica Acta* 68(12), 2725-2744, doi: 10.1016/j.gca.2003.11.024.

Bayon G., German C.R., Boella R.M, Milton J.A., Taylor R.N., and Nesbitt R.W. (2002), An improved method for extracting marine sediment fractions and its application to Sr and Nd isotopic analysis. *Chemical Geology* 187(3–4), 179-199, doi: 10.1016/S0009-2541(01)00416-8.

Belshaw N.S., Freedman P.A., O'Nions R.K., Frank M., and Guo Y. (1998), A new variable dispersion double-focusing plasma mass spectrometer with performance illustrated for Pb isotopes. *International Journal of Mass Spectrometry*, *181* (1-3), 51-58.

Cohen A.S., O'Nions R.K., Siegenthaler R., and Griffin W.L. (1988), Chronology of the pressure-temperature history recorded by a granulite terrain. *Contrib. Mineral. Petrol.*, *98*, 303-311.

Cook H.E., Johnson P.D., Matti J.C., and Zemmels I. (1975), Methods of sample preparation and X-ray data analysis (X-ray mineralogy laboratory, Deep Sea Drilling Project, University of California Riverside). In *Initial Reports of the Deep-Sea Drilling Project* 28, 999-1007.

Galer S.J.G., and O'Nions R.K. (1989), Chemical and isotopic studies of ultramafic inclusions from the San Carlos volcanic field, Arizona: a bearing on their petrogenesis. *J. Petrol.*, *30*, 1033-1064.

Garbe-Schönberg, C. D. (1993), Simultaneous determination of 37 trace elements in 28 international rock standards by ICP-MS, *Geostand. Newsl*., 17, 81–97, doi:10.1111/j.1751-908X.1993.tb00122.x.

Hein J.R., Schwab W.C., and Davis A.S. (1988), Co and Pt-rich ferromanganese crusts and associated substrate rocks from the Marshall Islands. *Marine Geology* 78, 255-283.

Henken-Mellies W.U., Beer J., Heller F., Hsü K.J., Shen C., Bonani G., Hofmann H.J., Suter M., and Wölfli W. (1990), ^{10}Be and ^{9}Be in South Atlantic DSDP Site 519: Relation to geomagnetic reversals and to sediment composition. *Earth and Planetary Science Letters* 98(3–4), 267-276, doi: 10.1016/0012-821X(90)90029-W.

Hoernle K., and Scientific Party (2003), Cruise Report M51/1. In *Ostatlantik - Mittelmeer - Schwarzes Meer, Cruise No. 51, 12 September - 28 December 2001*, Meteor-Berichte 03-1 (eds. C. Hemleben, K. Hoernle, B. B. Jorgensen and W. Roether, pp. 3-35. Hamburg, Germany: University of Hamburg.

I.O.C.-Intergovernmental Oceanographic Commission (2002), Geological Processes in the Mediterranean and Black Seas and North East Atlantic. Preliminary results of investigations during the TTR-11 cruise of RV Professor Logachev, July-September, 2001. In *IOC Technical Series* (eds. N. H. Kenyon, M. K. Ivanov, A. M. Akhmetzhanov and G. G. Akhmanov). Paris, France: UNESCO.

Kubik, P. W., and M. Christl (2010), ^{10}Be and ^{26}Al measurements at the Zurich 6 MV Tandem AMS facility, *Nucl. Instrum. Methods Phys. Res.*, Sect. B, 268, 880–883, doi:10.1016/j.nimb.2009.10.054.

Merle R. (2006), Age and origin of Tore-Madeira Rise: beginning of Atlantic Ocean spreading or hotspot track. Petrology, geochemistry, U-Pb geochronology and Pb-Sr-Hf isotopes. PhD, University of Nantes (in French).

Steiger R.H., and Jäger E. (1977), Subcommission on geochronology: Convention on the use of decay constants in geo- and cosmochronology. *Earth and Planetary Science Letters* 36(3), 359-362, doi: 10.1016/0012-821X(77)90060-7.

Tanaka T., Togashi S., Kamioka H., Amakawa H., Kagami H., Hamamoto T., Yuhara M., Orihashi Y., Yoneda S., Shimizu H., Kunimaru T., Takahashi K., Yanagi T., Nakano T., Fujimaki H., Shinjo R., Asahara Y., Tanimizu M., and Dragusanu C. (2000), JNdi-1: a neodymium isotopic reference in consistency with LaJolla neodymium. *Chemical Geology* 168(3–4), 279-281, doi: 10.1016/S0009-2541(00)00198-4.

Usui A., Mellin T.A., Nohara M., and Yuasa M. (1989), Structural stability of marine 10A manganates from the Ogasawara (Bonin) arc: implication for low-temperature hydrothermal activity. *Marine Geology* 86, 41-56.

New constraints on the Pb and Nd isotopic evolution of NE Atlantic water masses

Abstract

Time series of lead (Pb) and neodymium (Nd) isotope compositions were measured on three ferromanganese crusts recording the evolution of NE Atlantic water masses over the past 15 Ma. The crusts are distributed along a depth profile (~700-4600 m) comprising the present-day depths of Mediterranean Outflow Water and North East Atlantic Deep Water. A pronounced increase of the $^{206}Pb/^{204}Pb$ in the two deeper crusts starting at ~4 Ma and a decrease in $^{143}Nd/^{144}Nd$ in all three crusts took place between ~6-4 Ma and the present. These patterns are similar to isotope time series in the western North Atlantic basin and are consistent with efficient mixing between the two basins. However, the changes occurred 1-3 Ma earlier in the eastern basin indicating that the northeastern Atlantic led the major change in Pb and Nd isotope composition, probably due to a direct supply of Labrador Sea Water *via* a northern route. The Pb isotope evolution during the Pliocene-Pleistocene can generally be explained by mixing between two end-members corresponding to Mediterranean Outflow Water and North East Atlantic Deep Water but external sources such as Saharan dust are likely to have played a role as well. The Pb isotope composition of the shallowest crust that grew within the present-day Mediterranean Outflow Water does not show significant Pb isotope changes indicating that it was controlled by the same Pb sources throughout the past 15 Ma.

This Chapter has been published as:

Muiños, S. B., M. Frank, C. Maden, J. R. Hein, T. van de Flierdt, S. M. Lebreiro, L. Gaspar, J. H. Monteiro and A. N. Halliday (2008), New constraints on the Pb and Nd isotopic evolution of NE Atlantic water masses, *Geochem. Geophys. Geosyst.*, 9, Q02007, doi: 10.1029/2007GC001766.

III.1. Introduction

The strength of the present-day Meridional Overturning Circulation, which controls deep ventilation and meridional heat transport around the globe, has to a large extent been controlled by the strength of North Atlantic Deep Water (NADW) production. Three principal water masses contribute to the formation of NADW at high northern latitudes: Labrador Seawater (LSW), Denmark Strait Overflow Water (DSOW), and Iceland-Scotland Overflow Water (ISOW), to which variable amounts of Subpolar Mode Water are admixed (Schmitz and McCartney, 1993). In addition, it has been suggested that contributions of highly saline and warm Mediterranean Outflow Water (MOW) are important for the salt and temperature budget of the North Atlantic, thereby preconditioning water masses that form NADW (cf. Reid, 1978; Voelker et al., 2006). In the western north Atlantic, NADW flows south within the Western Boundary Undercurrent and reaches the eastern North Atlantic basin through gaps in the Mid-Atlantic Ridge such as the Romanche or Vema Fracture zones (cf. Broecker et al., 1985). North East Atlantic Deep Water (NEADW) is formed by mixing of a branch of ISOW, which did not flow into the North-western basin, with LSW, Lower Deep Water (LDW, which is essentially modified Antarctic Bottom Water (AABW)) and modified NADW (Lacan and Jeandel, 2005a).

NADW production and export to the Southern Ocean have been subject to temporal changes but the magnitude and timing of those changes has been a matter of debate. It has been argued that NADW export was not fully established until the closure of the Isthmus of Panama (beginning at around 12.5 Ma and final closure at ~3 Ma (Murdock et al., 1997 and references therein)). According to this hypothesis the closure caused an enhanced advection of warm and saline waters to the northern high-latitudes which then increased the production of NADW (Bartoli et al., 2005). In contrast, there are clear indications from carbon and neodymium isotope studies that the NADW export was stronger during the warm early Pliocene than it is today (Ravelo and Andreasen, 2000) and decreased after the major intensification of Northern Hemisphere Glaciation (NHG) at 2.7 Ma (Raymo et al., 1992; Frank et al., 2002). Moreover, based on Nd isotope records from the Walvis Ridge, Via and Thomas (2006) postulated an onset of NADW production in the early Oligocene, in agreement with sedimentological evidence (Davies et al., 2001).

Another important factor that probably influenced thermohaline circulation during the Miocene was the Messinian Salinity Crisis (MSC). During the MSC between 5.96 and 5.33 Ma (Krijsgsman et al., 1999), the Mediterranean was, at least periodically, isolated from the global ocean, which led to the deposition of large evaporate sequences. By the end of the MSC, the exchange of water between the Mediterranean Sea and the Atlantic was reestablished and highly saline and warm MOW entered the North Atlantic through the Strait of Gibraltar. Present MOW properties show the existence of two cores of this water mass: an upper core, centered at about 800 m, and a lower core, at 1200 m water depth (Madelain, 1970; Zenk, 1970; Ambar and Howe, 1979; Ambar et al., 1999; 2002). The changes during the Miocene MSC and the interruption of MOW inflow into the North Atlantic most likely had a profound impact on overturning circulation and northern hemisphere climate (Johnson, 1997; Rogerson et al., 2006).

In order to better understand long-term changes of ocean circulation and weathering inputs into the ocean on a million-year time scale, the radiogenic isotope compositions of Pb and Nd have been used as proxies. These elements have residence times on the order of or shorter than the global mixing time of the ocean and can therefore be used as proxies for water mass mixing (cf. Frank, 2002). Radiogenic isotopes are not influenced by biological fractionation processes, and change their values only as a function of water-mass mixing or by additions from external sources such as riverine, aeolian, or in the case of Pb, hydrothermal inputs (cf. Frank, 2002; van de Flierdt et al., 2004). In addition, exchange processes at the boundaries of the oceans such as shelf areas (termed boundary exchange) may alter the Nd isotopic composition of seawater (Lacan and Jeandel, 2005b) and submarine groundwater discharge may also play a role in controlling the dissolved Nd isotope signature of seawater (Johannesson and Burdige, 2007).

The present-day Nd isotope composition of water masses, as measured directly on seawater samples, shows that the most radiogenic isotope compositions are found in the North Pacific, whereas the least radiogenic values are found in the North Atlantic, generally reflecting the isotopic composition of the rocks surrounding the main ocean basins (cf. Frank, 2002). Newly formed NADW has an ε_{Nd} signature of -13.5 (Piegras and Wasserburg, 1982, 1987; Jeandel, 1993, Lacan and Jeandel, 2005a) (Nd isotope ratios are expressed as ε_{Nd} values; This notation refers to the deviation of the measured $^{143}Nd/^{144}Nd$ ratio from the chondritic uniform reservoir CHUR, which value is 0.512638, multiplied by 10,000). The

unradiogenic Nd isotope signature of NADW today mainly originates from the LSW component. This water mass today has a very unradiogenic signature (ε_{Nd} = -13.9 ± 0.4) (Lacan and Jeandel, 2005a) caused by weathering contributions from old Archean rocks which in the Baffin Bay area reach an ε_{Nd} as low as -26 (Stordal and Wasserburg, 1986). In comparison, DSOW (ε_{Nd} = -8.4 ± 1.4) and ISOW (ε_{Nd} = -8.2 ± 0.6) have much more radiogenic signatures (Piegras and Wasserburg, 1987; Lacan and Jeandel, 2005a). In the North-eastern Atlantic, NEADW has an Nd isotopic signature of -13.2 ± 0.4 (Lacan and Jeandel, 2005a) whereas modified NEADW show less negative ε_{Nd} values varying between -11.3 and -11.9 (Tachikawa et al., 1999; van de Flierdt et al., 2006). At shallower depth (0-1100 m), Nd isotope ratios of the seawater in the northeastern Atlantic show more negative values (ε_{Nd} down to -13) probably due to the contribution by partial dissolution of Saharan dust particles (Saharan dust has ε_{Nd} values between -12 to -14) (e.g. Grousset et al., 1988; Tachikawa et al., 1997). For deeper waters (below 2500 m) the dissolved Nd isotope signature can be explained by mixing between NADW and AABW (e.g., Frank et al., 2003). Southern Ocean waters, such as AABW and Antarctic Intermediate Water, have less radiogenic ε_{Nd} values (-7 to -9) (Piegras and Wasserburg, 1982; Bertram and Elderfield, 1993; Jeandel, 1993) as a result of the contribution of Pacific waters with higher ε_{Nd} values (-3 to -5) reflecting weathering of young volcanic rocks (Piegras and Jacobsen, 1988).

The pre-anthropogenic Pb isotope distribution in deep waters, which cannot be measured on seawater, has been recovered from ferromanganese crust surfaces (Abouchami and Goldstein, 1995; von Blanckenburg et al., 1996a) and shows that the most radiogenic compositions are found in the NW Atlantic (^{206}Pb/ ^{204}Pb >19.1) whereas less radiogenic values prevail in the Southern Ocean (^{206}Pb/ ^{204}Pb <18.9) and in the central North Pacific (e.g., ^{206}Pb/ ^{204}Pb < 18.7). The highly radiogenic Pb isotope values in the North Atlantic have been explained by incongruent weathering processes on the old cratonic landmasses of northern Canada and Greenland (von Blanckenburg and Nägler, 2001).

Changes in radiogenic isotope signatures recorded in fish teeth (e.g., Thomas, 2004; Martin and Scher, 2004; Scher and Martin, 2006; Thomas and Via, 2007) or planktonic *foraminifera* (Vance and Burton, 1999; Vance et al., 2004) deposited in marine sediments, or in ferromanganese crusts (hereafter called crusts) have been used as proxies (cf. Frank, 2002). Crusts are seawater precipitates which grow at very slow rates (about 0.5-10 mm/Ma) and

recorded the radiogenic isotope evolution of seawater as far back as 75 Ma (Klemm et al., 2005). Several time series studies based on ferromanganese crust time series in the western North Atlantic have shown that the ε_{Nd} of NADW has decreased significantly over the past 3 Ma (Burton et al., 1997, 1999; O'Nions et al., 1998). This was either caused by increased weathering contributions from old cratonic areas in northern Canada and Greenland or by an increased admixture of LSW. In the eastern North Atlantic similar patterns have been observed, though with a smaller amplitude (Abouchami et al, 1999; Reynolds et al., 1999). A contribution from LSW entering *via* a northern route (Sy et al., 1997; Paillet et al., 1998; Abouchami et al., 1999; Bower et al., 2002; Frank et al., 2003) has been suggested to have occurred in the eastern basin. In addition, MOW contributions (ε_{Nd} = -9.4 ± 0.3 (Spivack and Wasserburg, 1988; Abouchami et al., 1999; Tachikawa et al., 2004)) have clearly played a role for the radiogenic isotope composition of the water masses in the eastern basin, particularly at shallow depths.

We present new high-resolution and high-precision Pb and Nd isotope time series obtained from three crusts in the eastern North Atlantic Ocean. These data provide a 15 Ma isotopic history of water masses at different depths in the eastern North Atlantic, which varied as a function of changes in ocean circulation and weathering inputs.

III.2. Material and Methods

Three hydrogenous crusts covering water depths between ~700 and 4600 m in the eastern North Atlantic Ocean were analyzed for Pb and Nd isotopes, bulk element chemistry, and mineralogy. The samples were collected during Meteor Cruise 51/1 (2001) (Hoernle and Scientific Party, 2003) (Figure III.1. and Table III.1.) between the Portuguese southwest coast and Madeira Island. Crusts 3514-6 (Lion seamount) and 3511-1 (Josephine seamount) were collected east of the Madeira-Tore Rise, whereas crust 3513-14 was collected on the western flank of the Rise. The crusts were sampled continuously in steps of 0.5 mm for the top first centimeter of the crust and in steps of 1 mm for the remaining depths. Sampling was performed perpendicular to the macroscopic growth laminations using a computer-controlled drill with 10 mm diameter. The methods used for chemical preparation and purification of Nd and Pb were adopted from Cohen et al. (1988) and Galer and O'Nions

(1989), respectively. Nd and Pb isotope ratios were determined by MC-ICP-MS (*Nu Instruments*) at ETH Zürich. For the Pb isotope measurements, a Tl-doping procedure (e.g.,

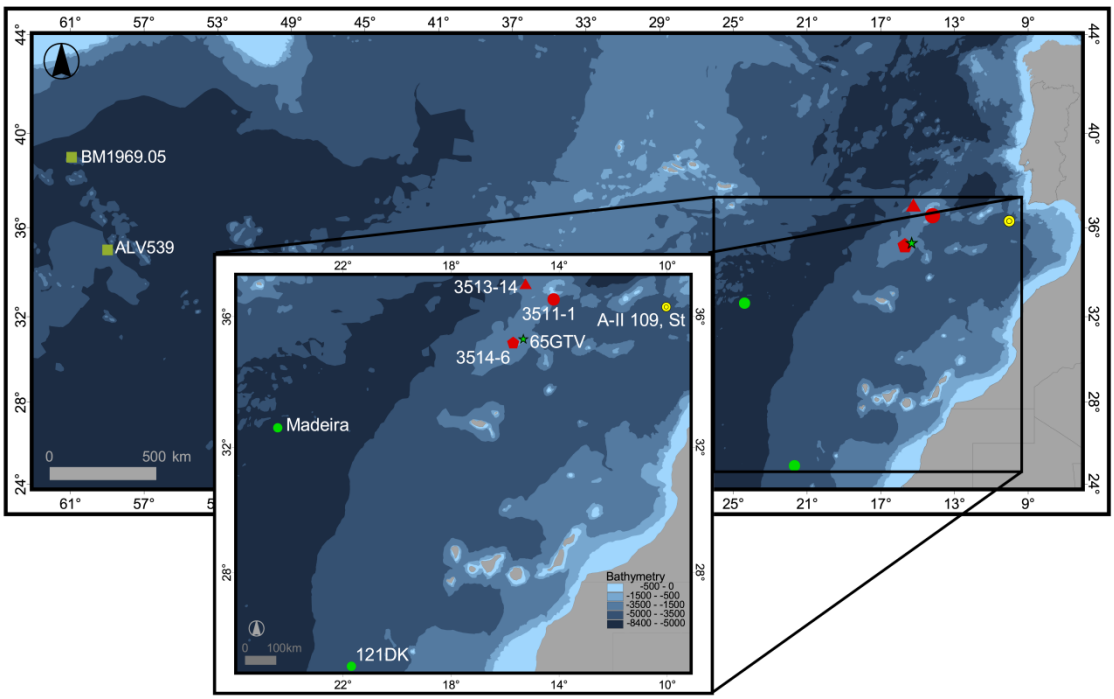

Figure III.1. Map showing the location of the three studied crusts (in red) plus 65GTV (green star) from a nearby location [*Abouchami et al.,* 1999]. Data from 121DK (Abouchami et al., 1999) and Madeira (Reynolds et al., 1999) (green circles), and the A-II 109, St. 95 ε_{Nd} profile (Piegras and Wasserburg, 1983) (yellow circle) from the NE Atlantic as well as crusts BM1969.05 and ALV539 (Burton et al., 1997, 1999; Reynolds et al., 1999) (dark green squares) from the NW Atlantic were also applied in our study (bathymetry from Gebco).

Belshaw et al., 1998) was applied. $^{143}Nd/^{144}Nd$ was normalized to $^{146}Nd/^{144}Nd = 0.7219$ for instrumental mass bias correction. Age corrected $\varepsilon_{Nd(T)}$ values were calculated using $^{147}Sm/^{144}Nd = 0.115$. Errors shown on the figures correspond to $2\sigma_{(SD)}$ external reproducibilities, obtained by repeated measurements of standard materials. All isotope ratios presented were normalized to standard values: JMC-Nd, with a $^{143}Nd/^{144}Nd$ ratio of 0.511833 cross-calibrated to the La Jolla standard (0.511858) was used. For the NIST SRM981 Pb standard the ratios used for external normalization are those given by Abouchami et al. (1999). For the Nd isotope measurements of different sessions, the 2σ external precision varied between 30 ppm and 33 ppm, whereas for Pb isotope

measurements the 2σ external precision was 116, 144, 172, 46, and 74 ppm for $^{206}Pb/^{204}Pb$, $^{207}Pb/^{204}Pb$, $^{208}Pb/^{204}Pb$, $^{207}Pb/^{206}Pb$, and $^{208}Pb/^{206}Pb$, respectively. In-run precision for each sample was better than the external reproducibility. The crusts were dated using $^{10}Be/^{9}Be$ profiling applying a 1.51 million year half life of ^{10}Be (Hofmann et al., 1987). The ^{10}Be data were measured at the AMS facility of ETH Zürich and Paul Scherrer Institute, Switzerland. The samples were measured applying a newly developed carrier-free method, in which the natural $^{10}Be/^{9}Be$ ratios were determined directly (Maden et al., 2004) (Table III.2.). The reduced accuracies of the older $^{10}Be/^{9}Be$ ratios were caused by the low ion currents extracted from the samples.

Table III.1. Locations and details of three crusts from Meteor cruise M51/1[a]

Sample	Name used in Text	Location	Latitude, ºN	Longitude, ºW	Water depth, m	Thickness,[b] mm	Growth Rates, mm/Ma	Base Age, Ma
417DR-6Mn	3514-6	Lion seamount, cone at SW margin	35º 12.7-13.0	15º 42.03-42.36	938-688	**23.5** 0-9.5 9.5-17 17-23.5	 1.37 2.45 1.25	15.2
410DR-1Mn	3511-1	Josephine seamount, S flank	36º 30.5-30.7	14º 12.48-13.04	2436-2161	**18** 0-10.5 10.5-18	 1.25 2.04	12.0
414DR-14Mn	3513-14	Madeira-Tore Rise, NW margin	36º 58.2	15º 44-90-44.80	4586-4603	**43** 0-5 5-43	 1.76 4.45	11.4

[a]The coordinates and depth ranges correspond to the "on" and "off" of the bottom data from each dredge station.
[b]The total thickness of the sample is given in bold; the depth intervals correspond to each depth interval with a different growth rate.

The samples were analyzed for bulk element chemistry by ICP-MS/AES at the National Oceanography Centre, Southampton, U.K. The chemical preparation of the samples included a first dissolution step in 6M HCl and a second dissolution step of the residue in hydrofluoric and perchloric acids, which were combined for the elemental analyses, of which only the Mn, Fe and Co concentrations are used in this study. Internal rock standards and blanks

were used to calibrate the data. X-ray diffraction analyses (for 3511-1 and 3514-6) were conducted on a Philips diffractometer, using Cu-Kα radiation and a carbon curved-crystal monochromator, at the United States Geological Survey. These analyses showed that the Fe-Mn oxyhydroxide fraction of the samples throughout consists of δMnO_2 (vernadite), the main mineral in crusts of hydrogenetic origin. The mineralogy, taken together with the Mn/Fe ratios (0.58 to 1.26) and the growth rates (see next section) confirm an entirely hydrogenetic origin and allows the crusts to be used as reliable archives of paleoceanographic events (Koschinsky et al., 1996**;** Hein et al., 2000).

III.3. Results

III.3.1. Dating

Growth rates obtained from the $^{10}Be/^{9}Be$ profiles vary between 1.3 and 4.5 mm/Ma (Figure III.2. and Tables III.1. and III.2.), which is in the range expected for hydrogenetic

Table III.2. The $^{10}Be/^{9}Be$ dating and growth rates

Depth, mm	Error, mm	$^{10}Be/^{9}Be \times 10^{-9}$	Absolute Error, $\times 10^{-9}$	Relative Error, %	Growth Rates, mm/ Ma	Ages, Ma	Error 2σ[a]	Linear Ages	Co, wt%
				3514-6					
0.00								0.00	0.585
0.50	0.50	26.96	1.97	7.30		0.48	±0.04	0.36	0.758
4.25	0.75	5.16	0.49	9.47	1.03	4.11	±0.39	3.10	0.565
9.50	1.00	1.33	0.28	20.96	1.77	7.08	±1.48	6.93	0.467
				3511-1					
0.00								0.00	0.565
3.00	0.50	20.86	2.27	10.90		2.78	±0.30	2.40	0.729
5.75	0.75	6.54	0.75	11.46	1.08	5.32	±0.61	4.60	1.026
10.25	0.75	1.78	0.31	17.26	1.58	8.17	±1.41	8.20	0.735
				3513-14					
0.00								0.00	0.760
5.00	0.50	13.71	1.05	7.65		1.05	±0.08	1.12	0.554
9.25	0.75	9.14	1.15	12.54	4.78	1.93	±0.24	2.08	0.268
18.50	0.50	4.20	0.39	9.32	5.42	3.64	±0.34	4.16	0.185
26.75	0.75	1.42	0.34	23.81	3.47	6.02	±1.43	6.01	0.142

[a]The σ values correspond to standard error of the mean (SEM).

ferromanganese crusts (e.g., Hein et al., 2000; Frank, 2002). Intermediate depth crust 3511-1 has an extrapolated surface $^{10}Be/^{9}Be$ ratio of ~$5x10^{-8}$, which corresponds to values expected for modern seawater precipitates in the eastern North Atlantic Ocean (von Blanckenburg et al., 1996b). The shallowest crust 3514-6 has a lower surface $^{10}Be/^{9}Be$ ratio of 2.7 x 10^{-8} and also deepest crust 3513-14 has a lower extrapolated surface $^{10}Be/^{9}Be$ ratio of 2.3 x 10^{-8}. The lower $^{10}Be/^{9}Be$ value in the shallowest crust is consistent with water column data from similar water depths in the northwestern Atlantic (Ku et al., 1990) and with admixture of waters from the Mediterranean (the location of the crust is presently bathed by MOW), which have very low $^{10}Be/^{9}Be$ ratios of ~1 x 10^{-8} (Brown et al., 1992). Alternatively, if the true actual surface $^{10}Be/^{9}Be$ ratio of all crusts were 5 x 10^{-8}, this would imply that a layer representing ~1.5 Ma of crust growth (~2 mm) is missing from the surface of shallowest crust 3514-6. Given that there are no macroscopically visible hints for erosion or dissolution at the surface of this crust, we consider this highly unlikely. For following interpretations we will therefore consider the $^{10}Be/^{9}Be$ ratio of 2.7x 10^{-8} as the correct surface value, but will briefly discuss the implications of a possibly missing surface layer in section 4.5. For deepest crust 3513-14 the low $^{10}Be/^{9}Be$ ratio may either imply that there is a thick layer representing 1.5 Ma of crust growth missing (~6.6 mm) or that the crust grew much more slowly at about 1.7 mm/Ma in the uppermost 5 mm, where we have no $^{10}Be/^{9}Be$ data. Such a lower growth rate is fully consistent with the growth rate variability derived from the Co constant flux method (Manheim, 1986; Frank et al., 1999a) which was consequently adopted for the applied age model in the upper 5 mm (Figure III.2.). The oldest part of the crusts 3514-6 and 3511-1 was not dated by $^{10}Be/^{9}Be$ but growth rates were determined by matching the Co constant flux method in each crust to $^{10}Be/^{9}Be$ in their respective younger part (Manheim, 1986; Frank et al., 1999a). The results of the Co method indicate that the average growth rates obtained from $^{10}Be/^{9}Be$ in the younger parts of crusts 3514-6 and 3511-1 were not significantly different from their older parts. The dating resulted in ages of 15.2 Ma, and 12.0 Ma for the bases of the crusts at 23.5 mm and 18 mm depth of crusts 3514-6 and 3511-1, respectively. For deep crust 3513-14, the Co-derived growth rate did not match the well-constrained $^{10}Be/^{9}Be$ growth rate, but indicates relatively constant growth below 5 mm, which is why the age model for this crust is only based on the extrapolated $^{10}Be/^{9}Be$ ratios below 5 mm depth.

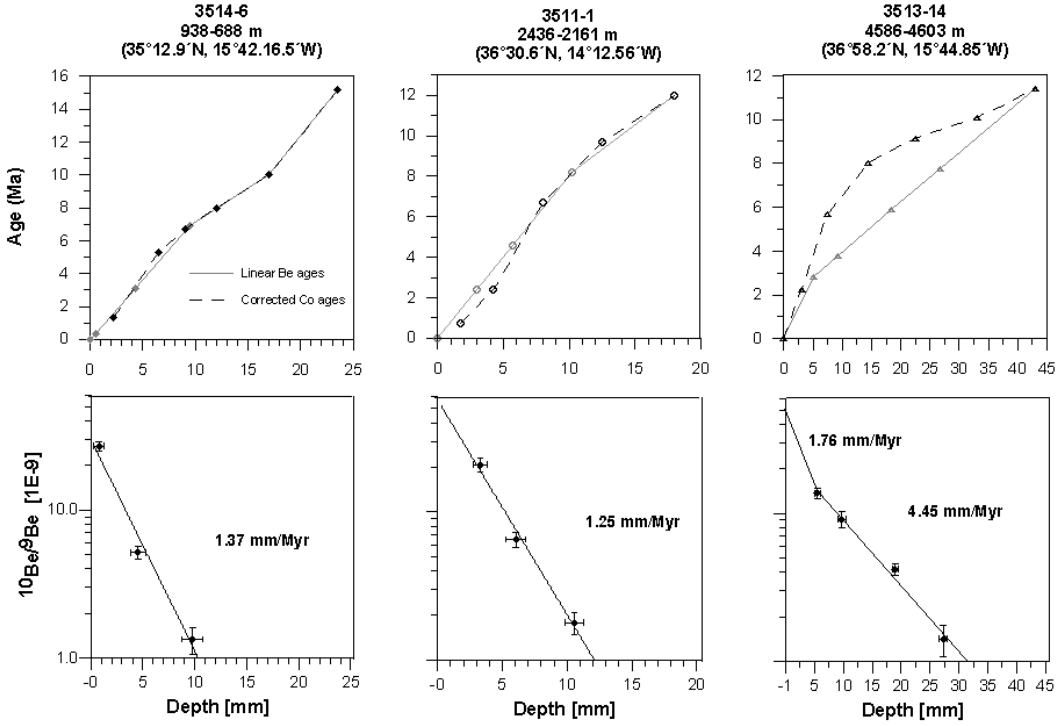

Figure III.2. Profiles of $^{10}Be/^{9}Be$ ratios for the three crusts studied versus depth. The ages of the applied age models given by the solid lines in the age versus depth plots were calculated with a half–life for ^{10}Be of 1.5 Ma. The growth rates and ages beyond the age range covered by $^{10}Be/^{9}Be$ data were determined using the Co constant flux method (Manheim, 1986; Frank et al., 1999a) and rectified to match the $^{10}Be/^{9}Be$-derived growth rate in the upper part of the two shallower crusts, respectively (dashed line).

III.3.2. Nd and Pb isotope time series

The three crusts display surface Pb and Nd isotope values ranging from 18.81 to 18.98 for $^{206}Pb/^{204}Pb$ and between –10.9 to –11.6 for ε_{Nd} (Table III.3., Figure III.3.). These values are in good agreement with values for other crust surfaces from the northeastern Atlantic (Abouchami et al., 1999; Reynolds et al., 1999; Claude-Ivanaj et al., 2001). Nevertheless, there are significant differences in the surface isotope ratios between the three crusts: Shallowest crust 3514-6, as well as crust 65GTV (Abouchami et al., 1999) from 1500 m water depth at essentially the same location (Figures III.1. and III.4.), show less radiogenic $^{206}Pb/^{204}Pb$ values (18.81 and 18.78, respectively) than the two deeper crusts (18.95 and 18.98). The time series of these four crusts are presented in Figure III.4. All four crusts recorded essentially constant Pb isotope ratios prior to 4 Ma, whereas crusts 3514-6 and 3511-1 show values around 18.8 and 65GTV and 3513-14 recorded values around 18.7.

Table III.3. Pb and Nd isotopic compositions of the crusts

Depth, mm	Mean Depth, mm	Age, Ma	$^{206}Pb/^{204}Pb$	$^{207}Pb/^{204}Pb$	$^{208}Pb/^{204}Pb$	$^{143}Nd/^{144}Nd$	$1\sigma^a$	$\varepsilon_{Nd(T)}$
				3514-6				
0 - 0,5	0,25	0,18	18,811	15,679	38,880	0,512077	± 3	-10,94
1 - 1,5	1,25	0,91	18,799	15,677	38,862	0,512091	± 3	-10,67
2 - 2,5	2,25	1,64	18,791	15,679	38,860	0,512104	± 3	-10,40
3 - 3,5	3,25	2,37	18,789	15,676	38,850	0,512113	± 3	-10,22
4 - 4,5	4,25	3,10	18,798	15,677	38,857	0,512119	± 2	-10,09
5 - 5,5	5,25	3,83	18,807	15,678	38,863	0,512119	± 3	-10,08
6 - 6,5	6,25	4,56	18,804	15,674	38,853	0,512123	± 3	-10,00
7 - 7,5	7,25	5,29	18,798	15,676	38,865	0,512117	± 3	-10,11
7 - 7,5	7,25	5,29				0,512137	± 5	-9,72
8 - 8,5	8,25	6,02	18,790	15,675	38,869	0,512125	± 3	-9,94
9 - 9,5	9,25	6,75	18,786	15,674	38,867	0,512134	± 2	-9,75
10 - 11	10,50	7,34	18,783	15,674	38,877	0,512134	± 3	-9,76
12 - 13	12,50	8,15	18,781	15,674	38,883	0,512134	± 2	-9,74
14 - 15	14,50	8,97	18,786	15,676	38,887	0,512146	± 2	-9,51
16 - 17	16,50	9,79	18,795	15,679	38,890	0,512157	± 3	-9,29
18 - 19	18,50	11,20	18,794	15,680	38,890	0,512159	± 3	-9,24
20 - 21	20,50	12,80	18,788	15,680	38,878	0,512182	± 4	-8,75
22 - 23	22,50	14,40	18,776	15,678	38,867	0,512160	± 3	-9,17
23 - 23,5	23,25	15,00	18,778	15,681	38,874	0,512171	± 3	-8,96
	23,00	15,20						
				3511-1				
0 - 0,5	0,25	0,20	18,956	15,686	39,040	0,512045	± 3	-11,56
1 - 1,5	1,25	1,00	18,915	15,682	39,004	0,512036	± 2	-11,73
2 - 2,5	2,25	1,80	18,873	15,680	38,953	0,512037	± 3	-11,71
3 - 3,5	3,25	2,60	18,836	15,680	38,907	0,512044	± 3	-11,55
4 - 4,5	4,25	3,40	18,811	15,678	38,868	0,512060	± 2	-11,24
5 - 5,5	5,25	4,20	18,803	15,679	38,854			
5 - 5,5	5,25	4,20	18,803	15,679	38,864	0,512071	± 2	-11,02
6 - 6,5	6,25	5,00	18,803	15,677	38,860	0,512078	± 3	-10,87
7 - 7,5	7,25	5,80	18,805	15,676	38,860	0,512089	± 3	-10,65
8 - 8,5	8,25	6,60	18,808	15,677	38,867	0,512093	± 2	-10,57
9 - 9,5	9,25	7,40	18,801	15,674	38,865	0,512109	± 3	-10,24
10 - 11	10,50	8,32	18,793	15,674	38,868	0,512102	± 3	-10,37
11 - 12	11,50	8,81	18,795	15,675	38,874	0,512103	± 2	-10,35
12 - 13	12,50	9,30	18,794	15,675	38,886	0,512107	± 3	-10,26
13 - 14	13,50	9,79	18,785	15,672	38,881	0,512114	± 3	-10,11
14 - 15	14,50	10,28	18,783	15,675	38,893	0,512120	± 3	-9,99
15 - 16	15,50	10,77	18,790	15,674	38,885	0,512142	± 3	-9,56
16 - 17	16,50	11,26	18,798	15,674	38,882	0,512152	± 3	-9,36
17 - 18	17,50	11,75	18,804	15,676	38,886	0,512193	± 3	-8,55
	18,00	12,00						

Table III.3. (continued)

Depth, mm	Mean Depth, mm	Age, Ma	$^{206}Pb/^{204}Pb$	$^{207}Pb/^{204}Pb$	$^{208}Pb/^{204}Pb$	$^{143}Nd/^{144}Nd$	1 σ^a	$\varepsilon_{Nd(T)}$
				3513-14				
0 - 0,5	0,25	0,14	18,982	15,689	39,090	0,512060	± 3	-11,27
1 - 1,5	1,25	0,71	18,937	15,690	39,048	0,512047	± 3	-11,53
2 - 2,5	2,25	1,28	18,886	15,685	38,970	0,512058	± 3	-11,31
3 - 3,5	3,25	1,85	18,856	15,682	38,926	0,512066	± 3	-11,16
4 - 4,5	4,25	2,41	18,845	15,681	38,916	0,512077	± 3	-10,94
5 - 5,5	5,25	2,94	18,845	15,683	38,923	0,512068	± 3	-11,11
6 - 6,5	6,25	3,16	18,836	15,678	38,903	0,512074	± 3	-10,99
7 - 7,5	7,25	3,39	18,836	15,681	38,910	0,512068	± 3	-11,11
8 - 8,5	8,25	3,61	18,834	15,680	38,902	0,512085	± 3	-10,77
9 - 9,5	9,25	3,84	18,809	15,679	38,909	0,512088	± 3	-10,71
10 - 11	10,50	4,12	18,807	15,678	38,898	0,512102	± 3	-10,43
12 - 13	12,50	4,57	18,798	15,679	38,869	0,512119	± 3	-10,09
14 - 15	14,50	5,02	18,771	15,672	38,836	0,512106	± 3	-10,34
16 - 17	16,50	5,47	18,750	15,672	38,829	0,512126	± 3	-9,95
18 - 19	18,50	5,92	18,732	15,670	38,814	0,512133	± 3	-9,81
20 - 21	20,50	6,37	18,739	15,667	38,806	0,512154	± 3	-9,40
22 - 23	22,50	6,81	18,734	15,669	38,811	0,512168	± 3	-9,12
24 - 25	24,50	7,26	18,730	15,672	38,809	0,512163	± 3	-9,21
26 - 27	26,50	7,71	18,722	15,668	38,795	0,512163	± 3	-9,20
28 - 29	28,50	8,16	18,727	15,671	38,808	0,512178	± 4	-8,90
30 - 31	30,50	8,61	18,719	15,669	38,799	0,512160	± 3	-9,27
32 - 33	32,50	9,06	18,720	15,670	38,805	0,512162	± 3	-9,22
34 - 35	34,50	9,51	18,714	15,668	38,797	0,512163	± 3	-9,20
36 - 37	36,50	9,96	18,699	15,668	38,791	0,512146	± 2	-9,52
38 - 39	38,50	10,41	18,702	15,667	38,794	0,512158	± 4	-9,29
40 - 41	40,50	10,86	18,707	15,669	38,803	0,512149	± 2	-9,47
42 - 43	42,50	11,31	18,715	15,669	38,811	0,512162	± 2	-9,22
	43,00	11,42						

[a]The σ values correspond to SEM.

After 4 Ma, the Pb isotope records of all crusts show a continuous increase in $^{206}Pb/^{204}Pb$ ratios similar to previously published records for other crusts from the eastern North Atlantic (Abouchami et al., 1999; Reynolds et al., 1999). The only exception is shallowest crust 3514-6, which stayed constant. There is a significant trend in the amplitude of change over the past ~4 Ma with water depth from essentially constant $^{206}Pb/^{204}Pb$ values at 700-900 m depth to a maximum change of 0.25 in the deepest crust (3513-14), which started to change already at ~6 Ma (Table III.4.). There is no indication that the striking constancy of the Pb isotope time series of the shallowest crust does not reflect a seawater signal. Potential substrate dissolution can be excluded because the Pb isotope composition of volcanic rocks from the same and nearby seamounts is very different from that of seawater

recorded by the crust (Geldmacher et al., 2006). In particular, the $^{207}Pb/^{204}Pb$ ratios (~15.50 to ~15.60) of the basaltic rocks are much lower than those of seawater derived from our samples, as well as from other hydrogenetic crusts in the area.

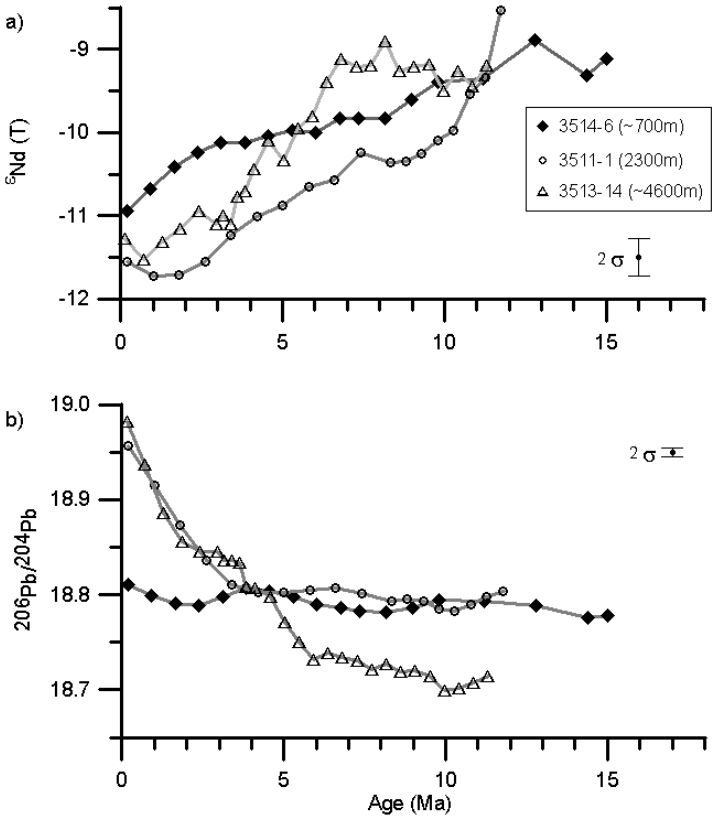

Figure III.3. Time series of a) $\varepsilon_{Nd\ (T)}$ and b) $^{206}Pb/^{204}Pb$ versus age for the three crusts studied. All error bars represent $2\sigma_{(SD)}$ external reproducibilities of repeated standard measurements.

The amplitudes and the timing of changes in the Nd isotope time series show significant differences among the crusts although, in contrast to the Pb isotopes, there is no clear trend in the amplitude of the changes with water depth. The shallowest crust shows a continuous overall decrease of 2 ε_{Nd} units between 15 Ma and the present. The decrease from 4 Ma to the present amounted to ~0.8 ε_{Nd} units. The intermediate depth crust also shows a continuous trend between 12 Ma ago and the present, but the amplitude was higher (~3 ε_{Nd} units) and there was no significant decrease over the past 4 Ma. The deepest crust shows

constant values between 11 and ~6 Ma followed by a decrease in ε_{Nd} from -9.5 to –11.5. This is the steepest gradient over the last ~4 Ma found in the records of our crusts, which resembles the pattern in the western North Atlantic.

III.4. Discussion

III.4.1. Present day situation

The crust surface ε_{Nd} values are -10.9, -11.6 and -11.3 for crusts 3514-6, 3511-1, and 3513-14, respectively. Despite the fact that the surface data integrate over several 100 kyr for each sample, the values are comparable to present-day water column data obtained at nearby locations (Piegras and Wasserburg, 1983; Spivack and Wasserburg, 1988; Tachikawa et al., 2004). Shallowest crust 3514-6 lies within the upper core of MOW and shows a Nd isotope signature (ε_{Nd} = -10.9) that agrees well with values for the corresponding water depth (ε_{Nd} = -10.6) of nearby water profile A-II 109, St. 95 (Piegras and Wasserburg, 1983) (Figures III.1. and III.5.). In the water profile A-II 109, St. 95 the ε_{Nd} signature in the core of MOW, at 1000 m water depth, is -9.8, reflecting the presence of a large fraction of MOW at this location.

The surfaces of the intermediate depth crust 3511-1 (corresponding to NEADW) and the deepest crust 3513-14 (NEADW, possibly recording minor AABW influence) show more negative ε_{Nd} values which are similar to the water-column data reported for the corresponding water depths at A-II 109, St. 95 (-12.2 and -11.8, respectively) as well as for samples from a study further south in the eastern North Atlantic (Tachikawa et al., 1999). The data of the intermediate depth crust are also in good agreement with values published for other crusts in the NE Atlantic: Crust 121DK (2000 m water depth) shows a ε_{Nd} surface value of -11.84, whereas the surface of crust 65GTV (1500 m water depth) shows a higher ε_{Nd} value of -10.2, in agreement with its proximity to the lower core of MOW (Abouchami et al., 1999). Data for the deepest crust agree with values for the surface of crust Madeira (~5100 m water depth) with an ε_{Nd} = -11.1 (Reynolds et al., 1999).

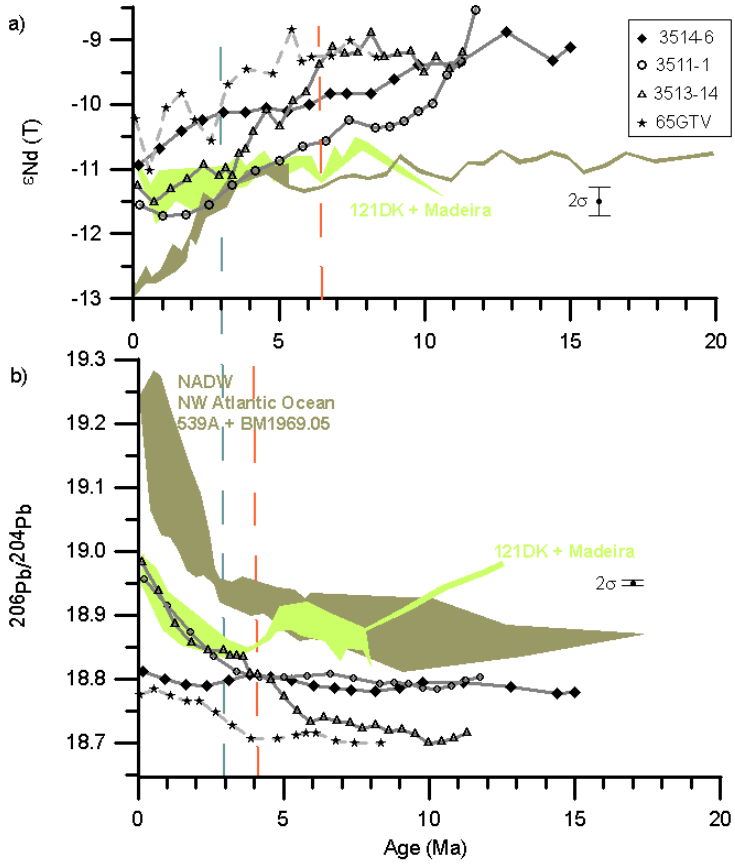

Figure III.4. Comparison of (a) Nd and (b) $^{206}Pb/^{204}Pb$ time series for our three crusts with other crusts from the northeastern and northwestern Atlantic: The data for 65GTV (Abouchami et al., 1999) are plotted as solid stars with dashed line. The data for 121DK (Abouchami et al., 1999) and Madeira (Reynolds et al., 1999) are plotted as a light green field. The data from the northwestern Atlantic, crusts BM1969.05 (39°N; 61°W) and ALV 539 (35°N; 59°W) (Burton et al., 1997, 1999; Reynolds et al., 1999) are plotted as a dark green field. Dashed vertical lines mark the major changes in patterns for the northeastern Atlantic (red) and northwestern Atlantic (blue).

Preanthropogenic Pb isotopic data cannot be extracted from modern seawater. We therefore compare our $^{206}Pb/^{204}Pb$ surface values with surface data of other northeastern Atlantic crusts. Our shallowest crust (upper MOW core) shows a $^{206}Pb/^{204}Pb$ value of 18.81, comparable with the 18.78 value of crust 65GTV (lower MOW core), which are the least radiogenic crusts (Abouchami et al., 1999). The intermediate and deepest crusts show more radiogenic $^{206}Pb/^{204}Pb$ isotopic values of 18.96 and 18.98, respectively, which are comparable with values for crusts 121DK and Madeira (18.95 and 18.99, respectively) from similar water depths (Abouchami et al., 1999; Reynolds et al., 1999; Claude-Ivanaj et al., 2001).

Table III.4. Overall variations of Nd and Pb from ~4 Ma toward the Present[a]

Sample	Water Depth, m	Location	Δ Nd	Overall change ε_{Nd} units	Δ Pb
3514-6	688-938	Lion seamount	0.8	2.0	0.02
65GTV[b]	1500	Lion seamount	1.3	2.0	0.07
121DK[b]	2000	Tropic seamount	0.8	0.8	0.11
3511-1	2161-2436	Josephine seamount	0.6	3.0	0.15
3513-14	4586-4603	Madeira-Tore Rise	2.0	2.5	0.25
Madeira[c]	5347-4867	Madeira Abyssal Plain	0.3	0.0	0.15

[a] ΔNd and ΔPb correspond to the calculated variation of Nd and Pb values from the age that the sample start to vary towards the present. For all crusts the starting age of the major variation is ~4 Ma, whereas deepest crust 3513-14 the start is at ~6 Ma. The overall change in ε_{Nd} values corresponds to the total variation through the profile.
[b] Abouchami et al. (1999).
[c] Reynolds et al. (1999).

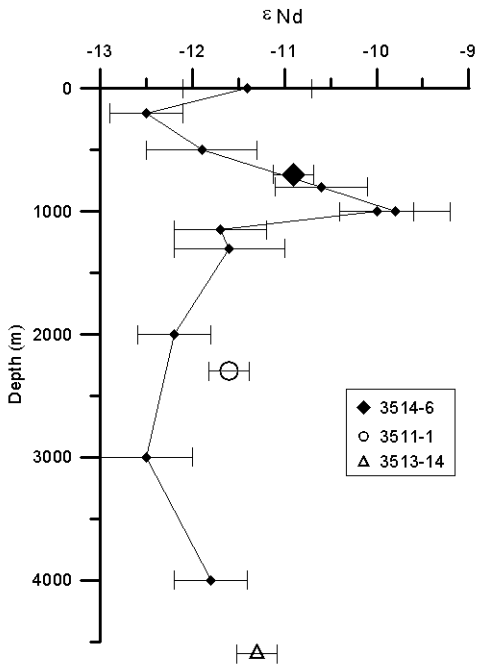

Figure III.5. Plot of $\varepsilon_{Nd(0)}$ as a function of depth at station A-II, 109 St. 95 (Piegras and Wasserburg, 1983), compared with the ε_{Nd} of the surfaces of our three crusts (3514-6, 3511-1 and 3513-14).

III.4.2. Mid-Miocene to Present water mass evolution

Previous studies have investigated Pb and Nd isotope time series in ferromanganese crusts from the western and eastern North Atlantic (Burton et al., 1997, 1999; O'Nions et al., 1998; Abouchami et al., 1999; Reynolds et al., 1999; Claude-Ivanaj et al., 2001, Frank et al., 2003). Western North Atlantic records show a consistent evolution of Nd and Pb isotope time series for NADW or a precursor of it over the past 3 Ma, although apparent differences in the timing of change have been observed (Burton et al., 1999). Eastern North Atlantic data show similar patterns in Pb and Nd isotope records but different absolute values, as well as timing and amplitudes of change. The Pb isotope changes in the deep northeastern Atlantic occurred about 1 Ma earlier than in the western basin and are shifted by about 0.3 in $^{206}Pb/^{204}Pb$ towards less radiogenic ratios. There is a common decreasing trend in all the Nd isotope time series that resembles records from the western North Atlantic over the past 3 Ma (Burton et al., 1997; 1999; O'Nions et al., 1998). However our new deep-water Nd isotope record shows an early decrease in ε_{Nd} (~6 Ma) that is of similar amplitude as western North Atlantic records from 3 Ma to the present, but is ~1.5 ε_{Nd} units more radiogenic. The marked changes observed in the Pb and Nd compositions of western NADW and NEADW were interpreted as a consequence of changes of style and intensity of continental weathering in northern Canada and Greenland or alternatively as a change in the signatures and contributions of water masses mixing to produce NADW since the onset of NHG 2.7 Ma ago (Burton et al., 1997, 1999; O'Nions et al., 1998; Reynolds et al., 1999; Foster and Vance, 2006). Increased mechanical weathering was invoked as the cause of increased erosional input of old cratonic material with low ε_{Nd}, which may have led to the decrease of ε_{Nd} in North Atlantic deep waters over the past 3 Ma (O'Nions et al., 1998). Alternatively, the contribution of LSW with its very unradiogenic Nd isotope composition may have increased over the past 3 Ma (Burton et al., 1999). Enhanced release of loosely bound radiogenic Pb from old cratonic rocks (incongruent weathering), rapidly eroded under glacial conditions, has been inferred to be the cause for the drastic increase in $^{206,207,208}Pb/^{204}Pb$ over the past 3-2 Ma (von Blanckenburg and Nägler, 2001; Foster and Vance, 2006). Despite the fact that the time series patterns of the eastern North Atlantic crusts generally resemble those of the western basin, it appears that the eastern North Atlantic led the major changes in Nd and Pb isotope compositions in three crusts from water depths between 1500 and 4600 m by about 1-3 Ma, which cannot be the result of dating

uncertainties. This difference in timing can not be explained by changes in weathering in northern Canada and Greenland associated with the onset of NHG but must rather have been associated with paleoceanographic changes that occurred prior to and during the early phase of the onset of NHG. These changes may for example have been related to the closure of the Isthmus of Panama. It has been reported that the gradual closure of the Isthmus of Panama had a major impact on intermediate and deep water circulation and an intensification of NADW export at ~4.6 Ma (Driscoll and Haug, 1998; Frank et al., 1999b; Reynolds et al., 1999). The early change in the eastern North Atlantic may thus have been caused by a diminished influence of LDW as suggested by Abouchami et al. (1999). There is, however, no clearly detectable shift towards less radiogenic Nd isotope and more radiogenic Pb isotope composition at 4 Ma in the records from the Romanche and Vema Fracture zones, the ultimate pathway of southern sourced water masses in the eastern North Atlantic Basin (Frank et al., 2003). More likely, therefore, the similarity of the overall patterns and the differences in amplitudes observed for Pb and Nd isotopes between the western and eastern basins over the past 4 Ma indicate an influence from efficient deep water-mass exchange between the two basins *via* a northern route, such as the Charlie-Gibbs Fracture Zone (CGFZ) (Sy et al., 1997; Paillet et al., 1998; Bower et al., 2002). In the more distant past (prior to ~2 Ma), the CGFZ could have dominated the exchange between the two basins. This may have enabled a pronounced early and direct transfer of the extremely unradiogenic Nd and radiogenic Pb isotope signature of LSW into the northeastern Atlantic basin prior to the change in the isotopic composition of NADW. This is supported by model calculations (Sy et al., 1997) which show that spreading of LSW under winter forcing conditions can occur at a more southerly location, leading to a more efficient export of this water mass to the eastern basin *via* northern fracture zones such as the CGFZ. Schott et al. (1999) reported the existence of phases of strong deep eastward flow through the CGFZ under present-day conditions. These authors conclude that the North Atlantic Current (NAC, which is a warm surface current transporting Gulf Stream waters to the eastern North Atlantic), also plays a crucial role for the pathways of deep water supply out of the eastern North Atlantic. According to their observations, if the NAC follows a more northerly route for an extended period of time, then the flow through the CGFZ can be pushed backwards, thus changing the composition of the northern deep circulation system. Moreover, Boessenkool et al. (2007) pointed out that convective change in the Labrador Sea may be more important in the

production of NADW than Greenland-Scotland Ridge (GSR) overflows, as the volume transport of the GSR overflows weakens when LSW formation intensifies. A scenario like this may explain the earlier and pronounced LSW influence we observe in the eastern basin records. It is interesting to note in this context that Wright and Miller (1996) suggested a correlation between the uplift of the GSR and reduced export of Northern Component Water (which is the precursor of NADW) also pointing towards a potentially more LSW dominated Northern Component Water in the past. Thomas and Via (2007) recently suggested that a rapid decrease in the Nd isotope signal in the Walvis Ridge of the southeastern Atlantic between 10.6 and 7.3 Ma, may have been caused by deep convection in the Labrador Sea and a corresponding change in the Nd isotope composition of NADW. Such a very early change is not observed in other equatorial and Southern Atlantic records but our shallow and intermediate records clearly also show a decrease in the Nd isotope signal since ~12 Ma (Figure III.4a.) that may already have been related to increased contributions from the Labrador Sea.

There is a clear similarity in the Pb and Nd pattern between the two shallowest records from the northeastern Atlantic, crusts 3514-6 and 65GTV, in that they show less radiogenic $^{206}Pb/^{204}Pb$ ratios and more radiogenic ε_{Nd} values than the other crusts from the northeastern Atlantic over the past 3 Ma (Figure III.4.). The continuous increase in $^{206}Pb/^{204}Pb$ from 4 Ma to present has the largest amplitude in the deeper crusts, which appears to have been controlled by an increasing direct influence of LSW on the Pb isotope signature at depth. The change in Pb isotopes in the deepest crust even appears to have started as early as 6 Ma. In contrast, the Nd isotopes show no systematic change with water depth. This may be due to the shorter residence time of Pb compared with Nd, which is more efficiently mixed in the ocean. More importantly, the original Pb isotope end-member signature of LSW has probably been even more extreme than that of the Nd isotopes, which is why such a strong and clearly resolvable LSW signal is observed at depth. Small differences in Pb isotope composition between the crusts prior to 4 Ma probably originated from local input sources. In general, however, the deep water Pb isotope signature in the eastern North Atlantic Basin seems to have been dominated by water mass mixing, consistent with the general assumption that the adsorption of Pb onto particles is not reversible (Henderson and Maier-Reimer, 2002 and references therein), which means that there has been no significant release of surface water Pb or dust-derived Pb to deep waters.

III.4.3 Influence of MOW and the Messinian Salinity Crisis

The Pb isotope time series of the shallowest crust 3514-6 is markedly different from all other time series in the North Atlantic and thus requires additional discussion. The relatively unradiogenic Pb isotope composition of this crust and crust 65GTV from 1500 m water depth is in agreement with the expected signal of MOW based on the geology of the continental landmasses surrounding the Mediterranean (Abouchami et al., 1999). The shallowest crust is located within the upper core of the MOW around 800 m depth (Ambar et al., 1999, 2002) and the long-term stability of the signal indicates a continuous presence of MOW at this location and water depth, integrated over glacial/interglacial time scales, over the past 15 Ma. There is no indication of any significant growth hiatus during the MSC (Figure III.2.), which would, however, also be difficult to detect in view of the coarse resolution of the $^{10}Be/^{9}Be$ data. This apparently contrasts the missing record of the MSC between 6 and 5.3 Ma (Krijsgsman et al., 1999), when the Atlantic-Mediterranean exchange was reduced in comparison to the present day (Flecker and Ellam, 2006). The continuous and invariable Pb isotope record may indicate that the Pb isotopes were controlled by advection of MOW combined with local external inputs, such as partial dissolution of detrital particles from the nearby continents (e.g., Saharan dust) (Abouchami et al., 1999; Tachikawa et al., 1999). In addition, there may be no indication of the MSC because MOW formed at least episodically and the corresponding isotopic signal reached the depth and location of crust 3514-6 during these short episodes. In fact, Flecker et al. (2002) and Flecker and Ellam (2006) argued that even during the deposition of the Upper Evaporite sequence in the Mediterranean, the outflow into the Atlantic was reduced but was not completely or continuously stopped. In support of this, Flecker et al. (2002) suggested that a complete isolation over the MSC is inconsistent with observed Sr isotopic offsets from coeval open-marine values and the high salinities required for evaporite precipitation. In order to explain the evaporite deposition during the MSC, Flecker and Ellam (2006) proposed an alternative hypothesis to the desiccation or connected-basin hypothesis which states that evaporite deposition was triggered by one, or potentially several, Atlantic transgressions that increased the mass of salt in the Mediterranean. In view of these results, it appears most likely that MOW formed episodically and that therefore the Pb and Nd isotope signatures, which integrate over several 100 kyr, did not record short term changes caused by the MSC. It is stressed here that the Pb isotopes recorded the continuous MOW signature

(combined with some external contributions most likely from dust) due to the short residence time of Pb at this location proximal to the Strait of Gibraltar, whereas the Nd isotope record was overprinted by mixing with other North Atlantic water masses due its longer residence time.

III.4.4. Pliocene-Pleistocene evolution of water masses from Pb isotopes

In order to identify the changes in the sources of Pb contributing to seawater Pb isotope compositions over the past 5 Ma, time slice reconstructions of the four crusts in the eastern North Atlantic, which essentially only differ in water depth, were carried out (Figure III.6.). The time slice plots show that the Pb isotope ratios of all crusts can essentially be explained by a mixture between two water masses, the proportions of which changed over time (circa 5 Ma, circa 4 Ma, circa 3 Ma, circa 1.5 Ma, and present). The unradiogenic end-member has been MOW for the two shallow locations, whereas the radiogenic end-member most likely has been NEADW (including LDW and a LSW component). In addition, an external source, most likely dust, must have contributed to the Pb isotope signatures. For the present-day situation, the Pb in crust 65GTV is the least radiogenic. It is emphasized here that the MOW field represents an already modified isotope composition which is based only on the data for crust 65GTV from 1500 m water depth (Abouchami et al., 1999). It is most likely that unmodified MOW is even less radiogenic (Figure III.6.).

Data for the interval 5 to 3 Ma indicate a dominance of the unradiogenic end-member, which then shift towards the radiogenic end-member, most pronouncedly for the present day. At around 1.5 Ma, a composition intermediate between the two end-members was reached, but was accompanied by a change in slope (see particularly Figure III.6b.). Despite the overall similarity of the data, this indicates a change in the contributing end-members. Aridity increased in the Saharan region since ~4 Ma (Rea, 1994) caused by repeated cooling during the Pliocene-Pleistocene. A change in the source area of the Sahara from which dust was derived may have changed the mixing proportions of Pb at 1.5 Ma. Partial dissolution of dust may also have contributed to the markedly constant Pb isotope composition of the shallowest crust. In support of this, the data for the shallowest crust plot on the 1.5 Ma time-slice line for the entire period between 5 Ma and the present. As the Pb residence time in the surface waters is very short, and because adsorption of Pb onto particles is in general not

reversible (Henderson and Maier-Reimer, 2002), the Pb isotope signature of the upper part of MOW, as recorded by the shallowest crust, must have been strongly influenced by dust inputs. In contrast the deep water Pb isotope composition was mainly controlled by ocean circulation and water mass mixing.

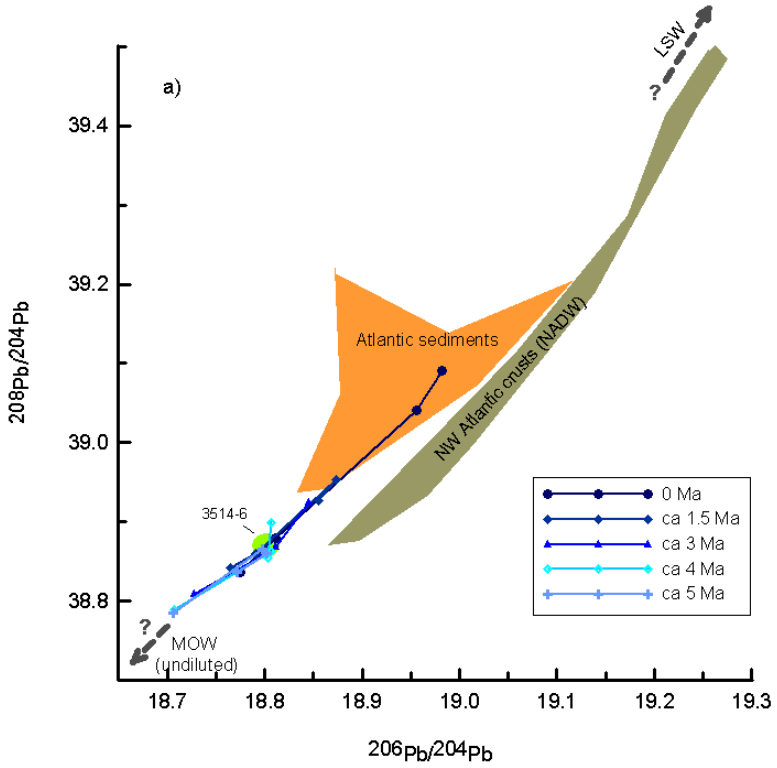

Figure III.6. Time slice connections (surface, 1.5, 3, 4, and 5 Ma) from the northeastern Atlantic crusts (65GTV, 3514-6, 3511-1, and 3513-14) in (a) $^{208}Pb/^{204}Pb$ versus $^{206}Pb/^{204}Pb$ and (b) $^{207}Pb/^{204}Pb$ versus $^{206}Pb/^{204}Pb$ space. The lines mark connections between the data of particular time slices (the legend in the graphics displays each time slice color). The green ellipse displays the field of crust 3514-6; it shows a nearly constant Pb isotope signature. The symbols and fields for the potential sources influencing the study area are: i) NW Atlantic crusts data (dark green field) defined by data from BM1969.05 and ALV539 (Burton et al., 1997, 1999; Reynolds et al., 1999) for the time range 0-5 Ma; ii) data from Atlantic sediments, interpreted as Saharan dust (orange field) is given by Sun (1980); iii) Saharan dust data (open grey diamond) is given by B. Hamelin (personal communication, 2003); The dashed dark grey lines indicate the possible endmember compositions of unmodified MOW (unradiogenic) and LSW (radiogenic) end-members.

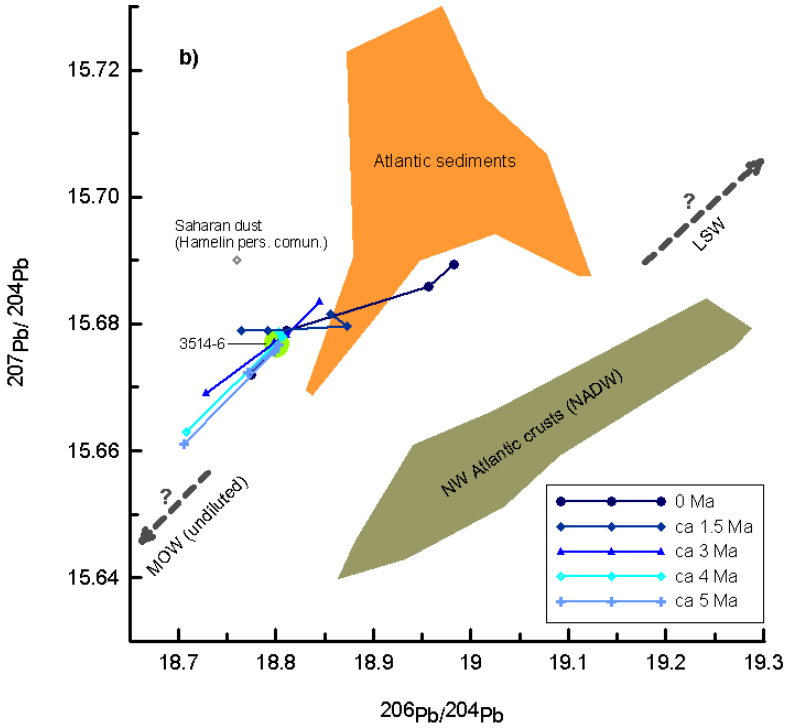

Figure III.6. (continued).

III.4.5. Alternative age model and implications for the shallow crust record

As mentioned in Section III.3.1., there is a possibility arising from its low surface $^{10}Be/^{9}Be$ ratio that the uppermost 2 mm of shallowest crust 3514-6, corresponding to ~1.5 Ma of growth, are missing due to erosion or dissolution. This would mean that this crust does have a relatively radiogenic ε_{Nd} value at the surface, previously interpreted as MOW influence. It would also imply that the decrease of the Nd isotopes at shallow depths started even 1.5 Ma earlier. In the case of Pb isotopes the record would still be very similar to the intermediate crust record prior to 4 Ma and remain constant until 1.5 Ma. Although such an erosional event cannot be completely excluded, the macroscopic evidence and the expected lower $^{10}Be/^{9}Be$ ratio at this water depth clearly argue against it. In addition, the Nd isotope signature of the surface of the crust agrees very well with values for the corresponding water depth of the water profile A-II 109, St. 95 (Piegras and Wasserburg, 1983) (Figure III.5.), which is why we consider the surface of this crust to be the true growth surface. However, even if there was an erosion or dissolution event, the overall interpretations of the Pb and Nd isotope ratios presented in sections III.4.1.- III.4.4. would not significantly change.

III.5. Conclusions

We present new time series of the Pb and Nd isotope evolution of water masses at different depths from the eastern North Atlantic of the past 15 Ma. The similarity between the Pb and Nd time series patterns from the northeastern and northwestern Atlantic over the past 4 Ma shows that there has been efficient mixing between the two basins. This and the fact that the northeastern Atlantic shows a major change in the trends 1-3 Ma earlier, reinforces the idea of an efficient export of LSW to the eastern Atlantic *via* a northern route such as across the CGFZ rather than through the equatorial fractures zones (Abouchami et al., 1999; Frank et al., 2003). A continuous decreasing trend in the Nd isotope composition at shallow and intermediate depths may indicate that waters from the Labrador Sea started to influence the eastern North Atlantic basin as early as at 12 Ma.

The evolution of water-mass mixing, from ~5 Ma to the present, as reconstructed from Pb isotopes, can be explained by a mixture between two principal end-members: an unradiogenic MOW end-member and a radiogenic NEADW end-member. It is likely that a local external input has influenced the Pb isotope evolution of the MOW. This is indicated by the invariant Pb isotope composition of the shallowest crust, located within the modern MOW, which is intermediate between the inferred undiluted MOW and NEADW end-members. This is probably due to the release of Pb from Saharan dust resulting from higher dust fluxes as a consequence of enhanced aridity. This crust has recorded an essentially constant MOW signal, despite the fact that the MSC occurred. This indicates that MOW was at least released episodically during that time and that the cessations of MOW were too short to be resolved in the ferromanganese crust record.

The enhanced $^{206}Pb/^{204}Pb$ gradient with water depth over the past ~4 Ma (Table III.4.) that we observe in our time series can best be explained by a stronger influence of LSW-derived Pb in the deeper crusts indicating that the Pb isotope composition of LSW must have been extremely radiogenic. Thus, the Pb isotope compositions of the shallower water masses have been controlled by a combination of local water mass mixing and external sources, such as dust, whereas those of the deeper water masses were mainly controlled by ocean circulation and water mass mixing.

Acknowledgments

We thank the Portuguese Science and Technology Foundation (FCT) for financial support of the projects INGMAR and PDCT/MAR/56823/2004. S.B.M. was supported by grant INGMAR-BICGEOQ1 and now grant SFRH/BD/22263/2005, both from FCT. We would also like to thank GRICES (Portugal) and DAAD (Germany) for traveling support. The $^{10}Be/^{9}Be$ ratios were measured at the Zurich AMS Facility jointly operated by the Swiss Federal Institute of Technology, Zurich and Paul Scherrer Institute, Villigen, Switzerland. The crew and scientific party of Meteor M51/1 cruise are also thanked as well as the Deutsche Forschungsgemeinschaft (DFG, German Research Council) for funding and Socfac program (National Oceanography Center, Southampton, U.K.) for ICP-MS/AES analyses. We also thank J. Fischer and L. Stramma for discussions and Mário Mil-Homens for help with the graphics. The editor Vincent Salters, as well as Ben Reynolds and one anonymous reviewer are thanked for their contribution to the improvement of the quality of this paper.

References

Abouchami, W., and S.L. Goldstein (1995), A lead isotopic study of Circum-Antarctic manganese nodules, *Geochimica et Cosmochimica Acta*, *59* (9), 1809-1820.

Abouchami, W., S.J.G. Galer, and A. Koschinsky (1999), Pb and Nd isotopes in NE Atantic Fe-Mn crusts: proxies for metal paleosources and paleocean circulation, *Geochimica et Cosmochimica Acta*, *63* (10), 1489-1505.

Ambar, I., and M.R. Howe (1979), Observations of the Mediterranean outflow-I Mixing in the Mediterranean Outflow, *Deep-Sea Research I*, *26A*, 535-554.

Ambar, I., L. Armi, A. Bower, and T. Ferreira (1999), Some aspects of time variability of the Mediterranean Water off south Portugal, *Deep-Sea Research I*, *46*, 1109-1136.

Ambar, I., N. Serra, M.J. Brogueira, G. Cabeçadas, F. Abrantes, P. Freitas, C. Gonçalves, and N. Gonzalez (2002), Physical, chemical and sedimentological aspects of the Mediterranean outflow off Iberia, *Deep-Sea Research II*, *49*, 4163-4177.

Bartoli, G., M. Sarnthein, M. Weinelt, H. Erlenkeuser, D. Garbe-Schonberg, and D.W. Lea (2005), Final closure of Panama and the onset of northern hemisphere glaciation, *Earth and Planetary Science Letters*, *237*, 33-44.

Belshaw, N.S., P.A. Freedman, R.K. O'Nions, M. Frank, and Y. Guo (1998), A new variable dispersion double-focusing plasma mass spectrometer with performance illustrated for Pb isotopes, *International Journal of Mass Spectrometry*, *181* (1-3), 51-58.

Bertram, C.J., and H. Elderfield (1993), The geochemical balance of the rare earth elements and neodymium isotopes in the oceans, *Geochimica et Cosmochimica Acta*, *57*, 1957-1986.

Boessenkool, K.P., I.R. Hall, H. Elderfield, and I. Yashayaev (2007), North Atlantic climate and deep-ocean flow speed changes during rhe last 230 years, *Geophysical Research Letters*, *34*, L13614, doi:10.1029/2007GL030285.

Bower, A.S., B.L. Cann, T. Rossby, W. Zenk, J. Gould, K. Speer, P.L. Richardson, M.D. Prater, and H.-M. Zhang (2002), Directly measured mid-depth circulation in the northeastern North Atlantic Ocean, *Nature*, *419*, 603-607.

Broecker, W.S., C. Rooth, and T.-H. Peng (1985), Ventilation of the Deep Northeastern Atlantic, *Journal of Geophysical Research*, *90*, 6940-6944.

Brown, E.T., C.I. Measures, J.M. Edmond, D.L. Bourlès, G.M. Raisbeck, and F. Yiou (1992), Continental inputs of beryllium to the oceans, *Earth and Planetary Science Letters*, *114*, 101-111.

Burton, K.W., H.-F. Ling, and R.K. O'Nions (1997), Closure of the Central American Isthmus and its effect on deep-water formation in the North Atlantic, *Nature*, *386*, 382-385.

Burton, K.W., D.-C. Lee, J.N. Christensen, A.N. Halliday, and J.R. Hein (1999), Actual timing of neodymium isotopic variations recorded by Fe-Mn crusts in the western North Atlantic, *Earth and Planetary Science Letters*, *171*, 149-156.

Claude-Ivanaj, C., A.W. Hofmann, I. Vlastélic, and A. Koschinsky (2001), Recording changes in ENADW composition over the last 340 ka using high precision lead isotopes in a Fe-Mn crust, *Earth and Planetary Science Letters, 188*, 73-89.

Cohen, A.S., R.K. O'Nions, R. Siegenthaler, and W.L. Griffin (1988), Chronology of the pressure-temperature history recorded by a granulite terrain, *Contrib. Mineral. Petrol.*, *98*, 303-311.

Davies, R., J. Cartwright, J. Pike, and C. Line (2001), Early Oligocene initiation of North Atlantic Deep Water formation, *Nature*, *410*, 917-920.

Driscoll, N.W., and G.H. Haug (1998), A short circuit in thermohaline circulation: A cause for Northern Hemisphere Glaciation, *Science*, *282* (5388), 436-438.

Flecker, R., S.d. Villiers, and R.M. Ellam (2002), Modelling the effect of evaporation on the salinity-$^{87}Sr/^{86}Sr$ relationship in modern and ancient marginal-marine systems: The Mediterranean Messinian Salinity Crisis, *Earth and Planetary Science Letters*, *203*, 221-233.

Flecker, R., and R.M. Ellam (2006), Identifying Late Miocene episodes of connection and isolation in the Mediterranean-Paratethyan realm using Sr isotopes, *Sedimentary Geology*, *188-189*, 189-203.

Foster, G.L., and D. Vance (2006), Negligible glacial-interglacial variation in continental chemical weathering rates, *Nature, 444*, 918-921.

Frank, M., R.K. O'Nions, J.R. Hein, and V.K. Banakar (1999a), 60 Myr records of major elements and Pb-Nd isotopes from hydrogenous ferromanganese crusts: Reconstruction of seawater paleochemistry, *Geochimica et Cosmochimica Acta*, *63*, 1689-1708.

Frank, M., B.C. Reynolds, and R.K. O'Nions (1999b), Nd and Pb isotopes in Atlantic and Pacific water masses before and after the closure of the Panama gateway, *Geology*, *27*, 1147-1150.

Frank, M. (2002), Radiogenic isotopes:tracers of past ocean circulation and erosional input, *Reviews of Geophysics*, *40*, 1001, doi:10.1029/2000RG00094.

Frank, M., N. Whiteley, S. Kasten, J.R. Hein, and R.K. O'Nions (2002), North Atlantic Deep Water export to the Southern Ocean over the past 14 Myr: Evidence from Nd and Pb isotopes in ferromanganese crusts, *Paleoceanography, 17*, 1022, 10.1029/2000PA000606.

Frank, M., T.v.d. Flierdt, A.N. Halliday, P.W. Kubik, B. Hattendorf, and D. Gunther (2003), Evolution of deepwater mixing and weathering inputs in the central Atlantic Ocean over the past 33 Myr, *Paleoceanography*, *18*, 1091, doi:10.1029/2003PA000919.

Galer, S.J.G., and R.K. O'Nions (1989), Chemical and isotopic studies of ultramafic inclusions from the San Carlos volcanic field, Arizona: a bearing on their petrogenesis, *J. Petrol.*, *30*, 1033-1064.

Geldmacher, J., K. Hoernle, A. Klugel, P.v.d. Bogaard, F. Wombacher, and B. Berning (2006), Origin and geochemical evolution of the Madeira-Tore Rise (eastern North Atlantic), *Journal of Geophysical Research*, *111*, B09206, doi:10.1029/2005JB003931.

Grousset, F.E., P.E. Biscaye, A. Zindler, J. Prospero, and R. Chester (1988), Neodymium isotopes as tracers in marine sediments and aerosols: North Atlantic, *Earth and Planetary Science Letters*, *87*, 367-378.

Hein, J.R., A. Koschinsky, M. Bau, F.T. Manheim, J.-K. Kang, and L. Roberts (2000), Cobalt-rich ferromanganese crusts in the Pacific, in *Handbook of Marine Mineral Deposits*, edited by D.S. Cronan, pp. 239-279, CRC Press, Boca Raton, Florida.

Henderson, G. and E. Maier-Reimer (2002), Advection and removal of ^{210}Pb and stable Pb isotopes in the oceans: A general circulation model study, *Geochim. Cosmochim. Acta, 66*, 257-272.

Hoernle, K., and S. Party (2003), Cruise Report M51/1, in *Ostatlantik - Mittelmeer - Schwarzes Meer, Cruise No. 51 - 28 December 2001.*, edited by C. Hemleben, K. Hoernle, B.B. Jorgensen, and W. Roether, pp. 3-35, Hamburg.

Hofmann, H.J., J. Beer, G. Bonani, H.R.v. Gunten, S. Raman, M. Suter, R.L. Walker, W. Wölfli, and D. Zimmermann (1987), ^{10}Be: half-life and AMS-standards, *Nuclear Instruments and Methods in Physics Research B*, *29*, 32-36.

Jeandel, C. (1993), Concentration and isotopic composition of Nd in the Southern Atlantic Ocean, *Earth and Planetary Science Letters*, *117*, 581-591.

Johannesson, K.H., and D.J. Burdige (2007), Balancing the global oceanic neodymium budget: Evaluating the role of groundwater, *Earth and Planetary Science Letters*, *253* (1-2), 129-142.

Johnson, R.G. (1997), Ice age initiation by an ocean-atmospheric circulation change in the Labrador Sea, *Earth and Planetary Science Letters*, *148*, 367-379.

Klemm, V., S. Levasseur, M. Frank, J.R. Hein and A.N. Halliday (2005), Osmium isotope stratigraphy of a marine ferromanganese crust, *Earth Planet. Sci. Lett*., *238,* 42-48.

Koschinsky, A., P. Halbach, J.R. Hein, and A. Mangini (1996), Ferromanganese crusts as indicators for paleoceanographic events in the NE Atlantic, *Geol Rudsch*, *85*, 567-576.

Krijgsman, W., F.J. Hilgen, I. Raffi, F.J. Sierro, and D.S. Wilson (1999), Chronology, causes and progession of the Messinian salinity crisis, *Nature*, *400*, 652-655.

Ku, T.L., M. Kusakabe, C.I. Measures, J.R. Southon, G. Cusimano, J.S. Vogel, D.E. Nelson, and S. Naraya (1990), Beryllium isotope distribution in the western North Atlantic: a comparison to the Pacific, *Deep-Sea Research*, *37* (5), 795-808.

Lacan, F., and C. Jeandel (2005a), Acquisition of the neodymium isotopic composition of the North Atlantic Deep water, *Geochemistry, Geophysics, Geosystems*, *6*, Q12008, doi:10.1029/2005GC000956.

Lacan F., and Jeandel C. (2005b), Neodymium isotopes as a new tool for quantifying exchange fluxes at the continent - ocean interface, *Earth Planet. Sci. Lett.*, *232*, 245-257.

Madelain, F.(1970), Influence de la topographie du fond sur l'écoulement Mediterranéen entre le Détroit de Gibraltar et le cap saint-Vincent, *Cahiers Océanographiques*, *22*, 43-61.

Maden, C., M. Doebeli, P.W. Kubik, M. Frank, and M. Suter (2004), Measurement of carrier-free ^{10}Be samples in AMS: the method and its potential, *Nuclear Instruments and Methods in Physics Research B*, *223-224*, 247-252.

Manheim, F.T. (1986), Marine cobalt resources, *Science*, *232*, 600-608.

Martin, E.E. and H.D. Scher (2004), Preservation of seawater Sr and Nd isotopes in fossil fish teeth: bad news and good news, *Earth Planet. Sci. Lett., 220*, 25-39.

Murdock, T.Q., A.J. Weaver, and A.F. Fanning (1997), Paleoclimatic response of the closing of the Isthmus of Panama in a coupled ocean-atmosphere model, *Geophysical Research Letters*, *24* (3), 253-256.

O'Nions, R.K., M. Frank, F. von Blanckenburg, and H.-F. Ling (1998), Secular variation of Nd and Pb isotopes in ferromanganese crusts from the Atlantic, Indian and Pacific Oceans, *Earth and Planetary Science Letters*, *155* (1-2), 15-28.

Paillet, J., M. Arhan, and M.S. McCartney (1998), Spreading of Labrador Sea Water in the eastern North Atlantic, *Journal of Geophysical Research*, *103* (C5), 10,223-10,239.

Piegras, D.J., and G.J. Wasserburg (1982), Isotopic composition of neodymium in waters from the Drake Passage, *Science*, *217*, 207-214.

Piegras, D.J., and G.J. Wasserburg (1983), Influence of the Mediterranean Outflow on the isotopic composition of neodymium in waters of the North Atlantic, *Journal of Geophysical Research*, *88* (C10), 5997-6006.

Piegras, D.J., and G.J. Wasserburg (1987), Rare earth transport in the western North Atlantic inferred from isotopic observations, *Geochimica et Cosmochimica Acta*, *51*, 1257-1271.

Piegras, D.J., and S.B. Jacobsen (1988), The isotopic composition of neodymium in the North Pacific, *Geochimica et Cosmochimica Acta*, *52*, 1373-1381.

Ravelo, A.C., and D.H. Andreasen (2000), Enhanced circulation during a warm period, *Geophys. Res. Lett., 27*, 1001-1004.

Raymo, M.E., D. Hodell, and E. Jansen (1992), Response of deep ocean circulation to initiation of northern hemisphere glaciation (3-2 Ma), *Paleoceanography, 7*, 645-672.

Rea, D.K. (1994), The paleoclimatic record provided by eolian deposition in the deep sea: The geologic history of wind, *Reviews of Geophysics*, *32*, 159-195.

Reid, J.L. (1978), On the mid-depth circulation of the salinity field in the North Atlantic Ocean, *J. Geophys. Res., 83*, 5063-5067.

Reynolds, B.C., M. Frank, and R.K. O'Nions (1999), Nd- and Pb-isotope time series from Atlantic ferromanganese crusts: implications for changes in provenance and paleocirculation over the last 8 Myr, *Earth and Planetary Science Letters*, *173*, 381-396.

Rogerson, M., E.J. Rohling and P.P.E. Weaver (2006), Promotion of meridional overturning by Mediterranean-derived salt during the last deglaciation, *Paleoceanography, 21*, PA4101, doi:10.1029/2006PA001306.

Scher, H.D. and E.E. Martin (2006), Timing and climatic consequences of the opening of Drake Passage, *Science, 312*, 428-430.

Schmitz, W.J. and M.S. McCartney (1993), On the North Atlantic circulation, *Rev. Geophys., 31*, 29-49.

Schott, F., L. Stramma, and J. Fischer (1999), Interaction of the North Atlantic Current with the deep Charlie Gibbs Fracture Zone throughflow, *Geophysical Research Letters*, *26* (3), 369-372.

Spivack, A.J., and G.J. Wasserburg (1988), Neodymium isotopic composition of the Mediterranean outflow and the eastern North Atlantic, *Geochimica et Cosmochimica Acta*, *52*, 2767-2773.

Stordal, M.C., and G.J. Wasserburg (1986), Neodymium isotopic study of Baffin Bay water: Sources of REE from very old terranes, *Earth and Planetary Science Letters*, *77*, 259-272.

Sun, S.-S. (1980), Lead isotopic study of young volcanic rocks from mid-ocean ridges, ocean islands and island arcs, *Phil. Trans. R. Soc. Lond*, *A297*, 409-445.

Sy, A., M. Rhein, J.R.N. Lazier, K.P. Koltermann, J. Meincke, and A. Putzka (1997), Surprisingly rapid spreading of newly formed intermediate waters across the North Atlantic Ocean, *Nature*, *386*, 675-679.

Tachikawa, K., C. Jeandel, and B. Dupré (1997), Distribution of rare earth elements and neodymium isotopes in settling particulate material of the tropical Atlantic Ocean (EUMELI site), *Deep-Sea Research I*, *44*, 1769-1792.

Tachikawa, K., C. Jeandel, and M. Roy-Barman (1999), A new approach to the Nd residence time in the ocean: the role of atmospheric inputs**,** *Earth and Planetary Science Letters, 170,* 433-446.

Tachikawa, K., M. Roy-Barman, A. Michard, D. Thouron, D. Yeghicheyan, and C. Jeandel (2004), Neodymium isotopes in the Mediterranean Sea: Comparison between seawater and sediment signals, *Geochim. Cosmochim. Acta, 68*, 3095-3106.

Thomas, D.J. (2004), Evidence for deep-water production in the North Pacific Ocean during the early Cenozoic warm interval, *Nature, 430*, 65-68.

Thomas, D.J., and R.K. Via (2007), Neogene evolution of Atlantic thermohaline circulation: Perspective from Walvis Ridge, southeastern Atlantic Ocean, *Paleoceanography*, *22*, PA 2212, 10.1029/2006PA001297.

van de Flierdt, T., Frank, M**.**, Lee, D.-C., Halliday, A.N., Reynolds, B.C., and Hein, J.R. (2004), New constraints on the sources and behavior of neodymium and hafnium in seawater from Pacific Ocean ferromanganese crusts, *Geochim. Cosmochim. Acta, 68,* 3827-3843.

van de Flierdt, T., L.F. Robinson, J.F. Adkins, S.R. Hemming, and S.L. Goldstein (2006), Temporal stability of the neodymium isotope signature of the Holocene to glacial North Atlantic, *Paleoceanography*, *21*, PA 4102, 10.1029/2006PA001294.

Vance, D., and K. Burton (1999), Neodymium isotopes in planktonic foraminifera: a record of the response of continental weathering and ocean circulation rates to climate change, *Earth and Planetary Science Letters*, *173*, 365-379.

Vance, D., A.E. Scrivner, P. Beney, M. Staubwasser, G.M. Henderson, and N.C. Slowey (2004), The use of foraminifera as a record of the past neodymium isotope composition of seawater, *Paleoceanography*, *19*, PA2009, 10.1029/2003PA000957.

Via, R.K., and Thomas, D.J. (2006), Evolution of Atlantic Thermohaline Circulation – Timing of the onset of Deep-water Production in the North Atlantic, *Geology*, *34*, 441-444.

Voelker, A.H.L., S.M. Lebreiro, J. Schonfeld, I. Cacho, H. Erlenkeuser, and F. Abrantes (2006), Mediterranean outflow strengthening during northern hemisphere coolings: A salt source for the glacial Atlantic?, *Earth and Planetary Science Letters*, *245*, 39-55.

von Blanckenburg, F., R.K. O'Nions, and J.R. Hein (1996a), Distribution and sources of pre-anthropogenic lead isotopes in deep ocean water from Fe-Mn crusts, *Geochimica et Cosmochimica Acta*, *60* (24), 4957-4963.

von Blanckenburg, F., R.K. O'Nions, N.S. Belshaw, A. Gibb, and J.R. Hein (1996b), Global distribution of beryllium isotopes in deep ocean water as derived from Fe-Mn crusts, *Earth and Planetary Science Letters*, *141*, 213-226.

von Blanckenburg, F., and F. Nägler (2001), Weathering versus circulation-controlled changes in radiogenic isotope tracer composition of the Labrador Sea and North Atlantic Deep Water, *Paleoceanography*, *16* (4), 424-434.

Wright, J.D., and K.G. Miller (1996), Control of North Atlantic Deep Water circulation by the Greenland-Scotland Ridge, *Paleoceanography*, *11* (2), 157-170.

Zenk, W. (1970), On the temperature and salinity structure of the Mediterranean Water in the Northeast Atlantic, *Deep-Sea Research*, *17*, 627-631.

Radiogenic Pb, Nd, and Sr isotope composition of the detrital fraction of Fe-Mn crusts from NE Atlantic seamounts: Tracers of detrital inputs over the past 12 million years

Abstract

The continental inputs of detrital material in the North East Atlantic Ocean have varied on different time scales in the past as a consequence of changes in aridity and atmospheric circulation in North Africa. In order to reconstruct past climatically driven changes of the continental inputs to the NE Atlantic we compared the radiogenic isotope composition of Pb, Nd and Sr of the detrital silicate fraction of hydrogenetic Fe-Mn crust surface scrapes and neighboring sediments to previous results obtained from pelagic sediments. Pb, Nd, and Sr time series of two Fe-Mn crusts dated by profiles of cosmogenic ^{10}Be and stable ^{9}Be were established to reconstruct the evolution of inputs for the past 12 million years.

Our data suggest that long-term changes of the continental inputs of detrital material in the NE Atlantic can best be explained by a mixture of two end-members (Anti-Atlas/North African Granites and African aerosols/Atlantic-Iberian Margin sediments) demonstrating the long-term prevalence of dry conditions in North Africa over the past ~12 Ma.

This Chapter will be submitted as a manuscript:
Muiños, S. B., M. Frank, J. R. Hein, B. Haley, C. Ehlert, R. Stumpf, J. H. Monteiro, A. Voelker and F. Abrantes (to be submitted), Radiogenic Pb, Nd, and Sr isotope composition of the detrital fraction of Fe-Mn crusts from NE Atlantic Seamounts: Tracers of detrital inputs over the past 12 million years.

IV.1. Introduction

Marine sediments including hydrogenetic ferromanganese (Fe-Mn) crusts are composed of authigenic, detrital, and biogenic fractions. The detrital fraction derives from riverine and aeolian inputs and weathering of local outcrops, whereas the authigenic fraction consists of metals mainly derived directly from seawater and/or pore waters and its radiogenic isotope composition reflects that of bottom seawater. After sinking through the water column and variable transport by currents the detrital fraction minerals are incorporated into the Fe-Mn oxides during accretion of the oxide colloids; Fe-Mn crusts form by direct precipitation of colloidal hydrated metal oxides from the water column onto hard-rock substrates and are characterized by slow growth rates (<10 mm/Ma) and extremely high specific-surface areas, which promotes the enrichment of trace elements through scavenging by the major oxides (e.g. Hein et al. 1997). During accretion, the detrital supply to the oceans is also incorporated into the crusts. Due to their slow growth, Fe-Mn crusts are considered to be condensed stratigraphic sections and can be used as recorders of the oceanic and climatic history of the past ~75 Ma (Klemm et al., 2005). Despite the fact that Fe-Mn crusts cannot be used for high-resolution studies, the major long-term changes in oceanic and climatic history can be reconstructed based on the study of radiogenic isotopes. In fact, Banakar et al. (2003) reconstructed the Himalayan erosion history over the past 25 Ma by studying the evolution of sedimentary pulses recorded by the detrital silicate fraction of a Fe-Mn crust from the central Indian Ocean.

In the NE Atlantic the detrital fraction of the marine sediments at present mainly originates from aeolian continental input (in particular Saharan dust; Prospero et al., 2002) but riverine input may also represent a significant component in some areas closer to the continental margins (e.g. Holz et al., 2007). Sources of atmospheric dust and continental aerosols are the world's deserts and adjacent arid areas, which are covered by sand dunes, arid soils, dry lake beds, and dust pans (Grousset and Biscaye, 2005). The prevailing winds transport these aerosols over large distances (Prospero, 1981). Despite the fact that all of North Africa is a potential dust source (Middleton and Goudie, 2002), the Sahara-Sahel region is at present the world's greatest source of mineral dust to the atmosphere (Prospero et al., 2002). Hunneeus et al. (2011) estimate that 800 teragrams (10^{12} g) of dust are emitted every year from North Africa, which corresponds to ~70% of the global dust budget and makes North Africa the largest world dust source.

The radiogenic isotope composition of Sr, Nd, and Pb of dust is a valuable tracer of dust provenance, and for the discrimination of different source areas (Biscaye et al., 1997). On the basis of available sediment Sr and Nd isotope data, Scheuvens et al. (2013) proposed seven main geographic regions on northern Africa as main contributing sources of dust to NE Atlantic sediments (Table IV.1.).

Table IV.1. Geographical regions of northern Africa with representative $^{87}Sr/^{86}Sr$ and $\varepsilon_{Nd(0)}$ values (from Scheuvens et al., 2013)

Source region	$^{87}Sr/^{86}Sr$	$\varepsilon_{Nd}(0)$
Northern region (Morocco, Algeria)	0.717-0.727	-17.1 to -8.3
Western region (Western Sahara, Mauritania)	0.720-0.738	-17.9 to -13.5
Senegal	0.715-0.737	-16.2 to -14.5
Tunisia	0.714	-9.5
Libya	0.715	-15.4 to -10.7
Egypt and northern Sudan	0.705-0.718	-11.0 to -3.9
Sub-Saharan (without Senegal)	0.715-0.724	-12.4 to -10.0

The continental inputs of detrital material in the NE Atlantic have varied on different time scales in the past as a consequence of changes in aridity and atmospheric circulation in North Africa. This is reflected in variations of the dust export as recorded by marine sediments. At present, the Saharan dust transport over the North East Atlantic occurs during the entire year but is stronger during spring and summer (e.g., Swap et al., 1996). The sources and trajectories of the dust particles deposited in the North Atlantic Ocean are controlled by the seasonal latitudinal shift of the Inter Tropical Convergence Zone (ITCZ) from 19°N during boreal summer to ~5°S during winter (e.g., Hamilton et al., 1945). During summer, when the ITCZ is at its northernmost position and the surface airflow over

northwestern Africa is controlled by the West African monsoon (which causes rainfall in the Sahel region), the primary westward dust transport occurs at high altitudes within the Saharan Air Layer (Prospero and Carlson, 1981). However, it is during spring and winter when major Saharan dust outbreaks occur. During these seasons, dust is transported within the Harmattan (essentially low altitude Trade Winds; e.g. Hamilton et al., 1945). The Harmattan is a cold, dry continental wind system that carries large amounts of dust from the Bodélé depression in Chad to the North Atlantic (e.g. Prospero and Lamb, 2003; Skonieczny et al., 2013). Thus, the amount of dust deposited and its provenance provide important information on the atmospheric circulation and transport and also about the climate of the dust's source areas (Grousset and Biscaye, 2005). However, Saharan dust events may involve large geographical domains and the identification of a single contributing source is unrealistic (Skonieczny et al., 2011; 2013). The multi-proxy approach of Skonieczny et al. (2011) for the 7-13 March 2006 major Saharan outbreak showed that even during a single major outbreak there were significant compositional changes of the dust deposited at Mbour, Senegal. In fact, marked differences in clay mineralogy, Sr and Nd compositions and also freshwater diatom taxa were observed from the beginning to the end of the outbreak which were linked to the progressive shift of the air mass trajectories during the event that resulted in the coverage of a large geographical domain (Skonieczny et al., 2011). In a more recent study of a three-year record of modern dust deposition at Mbour (Senegal) Skonieczny et al. (2013) found that the occurrence of some major deposition events during the winter-spring seasons, which originated in the western Sahara-Sahel region, is superimposed on the general seasonal pattern.

On glacial/interglacial time scales North African climate changed between arid to hyperarid conditions and wetter conditions (Cole et al., 2009). Based on Sr-Nd isotope data (Meyer et al., 2011) it seems that these conditions were linked to a latitudinal shift or to an expansion of the African rain belt (and associated wind belts) which have caused variations in the evaporation-precipitation balance. According to Meyer et al. (2011) during the Younger Dryas there was a prevalence of hyperarid conditions, while during the African Humid Period (AHP) the intensification of the monsoonal rainfall lead to much wetter conditions. With diminished monsoonal circulation northwest Africa returned to more arid conditions in the late Holocene (Meyer et al., 2011).

Regarding the long-term evolution (past ~8 Ma) of dust inputs into the Atlantic Ocean off northwest Africa, and the corresponding climatic evolution, Tiedemann et al. (1994) suggested that during the latest Miocene and earliest Pliocene (~7.2-4.7 Ma) both north and south Sahara regions were characterized by an humid climate. The onset of arid climates had different timings for each region. South Sahara aridification occurred stepwise since 4.6 Ma, with a major aridification around 3.5 and 2.1 Ma. The aridification of the North Sahara started later at 3.2 Ma, which approximately coincided with the onset of Northern Hemisphere Glaciation (NHG; Tiedemann et al., 1994).

Here we use the radiogenic isotope composition of Pb, Nd and Sr of the detrital silicate fraction of hydrogenetic Fe-Mn crusts and nearby sediment to reconstruct past changes of the input of material supplied by the continents to the North East Atlantic Ocean driven by climatic changes over the past ~12 Ma.

Published radiogenic isotope data of the study area were either focused on "present-day" values (Grousset et al., 1988; 1998; Chavagnac et al., 2007) or reached at the most as far back as the AHP (12 kyrs ago) and the Last Glacial Maximum (20 kyrs ago) (Grousset et al., 1998; Cole et al., 2009). Our results obtained from the surfaces of the Fe-Mn crusts, which we compare to "present-day" data obtained in various previous studies, correspond to a ~1-2 Ma integration including glacial/interglacial periods due to the slow growth rates of Fe-Mn crusts.

The first goal of our study is to demonstrate that the isotopic composition of the detrital fraction of the crusts represents Saharan dust input. Despite the low resolution of our time series our goal is also to reconstruct the changes in the input of detrital material into the Northeast Atlantic, and thus to contribute to a better understanding of the driving factors of these changes over the period of the past 12 Ma, for the older part of which no higher resolution sedimentary records are available to date.

IV.2. Material and Methods

We performed measurements on 57 sub-samples comprising 31 Fe-Mn crust surface scrapings, 15 samples from depth profiles of three selected crusts, six sediment samples,

and five duplicates. The samples of this study were collected from twelve seamounts in the NE Atlantic during cruises Trident 86, TTR-11 (I.O.C., 2002), Meteor 51/1 (Hoernle and Scientific Party, 2003), and Tore-Madeira (Merle, 2006). Sampling locations cover a wide geographic area in the NE Atlantic including seamounts in the Portuguese Exclusive Economic Zone (EEZ, and the proposed extended continental shelf), the western Mediterranean Sea and near the Canary Islands, and are distributed over a large depth range (Figure IV.1., Table IV.2.).

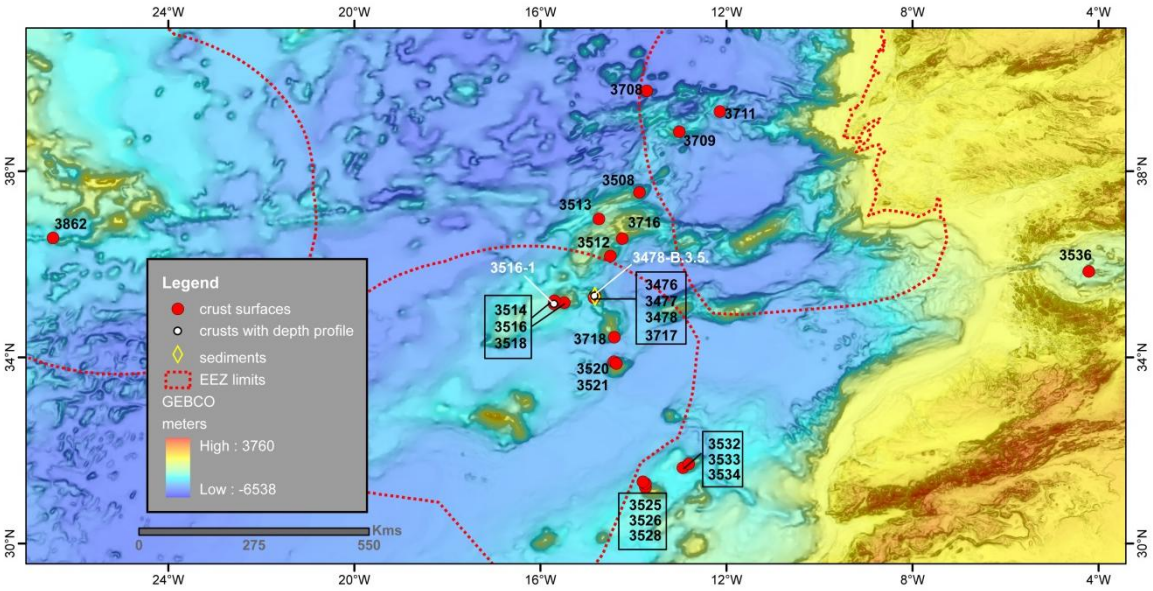

Figure IV.1. Map showing the location of the studied seamounts the samples studied.

The chemical preparation method for the complete separation of the detrital fraction from the authigenic Fe-Mn oxide fraction (seawater isotopic signature) was performed at the Marine Biogeochemistry Laboratory at LNEG-UGM (Alfragide) and essentially consisted of 6N HCl leaching of ~1g of Fe-Mn crust sample or sediment. The use of such a highly concentrated acid was chosen in order to avoid mixing of the detrital radiogenic isotope signatures with the seawater-derived Pb, Nd and Sr isotope signatures and we accepted that dissolution of a fraction of the detrital clays likely occurred during this procedure. The resulting solution was centrifuged and separated from the residue. The residue, hereafter

termed "detrital fraction", was rinsed three times with ultrapure water and was then freeze-dried. The detrital fraction was completely dissolved at GEOMAR, Kiel by a mixture of concentrated HF and HNO_3 (5:1). The methods used for subsequent chemical preparation and ion chromatographic purification of Nd, Pb, and Sr followed Cohen et al. (1988), Galer and O'Nions (1989) and Bayon et al. (2002), respectively, and were carried out at GEOMAR, Kiel. Pb, Nd and Sr isotope ratios were determined by MC-ICP-MS (*Nu Instruments*) at GEOMAR, Kiel.

For Pb isotope measurements, a standard bracketing method was applied (Albarède et al., 2004). All Pb isotope ratios presented were normalized to the NBS981 standard values given by Abouchami et al. (1999). The 2σ external reproducibility of the repeated standard measurements during different sessions on the mass spectrometer was ±0.003 for $^{206}Pb/^{204}Pb$, ±0.004 for $^{207}Pb/^{204}Pb$, ±0.012 for $^{208}Pb/^{204}Pb$, ±0.0008 for $^{208}Pb/^{206}Pb$, and ±0.0001 for $^{207}Pb/^{206}Pb$. The measured $^{143}Nd/^{144}Nd$ ratio was normalized to $^{146}Nd/^{144}Nd$ = 0.7219 for instrumental mass bias correction. All Nd isotope ratios presented were normalized to the accepted value of the JNdi-1 standard of 0.512115 (Tanaka et al., 2000). The 2σ external precision of the different Nd isotope measurement sessions was 46 and 47 ppm, respectively.

$^{87}Sr/^{86}Sr$ isotope ratios were corrected for interferences (^{86}Kr, ^{87}Rb) and instrumental mass bias using $^{86}Sr/^{88}Sr$ = 0.1194 (Steiger and Jäger, 1977). The Sr isotope ratios were normalized to the widely used NBS987 standard value of 0.710245 and the 2σ external reproducibility of repeated measurements varied between 23 and 48 ppm.

Two of the three selected Fe-Mn crusts from which we produced depth profiles, were dated by profiles of the radioactive cosmogenic ^{10}Be and stable ^{9}Be obtained from the authigenic, seawater-derived Fe-Mn fraction, which allowed that Pb, Nd and Sr time-series were produced. The chemical preparation of the samples for the ^{10}Be Accelerator Mass Spectrometry (AMS) measurements followed closely the method described by Henken-Mellies et al. (1990) (see Chapter II-Material Methods for a detailed presentation of the chemical methods applied). The samples of this study were measured at the Zürich AMS facility of the Paul Scherrer Institute and of the ETH Zürich, Switzerland. The ^{10}Be concentrations were normalized to the internal standard S2007N with a nominal $^{10}Be/^{9}Be$ ratio of 28.1×10^{-12} (Kubik and Christl, 2010). The 1σ statistical uncertainties of individual

Table IV.2. Location of samples

Sample ID	Field ID	Latitude (N)*[1]	Longitude (W)*[1]	Water Depth (m)*[1]	Seamount	Geographic Area
3476	TTR11-352GR	35.3150	-14.8317	1855	Nameless	Madeira
3477	TTR11-353GR	35.3117	-14.8300	1853	Nameless	Madeira
3478	TTR11-354GR	35.3167	-14.8350	1839	Nameless	Madeira
3508	M51/1-404DR	37.5417	-13.8725	1800	Teresa	Madeira
3512	M51/1-412DR	36.1725	-14.4962	2018	Josephine	Madeira
3513	M51/1-414DR	36.9700	-14.7475	4594	MTR	Madeira
3514	M51/1-417DR	35.2142	-15.7032	813	Lion	Madeira
3516	M51/1-419DR	35.1442	-15.7046	1859	Lion	Madeira
3518	M51/1-421DR	35.1725	-15.4882	1955	Lion	Madeira
3520	M51/1-425DR	33.9008	-14..4222	2685	Seine	Madeira
3521	M51/1-426DR	33.8683	-14.3680	1362	Seine	Madeira
3708	TM-D3B	39.7217	-13.7152	4140	Tore	Madeira
3709	TM-D5	38.8442	-13.0147	2803	Tore	Madeira
3711	TM-D9	39.2775	-12.1486	3110	Tore	Madeira
3716	TM-D17B	36.5517	-14.2388	1620	Josephine	Madeira
3717	TM-D19	35.2767	-14.8500	2198	Nameless	Madeira
3718	TM-D20	34.4258	-14.4173	3756	Unicorn	Madeira
3525	M51/1-448DR	31.3216	-13.8009	3043	Dacia	Canaries
3526	M51/1-449DR	31.2875	-13.7456	2622	Dacia	Canaries
3528	M51/1-451DR	31.2058	-13.7498	1845	Dacia	Canaries
3532	M51/1-456DR	31.5725	-12.9845	2637	Annika	Canaries
3533	M51/1-457DR	31.6267	-12.9382	1602	Annika	Canaries
3534	M51/1-458DR	31.7083	-12.8156	2128	Annika	Canaries
3536	M51/1-462DR	35.8450	-4.2125	1221	Ibn Batouta	Mediterranean
3862	TR86-8D	36.5667	-26.4833	2575	Azores	Azores

*[1] except for samples from the TTR-11 cruise that were collected by TV-Grab, all the other coordinates and water depths (M51/1- Meteor 51/1, TM-Tore-Madeira and TR-Trident 86) correspond to intermediate values from on- and off-bottom dredge locations. MTR means Madeira-Tore Rise.

^{10}Be measurements take into account both the counting statistics of the ^{10}Be ”events” and the reproducibility of repeated measurements, which were performed for each sample. On the same aliquots and on Fe-Mn nodule reference material NOD A1 the concentrations of

stable ^{9}Be, along with other elements (Sr, Ba, REEs, Hf, and Pb) were measured by ICP-MS at the ICPMS-Lab of the Institute of Geosciences, University of Kiel, Germany, using an AGILENT 7500cs ICP-MS instrument and following the procedure described by Garbe-Schönberg (1993). The determinations of the age models were carried out considering the recently revised ^{10}Be half-life of 1,387 Myr (Chmeleff et al., 2010).

IV.3. Results

IV.3.1. Distribution maps of $^{87}Sr/^{86}Sr$, $\varepsilon_{Nd(0)}$ and $^{206}Pb/^{204}Pb$ signatures

The distribution maps for $^{206}Pb/^{204}Pb$, ε_{Nd}, and $^{87}Sr/^{86}Sr$ signatures of the detrital fraction obtained from the surface scrapes of the Fe-Mn crusts and associated sediments are provided in Figures IV.2. to IV.4. (see also Tables IV.3., IV.4.).

The $^{206}Pb/^{204}Pb$ ratios (Figure IV.2.) ranged between 18.79 and 19.20 (average 18.89 for 24 measurements) for the detrital fraction of the crusts and between 18.67 and 18.84 (averaging 18.75 for 7 measurements) for the detrital fraction of the sediments; note that sedimentary Pb isotope data must be considered with caution because even though the sediments were recovered in the same TV-Grabs as the crusts, they likely include the uppermost surface sediment and may thus to some extent be contaminated by gasoline-derived anthropogenic Pb. Overall, $^{206}Pb/^{204}Pb$ values show no obvious geographic zonation. These values are in agreement with data reported by Sun (1980) for Atlantic Ocean sediments. Our least radiogenic values are comparable to typical $^{206}Pb/^{204}Pb$ ratios for Saharan dust of 18.70 reported by Abouchami and Zabel (2003) and of 18.76 given by B. Hamelin (personal communication, 2003)

The ε_{Nd} signature of the detrital fraction of the crust surfaces ranges from -9.2 to -13.1 (average -11.5 for 32 measurements), whereas the accompanying sediment samples range from -11.8 to -13.0 (average -12.3 for 8 measurements) (Figure IV.3.). These values are in good agreement with published values for the eastern North Atlantic region (Grousset et al., 1988; 1998; Grousset and Biscaye, 2005). The more radiogenic ε_{Nd} signatures found in our dataset most likely reflect contributions from the Mediterranean Sea as indicated by comparison to published values for Mediterranean Sea sediments ($-10 < \varepsilon_{Nd} < -2$; Frost et al.,

1986; Grousset et al., 1998). Moreover, and in contrast to the observations of Grousset et al. (1988) we do not find a geographic zonation of the $\varepsilon_{Nd(0)}$ distribution along the Azores-Mediterranean axis in our data.

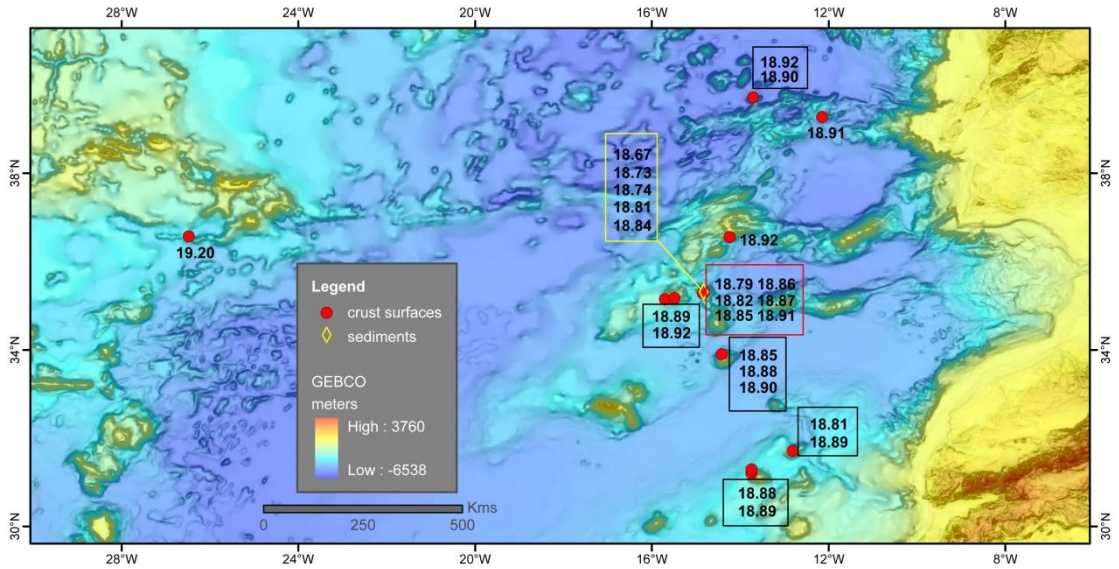

Figure IV.2. Map showing the distribution of the $^{206}Pb/^{204}Pb$ ratios of the detrital fraction of the Fe-Mn crusts surfaces and associated sediments.

$^{87}Sr/^{86}Sr$ ratios of the detrital fraction of the crust surface scrapes range from 0.7094 to 0.7204 (with an average value of 0.7121 for 33 measurements). The isotope signatures of the sediment samples range between 0.7097 and 0.7215 (average 0.7181 for 8 measurements). Overall our sample set shows no clear geographic zonation (Figure IV.4.). The values are all more radiogenic than the modern strontium isotope composition of seawater (0.70916) and are comparable with the values for subtropical Atlantic sediments (~0.715 to ~0.725; Grousset et al., 1998), cores GeoB 4223 (~0.7107 to ~0.7216) and GeoB 6007 (0.717-0.724) off Morocco (Meyer et al., 2011; 2013), as well as with the values given by Chavagnac et al. (2007) (0.7103 to 0.7121) for a mooring station at the Madeira Abyssal Plain (MAP; site Kiel 276).

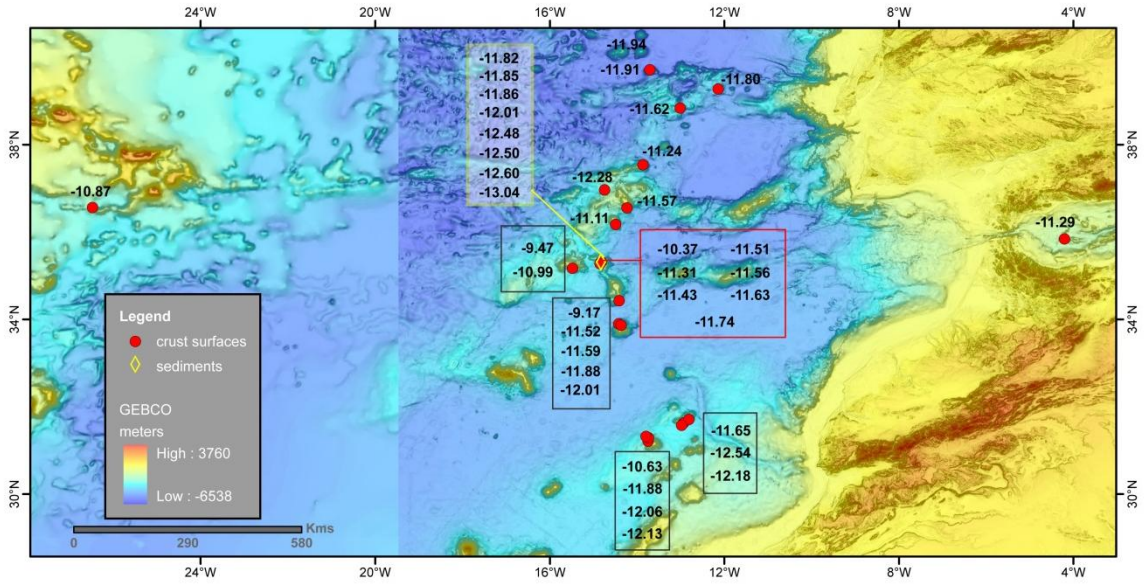

Figure IV.3. Map showing the distribution of the $\varepsilon_{Nd(0)}$ values of the detrital fraction of the Fe-Mn crusts surfaces and accompanying sediments.

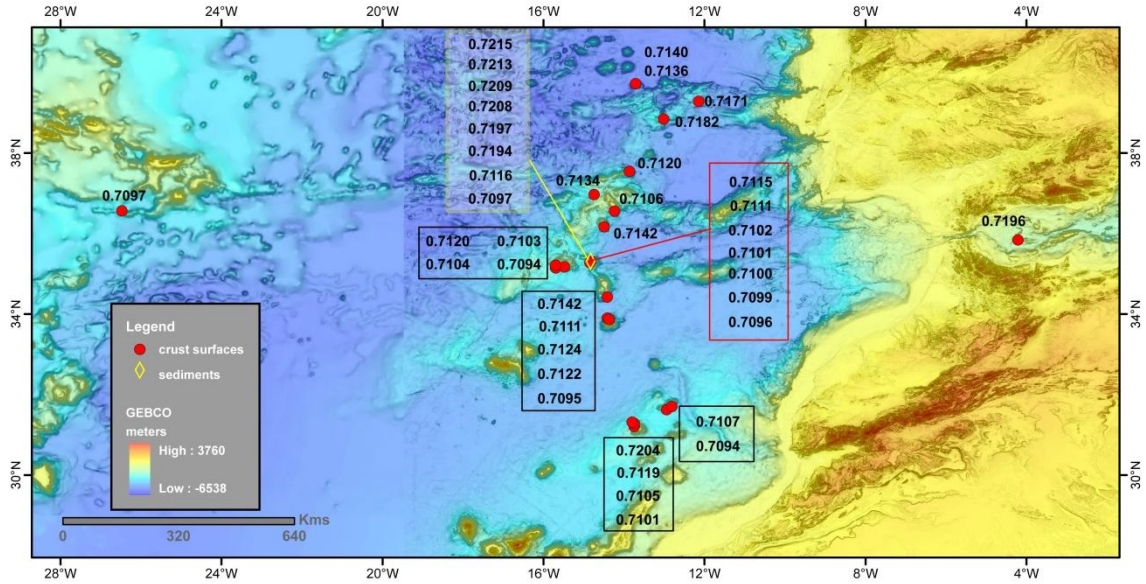

Figure IV.4. Map showing the distribution of the $^{87}Sr/^{86}Sr$ ratios of the detrital fraction of the Fe-Mn crusts surfaces and associated sediments.

In summary, a comparison of the data for the detrital material extracted from the Fe-Mn crusts and the sediments recovered together with them, as well as with sediment radiogenic

isotope data from the same or adjacent areas obtained in other studies (Sun, 1980; Grousset et al., 1988, 1998; Abouchami and Zabel, 2003; Chavagnac et al., 2007; Meyer et al., 2011; 2013), suggest that the signature of detrital material can be reliably extracted and that a reconstruction of the long-term changes of the detrital inputs into the eastern Atlantic Ocean using Fe-Mn crust records is viable.

Table IV.3. Pb, Nd and Sr isotopic composition of the crusts

Sample	$^{206}Pb/^{204}Pb$	$^{207}Pb/^{204}Pb$	$^{208}Pb/^{204}Pb$	$^{143}Nd/^{144}Nd$		$1\sigma^{*1}$	$\varepsilon_{Nd(T)}$	$^{87}Sr/^{86}Sr$
3476-B.3.2	18,850	15,670	38,913	0,512042	±	7	-11,6	0,7111
3476-B.3.3	18,863	15,674	38,931	0,512058	±	7	-11,3	0,7102
3477-B.3.4	18,907	15,679	38,986	0,512052	±	4	-11,4	0,7100
3477-B.3.4 DP	18,910	15,678	38,987	0,512036	±	6	-11,7	0,7099
3478-B.2.2	18,790	15,665	38,841	0,512107	±	34	-10,4	0,7115
3478-B.3.5	18,818	15,666	38,874	0,512045	±	8	-11,6	0,7101
3508-6				0,512062	±	9	-11,2	0,7120
3512-42				0,512068	±	9	-11,1	0,7142
3513-14				0,512009	±	9	-12,3	0,7134
3514-6								0,7120
3516-1	18,854	15,666	38,913					0,7104
3518-1	18,892	15,675	38,965	0,512074	±	5	-11,0	0,7094
3518-2	18,893	15,676	38,970	0,512153	±	6	-9,5	0,7103
3520-9	18,852	15,673	38,915	0,512047	±	7	-11,5	0,7111
3520-9 DP	18,884	15,678	38,962	0,512022	±	6	-12,0	0,7124
3520-16	18,896	15,678	38,972	0,512044	±	6	-11,6	0,7122
3521-6				0,512168	±	14	-9,2	0,7095
3708-1	18,918	15,677	38,977	0,512026	±	5	-11,9	0,7136
3708-1 DP	18,896	15,673	38,960	0,512027	±	7	-11,9	0,7140
3709-1				0,512043	±	7	-11,6	0,7182
3711-2	18,912	15,679	38,957	0,512033	±	6	-11,8	0,7171
3716-3	18,921	15,677	38,996	0,512045	±	5	-11,6	0,7106
3717-12	18,869	15,675	38,935	0,512048	±	5	-11,5	0,7096
3718-1				0,512029	±	8	-11,9	0,7142
3525-9				0,512020	±	7	-12,1	0,7204
3526-4	18,882	15,680	38,966	0,512016	±	5	-12,1	0,7120
3528-7	18,877	15,674	38,949	0,512029	±	7	-11,9	0,7101

3528-9	18,886	15,678	38,964	0,512093	±	6	-10,6	0,7105
3532-3				0,511967	±	11	-13,1	
3533-7	18,813	15,673	38,880	0,512041	±	7	-11,7	0,7095
3534-11	18,886	15,676	38,961	0,512014	±	5	-12,2	0,7107
3534-14	18,894	15,677	38,972	0,511995	±	7	-12,5	0,7107
3536-3				0,512059	±	4	-11,3	0,7196
3862	19,198	15,680	39,359	0,512081	±	6	-10,9	0,7097

*1 The σ values correspond to one standard error of the mean (SEM).

Table IV.4. Pb, Nd and Sr isotopic composition of the sediments.

Sample	$^{206}Pb/^{204}Pb$	$^{207}Pb/^{204}Pb$	$^{208}Pb/^{204}Pb$	$^{143}Nd/^{144}Nd$	$1\sigma^{*1}$	$\varepsilon_{Nd(T)}$	$^{87}Sr/^{86}Sr$
3476-A1	18.838	15.692	39.005	0.512022	± 7	-12.0	0.7208
3476-A2	18.808	15.679	38.971	0.511998	± 6	-12.5	0.7194
3477-A1	18.736	15.665	38.995	0.512030	± 6	-11.9	0.7213
3477-A1 DP	18.741	15.653	38.847	0.512030	± 6	-11.9	0.7197
3477-A2	18.728	15.662	38.795	0.511997		-12.5	0.7097
3477-A2 DP				0.511992		-12.6	0.7116
3478-A1	18.675	15.656	38.802	0.511970	± 7	-13.0	0.7209
3478-A2	18.741	15.597	38.267	0.512032	± 6	-11.8	0.7215

*1 The σ values correspond to one standard error of the mean (SEM).

IV.3.2. Dating

Two Fe-Mn crusts in the study area were dated by profiles of cosmogenic ^{10}Be/stable ^{9}Be (Table IV.5., Figure IV.5.). The average growth rate of crust 3478-B.3.5 from the Nameless seamount is 1.48 mm/Myr for the upper 10 mm and 2.74 mm/Myr between 10 and 17.5 mm depth. For crust 3516-1 from the Lion seamount a growth rate of 1.63 mm/Myr was obtained from the $^{10}Be/^{9}Be$ profiles. These rates are in accordance with expected values for marine ferromanganese crusts of hydrogenetic origin (e.g., Hein et al., 2000; Frank, 2002).

The extrapolated surface $^{10}Be/^{9}Be$ ratios (~4 to ~6 x 10^{-8}) are consistent with the values for present-day northeast Atlantic Deep Water (NEADW) corroborating undisturbed present-

day growth surfaces of our two crusts (von Blanckenburg et al., 1996). Both crusts show an exponential decrease of $^{10}Be/^{9}Be$ with depth in their upper parts, whereas in their older sections below 17.5 mm corresponding to an age of 8.4 Ma (Nameless seamount) and 13 mm corresponding to 7.4 Ma (Lion seamount) the $^{10}Be/^{9}Be$ in both crusts is essentially constant. This may indicate that the crusts had very high growth rates at the beginning of their deposition or that these data are already too old and too close to the $^{10}Be/^{9}Be$ background, which is what we adopted for further interpretation. With these growth rates, which we obtained using the revised ^{10}Be half life value of 1.387± 0.012 Ma (Chmeleff et al., 2010), we extrapolated the growth rates for the remainder of the profiles in each crust and assigned corresponding ages for initiation of accretion of 13.6 Ma and 12.3 Ma for crusts 3478-B.3.5 and 3516-1, respectively (in italics in Table IV.6.). These ages have to be considered with some caution because the growth rates in these older parts may have been much higher and we cannot exclude growth hiatuses within the sections for which the ages were extrapolated.

Table IV.5. The $^{10}Be/^{9}Be$ dating and growth rates

sub-sample	depth interval, mm	mean depth, mm	$^{10}Be/^{9}Be$, x 10^{-8}	growth rates, mm/Ma	Age, Ma
3478-B.3.5 A	0-1	0.50 ± 0.50	4.378 ± 0.158	**1.48**	0.34
3478-B.3.5 B	7-10	8.50 ± 1.50	0.293 ± 0.026	"	5.74
3478-B.3.5 C	14-17	15.75 ± 1.75	0.078 ± 0.006	**2.74**	8.39
3478-B.3.5 D	22-24	23.00 ± 1.00	0.055 ± 0.006	"	*11.04* [*1]
3478-B.3.5 E	28-30	29.00 ± 1.00	0.069 ± 0.006	"	*13.23* [*1]
3516-1 A	1	0.50 ± 0.50	4.193 ± 0.135	**1.63**	0.31
3516-1 B	6-8	7.00 ± 1.00	0.585 ± 0.030	"	4.29
3516-1 C	11-13	12.00 ± 1.00	0.124 ± 0.014	"	7.36
3516-1 D	15-17	16.00 ± 1.00	0.166 ± 0.012	"	*9.82* [*1]

[*1] These ages are based solely on extrapolation of the growth rates to the bases of the crusts. For both crusts the extrapolated ages beyond the interval of exponential $^{10}Be/^{9}Be$ decrease (8.4 and 7.4 Ma for 3478-B.3.5 and 3516-1, respectively), should be considered with caution.

IV.3.3. Pb, Nd and Sr Isotope Time Series

Time series of the Pb, Nd, and Sr isotope compositions of the detrital fractions were obtained for three crusts: i) 3476-B.3.3, 1,855 m water depth and ii) 3478-B.3.5, 1,839 m water depth both from Nameless seamount, and iii), crust 3516-1, 1,859 m water depth from Lion seamount. The crusts were collected at similar water depths but while the Nameless seamount crusts were collected in the northwestern region of the summit, the Lion crust was collected at the southwest flank of this seamount. The sampling locations at Lion and Nameless seamounts are separated by ~110 km (Figure IV.1.).

The three crusts display essentially identical surface detrital $^{206}Pb/^{204}Pb$ isotope ratios (18.80 to 18.81), and $^{87}Sr/^{86}Sr$ ratios ranging from 0.710 to 0.712 (Table IV.6., Figure IV.6.). Surface ε_{Nd} values range from -10.2 to -11.7. It is only the Nd isotope ratios of the Lion seamount crust that are significantly different (more radiogenic) from those of the Nameless seamount crusts, whereas there are no significant differences in Pb and Sr isotope ratios of the crust surfaces.

The two profiles from the Nameless seamount crusts are in good agreement with each other for all three-isotope systems (Figure IV.6.). In contrast, the Lion crust shows a less variable $^{206}Pb/^{204}Pb$ profile than the Nameless crusts but the data of all three crusts show somewhat less radiogenic Pb isotope signatures in their oldest parts and a nearly continuous trend towards more radiogenic values in the youngest parts (Figure IV.6.). For the Nd isotopes, the crusts from the Nameless seamount are systematically less radiogenic than the Lion crust throughout the profiles whereas for the Sr isotope ratios the profile of the Lion crust is only distinctly more radiogenic between 4 and 9 mm depth (Table IV.6., Figure IV.6.). Only one of the Nameless crusts was dated but both crusts from this seamount yield very similar records, which supports the reliability of both profiles. We will focus our interpretations on records of the dated crusts 3478-B.3.5 (Nameless seamount) and 3516-1 (Lion seamount) (Figure IV.7.).

The Nameless seamount crust (3478-B.3.5) shows a continuous increase from a $^{206}Pb/^{204}Pb$ ratio of 18.69 to 18.81 between 9.9 ± 1.1 Ma and the Present (Figure IV.7.; the errors assigned to the ages do not represent analytical uncertainties but reflect the depth range from which the crust material was recovered for each sample of the profiles). In contrast, the Lion seamount crust (3516-1) recorded essentially constant Pb isotope compositions

($^{206}Pb/^{204}Pb \approx 18.76$) between 10.4 ± 1.8 and 3.1 ± 1.2 Ma and then increased to the "present-day" value of 18.80. The amplitude of change of $^{206}Pb/^{204}Pb$ ratios in both crusts over time is small compared with the range of signatures observed in the crust surfaces. The signature of the Lion seamount crust has almost been constant between 18.76 and 18.80 when compared to the Nameless seamount crust, which changed from 18.69 to 18.81 over time.

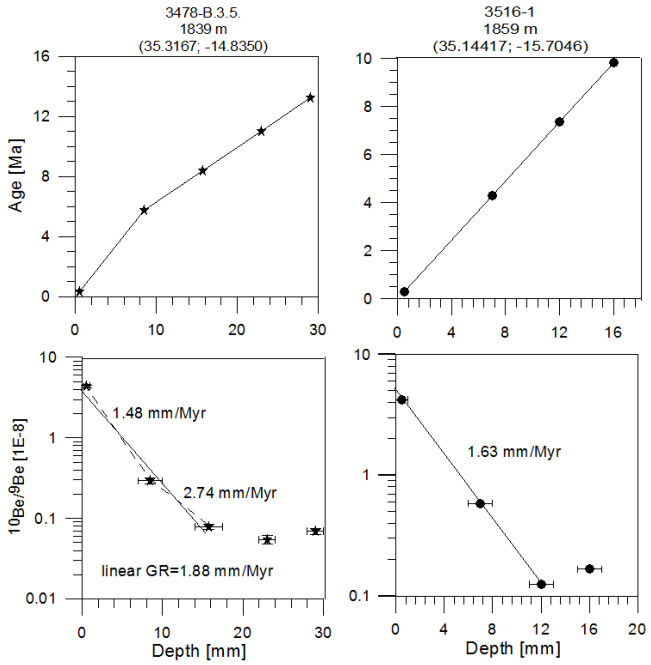

Figure IV.5. Profiles of $^{10}Be/^{9}Be$ ratios for the two crusts studied versus depth. The ages of the applied age models given by the solid lines in the age versus depth plots were calculated with a half–life for ^{10}Be of 1.387± 0.012 Ma and in the older part were extrapolated based on the growth rates obtained from the exponential decrease above.

Regarding the ε_{Nd} time series, the record of the Lion crust remained more radiogenic than the Nameless crust for the entire period of the last ~12 Ma. The time series resemble each other in that there was a trend to more radiogenic values starting at about ~10 Ma followed by a trend back to present-day to less radiogenic signatures. The Nameless crust record may become less radiogenic somewhat earlier than the Lion crust, although two of the samples in the middle of the record of the Lion crust could not be measured and the exact timing of the decrease can thus not be directly compared.

The strontium isotope evolution of the supply of detrital material is more distinct between the Lion and Nameless crusts although the overall variability is also small. The Nameless crust shows a Sr isotope peak with values of 0.7165 at ~10 Ma and then decreased steadily to $^{87}Sr/^{86}Sr$ signatures between 0.7100 and 0.7115 over the last ~8 Ma. The Lion crust displays less radiogenic values in the older part and then a continuous increase of the $^{87}Sr/^{86}Sr$ ratios to its maximum value of 0.7187 at 3.1 ± 1.2 Ma and it then decreased again to the present-day value of 0.7117.

Table IV.6. Pb, Nd and Sr isotopic composition of the depth profiles of 3 selected crusts

sub-sample	depth Interval, mm	mean depth, mm	Age, Ma	Age interval	$^{206}Pb/^{204}Pb$	$\varepsilon Nd(0)$	$^{87}Sr/^{86}Sr$
3478-B.3.5. A	0-7	3.5 ± 3.5	2.36	0.0-4.7	18.809	-11.7	0.7100
3478-B.3.5. B	7-13	10.0 ± 3.0	6.29	4.7-7.4	18.752	-10.9	0.7110
3478-B.3.5. C	13-17	15.0 ± 2.0	8.12	7.4-8.8	18.726	-10.9	0.7115
3478-B.3.5. D	17-23	20.0 ± 3.0	*9.94*[*1]	*8.8-11.0*	18.694	-11.9	0.7165
3478-B.3.5. E	23-30	26.5 ± 3.5	*12.31*[*1]	*11.0-13.6*	18.698	-11.4	0.7121
base age		30.0	***13.59***[*1]				
3516-1 A	0-3	1.5 ± 1.5	0.92	0.0-1.8	18.798	-10.2	0.7117
3516-1 B	3-7	5.0 ± 2.0	3.07	1.8-4.3	18.754	-9.3	0.7187
3516-1 C	7-10	8.5 ± 1.5	5.21	4.3-6.1	18.767		0.7155
3516-1 D	10-14	12.0 ± 2.0	7.36	6.1-8.6	18.761		0.7117
3516-1 E	14-20	17.0 ± 3.0	*10.43*[*1]	*8.6-12.3*	18.763	-10.6	0.7098
base age		20.0	***12.27***[*1]				
3476-B.3.3. A	0-7	3.5 ± 3.5			18.797	-11.2	0.7101
3476-B.3.3. B	7-13	10.0 ± 3.0			18.735	-11.1	0.7101
3476-B.3.3. C	13-18	15.5 ± 2.5			18.661	-11.7	0.7138
3476-B.3.3. D	18-25	21.5 ± 3.5			18.689	-11.6	0.7124
3476-B.3.3. 5	25-28	26.5 ± 1.5			18.739	-11.5	0.7119

[*1] These ages are based solely on extrapolation of the growth rates obtained from $^{10}Be/^{9}Be$ to the bases of the crusts and should be considered with caution (see chapter **IV.3.2.**).

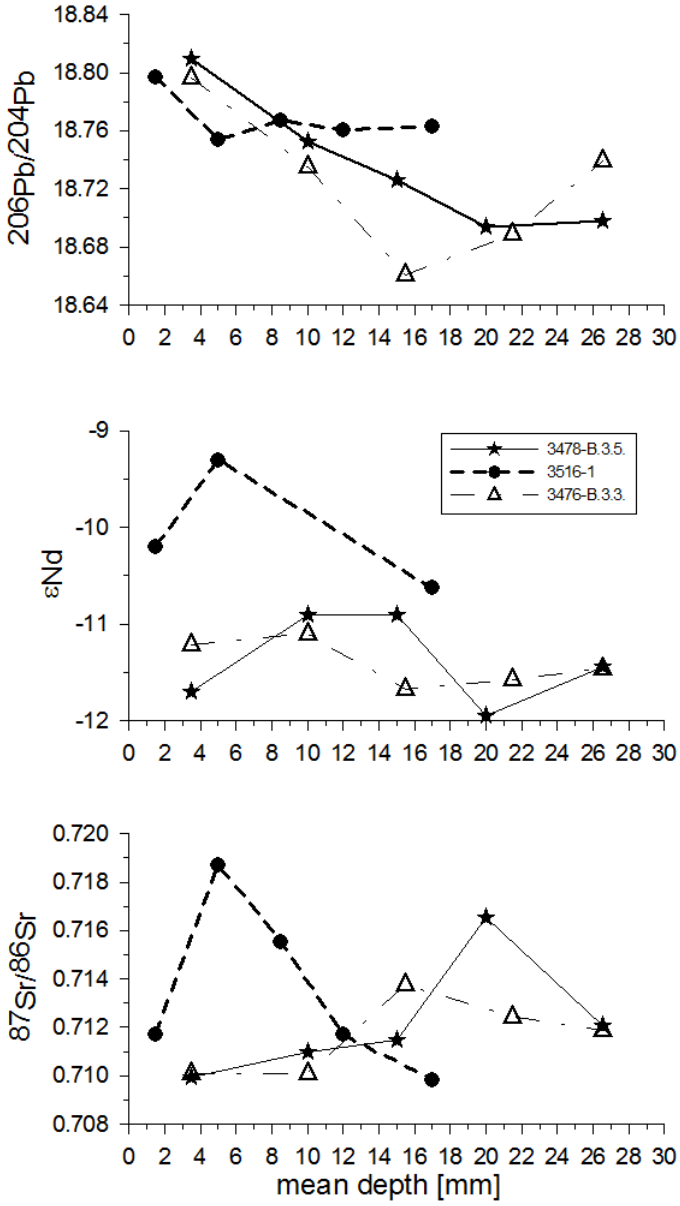

Figure IV.6. Profiles of $^{206}Pb/^{204}Pb$ (top), $\varepsilon_{Nd\ (T)}$ (middle) and $^{87}Sr/^{86}Sr$ (bottom) versus depth for the three crusts studied.

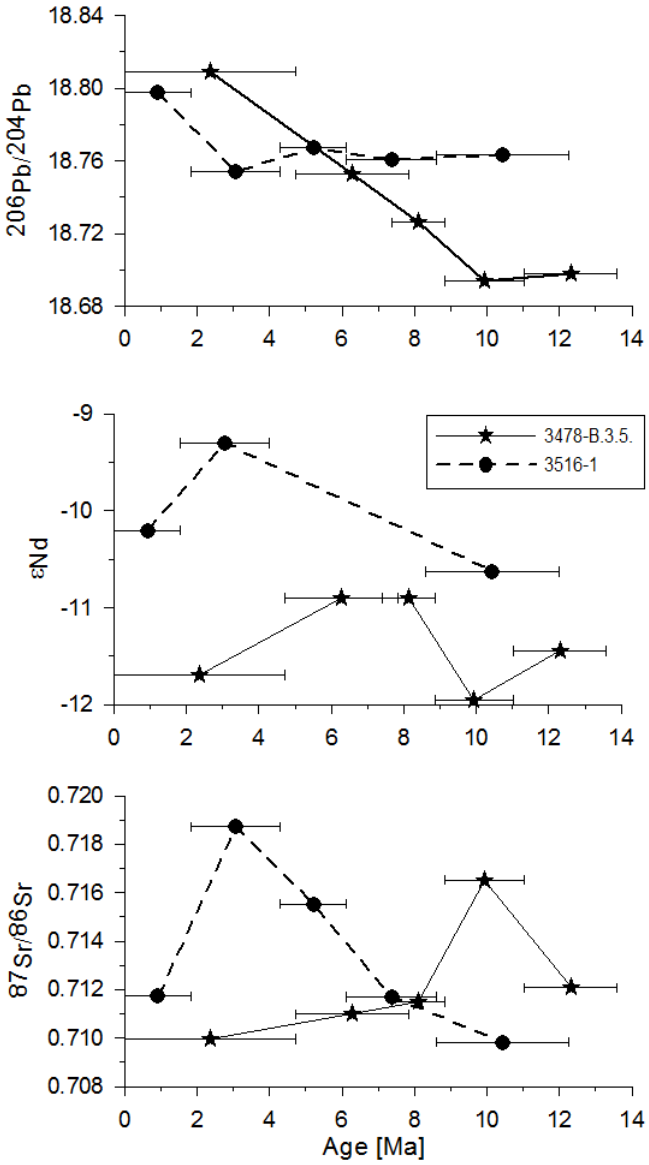

Figure IV.7. Time series of $^{206}Pb/^{204}Pb$ (top), $\varepsilon_{Nd\,(T)}$ (middle) and $^{87}Sr/^{86}Sr$ (bottom) versus age for the two crusts studied. The errors assigned to the ages do not represent analytical uncertainties but reflect the depth range from which the crust material was recovered for each sample of the profiles.

IV.4. Discussion

IV.4.1. Present-day situation

Based on the isotopic compositions of Nd, Sr, and Pb of the detrital fraction the main goal of this study is to identify the possible end-members/sources of the detrital input to our study area. In Table IV.7. we present a compilation of available Sr, Nd, and Pb isotopic signatures of possible source areas which help us to constrain our most likely end-members (Juteau et al., 1986; Abouchami et al., 2013; Scheuvens et al., 2013; Kumar et al., 2014).

Sr-Nd-Pb isotopic composition

In Figure IV.8. we present a comparison of the $^{87}Sr/^{86}Sr$ and ε_{Nd} signatures of the detrital fraction for the crust surfaces and sediment data along with literature data obtained from sediments reflecting the past 20,000 years (Grousset et al., 1988; 1998; Grousset and Biscaye, 2005; Chavagnac et al., 2007; Cole et al., 2009; Meyer et al., 2011; Stumpf et al., 2011; Meyer et al., 2013;) in order to identify the possible sources contributing detrital material to the study area.

The comparison shows that the ε_{Nd} values of the detrital material extracted from the crusts displays a larger range of values (~4 ε_{Nd} units) than that of the sediments. This implies that the sources of the detrital inputs may have been more variable in the past given that the difference probably results from the fact that the ε_{Nd} values in our samples reflect an integrated signal of the detrital inputs over ~1-2 Ma for each sample extracted from the crust surfaces.

The range of the $^{87}Sr/^{86}Sr$ signatures of our sample set is intermediate between the Chavagnac et al. (2007) data for the Anti-Atlas and the MAP Kiel 276 mooring station (Figure IV.8., blue and green vertical bars, respectively) and the data obtained from cores GeoB 4223 and GeoB 6007 off Morocco, which cover the last 12 kyrs (Meyer et al. 2011; 2013) (Figure IV.8., dark orange and orange rectangles, respectively).

On the basis of $^{87}Sr/^{86}Sr$ ratios, two distinct potential end-members exist for our sample set: A more radiogenic source similar to the Iberian Margin sediments (Stumpf et al., 2011) and to African aerosols (Grousset et al., 1998) (pink and orange fields in Figure IV.8.) and a less radiogenic field similar to the composition of Anti-Atlas/MAP Kiel 276 mooring station

(Chavagnac et al., 2007). The Sr isotopes do not allow distinguishing between the Iberian Margin and African aerosol sources (Grousset, personal communication, 2012).

The majority of the detrital sediment samples, and the detrital fractions of four Fe-Mn crust samples, namely 3525-9 (Dacia seamount-Canaries), 3536-3 (Ibn Batouta seamount-Mediterranean), 3709-1 and 3711-2 (both from Tore seamount-Madeira), show the most radiogenic Sr isotope compositions of our data set. The locations of these four Fe-Mn crust samples are generally closer to land and the signature of their detrital fraction may indicate a higher influence of proximal sources when compared to the crusts with less radiogenic values. The samples with less radiogenic Sr isotope values are more similar to the values of Anti-Atlas/Kiel 276 mooring station at the Madeira Abyssal Plain. According to Chavagnac et al. (2007) the possible source region for the Kiel 276 lithogenic particle flux is the Anti-Atlas Paleozoic Moroccan mountain belt, which is the most likely source region of the dust input to our sample locations as well.

When considering the Potential Source Areas (PSA) proposed by Scheuvens et al. (2013) our present-day data seem to indicate a mixture of several different sources (essentially PSA 1, PSA 2, PSA3 and PSA 6) contributing detrital material to our study area, consistent with multiple contributing sources even within one dust event (Skonieczny et al., 2011; 2013).

In Figures IV.9 and IV.10 we present the Pb isotope data of the crust surfaces and sediment samples along with available literature data. The majority of the detrital sediment samples show less radiogenic Pb isotope compositions, with sample 3478-A2 being the least radiogenic. The detrital Pb isotope signatures of the crust surfaces are in general more radiogenic than the sediment detrital data, with sample 3862 from the Azores being the most radiogenic. Our data plot between the data published for Atlantic sediments (Sun, 1980; blue field)/Iberian Margin Sediments (Stumpf et al. 2011; pink field) and NW African granites (Juteau et al. 1986; orange field and the two orange triangles-outliers) and a mix between these two end-members can explain our data in Pb-Pb isotope space (Atlantic sediments/Iberian Margin sediments *vs.* NW African granites). This is consistent with the above interpretation of Sr and Nd isotope data.

Table IV.7. Pb, Nd and Sr isotopic signatures' compilation of possible source areas contributing material to our study area

Potential Source Region		Geographic Area	Geology	$^{87}Sr/^{86}Sr$	$\varepsilon_{Nd}(0)$	$^{206}Pb/^{204}Pb$	$^{207}Pb/^{204}Pb$	$^{208}Pb/^{204}Pb$	ref.
PSA 1 < 0,720 / -13,5 to -9,5		Tunisia and northern Algeria	Tell Atlas: young orogenic mountain chain - Mesozoic	0,714-0,717	-13,5 to -9,5				1
PSA2 > 0,720 / < -13,5	PSA 2a	Foothills of Atlas Mountains	Anti-Atlas: Pre-Cambrian and lower Paleozoic	0,720-0,738	-17,9 to -13,5				1
	PSA 2b	Western Sahara, western Mauritania	basement rocks lowest						
PSA 3		Southern Algeria and Northern Mali		(0,721-0,726)	-12,4 to -12,1				1
PSA 4		Central Libya		0,715	-15,4 to -10,7				1
PSA 5		Western Chad incl. Bodélé depression		No data	-12,7				1
PSA 6		Southern Egypt, northern Sudan		0,706-0,718	-11,0 to -3,9				1
		Chad, Faya Largeau	Dust	0,715799	-11,1	18,6088	15,6819	38,6898	2
		Chad, Bodélé Depression "Si-rich component"	Deflatable diatomite lake-bed sediments	0,7276	-12,8	19,2060	15,7930	39,6480	2
		Chad, Bodélé Depression "Ca-rich component"	Sand-diatomite mixed material	0,7147	-10,1	18,9214	15,7198	39,263	2
		Mali	Soil	0,72087	-14,2	18,2830	15,6559	38,5548	3
		Mauritania	Soil	0,72312	-28,0	18,6561	15,7492	39,0615	3
		NW Africa	Granites	0,71453-0,81412	-9,6 to -8,9	18,704-19,222	15,623-15,684	38,645-38,905	4

References: 1-Scheuvens et al. (2013); 2- Abouchami et al. (2013); 3- Kumar et al. (2014); 4- Juteau et al. (1986).

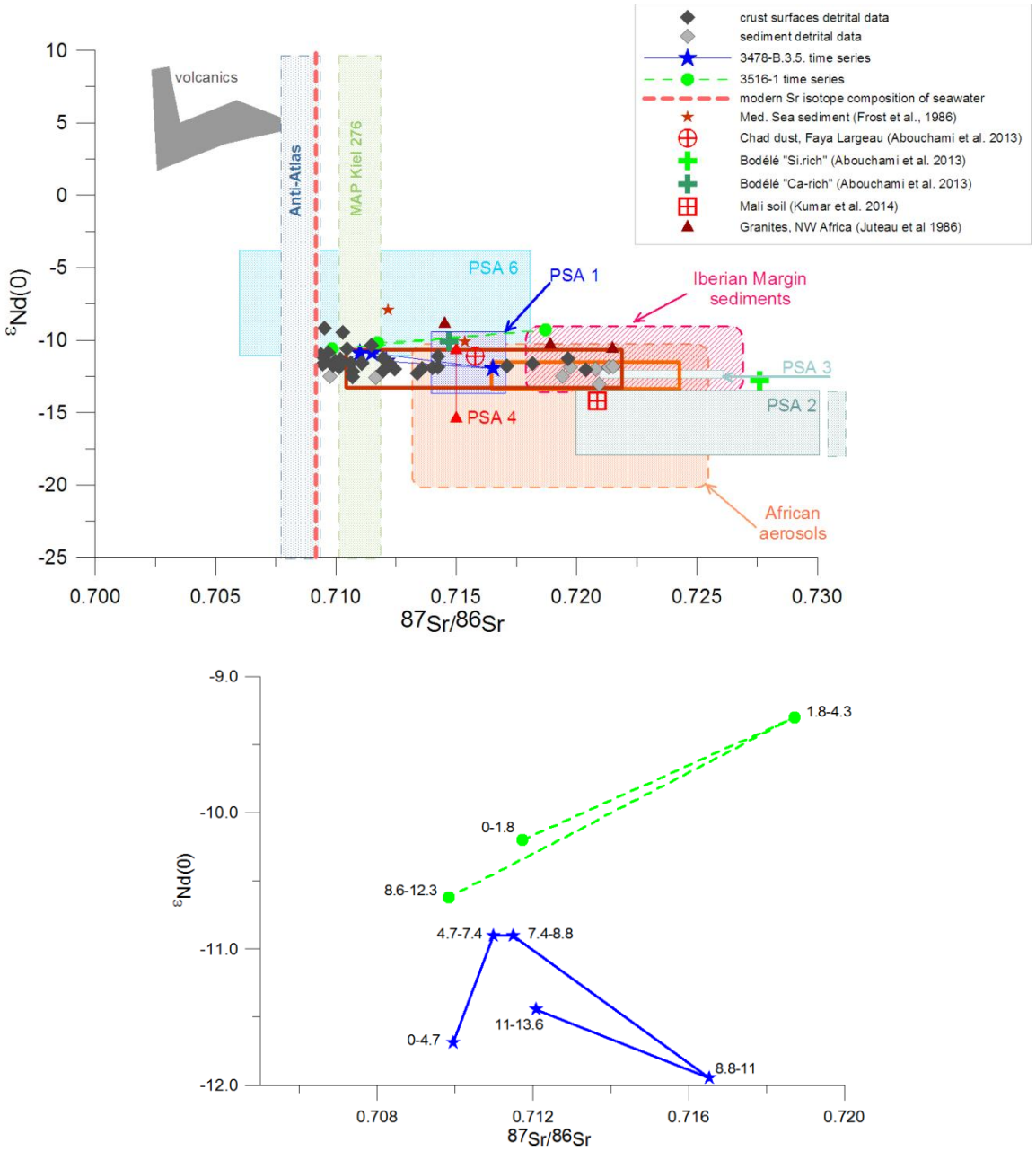

Figure IV.8. Upper plot: $^{87}Sr/^{86}Sr$ vs. ε_{Nd} plot including the data from this study and potential end member sources. $^{87}Sr/^{86}Sr$ Anti-Atlas field data and MAP Kiel 276 data (blue and green vertical bars) from Chavagnac et al. (2007, and references therein); Iberian margin sediments data (pink field) from Stumpf et al. (2011) and Grousset et al. (1998); Med. Sea sediment from Frost et al. (1986); African Aerosols data (orange field) from Grousset et al. (1992; 1998) and Grousset and Biscaye (2005). Sediments off Morocco from Meyer et al. (2011; dark orange field) and Meyer et al. (2013; orange field). Potential Source Areas (PSA) from Scheuvens et al. (2013; Table IV.7). Volcanics data (grey field) from Geldmacher et al. (2006). Other data please refer to "Legend". Lower plot: Close-up of our time series data.

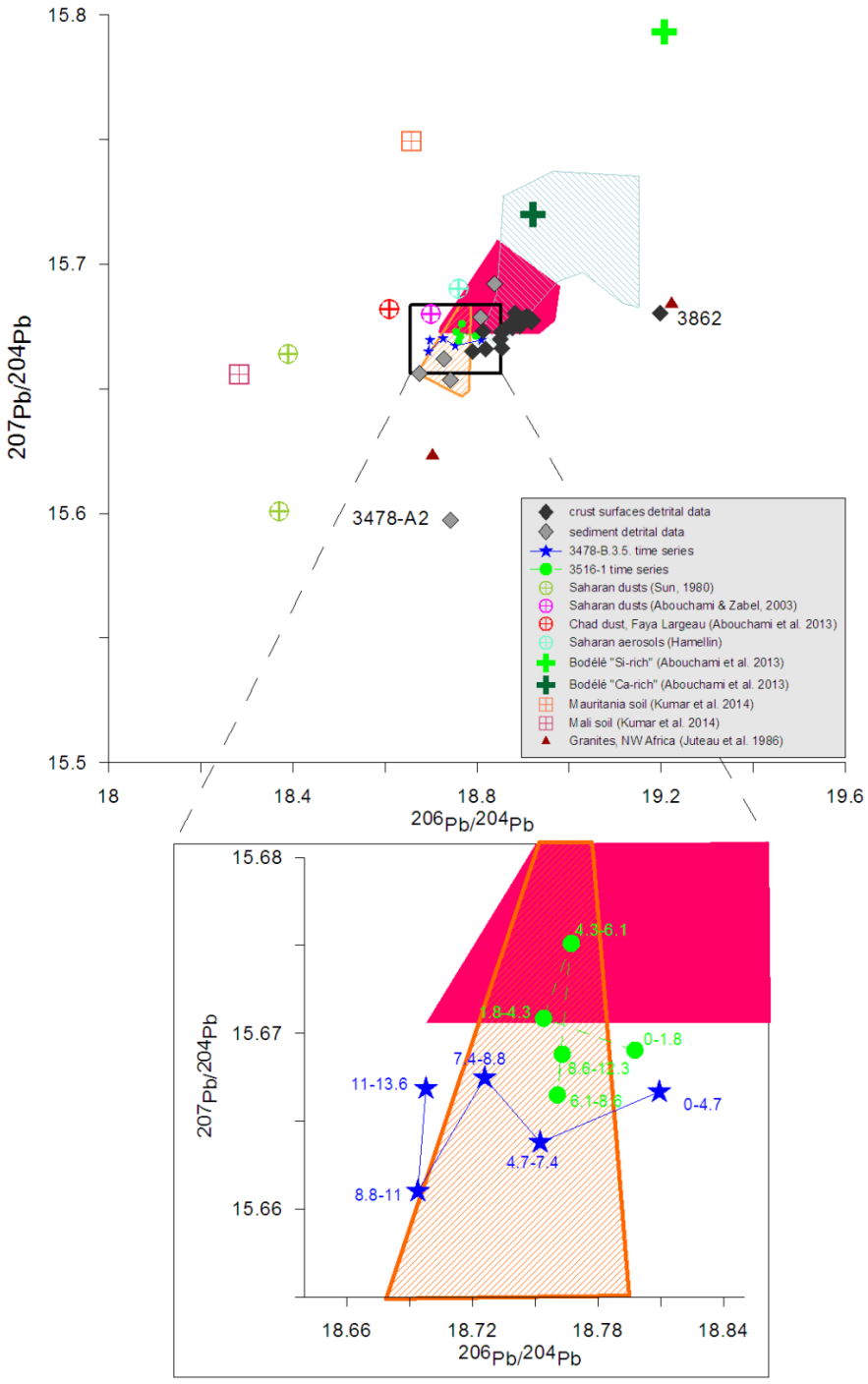

Figure IV.9. Upper plot: $^{206}Pb/^{204}Pb$ vs. $^{207}Pb/^{204}Pb$ plot including the data from this study and potential end member sources. Atlantic sediment Pb data (blue field) from Sun (1980); Iberian Margin sediments data (pink field) from Stumpf al. (2011); NW African Granites Pb data (orange field, complemented by dark orange triangles ("outliers") from Juteau et al (1986). Other data please refer to "Legend". Lower plot: Close-up of our time series data.

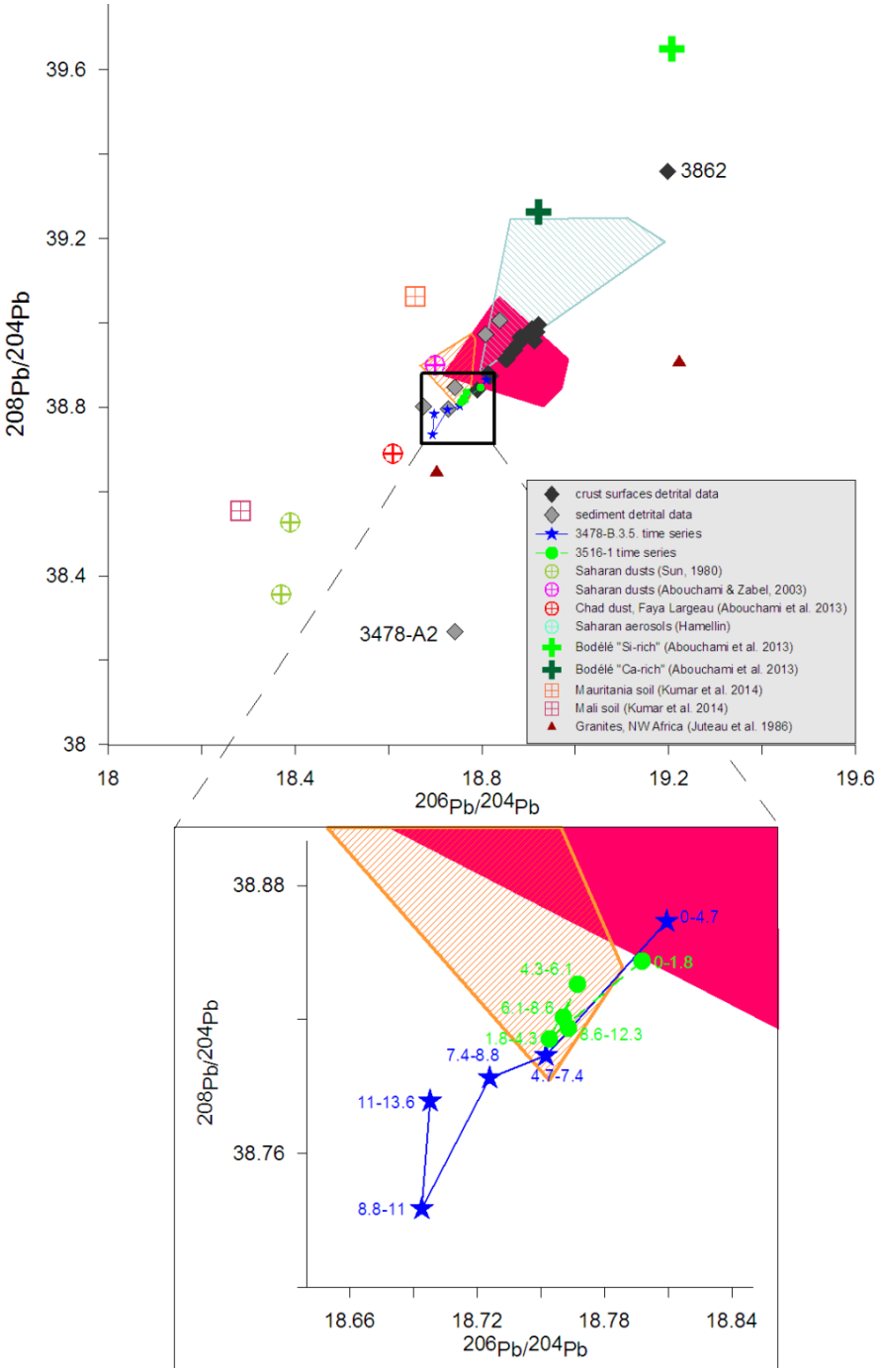

Figure IV.10. Upper plot: $^{206}Pb/^{204}Pb$ vs. $^{208}Pb/^{204}Pb$ plot including the data from this study and potential end member sources. Atlantic sediment Pb data (blue field) from Sun (1980); Iberian Margin sediments data (pink field) from Stumpf al. (2011); NW African Granites Pb data (orange field, complemented by dark orange triangles ("outliers") from Juteau et al (1986). Other data please refer to "Legend". Lower plot: Close-up of our time series data.

Our Sr-Nd-Pb isotopic data indicate a predominantly North African source. This is consistent with Abouchami et al. (2013) who pointed out that the majority of the tracer studies related to dust fluxes downwind of the Saharan plume indicate a North African region, such as Algeria, Mauritania, and Morocco, as the source.

IV.4.2. Time-series

Sr-Nd-Pb isotopic evolution

Considering the time-series data (close-up in Figures IV.8. -IV. 10.) the majority of the time series data plots in the field of the least radiogenic samples. However, and considering Figure IV.8. (close–up) both crusts show a peak towards more radiogenic Sr isotope compositions although at different times. Crust 3478-B.3.5 from the Nameless seamount shows a radiogenic Sr isotope peak about 10 Ma (time interval 11-8.8 Ma), whereas crust 3516-1 from the Lion seamount shows a peak at 3.1 Ma (time interval 4.3-1.8 Ma). Considering the Pb-Pb isotope space (Figure IV.9, close up) solely crust 3516-1 shows a peak towards more radiogenic compositions (Atlantic sediments/Iberian Margin sediments) but again with a different timing: 5.2 Ma (time interval 6.1-4.3 Ma).

In terms of $^{87}Sr/^{86}Sr$ ratios, this indicates a change from prevailing contributions from the Anti-Atlas/Moroccan sources to an Iberian Margin/African aerosol source. Considering the fact that the variations in both $^{87}Sr/^{86}Sr$ and the ε_{Nd} signatures correspond to the same changes in the source rocks (Meyer et al. 2013 and references therein) the different ε_{Nd} signature trends of each crust indicates that the source of the detrital input was somewhat different at ~3.1 Ma (closer to the Iberian Margin field) and at ~9.9 Ma (closer to African aerosols field).

These isotope excursion events occurred before and after the Mediterranean Salinity Crisis. The progressive restriction of the Thethys-Indian passage, which culminated in the isolation of the Mediterranean Sea from the Indian Ocean resulted in its final closure by the early Tortonian (~11 Ma) (Abrantes et al., 2012 and references therein). From ~11 Ma until ~7.25 Ma the connection between the Mediterranean and the Atlantic was represented by two small and shallow gateways: The Betic (southern Spain) and the Rifian (northern Morocco) corridors (e.g. Duggen et al., 2003 and references therein). As Africa and Europe

continued to converge, those paleocorridors closed completely and resulted in the Messinian Salinity Crisis between 5.96 and 5.33 Ma (Krijgsman et al., 1999). By 5.33 Ma the Strait of Gibraltar opened, either by global sea level rise at the end of the Miocene or by tectonics and erosion, and subsequently Atlantic waters flooded the Mediterranean again (e.g. Abrantes et al., 2012). Evidence for the opening of the Strait of Gibraltar and the initiation of the outflow of Mediterranean Water into the North Atlantic can be found in sediments from the Gulf of Cadiz (e.g. Hernández-Molina et al., 2014), and the continuous deposition of the Faro drift contourite deposit suggests that the Mediterranean Outflow Water (MOW) has prevailed at least since the early Pliocene (Abrantes et al., 2012).

For the ~3.1 Ma peak recorded by crust 3516-1 (Lion Seamount) a possible interpretation is that during the period from 4.3 to 1.8 Ma, distinct tectonic and paleoceanographic events took place in the Atlantic area. The closure of the Panama gateway, starting at around 12.5 Ma and with final closure at ~3 Ma (Murdock et al., 1997 and references therein; Osborne et al., 2014) led to major changes of the thermohaline circulation in the Atlantic Ocean, which culminated in the NHG at ~2.7 Ma ago (Raymo et al., 1992; Lunt et al., 2008). Moreover, Khélifi et al. (2009; 2014) suggested an intensification of the Mediterranean Outflow ~3.5-3.3 Ma ago as a result of major aridification of the Mediterranean region. It was also suggested by Khélifi et al. (2014) that an increase in salinity during that time period could have led to the lowering of the MOW plume by ~500 m. Additionally, and as reported by Hernandez-Molina et al. (2014), since the late Pliocene larger volumes of MOW circulating into the North Atlantic caused major depositional hiatuses, which are directly related to regional tectonic events and changes in the global thermohaline circulation. In fact, one of those major depositional hiatuses (3.2-3.0 Ma) occurred within the time period of the excursion in crust 3516-1 from Lion seamount. Hernandez-Molina et al. (2014) related that period of MOW intensification to the widespread circulation of NEADW.

The ~9.9 Ma (time interval 11-8.8 Ma) peak in crust 3478-B.3.5. may correspond to a major glacial-style period between 13 and ~9.5 Ma as referred to by Sarnthein et al. (1982), and the Saharan aerosol source signature of that event related to the gradual southward shift of the wind systems due to the Neogene northward drift of Africa. Additionally, the event was also concomitant with periods of deformation, exhumation, and erosion of the Atlas Mountains that occurred during the middle and late Miocene (Guímera et al., 2011; Ruiz et al., 2011; Ali et al., 2014).

Additionally, during glacial periods, the exposure of continental shelves, as a consequence of the lowering of sea level, contributed large amounts of terrigenous material to the deep ocean (e.g. Sarnthein and Diester-Haass, 1977).

Whether these isotope excursion events reflect "pure" glacial (dry) signal or a "pure" "tectonic" signal, is hard to unambiguously distinguish. Likely these events reflect a combination of both, as major tectonic changes influenced climate and hydrography, and by consequence, sedimentation along continental margins. In fact, one might argue that these distinct events that we observe in our record result from changes in the detrital material incorporated by the crusts resulting from changes in the prevailing circulation patterns caused by these major tectonic events.

The two peaks in the crusts are distinctly different taking into account that the growth rates are not significantly different between crusts (~1mm/Ma difference) for the considered period of time (~12 Ma). In addition the older peak is also present in the depth profile of the second crust 3476-B.3.3. from Nameless seamount (not dated) which closely resembles the isotopic record of crust 3478-B.3.5. from the same location. The fact that the two crust time series do not record radiogenic Sr peaks at the same time can result from a number of different factors, which are discussed below.

First, and considering the large amounts of time integrated by the sampling intervals it is not possible to ascribe a "true age" of an event: Possibly the simplest explanation for the ~10 Ma peak is to consider that the starting age of accretion of the Lion crust is not old enough to record that event- it may be possible that the event is even older than 10 Ma and so the Lion crust, being younger than that event, did not record the Sr isotope excursion. The same is true for the sampling intervals for the 3.1 Ma peak; if the first two intervals were merged (7 mm; 4.3 Ma) and reflect a similar period of time as the first interval of the Nameless seamount crust (7 mm; 4.7 Ma), the 3.1 Ma peak may have been missed.

Recent studies of the Sr isotope record of marine sediments proposed that the temporal Sr isotope variations are not only a function of the source but can also vary as a function of the weathering intensity and the type (chemical *versus* physical) of the weathering regimes (e.g. Blum and Erel, 2003; Jung et al., 2004; Colin et al., 2006; Meyer et al., 2011; 2013). It was suggested that low $^{87}Sr/^{86}Sr$ ratios of marine sediments are a consequence of more chemical weathering, which is dominant during humid periods, whereas higher $^{87}Sr/^{86}Sr$ ratios result

from a period of predominantly physical weathering, such as during arid conditions (Jung et al., 2004). Consequently physical weathering was dominant during glacial periods and resulted in higher $^{87}Sr/^{86}Sr$ ratios in the detrital fraction of the marine sediments, whereas during interglacial periods chemical weathering was dominant and the $^{87}Sr/^{86}Sr$ ratios were lower (e.g. Cole et al., 2006). As both peaks suggest arid (glacial) climatic conditions, probably the Sr isotope variations were controlled by mineral and/or grain-size sorting rather than by changes in the weathering regimes. In fact, the sorting of minerals or particle sizes can lead to marked isotope variations within a single source (cf. Goldstein and Hemming, 2003). In addition, minerals such as micas generally have high Rb/Sr ratios whereas feldspars have low Rb/Sr. The result of mineral sorting during transport by different sediment-transport mechanisms (e.g, ocean currents, wind) can lead to significant isotopic heterogeneities that are not related to particular source areas of the minerals (Goldstein and Hemming, 2003). In addition, coarse-grained material is generally enriched in Sr relative to Rb what leads to lower $^{87}Sr/^{86}Sr$ ratios. In contrast, fine-grained material is enriched in Rb relative to Sr, which results in higher $^{87}Sr/^{86}Sr$ ratios (Eisenhauer et al., 1999; Meyer et al., 2011). Under negligible chemical weathering conditions, Eisenhauer et al. (1999) showed that the Rb/Sr isotope systematics mainly reflects the average age of the source rocks and that the initial isotope ratio reflects the geological origin. This is consistent with (clay-rich) dust export to marine sediments under glacial (dry) conditions.

Additionally, several authors (e.g. Bozzano et al., 2002) acknowledge the difficulty in resolving the variability of dust source areas in time series studies, which is even greater when dealing with longer time scales.

Besides these effects of mineral sorting and incongruent weathering, the interaction of water masses with seamounts generates turbulent mixing and seamount-specific currents, such as Taylor columns, trapped waves, internal waves, etc., which influence the way sediments are deposited on and around the seamounts. These local physical oceanographic processes may play an important role in sediment dynamics and therefore for the interpretations of regional records like those addressed here (Hein et al., 2000; Turnewitsch et al., 2013). Depending on the shape of the seamount and its orientation relative to the impacting water masses, the patterns of sedimentation on adjacent seamounts can be vastly different. Turnewitsch et al. (2013) suggested that the reconstruction of paleo-flow in paleoceanographic studies may reflect variability in the higher-frequency paleo-flow

components rather than variability in the basin-scale net-flow component. These seamount-generated currents can influence sedimentation, erosion, and resuspension of the detrital material (Turnewitsch et al., 2013) and also re-suspend older sediment through slumping (Kayen et al., 1989).

In fact, during SO-83 Marflux 4 Cruise (Halbach and Scientific Crew, 1993), three seamounts on the northeast Atlantic were studied (Lion, Ampére and Tropic seamounts). The goal of the cruise/study was to obtain information on the variation of material fluxes from the water column to the seafloor and how the local oceanographic and morphologic conditions control the precipitation of authigenic deposits and of pelagic sedimentation. According to the SO-83 Marflux 4 Cruise report (Halbach and Scientific Crew, 1993), the steepest flanks of Lion Seamount are on the southern part of the area and so not too much sediment is expected to accumulate in those areas; sediment accumulation is greater on small plateaus along their northeastern slope. The SO-83 Marflux 4 core sites on Lion seamount covered different regions, depths, and environments; the southern areas face the open-ocean whereas the northeast flank (facing the Horseshoe Abyssal Plain-HAP) is more influenced by continental and Mediterranean sources (Halbach and Scientific Crew, 1993). The same should be valid for Nameless seamount which faces Lion seamount to the West and the HAP to the northeast.

Considering the present-day oceanographic setting of the area (Reid, 1978; Schmitz and McCartney, 1993; Ambar et al., 1999), the water-mass movements include the surface Azores Current from the West, an intermediate-depth flow of MOW from the West, and a deep-water flow from North-northwest (North Atlantic Deep Water for depths between ~1,600 to 4,000 m) and southwest/South (Antarctic Bottom Water for depths greater than 4,000 m). Considering these present-day currents impinging on the seamounts, we may expect that at ~1,800 m, where the samples are from, there should be (little) deposition on the summit and erosion, non-deposition, or resuspension on the flanks.

In summary, all the factors discussed above may contribute to an explanation for the distinct records we find in our crusts and more specifically in our time-series records. These are certainly complicating factors, but a plethora of papers have shown that regional and global paleoceanographic events can be recorded in crusts (e.g., Frank et al., 1999 and references therein). Furthermore, and considering the range of values for our crust surfaces, sediments

and time-series, the observed isotope excursions are not that pronounced and we consider the explanations presented above to be feasible in accounting for the differences found.

IV.5. Conclusions

We have studied the radiogenic isotope composition of Pb, Nd and Sr of the detrital silicate fraction of hydrogenetic Fe-Mn crusts and nearby sediments to try to reconstruct the continental inputs of detrital material in the NE Atlantic over the past ~12 Ma and the past climatic changes responsible for our records.

The first goal of our study was to demonstrate that the isotopic composition of the detrital fraction of the crusts represents Saharan dust input. Based on our data it is likely that the majority of the detrital inputs have been derived from Saharan dust fluxes, in particular from northern African source areas. In fact, the long-term isotopic evolution presented by the crusts can be explained by two end-members: The Anti-Atlas/North African Granites (less radiogenic) and the African aerosols/Atlantic-Iberian Margin sediments (radiogenic).

Despite the low resolution of our time series, the distinct variations we observe in our record were the result of changes in the detrital material incorporated by crusts, which likely resulted from changes in the prevailing circulation caused by major tectonic events. Also, the range of values for our crust surfaces, sediments and time-series, are not very large but do not likely reflect local conditions, rather they most probably represent a regional signal.

Overall, and most importantly, our data show that the prevailing climatic conditions over the past 12 Ma have not changed significantly and thus climate in North Africa, in particular the dry conditions, have been a long standing feature of the past up to 12 Ma as already pointed out by Tiedemann et al. (1994) for the past 5 Ma.

Acknowledgments

We thank the Portuguese Science and Technology Foundation (FCT) for financial support through Project PDCT/MAR/56823/2004; FCT also supported a fellowship to S.B.M. (SFRH/BD/22263/2005) co-financed by POCI 2010/EU. We would also like to thank GRICES (Portugal) and DAAD (Germany) for traveling support. Additional support to S.B.M. was provided by LNEG and IPMA fellowships. We acknowledge K. Hoernle, the crew and scientific party of Meteor M51/1 cruise as well as the Deutsche Forschungsgemeinschaft (DFG, German Research Council) for funding. We acknowledge J. Girardeau, the onboard scientific team, the University of Nantes and the French INSU-CNRS Institute for the financial support that made possible the collection of the samples from the Tore-Madeira Cruise and for kindly having made these samples available for this work. We also thank the co-chiefs of the TTR-11 Cruise, the onboard team and the UNESCO –IOC TTR Program for the samples collected during the TTR-11 cruise, which was funded by INGMAR Project (FCT). We thank F. Grousset for his help with the interpretation of Pb and Nd end-members. We also thank S. M. Lebreiro, L. M. Pinheiro for their help and discussions.

References

Abouchami, W., Galer, S.J.G. and Koschinsky, A., 1999. Pb and Nd isotopes in NE Atlantic Fe-Mn crusts: proxies for metal paleosources and paleocean circulation. *Geochimica et Cosmochimica Acta*, 63(10): 1489-1505.

Abouchami, W. et al., 2013. Geochemical and isotopic characterization of the Bodélé Depression dust source and implications for transatlantic dust transport to the Amazon Basin. *Earth and Planetary Science Letters*, 380: 112-123.

Abouchami, W. and Zabel, M., 2003. Climate forcing of the Pb isotope record of terrigenous input into the Equatorial Atlantic. *Earth and Planetary Science Letters*, 213(3-4): 221-234.

Abrantes, F. et al., 2012. 1 - Paleoclimate Variability in the Mediterranean Region. In: P. Lionello (Editor), *The Climate of the Mediterranean Region*. Elsevier, Oxford, pp. 1-86.

Albarède, F. et al., 2004. Precise and accurate isotopic measurements using multiple-collector ICPMS. *Geochimica et Cosmochimica Acta*, 68(12): 2725-2744.

Ali, S. et al., 2014. The provenance of Cretaceous to Quaternary sediments in the Tarfaya basin, SW Morocco: Evidence from trace element geochemistry and radiogenic Nd-Sr isotopes. *Journal of African Earth Sciences*, 90: 64-76.

Ambar, I., Armi, L., Bower, A. and Ferreira, T., 1999. Some aspects of time variability of the Mediterranean Water off south Portugal. *Deep-Sea Research I*, 46: 1109-1136.

Banakar, V.K., Galy, A., Sukumaran, N.P., Parthiban, G. and Volvaiker, A.Y., 2003. Himalayan sedimentary pulses recorded by silicate detritus within a ferromanganese crust from the Central Indian Ocean. *Earth and Planetary Science Letters*, 205(3-4): 337-348.

Bayon, G. et al., 2002. An improved method for extracting marine sediment fractions and its application to Sr and Nd isotopic analysis. *Chemical Geology*, 187(3-4): 179-199.

Biscaye, P.E. et al., 1997. Asian provenance of glacial dust (stage 2) in the Greenland Ice Sheet Project 2 Ice Core, Summit, Greenland. *Journal of Geophysical Research: Oceans*, 102(C12): 26765-26781.

Blum, J.D. and Erel, Y., 2003. 5.12 - Radiogenic Isotopes in Weathering and Hydrology. In: E.-i.-C.H.D. Holland and K.K. Turekian (Editors), *Treatise on Geochemistry*. Pergamon, Oxford, pp. 365-392.

Bozzano, G., Kuhlmann, H. and Alonso, B., 2002. Storminess control over African dust input to the Moroccan Atlantic margin (NW Africa) at the time of maxima boreal summer insolation: a record of the last 220 kyr. *Palaeogeography, Palaeoclimatology, Palaeoecology*, 183(1-2): 155-168.

Chavagnac, V. et al., 2007. Anti-Atlas Moroccan Chain as the source of lithogenic-derived micronutrient fluxes to the deep Northeast Atlantic Ocean. *Geophysical Research Lett*ers, 34(21): L21604.

Chmeleff, J., von Blanckenburg, F., Kossert, K. and Jakob, D., 2010. Determination of the 10Be half-life by multicollector ICP-MS and liquid scintillation counting. *Nuclear Instruments and Methods in Physics Research Section B: Beam Interactions with Materials and Atoms*, 268(2): 192-199.

Cohen, A.S., O'Nions, R.K., Siegenthaler, R. and Griffin, W.L., 1988. Chronology of the pressure-temperature history recorded by a granulite terrain. *Contributions to Mineralogy and Petrology*, 98(3):303-311. doi: 10.1007/BF00375181.

Cole, J.M., deMenocal, P.B., Goldstein, S.L. and Hemming, S.R., 2006. Terrigenous evidence from marine sediments for deglacial climate variability in Africa. *Geochimica et Cosmochimica Acta*, 70(18): A107.

Cole, J.M., Goldstein, S.L., deMenocal, P.B., Hemming, S.R. and Grousset, F.E., 2009. Contrasting compositions of Saharan dust in the eastern Atlantic Ocean during the last deglaciation and African Humid Period. *Earth and Planetary Science Letters*, 278(3-4): 257-266.

Duggen, S., Hoernle, K., van den Bogaard, P., Rupke, L. and Phipps Morgan, J., 2003. Deep roots of the Messinian salinity crisis. *Nature*, 422(6932): 602-606.

Eisenhauer, A. et al., 1999. Grain size separation and sediment mixing in Arctic Ocean sediments: evidence from the strontium isotope systematic. *Chemical Geology*, 158(3-4): 173-188.

Frank, M., 2002. Radiogenic isotopes: tracers of past ocean circulation and erosional input. *Reviews of Geophysics*, 40(1): 1-38.

Frank, M., O'Nions, R.K., Hein, J.R. and Banakar, V.K., 1999. 60Myr records of major elements and Pb-nd isotopes from hydrogenous ferromanganese crusts: Reconstruction of seawater paleochemistry. *Geochimica et Cosmochimica Acta*, 63(11/12): 1689-1708.

Frost, C.D., O'Nions, R.K. and Goldstein, S.L., 1986. Mass balance for Nd in the Mediterranean Sea. *Chemical Geology*, 55(1-2): 45-50.

Galer, S.J.G. and O'Nions, R.K., 1989. Chemical and isotopic studies of ultramafic inclusions from the San Carlos volcanic field, Arizona: a bearing on their petrogenesis. *Journal of Petrology*, 30: 1033-1064.

Garbe-Schönberg, C.-D., 1993. Simultaneous determination of thirty-seven trace elements in twenty-eight international rock standards by ICP-MS. *Geostandards Newsletter*, 17(1): 81-97.

Geldmacher, J. et al., 2006. Origin and geochemical evolution of the Madeira-Tore Rise (eastern North Atlantic). *Journal of Geophysical Research*, 111: B09206, doi:10.1029/2005JB003931.

Goldstein, S.L. and Hemming, S.R., 2003. 6.17 - Long-lived Isotopic Tracers in Oceanography, Paleoceanography, and Ice-sheet Dynamics. In: E.-i.-C.H.D. Holland and K.K. Turekian (Editors), *Treatise on Geochemistry*. Pergamon, Oxford, pp. 453-489.

Grousset, F.E. and Biscaye, P.E., 2005. Tracing dust sources and transport patterns using Sr, Nd and Pb isotopes. *Chemical Geology*, 222: 149-167.

Grousset, F.E., Biscaye, P.E., Zindler, A., Prospero, J. and Chester, R., 1988. Neodymium isotopes as tracers in marine sediments and aerosols: North Atlantic. *Earth and Planetary Science Letters*, 87: 367-378.

Grousset, F.E. et al., 1998. Saharan wind regimes traced by the Sr-Nd isotopic composition of subtropical Atlantic sediments: Last Glacial maximum vs Today. *Quaternary Science Reviews*, 17(4-5): 395-409.

Grousset, F.E., Rognon, P., Coudé-Gaussen, G. and Pédemay, P., 1992. Origins of peri-saharan dust deposits traced by their Nd and Sr isotopic composition. *Palaeogeography, Palaeoclimatology, Palaeoecology*, 93: 203-212.

Guímera, J., Arboleya, M.L. and Teixell, A., 2011. Structural control on present-day topography of a basement massif: the Central and Eastern Anti-Atlas (Morocco). *Geologica Acta*, 9(1): 55-65. doi: 10.1344/105.000001643.

Halbach, P. and Crew, S., 2003. Marine geological and geochemical investigations of sediments, precipitates and hard rocks from three seamounts in the NE Atlantic to identify element fluxes. *Technical cruise report of the RV Sonne cruise SO 83* - MARFLUX 4; BMFT project 03R424A6 and MAST contract 0022C. Freie Universitat Berlin, Berlin, 166 pp.

Hamilton, R.A., Archbold, J.W. and Douglas, C.K.M., 1945. Meteorology of Nigeria and adjacent territory. *Quarterly Journal of the Royal Meteorological Society*, 71(309-310): 231-264.

Hein, J.R. et al., 2000. Cobalt-Rich ferromanganese crusts in the Pacific. In: D.S.Cronan (Editor), *Handbook of Marine Mineral Deposits*. CRC Press, pp. 239-279.

Hein, J.R. et al., 1997. Iron and manganese oxide mineralization in the Pacific. In: K. Nicholson, J.R. Hein, J.R. Bühn and S. Dasgupta (Editors), *Manganese Mineralization: Geochemistry and mineralogy of terrestial and marine deposits. Geological Society Special Publication 119*, pp. 123-138.

Henken-Mellies, W.U. et al., 1990. ^{10}Be and ^{9}Be in South Atlantic DSDP Site 519: Relation to geomagnetic reversals and to sediment composition. *Earth and Planetary Science Letters*, 98(3-4): 267-276.

Hernández-Molina, F.J. et al., 2014. Onset of Mediterranean outflow into the North Atlantic. *Science*, 344(6189): 1244-1250.

Hoernle, K. and Party, S., 2003. Cruise Report M51/1. In: C. Hemleben, K. Hoernle, B.B. Jorgensen and W. Roether (Editors), *Ostatlantik - Mittelmeer - Schwarzes Meer, Cruise No. 51 - 28 December 2001*., Hamburg, pp. 3-35.

Holz, C., Stuut, J.-B.W., Henrich, R.d. and Meggers, H., 2007. Variability in terrigenous sedimentation processes off northwest Africa and its relation to climate changes: Inferences from grain-size distributions of a Holocene marine sediment record. *Sedimentary Geology, From Particle Size to Sediment Dynamics*, 202(3): 499-508.

Huneeus, N. et al., 2011. Global dust model intercomparison in AeroCom phase I. *Atmospheric Chemistry and Physics*. J1 - ACP, 11(15): 7781-7816.

I.O.C.-Intergovernmental.Oceanographic.Commission, 2002. Geological Processes in the Mediterranean and Black Seas and North East Atlantic. *Preliminary results of investigations during the TTR-11 cruise of RV Professor Logachev, July-September, 2001*. In: N.H. Kenyon, M.K. Ivanov, A.M. Akhmetzhanov and G.G. Akhmanov (Editors). IOC Technical Series. UNESCO, pp. 89.

Jung, S.J.A., Davies, G.R., Ganssen, G.M. and Kroon, D., 2004. Stepwise Holocene aridification in NE Africa deduced from dust-borne radiogenic isotope records. *Earth and Planetary Science Letters*, 221(1-4): 27-37.

Kayen, R.E. et al., 1989. Morphology of sea-floor landslides on Horizon Guyot: application of steady-state geotechnical analysis. *Deep Sea Research Part A. Oceanographic Research Papers*, 36(12): 1817-1839.

Khélifi, N. et al., 2009. A major and long-term Pliocene intensification of the Mediterranean Outflow, 3.5-3.3 Ma ago. *Geology*, 37: 811-814.

Khélifi, N., Sarnthein, M., Frank, M., Andersen, N. and Garbe-Schönberg, D., 2014. Late Pliocene variations of the Mediterranean outflow. *Marine Geology*, 357: 182-194.

Klemm, V., Levasseur, S., Frank, M., Hein, J.R. and Halliday, A.N., 2005. Osmium isotope stratigraphy of a marine ferromanganese crust. *Earth and Planetary Science Letters*, 238(1-2): 42-48.

Krijgsman, W., Hilgen, F.J., Raffi, I., Sierro, F.J. and Wilson, D.S., 1999. Chronology, causes and progression of the Messinian salinity crisis. *Nature*, 400: 652-655.

Kubik, P.W. and Christl, M., 2010. ^{10}Be and ^{26}Al measurements at the Zurich 6 MV Tandem AMS facility. *Nuclear Instruments and Methods in Physics Research Section B: Beam Interactions with Materials and Atoms*,

Proceedings of the Eleventh International Conference on Accelerator Mass Spectrometry, 268(7-8): 880-883.

Kumar, A. et al., 2014. A radiogenic isotope tracer study of transatlantic dust transport from Africa to the Caribbean. *Atmospheric Environment*, 82: 130-143.

Lunt, D., Valdes, P., Haywood, A. and Rutt, I., 2008. Closure of the Panama Seaway during the Pliocene: implications for climate and Northern Hemisphere glaciation. *Climate Dynamics*, 30(1): 1-18. doi: 10.1007/s00382-007-0265-6.

Merle, R., 2006. Age and origin of Tore-Madeira Rise: beginning of Atlantic Ocean spreading or hotspot track. Petrology, geochemistry, U-Pb geochronology and Pb-Sr-Hf isotopes. PhD Thesis, University of Nantes, Nantes (in French).

Meyer, I., Davies, G.R. and Stuut, J.-B.W., 2011. Grain size control on Sr-Nd isotope provenance studies and impact on paleoclimate reconstructions: An example from deep-sea sediments offshore NW Africa. *Geochemistry, Geophysics, Geosystems*, 12(3): Q03005.

Meyer, I., Davies, G.R., Vogt, C., Kuhlmann, H. and Stuut, J.-B.W., 2013. Changing rainfall patterns in NW Africa since the Younger Dryas. *Aeolian Research*, 10: 111-123.

Middleton, N.J. and Goudie, A.S., 2001. Saharan dust: sources and trajectories. *Transactions of the Institute of British Geographers*, 26(2): 165-181.

Murdock, T.Q., Weaver, A.J. and Fanning, A.F., 1997. Paleoclimatic response of the closing of the Isthmus of Panama in a coupled ocean-atmosphere model. *Geophysical Research Letters*, 24(3): 253-256.

Osborne, A.H. et al., 2014. The seawater neodymium and lead isotope record of the final stages of Central American Seaway closure. *Paleoceanography*, 29(7): 2014PA002676.

Prospero, J.M., 1981. Eolian transport to the World Ocean. In: C.E. Emiliani (Editor), *The Oceanic Lithosphere*. Wiley Interscience, New York, pp. 801-874.

Prospero, J.M. and Carlson, T.N., 1981. Saharan Air Outbreaks Over the Tropical North Atlantic. In: G.H. Liljequist (Editor), *Weather and Weather Maps. Contributions to Current Research in Geophysics*. Birkhäuser Basel, Basel, pp. 677-691. doi:10.1007/978-3-0348-5148-0_17.

Prospero, J.M., Ginoux, P., Torres, O., Nicholson, S.E. and Gill, T.E., 2002. Environmental Characterization of global sources of atmospheric soil dust identified with the Nimbus 7 Total Ozone Mapping Spectrometer (TOMS) absorbing aerosol product. *Reviews of Geophysics*, 40(1): 1002.

Prospero, J.M. and Lamb, P.J., 2003. African Droughts and Dust Transport to the Caribbean: Climate Change Implications. *Science*, 302(5647): 1024-1027.

Raymo, M.E., Hodell, D. and Jansen, E., 1992. Response of deep ocean circulation to initiation of Northern Hemisphere Glaciation (3-2Ma). *Paleoceanography*, 7(5): 645-672.

Reid, J.L., 1978. On the middepth circulation and salinity field in the North Atlantic Ocean. *Journal of Geophysical Research: Oceans*, 83(C10): 5063-5067.

Ruiz, G.M.H. et al., 2011. From central Atlantic continental rift to Neogene uplift - western Anti-Atlas (Morocco). *Terra Nova*, 23(1): 35-41.

Sarnthein, M. and Diester-Haass, L., 1977. Eolian-sand turbidites. *Journal of Sedimentary Research*, 47(2): 868-890.

Sarnthein, M. et al., 1982. Atmospheric and Oceanic Circulation Patterns off Northwest Africa During the Past 25 Million Years. In: U. von Rad, K. Hinz, M. Sarnthein and E. Seibold (Editors), *Geology of the Northwest African Continental Margin SE - 24*. Springer Berlin Heidelberg, pp. 545-604.

Scheuvens, D., Schütz, L., Kandler, K., Ebert, M. and Weinbruch, S., 2013. Bulk composition of northern African dust and its source sediments - A compilation. *Earth-Science Reviews*, 116: 170-194.

Schmitz, J., W.J and McCartney, M.S., 1993. On the North Atlantic circulation. *Reviews of Geophysics*, 31(1): 29-49.

Skonieczny, C. et al., 2013. A three-year time series of mineral dust deposits on the West African margin: Sedimentological and geochemical signatures and implications for interpretation of marine paleo-dust records. *Earth and Planetary Science Letters*, 364: 145-156.

Skonieczny, C. et al., 2011. The 7-13 March 2006 major Saharan outbreak: Multiproxy characterization of mineral dust deposited on the West African margin. *Journal of Geophysical Research: Atmospheres*, 116(D18): D18210.

Steiger, R.H. and Jäger, E., 1977. Subcommission on geochronology: Convention on the use of decay constants in geo- and cosmochronology. *Earth and Planetary Science Letters*, 36(3): 359-362.

Stumpf, R., Frank, M., Schönfeld, J. and Haley, B.A., 2011. Climatically driven changes in sediment supply on the SW Iberian shelf since the Last Glacial Maximum. *Earth and Planetary Science Letters*, 312(1-2): 80-90.

Sun, S.-S., 1980. Lead isotopic study of young volcanic rocks from mid-ocean ridges, ocean islands and island arcs. *Phil. Trans. R. Soc. Lond*, A297: 409-445.

Swap, R., Ulanski, S., Cobbett, M. and Garstang, M., 1996. Temporal and spatial characteristics of Saharan dust outbreaks. *Journal of Geophysical Research: Atmospheres*, 101(D2): 4205-4220.

Tanaka, T. et al., 2000. JNdi-1: a neodymium isotopic reference in consistency with LaJolla neodymium. *Chemical Geology*, 168(3-4): 279-281.

Tiedemann, R., Sarnthein, M. and Shackleton, N.J., 1994. Astronomic timescale for the Pliocene Atlantic $\delta^{18}O$ and dust flux records of Ocean Drilling Program Site 659. *Paleoceanography*, 9(4): 619-638.

Turnewitsch, R. et al., 2013. Deep-sea fluid and sediment dynamics - Influence of hill- to seamount-scale seafloor topography. *Earth-Science Reviews*, 127: 203-241.

von Blanckenburg, F., O'Nions, R.K. and Hein, J.R., 1996. Distribution and sources of pre-anthropogenic lead isotopes in deep ocean water from Fe-Mn crusts. *Geochimica et Cosmochimica Acta*, 60(24): 4957-4963.

Deep-Sea Fe-Mn crusts from the Northeast Atlantic Ocean: Composition and resource considerations

Abstract

Eighteen deep-sea ferromanganese crusts (Fe-Mn crusts) from 10 seamounts in the northeast Atlantic were studied. Samples were recovered from water depths of ~1,200 to ~4,600 m from seamounts near Madeira, the Canary and Azores islands, and one sample from the western Mediterranean Sea.

The mineralogical and chemical compositions of the samples indicate that the crusts are typical continental margin, hydrogenetic Fe-Mn crusts. The Fe-Mn crusts exhibit a Co+Cu+Ni maximum of 0.96 wt%. Platinum-group element contents analyzed for five samples showed Pt contents from 153 to 512 ppb.

The resource potential of Fe-Mn crusts within and adjacent to the Portuguese Exclusive Economic Zone (EEZ) is evaluated to be comparable to that of crusts in the central Pacific, indicating that these Atlantic deposits may be an important future resource.

This Chapter has been published as:
Susana Bolhão Muiños , James R. Hein , Martin Frank , José Hipólito Monteiro, Luís Gaspar , Tracey Conrad , Henrique Garcia Pereira and Fátima Abrantes (2013): Deep-sea Fe-Mn Crusts from the Northeast Atlantic Ocean: Composition and Resource Considerations, Marine Georesources & Geotechnology, 31:1, 40-70, doi:10.1080/1064119X.2012.661215.

V.1. Introduction

Manganese and ferromanganese oxide deposits in the oceans occur as nodules, crusts, and massive beds. These deposits have been classified as diagenetic, hydrogenetic, hydrothermal, and mixed-type deposits (Halbach 1986; Hein et al. 1997; Wen et al. 1997). Hydrogenetic crusts (Fe-Mn crusts) form by direct precipitation of colloidal hydrated metal oxides from the water column onto hard-rock substrates.

The first investigations of hydrogenetic Fe-Mn crusts on seamounts were carried out in the Pacific Ocean (Craig et al. 1982; Halbach et al. 1982, 1989b; Hein et al. 1988). The preconditions required for Fe-Mn crust formation, such as the occurrence of isolated volcanic edifices, strong currents that keep the edifices free of sediment, and an oxygen-minimum zone (OMZ) are also found in the Atlantic Ocean (Koschinsky et al. 1995). Indeed, previous results from NE Atlantic seamounts indicate widespread presence of Fe-Mn crusts of hydrogenetic origin (Koschinsky et al. 1995, 1996; Gaspar 2001; Muiños et al. 2002; Muiños 2005). Hydrogenetic precipitation is dependent on water-mass properties and is characterized by slow growth rates (<10 mm/Ma) and generation of an extremely high specific-surface area, which promotes the enrichment of trace elements through scavenging by the major oxides (e.g. Hein et al. 1997). Seamounts act as obstructions to oceanic water-mass flow thereby creating seamount-generated currents of enhanced energy relative to flows away from the seamounts. These currents, which are strongest along the outer rim of the summit region of seamounts, promote the formation of thick crusts, enhanced turbulent mixing, and produce upwelling, leading to increased primary productivity and thus maintenance of the OMZ (summarized in Hein et al. 2000). Manganese oxides and associated trace metals are concentrated in the OMZ, which are then scavenged onto crusts under oxic conditions resulting from the turbulent mixing around seamounts.

Our study area in the northeast Atlantic (Figure V.1.) is influenced by the Mediterranean Outflow Water (MOW), which is characterized by relatively high salinity and temperature and low oxygen content compared to surrounding water masses. Because manganese is soluble under low-oxygen conditions, this water mass is a reservoir for Mn^{2+} in solution between 800 and 1,200 m water depth, which corresponds to the upper and lower cores of the MOW (Madelain 1970; Zenk 1970; Ambar and Howe 1979; Ambar et al. 1999, 2002).

Fluctuations in the intensity of the OMZ and MOW may have influenced the composition of the Fe-Mn crusts (Koschinsky et al. 1996).

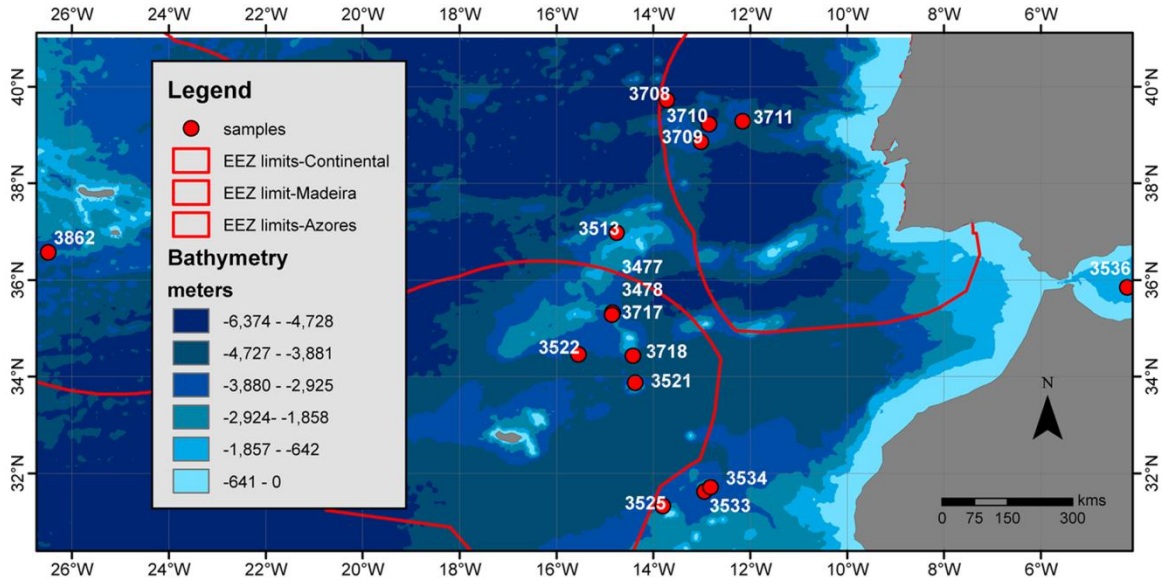

Figure V.1. Map showing bathymetry, the location of the sample sites, and the limits of the Portuguese EEZ.

Hydrogenetic precipitation promotes the enrichment of crusts in potentially economically important trace metals such as Co, Ni, Te, rare earth elements (REEs), and platinum-group elements (PGEs), and thus there is a growing recognition of Fe-Mn crusts as potential metal resources. With growing markets for metals in Asia, as well as the rapid development of high-tech and green-tech applications, the demand for rare metals will increase dramatically in the near future (Hein et al. 2010).

Significantly, to our knowledge, there is a lack of technology needed for detailed exploration and extraction of Fe-Mn crusts, which may be slowing development. However, much proprietary engineering research has been undertaken in a number of countries. Environmental studies are also in their infancy and should be addressed as stipulated in the United Nations Convention on the Law of the Sea and International Seabed Authority regulations. Accompanying the accelerating economic interest in Fe-Mn crusts, the

International Seabed Authority passed regulations for exploration for Fe-Mn crusts during its 18th Session in July 2012.

Much work has been done on marine Fe-Mn deposits, but studies of Atlantic Ocean deposits are still scarce compared to those from the Pacific Ocean. The aims of this study are to determine the composition of Fe-Mn crusts from the northeast Atlantic, in particular those within the Portuguese EEZ, and to consider their resource potential.

V.2. Material and Methods

Samples were collected from ten seamounts in the northeast Atlantic during cruises Trident 86, TTR-11 (I.O.C. 2002), Meteor 51/1 (Hoernle and Scientific Party 2003), and Tore-Madeira (Merle 2006). Sampling occurred over a wide geographic range including seamounts in the Portuguese EEZ and near the Canary Islands. Sampling locations are distributed over a large depth range and the growth and composition of the Fe-Mn crusts were influenced by different chemical and oceanographic environments that are broadly representative of the study area (Figure V.1. and Table V.1.).

The chemical and mineralogical data represent analyses of bulk samples. All crusts were analyzed by X-ray diffraction on a Philips diffractometer using Cu-Kα radiation and carbon monochromator at the United States Geological Survey (USGS). The interpretation of the diffractograms and identification of mineralogical phases were also performed at the USGS using the program X´Pert High Score of Philips (PANalytical). We follow the nomenclature of Usui et al. (1989) for manganese minerals. The semi-quantitative determination of mineral content is based on the relative intensity of the peaks and previously determined weighing factors (Cook et al. 1975; Hein et al. 1988).

Major elements (Fe, Mn, Si, Al, Ca, Mg, Na, K, Ti, P) were analyzed by fused-disk X-ray fluorescence; S, Ba, Cr, Cu, Li, Ni, Sr, V, Zn, and Zr by 4-acid digestion and inductively coupled plasma-optical emission spectrometry (ICP-OES); Ag, As, Be, Bi, Cd, Co, Ga, Ge, Hf, In, Mo, Nb, Pb, Rb, Sb, Sc, Sn, Ta, Tl, W, and Cs were analyzed by 4-acid digestion and ICP-mass spectrometry (MS); Th, U, Y, and REEs were analyzed by lithium metaborate fusion and ICP-MS; Se and Te by 4-acid digestion, hydride-generation, and atomic absorption spectrometry

(AAS), Hg by cold vapor AAS, and Cl^- was analyzed by the specific-ion electrode method. Based on duplicate analyses of 10% of the samples, precision was better than 5% for S, As, Ba, Be, Bi, Cd, Co, Cr, Cu, Ga, Ge, In, Li, Mo, Ni, Pb, Rb, Sc, Se, Sr, Te, Th, Tl, U, V, Zn, REEs, Cl^-, and Cs and better than 10% for Sb, Sn, W, and Hg. For a few elements, precision varies widely and data should be used with that in mind: Ag (10-33%), Hf (11-28%), Nb (15-24%), Ta (13-24%), and Zr (5-16%). Five samples were also analyzed for PGE and Au contents by fire assay and ICP-MS. Analytical accuracy was calculated using international standards AMIS0056 and HGMNEW and is better than 5% for Os and Ru, better than 10% for Ir, Pd, and Pt, 13% for Au, and varies from 5-17% for Rh.

Table V.1. Location of samples

Sample ID	Field ID	Latitude (N)*[1]	Longitude (W)*[1]	Water Depth (m)*[1]	Seamount	Geographic Area
3477-B.3.4	TTR11-353GR	35.3117	-14.8300	1853	Nameless	Madeira
3478-B.3.5	TTR11-354GR	35.3167	-14.8350	1839	Nameless	Madeira
3717-12	TM-D19	35.2767	-14.8500	2198	Nameless	Madeira
3521-6	M51/1-426DR	33.8683	-14.3680	1362	Seine	Madeira
3522-4	M51/1-428DR	34.4567	-15.5387	2946	Godzilla	Madeira
3718-1	TM-D20	34.4258	-14.4173	3756	Unicorn	Madeira
3513-13	M51/1-414DR	36.9700	-14.7475	4594	MTR-Josephine	Madeira
3513-14	M51/1-414DR	36.9700	-14.7475	4594	MTR-Josephine	Madeira
3513-16	M51/1-414DR	36.9700	-14.7475	4594	MTR-Josephine	Madeira
3708-1	TM-D3B	39.7217	-13.7152	4140	Tore	Madeira
3709-1	TM-D5	38.8442	-13.0147	2803	Tore	Madeira
3710-1	TM-D6B	39.2158	-12.8464	4245	Tore	Madeira
3711-2	TM-D9	39.2775	-12.1486	3110	Tore	Madeira
3525-9	M51/1-448DR	31.3216	-13.8009	3043	Dacia	Canaries
3533-7	M51/1-457DR	31.6267	-12.9382	1602	Annika	Canaries
3534-14.1	M51/1-458DR	31.7083	-12.8156	2128	Annika	Canaries
3536-3	M51/1-462DR	35.8450	-4.2125	1221	Ibn Batouta	Mediterranean
3862	TR86-8D	36.5667	-26.4833	2575	Azores	Azores

*[1] except for samples from the TTR-11 cruise that were collected by TV-Grab, all the other coordinates and water depths (M51/1- Meteor 51/1, TM-Tore-Madeira and TR-Trident 86) correspond to intermediate values from on- and off-bottom dredge locations. MTR means Madeira-Tore Rise.

Q-Mode factor analyses used the Varimax method (Klovan and Imbrie 1971). All communalities are >0.94 and values between -0.1575 and 0.1575 were not considered because they are below the level of statistical significance assuming a multi-Gaussian distribution.

The extent of the area covered by seamounts was determined using ArcGIS® and ETOPO bathymetry (Amante and Eakins 2009; http://www.ngdc.noaa.gov/mgg/global/global.html).

V.3. Mineralogy and chemical composition of the crusts

All Fe-Mn crust samples are composed predominately of δ-MnO_2 (vernadite), the mineral most characteristic of hydrogenetic Fe-Mn deposits found globally. The mineral δ-MnO_2 is epitaxially intergrown with X-ray amorphous iron oxyhydroxide (δ-FeO(OH)-feroxyhyte; Burns and Burns 1977; Varentsov et al. 1991; Hein et al. 2000). Detrital minerals, such as quartz and feldspar, and biogenic and diagenetic minerals, such as calcite and carbonate fluorapatite (CFA) are present in minor to moderate amounts (Table V.2.). In addition, two samples contain minor amounts of 10 Å manganate (probably todorokite), which may reflect a lower oxidation potential of seawater caused by increased biological productivity, as suggested by Hein et al. (2000) for some occurrences in the Pacific Ocean, or may indicate a minor hydrothermal contribution. Minor amounts of goethite are also present in the majority of the samples and can reflect a number of different processes, including: (1) increased inputs of Fe from continental sources (Bruland et al. 2001); (2) too much Fe present for the vernadite structure to accommodate (De Carlo 1991, and references therein); (3) the enhanced supply of Fe from the dissolution of calcareous tests for crusts below the calcite compensation depth (CCD), as suggested by von Stackelberg et al. (1984) for goethite in some layers of a deep-water Fe-Mn crust (4,830 m) collected in the Clarion-Clipperton nodule belt; and (4) as suggested by Hein et al. (2000), goethite is found only in the older parts of 5% of 640 crust samples analyzed from Pacific Ocean sites and may result from the maturation of X-ray amorphous Fe oxyhydroxide. Most Atlantic crusts in our study do not originate from below or near the CCD and their Fe concentrations are not greater

than those of many crusts without goethite, so that explanations (1) and (4) may be most likely for the occurrence of goethite in the Atlantic samples.

Table V.2. X-ray Diffraction Mineralogy of Fe-Mn samples

Sample	δ-MnO_2 (%)	Others*[2]
3477-B.3.4	95	feldspar; todorokite; quartz; goethite
3478-B.3.5	93	goethite; calcite; plagioclase; quartz
3513-13	94	goethite; plagioclase; quartz
3513-14	94	goethite; quartz; plagioclase
3513-16	85	quartz; goethite; feldspar; kaolinite
3521-6	92	CFA; low Mg-calcite; goethite
3522-4	99	calcite
3708-1	94	quartz; goethite
3709-1	91	quartz; goethite; plagioclase
3710-1	95	quartz; goethite
3711-2	87	calcite; quartz; goethite
3717-12	97	goethite; plagioclase; quartz
3718-1	87	quartz; goethite; aragonite; plagioclase
3525-9	99	calcite; quartz
3533-7	85	CFA; goethite
3534-14.1	93	goethite; feldspar; quartz; calcite
3536-3	71	calcite; Mg-calcite; todorokite; goethite; quartz
3862	96	goethite

*[2] in approximate decreasing abundance; CFA means carbonate fluorapatite.

The Fe-Mn crust samples have Fe contents from 12.5 to 23.2 wt % with an average of 17.9 wt % and Mn contents from 9.3 to 17.0 wt% with a mean of 13.7 wt % (Table V.3.). These concentrations result in Fe/Mn ratios of 0.88 to 1.96 with a mean of 1.33, which is in the

range typical of continental margin hydrogenetic Fe-Mn crusts (Hein et al. 2000). Silicon and Al concentrations range from 1.21 to 13.0 wt % and 0.73 to 4.66 wt % with average values of 4.45 and 2.04 wt %, respectively; Si/Al ratios vary between 0.83 and 5.32, with an average value of 2.05. The Si/Al ratios of the volcanic rocks in the area (Geldmacher et al. 2006; Merle et al. 2006) cluster around 2.8. Sample 3708-1 from Unicorn Seamount has a Si/Al ratio of 5.32 indicating the presence of biogenic silica or eolian quartz. An explanation for the low Si/Al ratios is more difficult but preferential incorporation of feldspar over quartz or sorption of Al hydroxide as suggested by Koschinsky and Halbach (1995) could explain those ratios. Calcium concentrations range from 0.99 to 12.7 wt % with a mean value of 3.23 wt %, and P varies from 0.21 to 4.28 wt %, averaging 0.65 wt %. Cobalt, Cu, and Ni show minimum concentrations of 931, 315, and 1,240 ppm and maximum concentrations of 5,440, 2,050, and 3,980 ppm, respectively. Cobalt has a mean concentration of 3,408 ppm, copper averages 872 ppm, and nickel 2,197 ppm. The Co+Cu+Ni maximum is 0.96 wt %, with a mean of 0.64 wt %. These values and the Fe/Mn ratios are consistent with a predominantly hydrogenetic origin of continental margin Fe-Mn crusts. Some compositional data points fall outside the typical open-ocean hydrogenetic field (Figure V.2.), but do fall within the field typical for Pacific continental margin and small ocean basin Fe-Mn crusts. These continental-margin-type crusts show lower total Co+Cu+Ni and higher Fe, Si, Al, and Cr contents than open-ocean crusts, reflecting the higher terrigenous input per unit area for the Atlantic (Koschinsky et al. 1995; Hein et al. 2000).

Tellurium is also an important element because of its potential economic value in the solar cell industry (Hein et al. 2010). In our samples, Te ranges from 11 to 71 ppm with an average value of 43 ppm. Hein et al. (2003) reported mean concentrations of Te for Pacific and Atlantic hydrogenetic Fe-Mn crusts of 50 ppm, which is consistent with our data. Vanadium, W, Zr, and Th also have notably high concentrations in our samples (Table V.3.).

Differences in crust composition based on subregions of our study area (Mediterranean, Canaries, Tore, Madeira-Tore Rise (MTR), and Azores) are presented in Figure V.3. using data averaged from Table V.3. for each subregion (see Table V.1.). It should be stressed that for Mediterranean and Azores subregions, only one sample is available, which should be taken in to consideration when comparing to the average values from the remaining

Table V.3. Chemical composition

		3521-6	DUP-3521-6	3522-4	3525-9	3536-3	3708-1	3709-1	3710-1	3711-2	3718-1
Fe	wt%	17.8	N.A.	20.3	22.9	12.5	17.8	16.9	20.8	18.0	17.9
Mn		13.5	N.A.	16.1	14.3	14.2	13.8	15.3	10.6	11.9	12.1
Si		1.21	N.A.	2.20	2.34	3.65	5.94	6.78	4.96	3.87	9.77
Al		1.47	N.A.	1.46	1.33	2.62	3.05	2.07	3.05	1.76	1.84
Ca		6.05	N.A.	2.54	2.16	8.58	1.50	1.72	1.40	5.06	1.49
Mg		1.92	N.A.	1.18	1.09	4.06	1.49	1.21	1.28	1.08	0.98
Na		0.91	N.A.	1.05	1.00	0.53	1.12	1.31	0.87	1.00	1.26
K		0.25	N.A.	0.30	0.29	0.49	0.48	0.51	0.44	0.43	0.60
Ti		1.10	N.A.	0.91	0.98	0.10	0.80	0.61	0.93	0.88	0.50
P		1.46	N.A.	0.42	0.46	0.21	0.41	0.33	0.46	0.38	0.29
S		0.39	0.40	0.32	0.28	0.23	0.26	0.24	0.21	0.25	0.20
Fe/Mn		1.3	--	1.3	1.6	0.9	1.3	1.1	2.0	1.5	1.5
Si/Al		0.83	--	1.51	1.75	1.39	1.95	3.27	1.62	2.20	5.32
Ag	ppm	0.29	0.10	0.34	0.23	0.04	0.12	0.12	0.11	0.11	0.24
As		455	416	317	373	328	250	233	298	272	244
Ba		884	904	1270	1450	953	977	1240	740	882	1540
Be		9.5	9.0	11	12	3.7	9.3	8.6	8.3	7.8	8.7
Bi		33	31	31	25	6.5	22	24	24	22	16
Cd		4.0	3.7	4.6	4.0	2.8	7.4	3.8	5.3	2.9	2.4
Co		5440	5230	4000	3380	931	3250	3440	3180	3260	2510
Cr		101	109	21	78	61	49	121	54	35	30
Cu		426	422	784	592	317	1420	1040	786	368	1410
Ga		8.6	8.1	9.6	13	7.8	14	15	13	9.8	14
Ge		0.8	0.8	0.7	0.9	0.2	0.6	0.5	0.6	0.7	0.4
Hf		8.4	3.7	8.2	3.9	0.36	3.3	1.7	3.3	1.6	7.1
In		0.12	0.11	0.10	0.12	0.05	0.12	0.14	0.20	0.10	0.13
Li		18	18	8	6	117	49	22	22	11	11
Mo		328	314	444	464	184	308	387	228	299	446
Nb		68	36	58	50	5.2	34	41	41	31	43
Ni		2350	2420	1830	1400	2790	2570	2650	1290	1240	1440
Pb		1860	1930	1880	1740	519	1110	1230	1120	1320	1000

Table V.3. (Continued)

		3521-6	DUP-3521-6	3522-4	3525-9	3536-3	3708-1	3709-1	3710-1	3711-2	3718-1
Rb	ppm	5,4	4,9	6,1	6,6	18	14	14	15	15	19
Sb		46	39	46	57	26	38	45	43	32	47
Sc		20	18	13	16	12	15	11	20	14	9,1
Se		<0.2	<0.2	0,4	0,5	<0.2	0,5	0,3	0,6	0,4	<0.2
Sn		7,6	6,7	5,4	5,3	1,7	4,8	6,3	10	4,9	4,4
Sr		1380	1400	1290	1320	557	849	1040	719	1070	916
Ta		2,3	1,2	1,8	1,8	<0.05	0,85	0,42	1,2	0,60	0,63
Te		71	67	47	42	11	34	43	46	42	32
Th		54	54	37	44	24	40	46	75	66	49
Tl		118	112	142	49	38	116	140	75	65	60
U		15	15	14	14	4,7	11	10	11	12	6,6
V		914	997	962	1030	599	737	660	795	793	764
W		64	50	109	108	36	66	80	48	64	53
Zn		463	475	557	560	566	594	548	473	435	622
Zr		214	240	137	72	16	173	57	180	212	128
La		356	343	294	371	53,8	196	211	229	327	141
Ce		1120	1080	1270	1570	250	1100	1370	1540	1360	1280
Pr		77,8	74,8	66,9	84,1	14,2	49,1	51,7	57,8	80,1	32,3
Nd		297	286	251	316	55,3	186	188	214	298	112
Sm		70,1	66,8	57,2	71,6	15,8	46,6	43,6	53,2	70,0	25,8
Eu		16,7	16,2	13,9	17,1	3,79	11,0	10,1	13,1	16,3	5,68
Gd		77,7	74,1	63,3	78,4	17,6	50,0	42,2	58,5	71,2	22,6
Tb		12,1	11,6	9,99	12,3	2,96	8,27	6,62	9,34	11,0	3,62
Dy		65,0	62,4	50,8	63,2	15,9	43,0	33,2	49,1	55,3	17,1
Y		340	333	184	230	77,9	164	103	182	186	46,1
Ho		14,9	14,3	11,1	13,5	3,50	9,54	7,03	10,7	11,6	3,35
Er		42,1	41,3	29,7	37,6	10,1	26,8	19,2	30,0	31,4	9,45
Tm		5,90	5,81	4,29	5,21	1,48	3,96	2,74	4,50	4,30	1,38
Yb		35,6	34,7	26,1	32,1	8,9	24,6	17,3	28,0	25,6	8,8
Lu		5,62	5,37	3,93	4,73	1,34	3,87	2,60	4,32	3,75	1,37
Hg	ppb	14	14	13	7	7	10	8	25	11	10
Cl⁻	ppm	>5000	>5000	>5000	>5000	3120	>5000	>5000	>5000	>5000	>5000

Table V.3. (Continued)

		3862	3477-B.3.4	3478-B.3.5	3513-13	DUP-3513-13	3513-14	3513-16	3533-7	3534-14.1	3717-12
Fe	wt%	23.2	17.6	16.6	16.6	N.A.	15.7	12.6	14.0	21.4	20.3
Mn		13.3	17.0	16.3	13.4	N.A.	13.2	9.3	13.5	13.2	15.5
Si		1.57	3.09	3.36	4.47	N.A.	5.94	13.0	1.30	2.48	2.32
Al		1.29	1.74	1.73	2.45	N.A.	2.65	4.66	0.73	1.49	1.23
Ca		2.04	1.92	3.34	1.40	N.A.	1.28	0.99	12.7	2.17	1.87
Mg		1.24	1.48	1.57	1.32	N.A.	1.36	1.83	1.13	1.32	1.10
Na		1.13	1.25	1.16	1.22	N.A.	1.13	1.27	0.84	0.98	1.14
K		0.24	0.51	0.49	0.45	N.A.	0.68	1.59	0.37	0.31	0.46
Ti		2.37	0.67	0.57	0.83	N.A.	0.52	0.74	0.29	1.01	0.32
P		0.51	0.38	0.41	0.39	N.A.	0.31	0.24	4.28	0.51	0.31
S		0.29	0.30	0.26	0.24	0.23	0.18	0.14	0.31	0.27	0.26
Fe/Mn		1.7	1.0	1.0	1.2	--	1.2	1.4	1.0	1.6	1.3
Si/Al		1.21	1.77	1.95	1.82	--	2.24	2.79	1.79	1.66	1.88
Ag	ppm	0.44	0.34	0.14	0.12	0.15	0.18	0.23	0.05	0.12	0.04
As		439	316	278	214	213	207	129	279	419	346
Ba		1450	1320	1360	955	958	1170	769	2180	991	1550
Be		12	8.8	8.0	7.2	7.1	8.1	5.5	7.3	12	11
Bi		15	30	23	18	18	18	14	15	24	25
Cd		4.6	3.7	4.0	4.7	4.6	5.0	3.8	2.5	3.4	2.7
Co		4270	4930	4060	3860	3800	2020	1650	2640	4330	1970
Cr		72	51	50	31	33	67	27	49	60	111
Cu		382	970	969	1140	1130	2050	2010	315	454	449
Ga		14	16	16	14	14	19	19	8.0	10	13
Ge		1.0	0.5	0.5	0.7	0.7	0.6	0.3	0.4	0.7	0.6
Hf		6.5	12	5.8	2.4	3.1	5.5	7.3	0.86	3.0	1.2
In		0.10	0.14	0.11	0.19	0.19	0.29	0.31	0.06	0.09	0.16
Li		11	26	33	27	26	43	63	13	11	7
Mo		371	379	341	289	289	360	164	278	350	548
Nb		74	68	41	29	41	43	58	11	50	11
Ni		1330	3670	3980	2010	1990	2590	2590	1990	1590	2210
Pb		991	2100	1720	943	953	863	539	1330	1650	1060

Table V.3. (Continued)

		3862	3477-B.3.4	3478-B.3.5	3513-13	DUP-3513-13	3513-14	3513-16	3533-7	3534-14.1	3717-12
Rb		3,2	12	12	12	12	20	34	8,3	6,5	11
Sb		47	55	48	32	32	34	27	37	47	56
Sc		21	10	8,6	14	14	13	17	7,4	17	11
Se		0,3	<0.2	<0.2	0,3	0,3	<0.2	0,3	<0.2	0,4	<0.2
Sn		8,1	7,2	5,5	3,8	3,8	3,7	3,4	2,1	5,0	4,9
Sr		1340	1130	1030	1090	1060	745	484	1470	1090	1170
Ta		4,1	1,2	0,60	0,84	1,1	0,99	1,8	0,38	1,2	0,12
Te		49	66	56	40	41	25	33	32	58	34
Th		43	39	37	61	59	69	50	17	52	45
Tl		73	195	169	122	123	120	61	85	73	143
U		19	9,7	8,6	9,6	9,3	7,6	5,1	9,2	14	8,3
V		1130	848	797	662	644	612	270	861	974	904
W		54	115	92	57	57	64	25	84	72	121
Zn		650	724	755	468	475	604	547	576	538	652
Zr		75	151	88	122	178	204	104	88	139	55
La		390	190	174	282	270	189	120	181	324	265
Ce		1460	1210	1100	1450	1400	1290	972	662	1260	1400
Pr		90,8	40,8	39,2	70,3	67,2	52,8	30,9	36,8	71,7	61,8
Nd		339	153	145	254	244	191	113	142	269	229
Sm		78,9	34,4	33,4	61,6	59,2	48,3	27,9	31,9	62,7	52,4
Eu		18,8	8,10	7,85	14,5	13,8	11,2	6,50	7,38	14,9	12,4
Gd		85,0	35,0	34,4	62,0	59,5	46,6	27,0	36,1	68,5	51,1
Tb		13,6	5,61	5,30	9,87	9,55	7,37	4,32	5,62	10,8	7,87
Dy		69,8	29,0	26,8	49,3	47,5	36,5	21,6	30,7	55,8	38,4
Y		269	110	100	164	158	120	79,9	159	217	111
Ho		15,4	6,29	5,85	10,4	9,92	7,49	4,52	7,12	12,4	8,03
Er		41,8	17,6	16,1	27,9	27,1	20,8	11,9	20,0	34,0	21,4
Tm		5,82	2,48	2,26	4,03	3,80	2,92	1,78	2,84	4,80	2,97
Yb		35,0	15,5	14,0	23,8	23,6	18,4	11,1	17,3	29,3	18,3
Lu		5,19	2,48	2,26	3,76	3,54	2,75	1,68	2,67	4,42	2,81
Hg	ppb	292	7	8	8	9	6	8	6	9	8
Cl^-	ppm	>5000	>5000	>5000	>5000	>5000	>5000	>5000	3640	>5000	>5000

All Cs concentrations < 5ppm

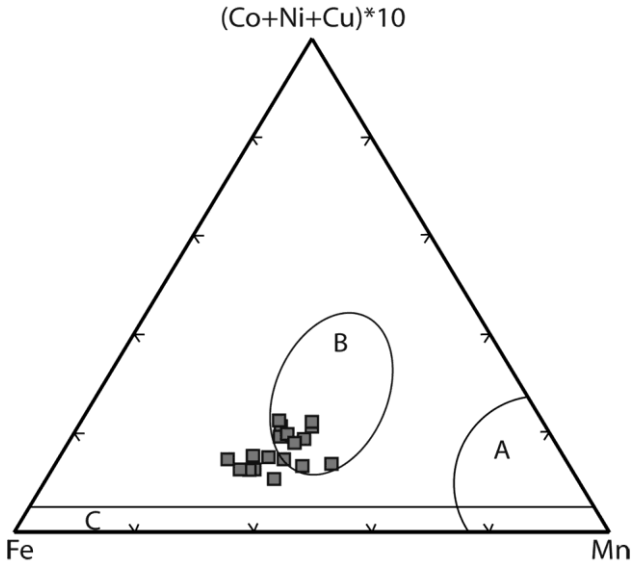

Figure V.2. Ternary diagram. All data plotted as wt %. The fields are: (A) diagenetic, (B) hydrogenetic, and (C) hydrothermal. Ternary plot software from (www.crog.org/cedric/dplot).

subregions. We also distinguish between the different MTR seamounts: MTR-Josephine and South MTR seamounts (which includes Nameless, Unicorn, Seine and Godzilla seamounts). South MTR seamounts is the subregion with the highest average values of Co+Ni+Cu, Co, Ni, Zn, Mo, Tl, W, Te, and Bi. The Mediterranean subregion is systematically lower for all elements, with the exceptions of Ni and Zn. The Canaries subregion shows the highest P contents, which will be discussed in the section on phosphatization, and the Azores subregion shows the higher concentrations of Ti (2.37 wt%), which may include a significant detrital source as well as the typical adsorption of Ti from seawater.

Changes in the geochemical composition of Fe-Mn crusts with water depth, such as increased Cu, Ni, Si, and Al concentrations with increasing water depth have been identified previously (e.g. Cronan 1977, 1997; Mangini et al. 1987; Hein et al. 1997). Increased Ni contents with water depth are not found in our sample set (Figure V.4.). There is an apparent increase of Cu content with water depth, which might be caused by the release of Cu during dissolution of carbonate material close to the CCD (Halbach et al. 1979 and references therein; Cronan 1997; Verlaan et al. 2004). Planktonic organisms extract metals from surface waters for metabolic processes and through scavenging. Dissolution of the carbonate tests and oxidation of the organic matter then release these metals at depth. The

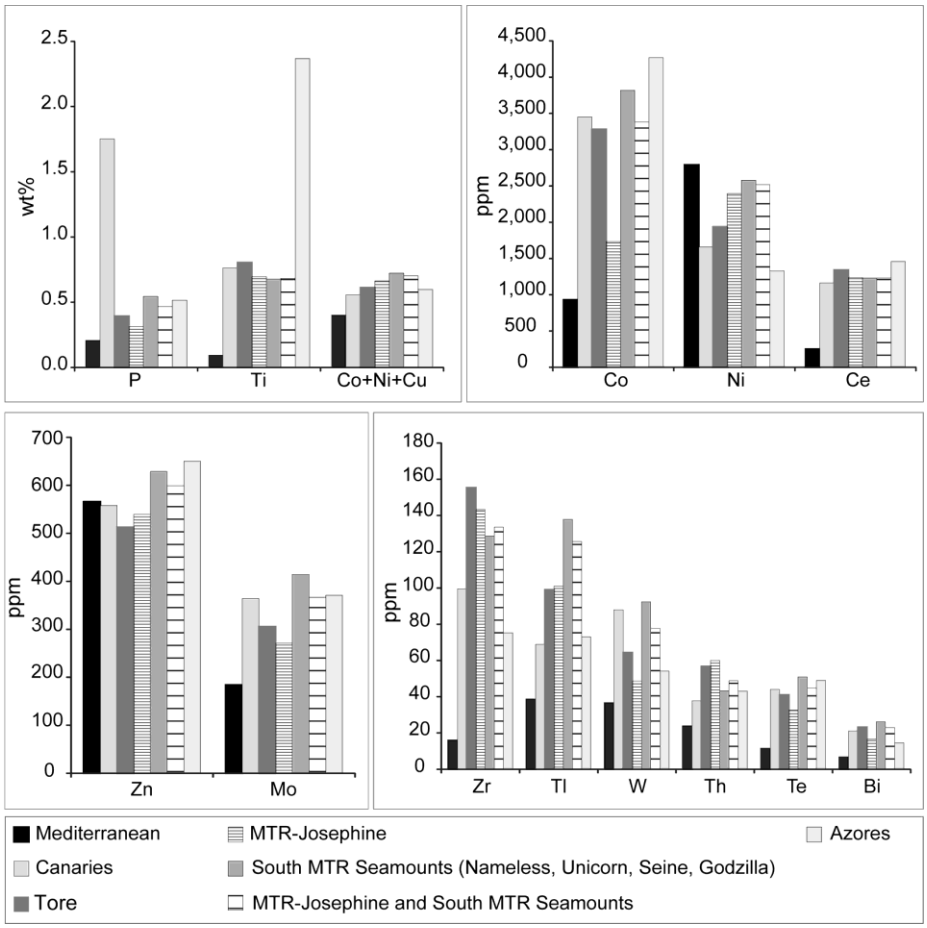

Figure V.3. Trace-metal concentrations in different subregions of the study area. Data correspond to averages of analyses in Table V.3. (See also Table V.1.).

CCD in the North Atlantic lies at about 4,700-4,800 m (van Andel 1975; Broecker and Peng 1982). Our most Cu-enriched samples are from ~4,600 m water depth. Cronan (1997) found that for Pacific manganese nodules, the highest Cu contents are not present in the deepest water nodules below the CCD, but in those located slightly above the CCD at around 5,000 m water depth. The increased deep-water Cu concentrations may thus be the result of a reduction in sedimentation rate associated with the loss of carbonate tests by dissolution near the CCD. That loss would lead to an increase in the concentration of organic phases in the sediments, whose decay would promote diagenetic reactions that enrich Cu and increase Al and Si contents (Cronan 1997). Our dataset supports this and shows similar increases with water depth for Cu, Al, and Si, and an opposite trend for Ca (Figure V.4.). Dissolution of carbonate tests may influence geochemistry within the calcite lysocline at depths from

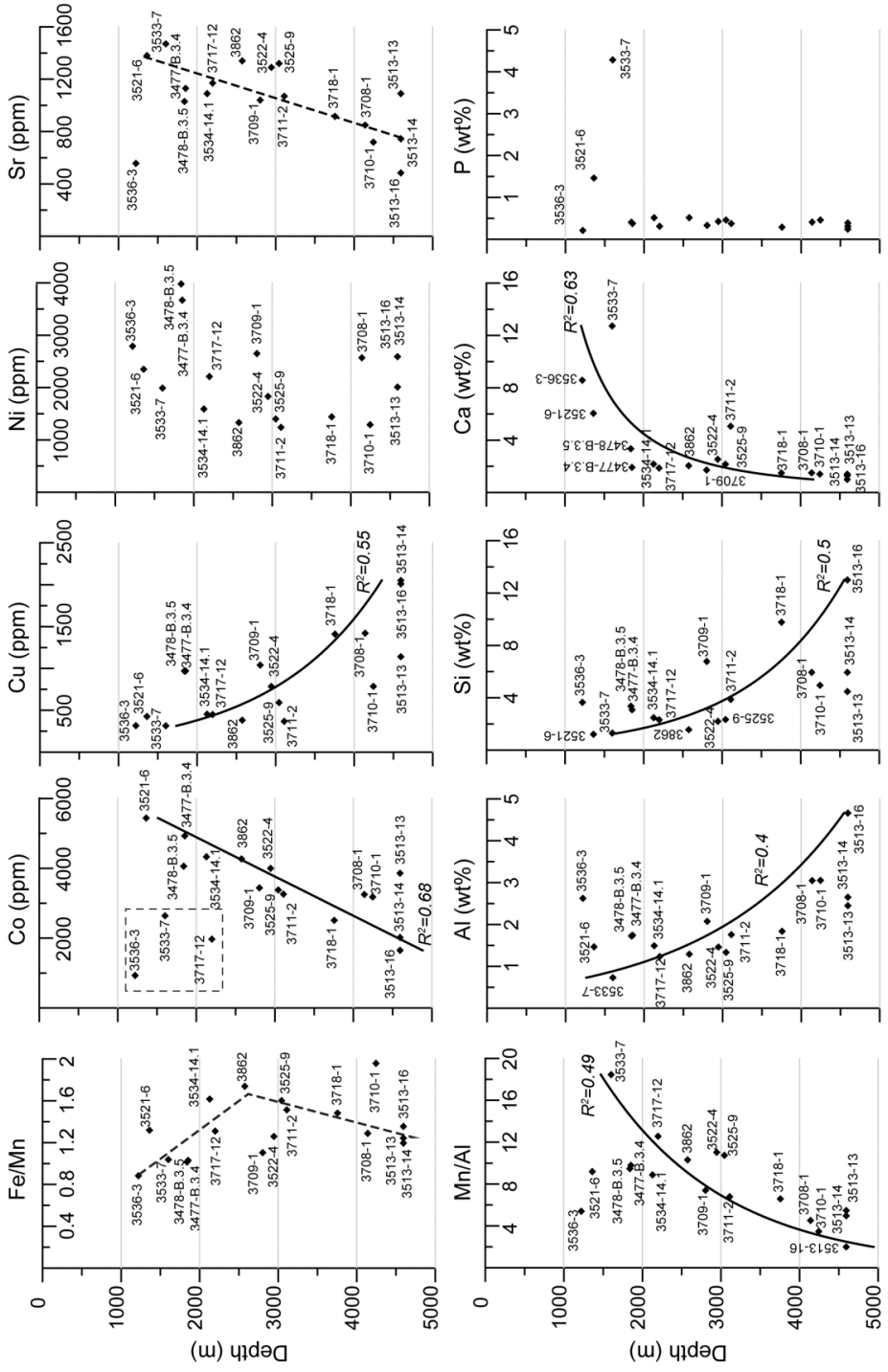

Figure V.4. Distribution of selected elements with water depth. Dashed lines correspond to hand-drawn trends, others are regression lines; dashed box in Co illustrates the group of samples not considered for regression lines.

about 2,600 to 3,000 m as indicated by a significant change in the slope of the Ca pattern and a change from increasing Fe/Mn to decreasing Fe/Mn with depth (Figure V.4.).

V.3.1. Rare Earth Elements

Chondrite-normalized REE patterns (Figure V.5a.) show enrichment of light REEs (LREEs) relative to heavy REEs (HREEs), a strong positive Ce anomaly, and a small positive Gd anomaly, which are typical of Fe-Mn crusts of hydrogenetic origin. Shale-normalized patterns (Figure V.5b.) are also characteristic of hydrogenetic Fe-Mn crusts in that they show pronounced middle REEs (MREEs) enrichment (Nath et al. 1992 and references therein). No direct relationship with water depth or geographic location is discernable, with the exception of crust 3536-3 from the Mediterranean Sea in which REEs concentrations are much lower. All samples are highly enriched in REEs relative to seawater and the Earth's crust, with up to 0.29 wt. % total REEs, crust 3536-3 being the exception with only 475 ppm total REEs. This sample grew in the Mediterranean Sea and precipitation of the oxides was governed by waters in the Alboran Basin mixed with Atlantic waters that entered through the Strait of Gibraltar. The waters from the Mediterranean are characterized by low oxygen contents and a low redox potential. Also, this sample and sample 3533-7 show less pronounced Ce anomalies. The presence of positive Ce anomalies is caused by scavenging of Ce from seawater by hydrous Fe-Mn oxides (Goldberg et al. 1963; Elderfield et al. 1981) and its preferential retention relative to the other REEs in the oxide phase through surface oxidation (Bau et al. 1996). According to Kuhn et al. (1998), and given that Ce (III) oxidation is characterized by slow reaction kinetics (Sholkovitz and Schneider 1991; Moffet 1994), the size of the Ce anomaly will depend on the duration that the Fe-Mn precipitates are in contact with seawater. De Carlo (1991) suggested that variations in the REEs abundances and the extent of fractionation between LREEs and HREEs primarily reflect changes in the mineralogical composition of the crusts. De Carlo (1991) also pointed out that care must be taken when using Ce anomalies calculated from bulk REE data as indicators of paleoredox conditions, given that the Ce anomaly is not only sensitive to variations in Ce content but also to variations in the concentrations of trivalent REEs, which are associated primarily with Fe and/or phosphate phases, whereas Ce is associated with the Mn phase. The Ce anomaly may not solely reflect Ce redox cycling and the REEs may provide indirect rather

than direct evidence of changes in the depositional conditions that result from controls on the Fe/Mn ratio. Accordingly, the low REE contents of crust 3536-3 are most likely the result of hydrothermal or diagenetic contributions characterized by fast growth rates and high Ni and Li contents.

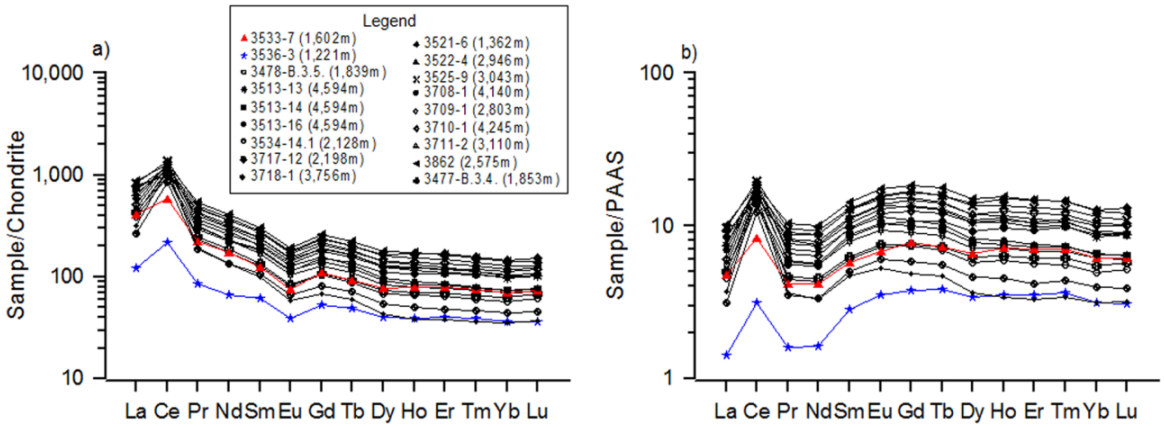

Figure V.5. a) Chondrite-normalized REE patterns. Normalization values from Anders and Grevesse (1989); b) Shale-normalized REE patterns. Normalization values for Post-Archean Australian Shale from Taylor and McLennan (1985); water depth listed after sample number in the Legend.

V.3.2. Platinum-Group Elements

Fe-Mn crusts are highly enriched in PGEs (Ir, Ru, Rh, Pt, Pd), especially Pt, compared to Earth's crustal abundances (Hein et al. 2000). Based on the five samples analyzed for PGEs, the Pt contents vary between 153 and 512 ppb, with an average value of 283 ppb; Rh, Ru, Pd, and Ir show concentrations up to 39, 21, 19, and 10 ppb, respectively (Table V.4.).

The processes of Pt enrichment in Fe-Mn crusts are not fully understood. Several mechanisms have been proposed for this enrichment, such as reduction or oxidation reactions, diagenetic or cosmogenic input, and enrichment related to phosphatization (Halbach et al. 1989a, 1990; Vonderhaar et al. 2000; Hein et al. 2005). We consider that the oxidative enrichment is the most likely general mechanism for high Pt concentrations; tetravalent Pt would be the final product, as it is also the case for Ce, whereas Te is hexavalent (Hein et al. 2003). The most likely mechanism is that Pt is sorbed from seawater

and then oxidized on the surface of the FeO(OH) (Hodge et al. 1985; Hein et al. 1997; Hein et al. 2003; Banakar et al. 2007).

Table V.4. PGE concentrations and ratios in five Fe-Mn crusts

Sample ID	Depth (m)	Fe (wt%)	Mn (wt%)	Co (wt%)	Ce (wt%)	Fe/Mn	Ir (ppb)	Ru (ppb)	Rh (ppb)	Pt (ppb)	Pd (ppb)	Au (ppb)	Pt/Pd	Ru/Rh	Pd/Ir	Pt/Ir	Pd/Ru	Pt/Ru	Pt/Au
3533-7	1602	14.0	13.5	0.26	0.07	1.04	5	14	14	153	19	------	8.1	1.0	3.8	31	1.4	11	------
3478-B.3.5	1839	16.6	16.3	0.41	0.11	1.01	10	21	39	512	14	9	37	0.54	1.4	51	0.67	24	57
3534-14.1	2128	21.4	13.2	0.20	0.13	1.62	6	17	25	231	11	------	21	0.68	1.8	39	0.65	14	------
3513-14	4594	15.7	13.2	0.17	0.10	1.20	6	18	18	223	10	------	22	1.0	1.7	37	0.56	12	------
3513-16	4594	12.6	9.3	0.43	0.13	1.35	6	13	27	296	15	------	20	0.48	2.5	49	1.2	23	------

V.4. Interelement relationships and mineral phases

A correlation coefficient matrix for selected elements (Table V.5.) shows that Fe is positively correlated (99% Confidence Interval-CI) with Ti, Mo, and REEs (the correlation is better with LREEs and MREEs) and to a lesser extent (95% CI) with Y and Co. Manganese is positively correlated with W, Tl, and Pb at the 99% CI, and also with Zn, Mo, Ni, and Bi at 95% CI, and shows negative correlations with the REEs (except La, Pr, and Nd). Cobalt shows strong positive correlations (99% CI) with Te, Pb, Nb, Bi, and some REEs (La, Pr, Nd, Tb, Dy, Ho, Er, Yb), and the correlations are better with the MREEs and HREEs. Tellurium also shows positive correlations with the same elements as Co, but Te shows lower correlation coefficients with Bi and the REEs. Both Co and Te show higher coefficients with Fe than with Mn and both show negative correlations with elements characteristic of the detrital-aluminosilicate fraction, which was also found for Te in open-ocean crusts (Hein et al. 2003).

Q-Mode factor analysis produces five factors that explain 97.3% of total variance of the data. Considering the mineralogical composition of the samples, we conclude that the five factors represent the Fe oxyhydroxide, aluminosilicate, biogenic (which may also include

Table V.5. Correlation Coefficient Matrix for selected elements

	Fe	Mn	Fe/Mn	Si	Al	Ca	Ti	P	Bi	Co	Cu	Mo	Nb	Ni	Pb	Te	Th	Tl	W	Zn	Zr
Fe																					
Mn	0.167																				
Fe/Mn	0.720	-0.552																			
Si	-0.449	-0.567	0.023																		
Al	-0.473	-0.584	0.036	0.795																	
Ca	-0.434	0.058	-0.417	-0.426	-0.381																
Ti	0.648	-0.153	0.634	-0.234	-0.139	-0.316															
P	-0.241	-0.023	-0.202	-0.358	-0.424	0.794	-0.145														
Bi	0.363	0.489	-0.030	-0.409	-0.459	-0.065	-0.064	0.108													
Co	0.503	0.362	0.187	-0.483	-0.434	-0.153	0.561	0.053	0.597												
Cu	-0.382	-0.291	-0.118	0.802	0.708	-0.549	-0.190	-0.339	-0.138	-0.283											
Mo	0.616	0.564	0.089	-0.313	-0.642	-0.323	0.075	-0.143	0.521	0.246	-0.148										
Nb	0.369	0.004	0.317	0.036	0.047	-0.442	0.664	-0.258	0.318	0.660	0.168	0.088									
Ni	-0.540	0.519	-0.779	0.085	0.191	0.030	-0.423	-0.083	0.040	0.034	0.306	-0.131	0.019								
Pb	0.442	0.587	-0.017	-0.567	-0.599	0.029	0.153	0.164	0.851	0.798	-0.356	0.441	0.462	0.145							
Te	0.463	0.301	0.224	-0.402	-0.343	-0.181	0.469	0.000	0.547	0.928	-0.280	0.185	0.692	0.122	0.809						
Th	0.198	-0.458	0.512	0.320	0.337	-0.564	0.203	-0.418	0.084	0.135	0.395	-0.042	0.225	-0.302	-0.084	0.147					
Tl	-0.018	0.722	-0.481	-0.205	-0.183	-0.233	-0.141	-0.088	0.486	0.465	0.165	0.369	0.194	0.683	0.519	0.468	0.003				
W	0.411	0.821	-0.224	-0.546	-0.622	-0.057	-0.152	0.064	0.706	0.345	-0.294	0.738	0.004	0.223	0.707	0.342	-0.280	0.626			
Zn	-0.005	0.572	-0.383	-0.051	-0.207	-0.116	-0.095	-0.078	-0.048	-0.004	0.140	0.363	0.065	0.605	0.166	0.081	-0.471	0.477	0.427		
Zr	0.109	-0.289	0.315	0.027	0.122	-0.173	0.186	-0.014	0.399	0.406	0.242	-0.106	0.346	-0.166	0.289	0.357	0.679	0.146	-0.146	-0.395	
La	0.797	0.074	0.577	-0.561	-0.510	-0.184	0.721	0.002	0.404	0.642	-0.453	0.432	0.413	-0.542	0.471	0.525	0.276	-0.012	0.284	-0.315	0.275
Ce	0.757	-0.019	0.655	-0.029	-0.142	-0.722	0.506	-0.377	0.367	0.438	0.106	0.545	0.390	-0.412	0.282	0.400	0.652	0.183	0.285	-0.122	0.317
Pr	0.771	0.011	0.605	-0.508	-0.418	-0.232	0.733	-0.034	0.362	0.614	-0.375	0.368	0.392	-0.559	0.403	0.486	0.383	-0.001	0.220	-0.377	0.347
Nd	0.782	0.037	0.590	-0.527	-0.433	-0.225	0.728	-0.069	0.347	0.587	-0.405	0.385	0.382	-0.549	0.395	0.456	0.341	-0.037	0.230	-0.356	0.296
Sm	0.734	-0.079	0.624	-0.443	-0.318	-0.248	0.751	-0.119	0.265	0.504	-0.319	0.304	0.374	-0.609	0.263	0.347	0.394	-0.129	0.087	-0.435	0.363
Eu	0.569	-0.128	0.529	-0.285	-0.356	-0.110	0.684	0.078	0.328	0.542	-0.249	0.292	0.491	-0.441	0.388	0.449	0.314	-0.093	0.094	-0.244	0.365
Gd	0.739	-0.050	0.621	-0.554	-0.363	-0.143	0.770	0.013	0.301	0.576	-0.417	0.230	0.421	-0.558	0.357	0.452	0.299	-0.119	0.131	-0.402	0.338
Tb	0.530	0.433	0.153	-0.665	-0.501	-0.067	0.324	0.198	0.520	0.622	-0.305	0.371	0.116	-0.045	0.590	0.510	0.211	0.499	0.576	-0.030	0.319
Dy	0.724	-0.040	0.607	-0.589	-0.392	-0.110	0.737	-0.010	0.315	0.611	-0.462	0.213	0.394	-0.545	0.384	0.492	0.330	-0.110	0.098	-0.430	0.399
Y	0.559	-0.053	0.476	-0.614	-0.390	0.124	0.693	0.234	0.338	0.649	-0.505	0.065	0.440	-0.435	0.433	0.531	0.113	-0.134	0.033	-0.427	0.371
Ho	0.639	0.328	0.307	-0.653	-0.508	-0.103	0.676	0.142	0.217	0.611	-0.362	0.337	0.273	-0.173	0.402	0.478	0.114	0.317	0.371	0.085	0.166
Er	0.729	0.076	0.536	-0.607	-0.387	-0.109	0.728	0.051	0.420	0.682	-0.427	0.221	0.408	-0.444	0.474	0.524	0.205	-0.013	0.210	-0.347	0.341
Tm	0.493	0.002	0.366	-0.394	-0.335	0.027	0.669	0.076	0.200	0.423	-0.348	0.205	0.504	-0.292	0.254	0.325	-0.105	-0.227	0.018	-0.095	-0.022
Yb	0.706	-0.018	0.590	-0.599	-0.426	-0.021	0.743	0.114	0.358	0.627	-0.505	0.210	0.471	-0.548	0.434	0.526	0.239	-0.083	0.127	-0.415	0.395
Lu	0.293	-0.056	0.259	-0.349	-0.258	0.096	0.720	0.128	-0.032	0.486	-0.316	0.027	0.521	-0.163	0.118	0.403	-0.042	-0.058	-0.221	-0.082	0.142
H2O Depth	-0.002	-0.561	0.385	0.661	0.651	-0.626	0.093	-0.371	-0.167	-0.259	0.748	-0.146	0.050	-0.282	-0.455	-0.323	0.658	-0.162	-0.371	-0.299	0.342

Correlation Coefficient matrix 18 samples
n= 18 for all elements
95% confidence level is |0.468|
99% confidence level is |0.582|

	Fe	Mn	Fe/Mn	Si	Al	Ca	Ti	P	Bi	Co	Cu	Mo	Nb	Ni	Pb	Te	Th	Tl	W	Zn	Zr

	Zr	La	Ce	Pr	Nd	Sm	Eu	Gd	Tb	Dy	Y	Ho	Er	Tm	Yb	Lu
La	0.275															
Ce	0.317	0.672														
Pr	0.347	0.985	0.711													
Nd	0.296	0.989	0.684	0.993												
Sm	0.363	0.950	0.646	0.972	0.978											
Eu	0.365	0.834	0.584	0.816	0.822	0.793										
Gd	0.338	0.957	0.582	0.961	0.969	0.964	0.790									
Tb	0.319	0.662	0.527	0.690	0.667	0.575	0.447	0.641								
Dy	0.399	0.947	0.547	0.953	0.959	0.960	0.763	0.981	0.626							
Y	0.371	0.848	0.305	0.829	0.835	0.833	0.736	0.911	0.545	0.926						
Ho	0.166	0.740	0.528	0.762	0.747	0.686	0.566	0.749	0.868	0.713	0.633					
Er	0.341	0.913	0.545	0.917	0.921	0.906	0.754	0.950	0.701	0.946	0.919	0.760				
Tm	-0.022	0.662	0.257	0.595	0.641	0.633	0.745	0.690	0.200	0.657	0.759	0.434	0.701			
Yb	0.395	0.895	0.483	0.892	0.889	0.882	0.736	0.944	0.614	0.939	0.929	0.723	0.904	0.667		
Lu	0.142	0.530	0.098	0.499	0.507	0.534	0.589	0.575	0.158	0.592	0.723	0.472	0.554	0.791	0.654	
H2O Depth	0.342	-0.064	0.454	0.059	0.013	0.128	0.010	0.001	-0.106	-0.051	-0.218	-0.123	-0.038	-0.236	-0.141	-0.298

	Zr	La	Ce	Pr	Nd	Sm	Eu	Gd	Tb	Dy	Y	Ho	Er	Tm	Yb	Lu

hydrothermal Mn), hydrogenetic Mn, and CFA phases (Figure V.6.), which is in agreement with previous work (Muiños 2005) that used a slightly different dataset and statistical tool (Pereira et al. 2003) and with investigations of globally distributed crusts (Frank et al. 1999). It is also worth noting that the number of samples being smaller than the number of variables does not affect the results, as discussed in Muiños (2005). The identified phases are comparable to the phases commonly found for Pacific and Indian Ocean Fe-Mn crusts.

V.5. Phosphatization

Phosphorus contents of our data set vary from 0.21 to 0.51 wt% (a factor of two) throughout the entire region and water depths (Figure V.4.). However, two samples, 3521-6 (Seine seamount) and 3533-7 (Annika seamount) are exceptions in that they show high P contents of 1.46 and 4.28 wt%, respectively, consistent with the CFA mineral component (Table V.2.). Regardless of these two samples, P seems to increase to the North and South of the Gibraltar: Samples from the MTR area (MTR-Josephine, Nameless, Unicorn, and Godzilla seamounts) show average P contents of 0.34 wt% while samples to the North (Tore) and South (Canaries) show higher average P values of 0.40 and 0.49 wt%, respectively.

Based on our limited dataset, phosphatization took place within the water-depth range of 1,200 to 1,500 m, but may also have occurred at shallower depths. That water-depth range corresponds to the lower core of MOW characterized by low dissolved oxygen contents and therefore low oxidation potential. This relationship was also pointed out by Koschinsky et al. (1996) and provides an indication of the influence of the prevailing oceanographic conditions in the area on the compositions of the crusts. Hein et al. (1993) suggested that during stable, warm climatic conditions dissolved phosphorous derived from intense chemical weathering on continents accumulated in the deep sea in large quantities. With the expansion of Antarctic glaciation and intensification of ocean circulation, the phosphorous-rich deep waters were redistributed by upwelling and turbulent mixing at the seamounts to intermediate water depths and may have been temporarily stored in the OMZ. Koschinsky and Halbach (1995) proposed a model for precipitation of hydrogenetic Fe-Mn crusts, with crusts being formed below the OMZ, as the result of the mixture of Mn^{2+}-rich and O_2-poor

waters with Mn^{2+}-poor and O_2-rich deep waters. Halbach et al. (1982, 1989b) and Koschinsky et al. (1997) linked the phosphatization with the expansion of the OMZ as the result of increased surface-water productivity. The expansion of the OMZ led to the impregnation with CFA of the extant crusts. Despite the fact that a phosphatized old crust generation is missing in Atlantic crusts, Koschinsky et al. (1996) noted phosphatization episodes within a 8.5 Ma record from a crust collected from Lion Seamount in the NE

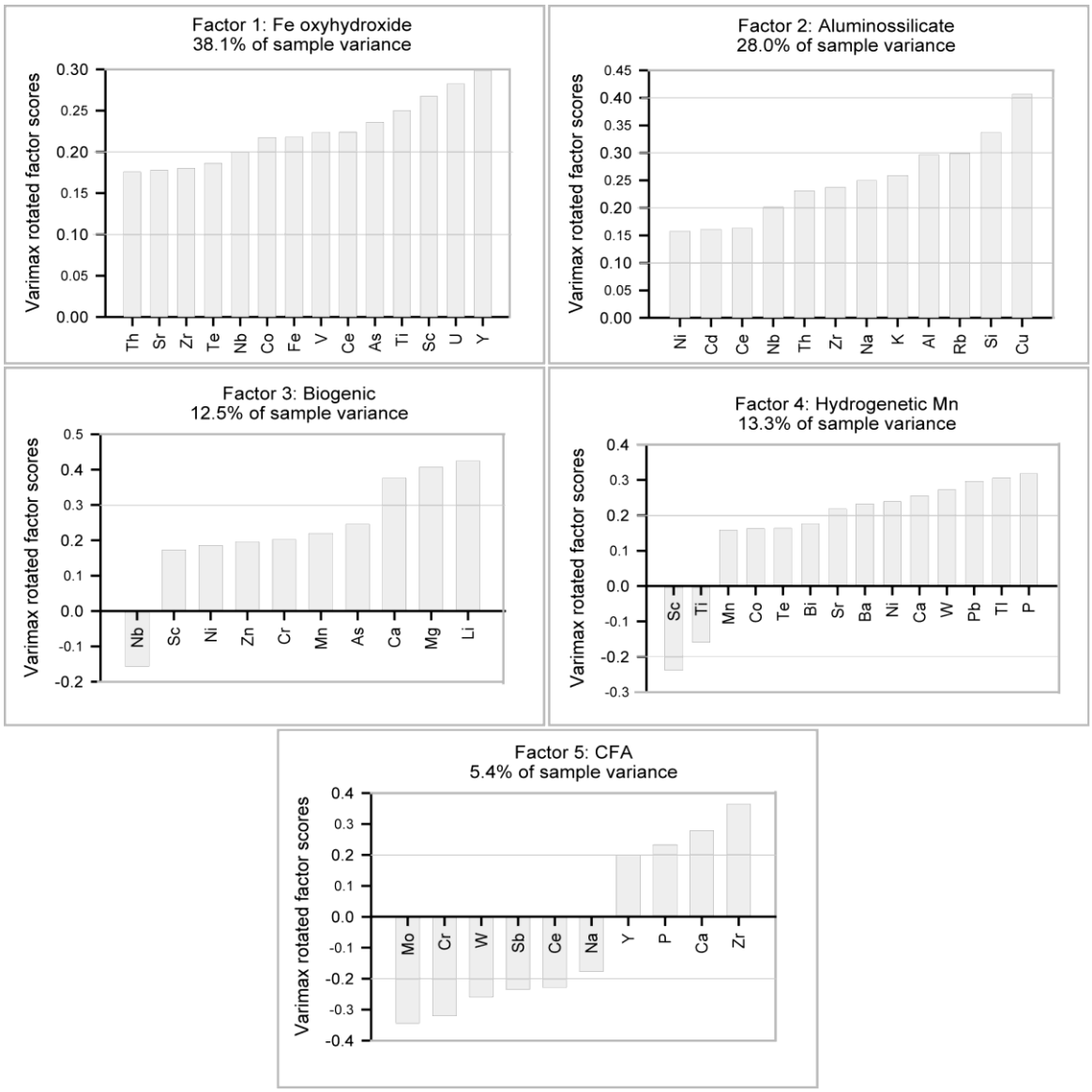

Figure V.6. Graphic display of Q-Mode rotated factor scores for five factors; CFA means carbonate fluorapatite.

Atlantic Ocean, which may at least in part correspond to the 6 Ma event of phosphatization of limestone that occurred on Lighthill seamount off Morocco (Jones et al. 2002). The phosphatization was most likely a consequence of episodes of increased productivity and biogenic particle flux and is much younger than the phosphatization episodes in the Pacific (Hein et al. 1993).

Thus, the most probable explanation for shallow-water phosphatization is an interaction of the OMZ and MOW to produce an extended depth range for O_2-poor and Mn^{2+}-and dissolved P-rich waters, which reached down the slopes of some seamounts covered with Fe-Mn crusts. As a consequence, crust accretion may have been prohibited and precipitation of CFA promoted at these relatively shallow depths in the Atlantic Ocean (Hein et al. 2000 and references therein).

V.6. Resource considerations

Fe-Mn deposits in the Portuguese EEZ may become an important future resource but there is a clear need for studies to better understand their origin and distribution. During the oceanographic cruises mentioned above, as well as during the SO 83 cruise (Halbach and Scientific Crew 1993), samples of Fe-Mn nodules and crusts were collected on various seamounts from the northeast Atlantic. Despite the fact that the sampling was not systematic, and knowledge of the area needs to be augmented, we present a first-order evaluation of the possible resource potential of Fe-Mn crusts within and adjacent to the Portuguese EEZ, based on criteria developed by Hein et al. (2009).

V.6.1. Grade

According to Hein et al. (2009), large seamount summit areas with high grades of Co, Ti, REEs, Te, Ni, Th, Mn, Pt, etc, will be preferentially chosen for mining the crusts. It is also stressed that the grade will depend on the ability to collect Fe-Mn crusts without their substrate rocks, which would of course result in a decrease in the metal grade. Figure V.7. shows the concentrations of selected trace metals that offer an economic potential for the future for the crusts analyzed here compared to data for crusts from different ocean basins

(from Hein 2004). Average metal concentrations in our dataset are comparable to average concentrations for Indian Ocean Fe-Mn crusts except for Zr, which is significantly higher in Indian Ocean crusts. For most of the metals, average concentrations for our dataset are in the range of the average Atlantic concentrations given by Hein (2004), except also for Zr and Pt. In comparison to central Pacific crusts, the average compositions of the crusts analyzed here are systematically lower, with the exceptions of Th, which is enriched in Atlantic and Indian crusts, and Te and Ce, which show similar concentrations. Nevertheless, if we consider the maximum values for our samples, the concentrations are similar to average central Pacific concentrations, except once again for Zr. The highest Co concentrations in our crusts of up to 0.54% Co are found in the shallower-water samples (on Seine and Nameless Seamounts; Figure V.4.). Further exploration is warranted within those areas and also regionally to possibly locate larger areas with mean crust grades similar to the maximum concentrations found for individual crusts analyzed here.

V.6.2. Tonnage (thickness)

Tonnages were calculated based on average thicknesses of crusts in our dataset for Nameless, Unicorn, and MTR seamounts (Table V.6.). Considering data in Table V.6., the surface area above 2,500 m water depth, and a mean wet-bulk density of crusts of 1.95 g/cm^3, we calculate the crust tonnage for Nameless, Unicorn, and MTR to be 7.1x10^7, 1.3x10^8, and 1.1x10^9 metric tons of wet crust respectively.

Considering the average concentrations for Co, Ni, Ce, Te, and Pt of 0.34%, 0.22%, 0.13%, 0.0043% and 3x10^{-8}%, respectively, we calculate maximum tonnages of these metals (Figure V.8. and Table V.6.) with consideration for dilution resulting from recovery of substrate rock and unavailability of crusts for recovery due to other factors (see Hein et al. 2009 for discussion).

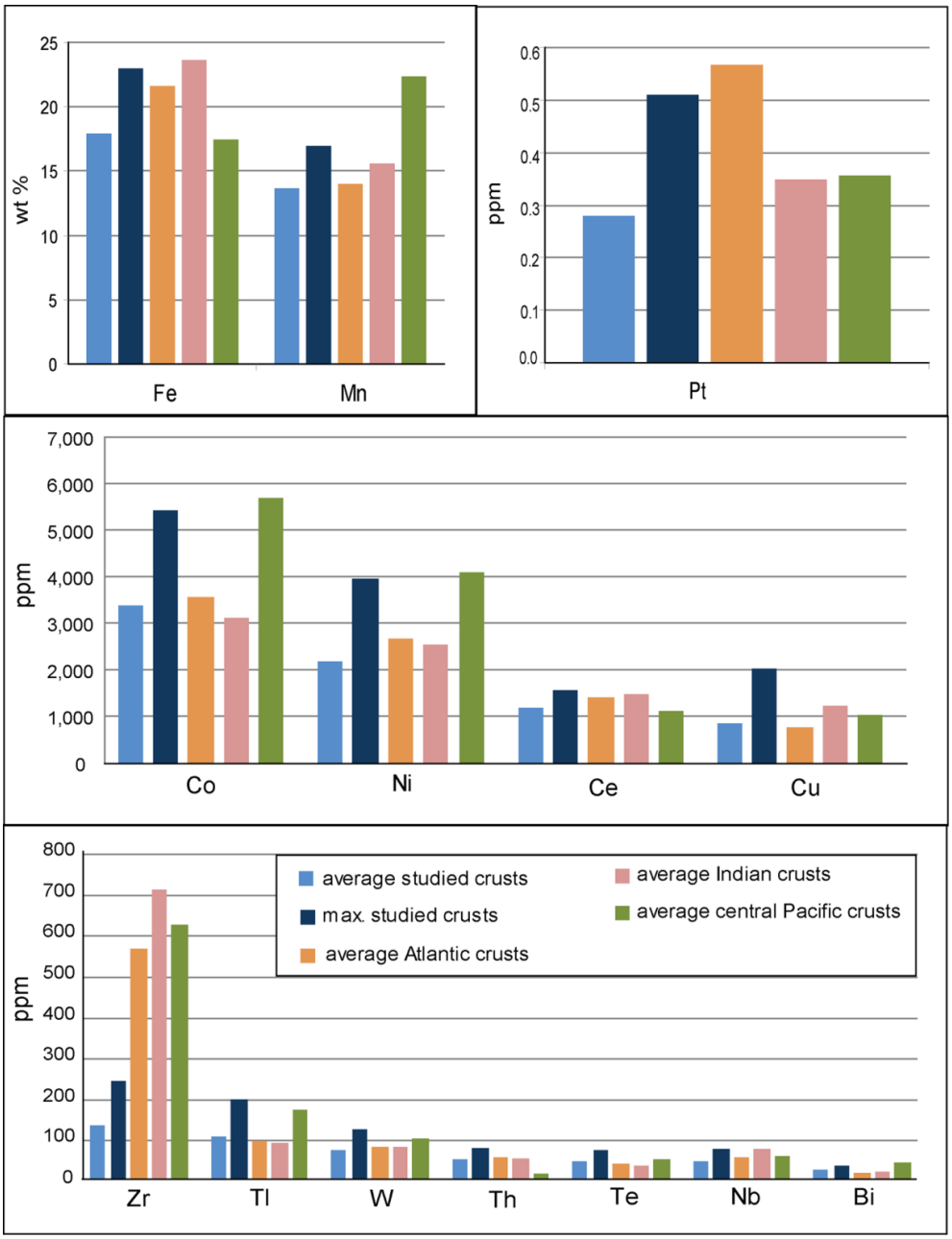

Figure V.7. Trace-metal concentrations in different ocean basins and in crusts analyzed here. Mean concentrations for Atlantic, Indian, and central Pacific crusts from Hein (2004).

V.6.3. Area Permissible for crust coverage

Due to the absence of detailed sampling and the lack of backscatter side-scan sonar data, a comprehensive and more accurate calculation of the area of crust-coverage is not possible. Despite these limitations, we calculated surface areas using ArcMap's 3D analyst, ArcGIS® from ETOPO bathymetry and present those data considering reductions in areas potentially exploitable that result from water depth constraints, limitations in our knowledge of sediment cover and topography, and the necessity for biological corridors, based on the case study of Hein et al. (2009). The 2,500 m water depth limit proposed by Hein et al. (2009) is also used here even though some Fe-hosted metals increase with water depth, especially copper, which shows increased concentrations in crusts deeper than 3,000 m (Figure V.4.). We consider that the 2,500 m water depth limit should be maintained because Cu is of limited economic potential either below or above the 2,500 m water depth and because the most economically important Fe-hosted metal –Te – does not show increasing concentrations with depth. In addition, most resource studies for the Pacific consider the 2,400-2,500 m as depth limit for calculations, and so comparisons of our data with Pacific data would not be valid using a different water depth limit.

Table V.6. Calculation of seamount and ridge surface areas for selected seamounts in the study area, crust mean thicknesses, and metric tons of selected metals based on a crust mean wet-bulk density of 1.95 g/cm^3

Seamount	Mean Thickness (cm)	Surface area above 2,500 m water depth (km^2)	Co (Tons)	Ni (Tons)	Ce (Tons)	Te (Tons)	Pt (Tons)
Nameless	8	454	$2.4x10^5$	$1.6x10^5$	$9.0x10^6$	$3.0x10^3$	$2.1x10^{-2}$
Unicorn	4	1948	$4.5x10^5$	$2.9x10^7$	$1.7x10^5$	$5.7x10^3$	$4.0x10^{-2}$
MTR	7	8492	$3.8x10^6$	$2.5x10^8$	$1.4x10^6$	$4.8x10^4$	$3.4x10^{-1}$

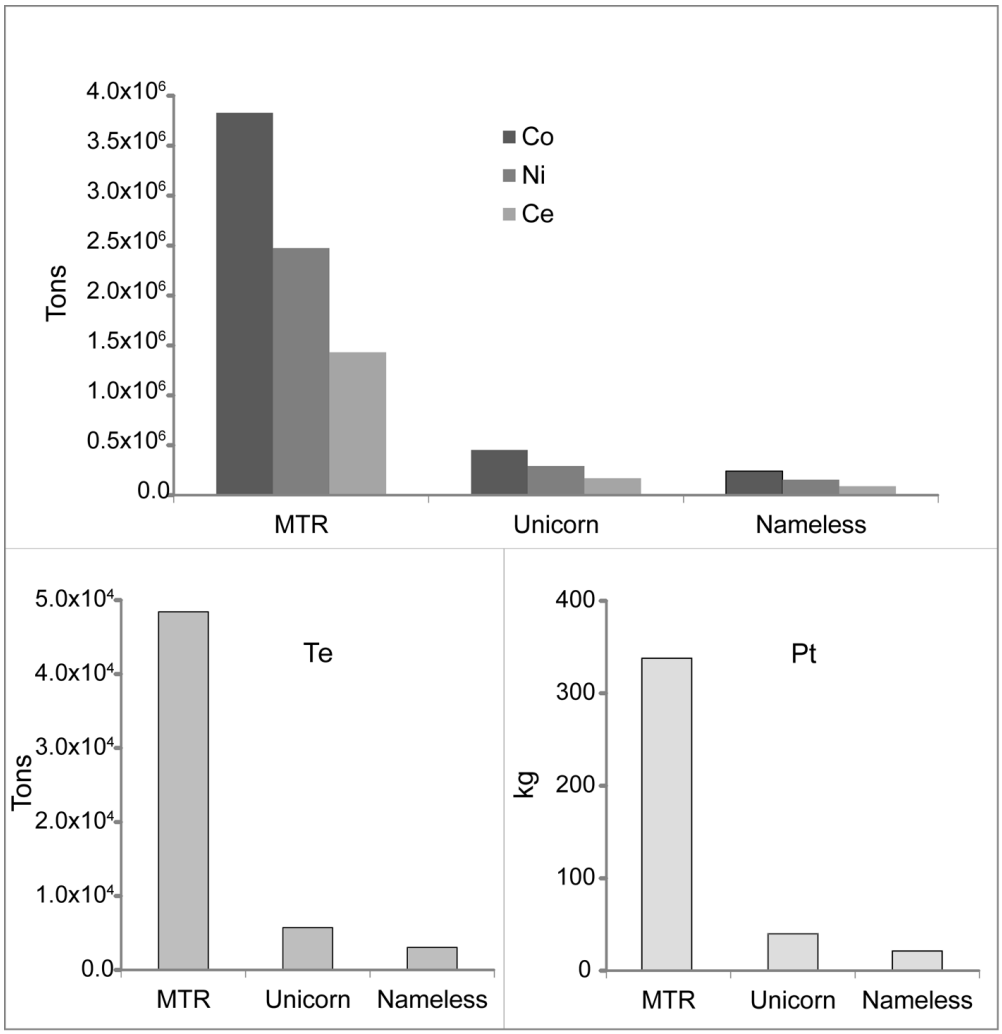

Figure V.8. Histogram of metric tons for different metals on the basis of average crust thicknesses for Nameless, Unicorn, and MTR seamounts.

We consider the following: (i) a large area represented by MTR (total surface area of 41,872 km^2); (ii) a medium-sized area, represented by the combined areas of Lion, Nameless, Dragon, and Unicorn Seamounts (total surface area of 7,824 km^2); and (iii) a small area represented by the combined areas of Lion and Nameless seamounts (total surface area of 3,676 km^2) (Figure V.9.). The choice of Nameless, Lion, Dragon, and Unicorn seamounts was made because we expect that these seamounts located to the south of MTR may represent a suitable exploration area based on their depths, specific oceanic currents, and metal concentrations. Area calculations and reductions for the three scenarios are illustrated in Figure V.10.

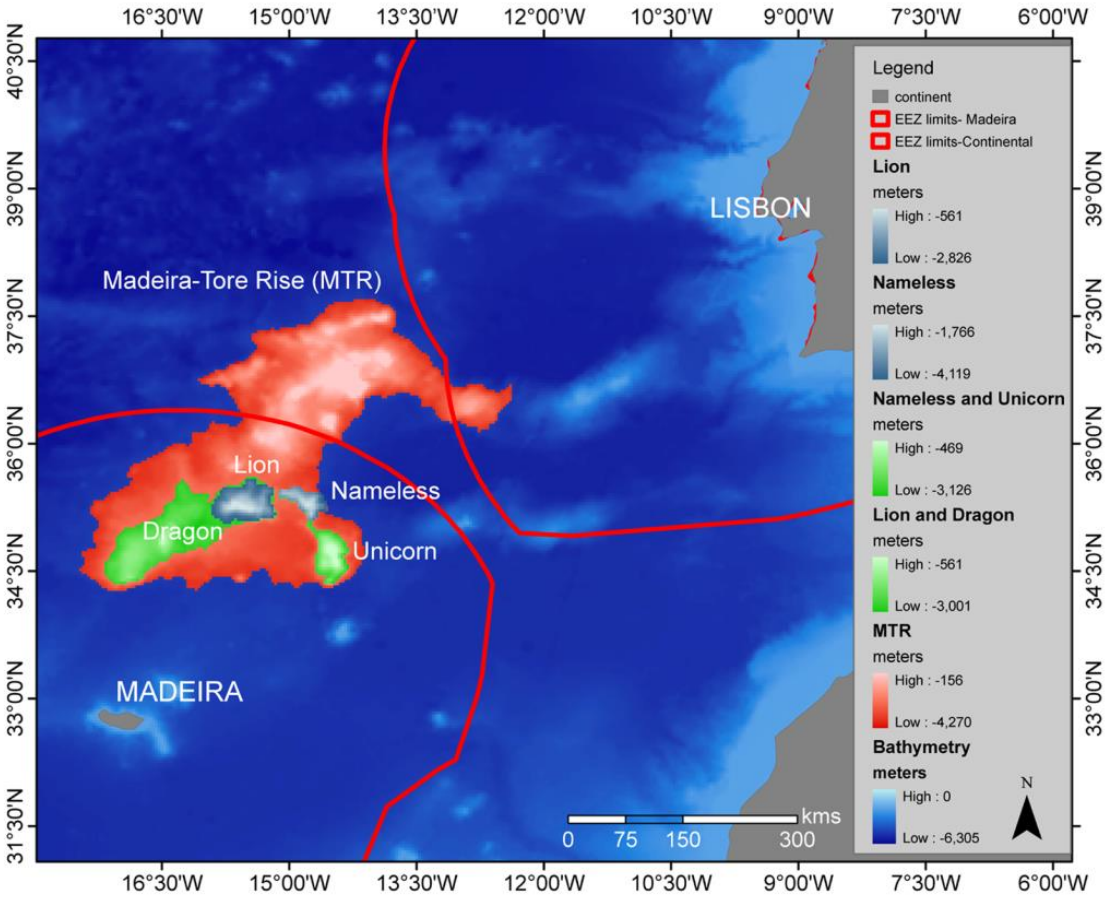

Figure V.9. Madeira -Tore Rise; Lion and Dragon, and Nameless and Unicorn; and Lion and Nameless contour polygons used for surface area calculations.

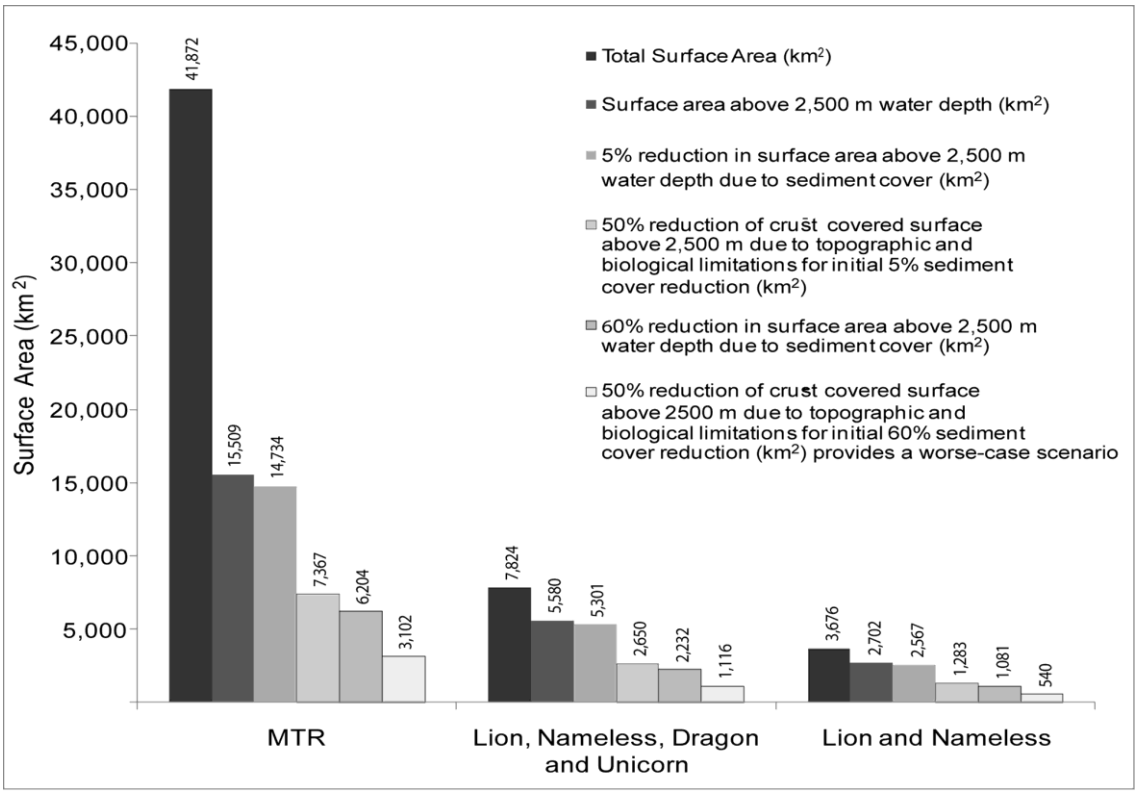

Figure V.10. Histogram of total surface area and surface area above 2,500 m water depth for the three scenarios that consider different sizes of seamount areas. Other bars represent reductions in size of areas where crusts might be available because of sediment cover and other considerations (see Hein et al. 2009).

Hein et al. (2009) calculated surface areas for two case studies: (i) a large guyot (total surface area of 11,761 km^2) and (ii) an average-size guyot (total surface area of 3,495 km^2). Considering the worst-case scenario (50% reduction of crust-covered surface above 2,500 m water depth due to topographic and biological limitations for initial 60% sediment cover reduction), Hein et al. (2009) obtained, respectively, 615 km^2 and 231 km^2 of permissible area. A worst-case scenario for our dataset would yield surface areas of 3,102, 1,116, and 540 km^2, for the three groups described above, respectively (Figure V.10.). Considering these surface areas, a wet bulk density of 1.95 g/cm^3, an annual production of 1 million tons, and assuming a general mean crust thickness of 3 cm rather than using the limited dataset that we have for crust thicknesses from each seamount, the area needed to maintain a 20-year mine site is 342 km^2, which can be potentially accommodated by all three groups. These results are comparable to the results obtained by Hein et al. (2009) for central equatorial Pacific seamounts.

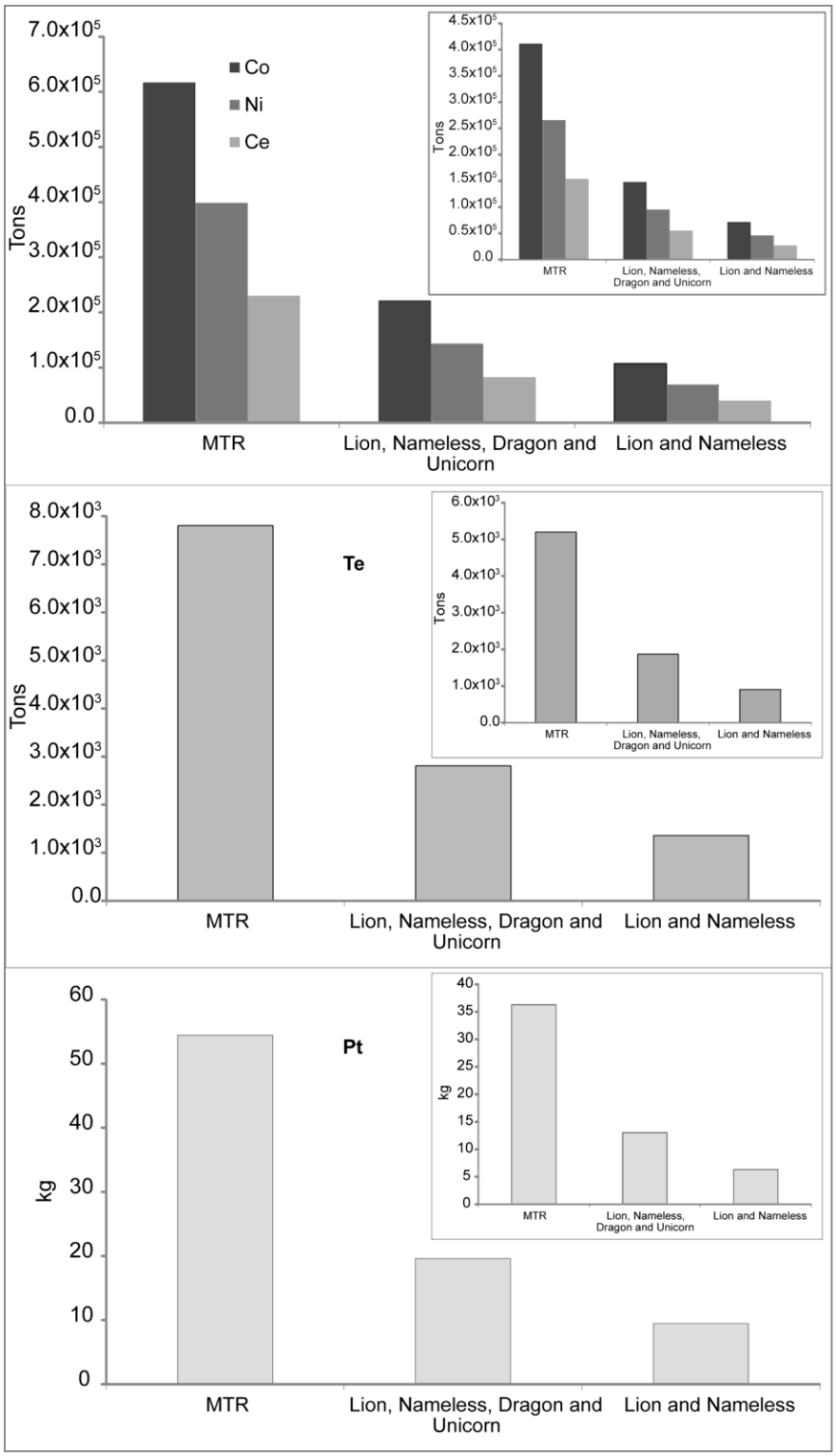

Figure V.11. Histogram of calculated tonnages (wet weight) for different metals considering the worst-case scenario of surface area reductions. Insets plots show areas corresponding to calculated tonnages based on dry weight.

We also calculated metal tonnages considering the above conditions (worst-case scenario and 3 cm mean crust thickness). The metal concentrations used for these calculations are the ones given previously. We also calculated the dry-tonnages using a mean dry-bulk density of crusts of 1.3 g/cm^3 (Hein et al. 2000). In Figure V.11. we present a histogram of calculated tonnages (wet- and dry-weight) for the metals considered. Maximum tonnages (resulting from large area calculations) for Co, Ni, Ce, Te and Pt are $6.2x10^5$, $4.0x10^5$, $2.3x10^5$, $7.8x10^3$ and $5.4x10^{-2}$ tons, respectively. Considering the small area, our calculations result in $1.1x10^5$, $6.9x10^4$, $4.0x10^4$, $1.4x10^3$ and $9.5x10^{-3}$ tons for the same metals, respectively. Our results show that the study area within the Portuguese EEZ (and adjacent areas in International Waters, for MTR; Figure V.11.) is comparable to that of areas in the central Pacific Ocean presented in Hein et al. (2009). Exploration beyond reconnaissance may now be warranted and should include detailed sampling, backscatter side-scan sonar, bathymetric mapping, and detailed mapping of crust thicknesses, etc., in order to better constrain the assumptions made here and to allow for a quantitative resource evaluation.

V.7. Conclusions

The objective of this study was to determine the composition of Fe-Mn crusts from the northeast Atlantic and to consider gaps in our knowledge needed for a quantitative resource potential of these deposits. The compositions of the studied crusts are typical for hydrogenetic crusts adjacent to continental margins. Specific compositional differences are found that likely indicate specific local conditions during crust accretion, for example higher Co, Ni, and Zr in Pacific crusts and higher Th in Atlantic crusts.

The enrichment of trace metals of economic interest in Fe-Mn crusts is of particular importance for their potential as a resource (i.e. Te and REEs), and is of specific interest for the resource potential of these deposits within the Portuguese EEZ. Based on the criteria of Hein et al. (2009), we calculated tonnages for specific metals in chosen areas in and adjacent to the Portuguese EEZ. Our results indicate that the study area is comparable to parts of the central Pacific Ocean and may represent an important metal resource for the future. Further studies are warranted in order to better constrain and quantify the results presented here.

Acknowledgments

We thank the Portuguese Science and Technology Foundation (FCT) for financial support through Project PDCT/MAR/56823/2004; FCT also supported a fellowship to S.B.M. (SFRH/BD/22263/2005) co-financed by POCI 2010/EU. Additional support to S.B.M. was provided by a LNEG fellowship. We acknowledge K. Hoernle, the crew and scientific party of Meteor M51/1 cruise as well as the Deutsche Forschungsgemeinschaft (DFG, German Research Council) for funding. We acknowledge J. Girardeau, the onboard scientific team, the University of Nantes and the French INSU-CNRS Institute for the financial support that made possible the collection of the samples from the Tore-Madeira Cruise and for kindly having made these samples available for this work. We also thank the co-chiefs of the TTR-11 Cruise, the onboard team and the UNESCO –IOC TTR Program for the samples collected during the TTR-11 cruise, which was funded by INGMAR Project (FCT). We also thank S. M. Lebreiro, L. M. Pinheiro, R. Dunham, J. Noiva, J. Dias, F. Neves, C. Lopes and M. Mil-Homens for their help and discussions. The editors and two anonymous reviewers are thanked for their contribution to the improvement of this paper.

References

Amante, C., and B.W. Eakins. 2009. *ETOPO1 1 Arc-Minute Global Relief Model: Procedures, Data Sources and Analysis.* Vol. March 2009, *NOAA Technical Memorandum NESDIS NGDC-24*.

Ambar, I., L. Armi, A. Bower, and T. Ferreira. 1999. Some aspects of time variability of the Mediterranean Water off south Portugal. *Deep-Sea Research I* 46:1109-1136.

Ambar, I., and M.R. Howe. 1979. Observations of the Mediterranean outflow-I Mixing in the Mediterranean Outflow. *Deep-Sea Research I* 26A:535-554.

Ambar, I., N. Serra, M.J. Brogueira, G. Cabeçadas, F. Abrantes, P. Freitas, C. Gonçalves, and N. Gonzalez. 2002. Physical, chemical and sedimentological aspects of the Mediterranean outflow off Iberia. *Deep-Sea Research II* 49:4163-4177.

Anders, E., and N. Grevesse. 1989. Abundances of the elements: Meteoritic and solar. *Geochimica et Cosmochimica Acta* 53:197-214.

Banakar, V.K., J.R. Hein, R.P. Rajani, and A.R. Chodankar. 2007. Platinum group elements and gold in ferromanganese crusts from Afanasiy-Nikitin seamount, equatorial Indian Ocean: Sources and fractionation. *Journal of Earth System Science* 116: 3-13.

Bau, M., A. Koschinsky, P. Dulski, and J.R. Hein. 1996. Comparison of the partitioning behaviors of yttrium, rare-earth elements, and titanium between hydrogenetic marine ferromanganese crusts and seawater. *Geochimica et Cosmochimica Acta* 60: 1709-1725.

Broecker, W.S., and T.-H. Peng. 1982. *Tracers in the Sea*. Palisades, New York: Lamont-Doherty Geological Observatory, Columbia University.

Bruland, K.W., E.L. Rue, and G.J. Smith. 2001. Iron and macronutrients in California coastal upwelling regimes: Implications for diatom blooms. *Limnology and Oceanography* 46:1661-1674.

Burns, R. G., and V. M. Burns. 1977. Mineralogy. In *Marine Manganese Deposits*, edited by G. P. Glasby, 185-248.

Amsterdam: Elsevier.

Cook, H.E., P.D. Johnson, J.C. Matti, and I. Zemmels. 1975. Methods of sample preparation and X-ray data analysis (X-ray mineralogy laboratory, Deep Sea Drilling Project, University of California Riverside). In *initial Reports of the Deep-Sea Drilling Project* 28, 999-1007.

Craig, James D., James E. Andrews, and Maurice A. Meylan. 1982. Ferromanganese Deposits in the Hawaiian Archipelago. *Marine Geology* 45:127-157.

Cronan, D. S. 1977. Deep- sea nodules: distribution and geochemistry. In *Marine Manganese Deposits*, edited by G. P. Glasby, 11-44. Amsterdam: Elsevier.

———. 1997. Some controls on the geochemical variability of manganese nodules with particular reference to the tropical South Pacific. In *Manganese Mineralization: Geochemistry and mineralogy of terrestrial and marine deposits*, *Geological Society Special Publication 119,* edited by K. Nicholson, J. R. Hein, J. R. Buhn and S. Dasgupta, 139-151. Bath, U.K.: The Geological Society.

De Carlo, E. H. 1991. Paleoceanographic implications of rare earth element variability within a Fe-Mn crust from the central Pacific Ocean. *Marine Geology* 98:449-467.

Elderfield, H., C. J. Hawkesworth, M. J. Greaves, and S. E. Calvert. 1981. Rare earth element geochemistry of oceanic ferromanganese nodules and associated sediments. *Geochimica et Cosmochimica Acta* 45:513-528.

Frank, M., R. K. O'Nions, J. R. Hein, and V. K. Banakar. 1999. 60 Ma records of major elements and Pb-Nd isotopes from hydrogenous ferromanganese crusts: Reconstruction of seawater paleochemistry. *Geochimica Cosmochimica Acta* 63:1689-1708.

Gaspar, L. 2001. Química e mineralogia de depósitos de ferromanganês da montanha submarina Lion, ZEE da Madeira, Portugal. Paper read at Actas do VI Congresso de Geoquímica dos Países de Língua Portuguesa/XII Semana da Geoquímica, at Faro, Portugal, April 9 -12.

Geldmacher, J., K. Hoernle, A. Klugel, P. v.d. Bogaard, F. Wombacher, and B. Berning. 2006. Origin and geochemical evolution of the Madeira-Tore Rise (eastern North Atlantic). *Journal of Geophysical Research* 111:B09206, doi: 10.1029/2005JB003931.

Goldberg, E.D., M. Koide, R.A. Schmitt, and R.H. Smith. 1963. Rare earth distribution in the marine environment. *Journal of Geophysical Research* 68:4209-4217.

Halbach, P. 1986. Process controlling the heavy metal distribution in Pacific ferromanganese nodules and crusts. *Geologische Rundschau* 75:235-247.

Halbach, P., and Scientific Crew. 1993. Marine geological and geochemical investigations of sediments, precipitates and hard rocks from three seamounts in the NE Atlantic to identify element fluxes. In *Technical cruise report of the RV Sonne cruise SO 83 - MARFLUX 4; BMFT project 03R424A6 and MAST contract 0022C*. Berlin, Germany: Freie Universitat Berlin.

Halbach, P., F.T. Manhein, and P. Otten. 1982. Co-rich ferromanganese deposits in the marginal seamount regions of the central pacific basin: results of the Midpac'81. *Erzmetall* 35:447-453.

Halbach, P., E.Rehm, and V. Marchig. 1979. Distribution of Si, Mn, Ge, Ni, Cu, Co, Zn, Pb, Mg, and Ca in Grain-Size Fractions of Sediment Samples from a Manganese Nodule Field in the Central Pacific Ocean. *Marine Geology* 29:237-252.

Halbach, P., C. Kriete, B. Prause, and D. Puteanus. 1989a. Mechanisms to explain the platinum concentration in ferromanganese seamount crusts. *Chemical Geology* 76:95-106.

Halbach, P. E., C-D. Sattler, F. Teichmann, and M. Washner. 1989b. Cobalt-rich and platinum- bearing manganese crust deposits on seamounts: nature, formation, and metal potential. *Marine Mining* 8:23-39.

Halbach, P., B. Prause, K. Koch, M. Westholt. 1990. Platinum and Palladium in Co-Rich Ferromanganese Crust Deposits. *Marine Mining* 9:117-126.

Hein, J.R. 2004. Cobalt-rich ferromanganese crusts: Global distribution, composition, origin and research activities. In *Minerals other than Polymetallic nodules of the International Seabed Area. Proceedings of a Workshop held on 26-30 June 2000,* 188-256. Kingston, Jamaica: International Seabed Authority.

Hein, J.R., T.A. Conrad, and R.E. Dunham. 2009. Seamount Characteristics and Mine-Site Model Applied to

Exploration- and Mining-Lease-Block Selection for Cobalt-Rich Ferromanganese Crusts. *Marine Georesources and Geotechnology* 27:160-176, doi:10.1080/10641190902852485.

Hein, J.R., T.A. Conrad, and H. Staudigel. 2010. Seamount Mineral Deposits, a source of rare metals for high-technology industries. *Oceanography* 23 (1):184-189.

Hein, J. R., A. Koschinsky, M. Bau, F. T. Manheim, J-K Kang, and L. Roberts. 2000. Cobalt-Rich ferromanganese crusts in the Pacific. In *Handbook of Marine Mineral Deposits*, edited by D. S. Cronan, 239-279. Boca Raton, Florida: CRC Press.

Hein, J. R., A. Koschinsky, P. Halbach, F. T. Manheim, M. Bau, J-K Kang, and N. Lubick. 1997. Iron and manganese oxide mineralization in the Pacific. In *Manganese Mineralization: Geochemistry and mineralogy of terrestrial and marine deposits*, *Geological Society Special Publication 119,* edited by K. Nicholson, J. R. Hein, J. R. Buhn and S. Dasgupta, 123-138. Bath, U.K.: The Geological Society.

Hein, J. R., A. Koschinsky, and A. N. Halliday. 2003. Global occurrence of tellurium-rich ferromanganese crusts and a model for the enrichment of tellurium. *Geochimica et Cosmochimica Acta* 67 (6):1117-1127.

Hein, J. R., A. Koschinsky, and B. McIntyre. 2005. The global enrichment of platinum group elements in marine ferromanganese crusts. *In Extended Abstracts, 10th International Platinum Symposion*, edited by T.O. Törmänen and T.T. Alapeti, 7-11 August 2005, Oulu, Finland, 98-101.

Hein, J.R., W.C. Schwab, and A.S. Davis. 1988. Co and Pt-rich ferromanganese crusts and associated substrate rocks from the Marshall Islands. *Marine Geology* 78:255-283.

Hein, J. R., H-W. Yeh, S. H. Gunn, W. V. Sliter, L. M. Benninger, and C-H. Wang. 1993. Two major Cenozoic episodes of phosphogenesis recorded in Equatorial Pacific seamount deposits. *Paleoceanography* 8 (2):293-311.

Hodge, V.F., M. Stallard, M. Koide and E.D. Goldberg. 1985. Platinum and the platinum anomaly in the marine environment. *Earth and Planetary Science Letters* 72:158-162.

Hoernle, K., and Scientific Party. 2003. Cruise Report M51/1. In *Ostatlantik - Mittelmeer - Schwarzes Meer, Cruise No. 51, 12 September - 28 December 2001*, Meteor-Berichte 03-1, edited by C. Hemleben, K. Hoernle, B. B. Jorgensen and W. Roether, 3-35. Hamburg, Germany: University of Hamburg.

I.O.C.-Intergovernmental Oceanographic Commission. 2002. Geological Processes in the Mediterranean and Black Seas and North East Atlantic. Preliminary results of investigations during the TTR-11 cruise of RV Professor Logachev, July-September, 2001. In *IOC Technical Series*, edited by N. H. Kenyon, M. K. Ivanov, A. M. Akhmetzhanov and G. G. Akhmanov. Paris, France: UNESCO.

Jones, E.J.W., M.K. BouDagher-Fadel, and M.F. Thirlwall. 2002. An investigation of seamount phosphorites in the Eastern Equatorial Atlantic. *Marine Geology* 183:143-162.

Klovan, J.E., and J. Imbrie. 1971. An algorithm and FORTRAN-IV program for large-scale Q-mode factor analysis and calculation of factor scores. *Mathematical Geology* 3:61-77.

Koschinsky, A., M. van Gerven, and P. Halbach. 1995. First investigations of massive ferromanganese crusts in the NE Atlantic in comparison with hydrogenetic Pacific occurrences. *Marine Georesources and Geotechnology* 13:375-391.

Koschinsky, A., and P. Halbach. 1995. Sequential leaching of marine ferromanganese precipitates: Genetic implications. *Geochimica et Cosmochimica Acta* 59:5113-5132.

Koschinsky, A., P. Halbach, J. R. Hein, and A. Mangini. 1996. Ferromanganese crusts as indicators for paleoceanographic events in the NE Atlantic. *Geologische Rundschau* 85:567-576.

Koschinsky, A., A. Stascheit, M. Bau, and P. Halbach. 1997. Effects of phosphatization on the geochemical and mineralogical composition of marine ferromanganese crusts. *Geochimica et Cosmochimica Acta* 61 (19):4079-4094.

Kuhn, T., M. Bau, N. Blum, and P. Halbach. 1998. Origin of negative Ce anomalies in mixed hydrothermal-hydrogenetic Fe-Mn crusts from the Central Indian Ridge. *Earth and Planetary Science Letters* 163:207-220.

Madelain, F. 1970. Influence de la topographie du fond sur l'écoulement Mediterranéen entre le Détroit de Gibraltar et le cap Saint-Vincent. *Cahiers Océanographiques* 22:43-61.

Mangini, A., P. Halbach, D. Puteanus, and M. Segl. 1987. Chemistry and Growth of Central Pacific Mn-Crusts and

Their Economic Importance. In *Marine Minerals, Advances in Research and Resource Assessment*, edited by P. G. Teleki, M. R. Dobson, J. R. Moore and U. v. Stackelberg, 205-220. Dordrecht Germany: D. Reidel Publishing Company.

Merle, R. 2006. Age and origin of Tore-Madeira Rise: beginning of Atlantic Ocean spreading or hotspot track. Petrology, geochemistry, U-Pb geochronology and Pb-Sr-Hf isotopes. PhD, University of Nantes, Nantes (in French).

Merle, R., U. Schärer, J. Girardeau, and G. Cornen. 2006. Cretaceous seamounts along the continent-ocean transition of the Iberian margin: U-Pb ages and Pb-Sr-Hf isotopes. *Geochimica et Cosmochimica Acta* 70 (19):4950-4976.

Moffet, J.W. 1994. A radiotracer study of cerium and manganese uptake onto suspended particles in Chesapeake Bay. *Geochimica et Cosmochimica Acta* 58:695-703.

Muiños, S.B. 2005. Contribuição da análise multivariada para o estudo de crostas submarinas de ferro e manganês do Atlântico Nordeste. Master, Instituto Superior Técnico, Universidade Técnica de Lisboa, Lisbon (in Portuguese).

Muiños, S.B., L. Gaspar, J.H. Monteiro, R. Salgueiro, J.F. Ramos, V.H. Magalhães, and T. Rodrigues. 2002. Ferromanganese deposits from the Nameless Seamount: Preliminary results. In *IOC Workshop Report* 183:27-30.

Nath, B.N., V. Balaram, M. Sudhakar, and E.W.L. Plueger. 1992. Rare-earth element geochemistry of ferromanganese deposits from the Indian Ocean. *Marine Chemistry* 38:185-208.

Pereira, H.G., Renca, S. and J. Saraiva. 2003. A case study on geochemical anomaly identification through principal components analysis supplementary projection. *Applied Geochemistry* 18:37-44.

Sholkovitz, E.R., and D.L. Schneider. 1991. Cerium redox cycles and rare earth elements in the Sragasso Sea. *Geochimica et Cosmochimica Acta* 55:2737-2743.

Taylor, S.R., and S.M. McLennan. 1985. *The Continental Crust: Its Composition and Evolution*. Oxford: Blackwell.

Usui, A., T.A. Mellin, M. Nohara, and M. Yuasa. 1989. Structural stability of marine 10A manganates from the Ogasawara (Bonin) arc: implication for low-temperature hydrothermal activity. *Marine Geology* 86:41-56.

van Andel, T.H. 1975. Mesozoic-Cenozoic calcite compensation depth and the global distribution of calcareous sediments. *Earth and Planetary Science Letters* 21:455-480.

Varentsov, I.M., V.A. Drits, A.I. Gorshkov, A.V. Sivtsov, and B.A. Sakharov. 1991. Mn-Fe oxyhydroxide crusts from the Krylov seamount (eastern Atlantic): Mineralogy, geochemistry and genesis. *Marine Geology* 96:53-70.

Verlaan, P. A., D. S. Cronan, and C. L. Morgan. 2004. A comparative analysis of compositional variations in and between marine ferromanganese nodules and crusts in the South Pacific and their environmental controls. *Progress in Oceanography* 63:125-158.

Vonderhaar, D.L., G.M. McMurty, D. Garbe-Schönberg, D. Stüben, and B.K. Esser. 2000. Platinum and other related element enrichment in Pacific ferromanganese crust deposits. In *Marine authigenesis: From global to microbial*, *SEPM Special Publication 66*, edited by C.R. Glenn, L. Prévôt-Lucas and J. Lucas, 287-308. Tulsa, Oklahoma: SEPM.

von Stackelberg, U., H. Kuzendorf, V. Marchig, and R. Gwodz. 1984. Growth history of a large ferromanganese crust from the equatorial north pacific nodule belt. *Geologisches Jahrbuch* A75:213-235.

Wen, X., E.H. De Carlo, and Y.H. Li. 1997. Interelement relationships in ferromanganese crusts from the central Pacific ocean: their implications for crust genesis. *Marine Geology* 136:277-297.

Zenk, W. 1970. On the temperature and salinity structure of the Mediterranean Water in the Northeast Atlantic. *Deep-Sea Research* 17:627-631.

Summary and Outlook

An integrated approach, considering Fe-Mn crusts both as paleoceanographic archives and as potentially economic resources, was adopted in this thesis. The present work aimed at determining the paleoceanographic, geological and chemical conditions responsible for the formation of hydrogenetic ferromanganese deposits on northeast Atlantic seamounts, as well as their concentration of trace metals of economic interest and the ways in which the chemical and isotopic compositions of the crusts reflect paleoclimatic and paleoceanographic conditions in the northeast Atlantic Ocean. The following conclusions are based on the results discussed in the main chapters of the thesis.

Taking into account the three sample sets used, a total of 28 sampling sites corresponding to 13 seamounts were studied. These sites are distributed over a wide geographic area and depth range and, despite the fact that the sampling was not exhaustive, are representative of the study area. Of the 28 sampling sites ~47% comprise depths between 1,500 and 2,500 m, which is the depth where the thickest and most trace metal enriched Fe-Mn crusts occur. If the depth range of 1,500 to 3,500 m is considered, ~75% of the sampling sites are included.

The mineralogical and chemical compositions indicate that samples are typical continental margin-type Fe-Mn crusts (Chapter V). The crusts are predominantly composed of δ-MnO_2 (vernadite), which is the mineral characteristic of hydrogenetic Fe-Mn deposits. The Fe and Mn contents average 17.9 wt % and 13.7 wt %, respectively, to which corresponds a mean Fe/Mn ratio of 1.33. Co, Ni, and Cu contents average 3,408 ppm, 2,197 ppm and 872 ppm, respectively, with maximum total Co+Cu+Ni value of 0.96 wt % (average is 0.64 wt %). These values and the Fe/Mn ratios are consistent with a predominantly hydrogenetic origin of continental margin Fe-Mn crusts. The continental margin crusts show lower total Co+Cu+Ni and higher Fe, Si, Al, and Cr contents reflecting the higher contribution of terrigenous inputs. In fact, this terrigenous input can be identified in the mineralogical content (e.g. quartz, feldspars) as well as in the variations of their radiogenic isotope

compositions, as has been shown in Chapter IV by studying the detrital fraction of the Fe-Mn crusts.

The differences in crust composition by subregion indicate that the highest average values of Co+Cu+Ni, Co, Ni, Zn, Mo, Tl, W, Te, and Bi are found in the South Madeira-Tore Rise seamounts. In contrast, the Mediterranean subregion has systematically lower contents for all elements with the exception of Ni and Zn. The Canaries and Azores subregions show the highest values of P and Ti, respectively. These values may be related, respectively, to the presence of diagenetic minerals and detrital sources.

Changes in composition with water depth are also identified. Cu, Al, and Si contents increase with increasing water depth whereas Ca shows an opposite trend. This likely reflects the influence of dissolution of carbonate tests in the geochemistry within the calcite lysocline as indicated by a change in the slope of the Ca pattern and a change from increasing Fe/Mn to decreasing Fe/Mn ratios with depth at ~2,600 to 3,000 m.

All samples are highly enriched in REEs (up to 0.29 wt %) and PGEs (up to 512 ppb). However, there is no clear relationship with water depth and geographic location with the exception of the sample from the Mediterranean subregion that shows lower REEs concentrations (475 ppm total REEs).

A first-order evaluation of the preliminary resource potential of Fe-Mn crusts within the Portuguese EEZ was performed (Chapter V). The results indicate that the study area in the northeast Atlantic is comparable to some parts of the highly prospective Central Pacific Ocean in terms of grade and tonnage needed for a 20-year mine site. Thus, Fe-Mn deposits in the Portuguese EEZ may become an important resource. However, quantitative data specifically related to NE Atlantic seamounts and plateaus are required to provide the constraints necessary for a quantitative resource assessment and to better determine the origin and distribution of the crusts.

These deposits are formed by direct precipitation of the elements from the water column, and so their chemical composition reflects the oceanographic conditions present at the time of formation. Detailed knowledge of the area's paleoceanography is crucial for a better understanding of the composition and formation of these deposits.

In which way the geological, paleoceanographic and paleoclimatic conditions have influenced the chemistry of the Fe-Mn crusts has been reconstructed using the radiogenic isotope signatures of Pb, Nd and Sr recorded in dated Fe-Mn crusts.

The Pb and Nd isotopic compositions of three Fe-Mn crusts distributed along a water depth profile (Chapter III) show that the present-day prevailing water masses for the considered depths are MOW and NEADW. The long-term changes in ocean circulation based on the time series of Pb and Nd isotopes indicate that major tectonic and paleoceanographic events during the time period studied have been recorded: a) The change towards more radiogenic $^{206}Pb/^{204}Pb$ values, and towards less radiogenic ε_{Nd} values at ~4 Ma, as a result of the major paleoceanographic changes that occurred prior to and during the onset of the NHG related to the gradual closure of the Isthmus of Panama and that culminated in the cessation of water exchange between the Atlantic and the Pacific around 4-3 Ma; b) The apparently missing reflection of the Messinian Salinity Crisis that may indicate that MOW was released at least episodically and that the cessations were too short to be recorded in the Fe-Mn crust record. However, the long-term stable and relatively unradiogenic Pb isotope composition of the shallowest crust points to a continuous presence of the MOW signal with contributions from external detrital inputs.

In order to address the external detrital inputs contributing to the NE Atlantic, and to reconstruct past climatically driven changes, the radiogenic isotope composition of Pb, Nd and Sr of the detrital silicate fraction of hydrogenetic Fe-Mn crust surface scrapings and neighboring sediments was studied (Chapter IV). The results show that the input of detrital material to the NE Atlantic likely has mainly been derived from the Sahara, in particular from northern African source areas (such as the Anti-Atlas). Most importantly, the data reveal that the prevailing dry conditions in North Africa have been a long standing feature of the past up to 12 Ma. Also, and despite the low resolution of the detrital time series of this study, the distinct major long-term changes in oceanic and climatic history are recorded by crusts and can be reliably reconstructed based on the study of radiogenic isotopes. In fact, the distinct variations we observe in our record most probably represent a regional signal and likely result from changes in the detrital material incorporated by crusts as a result of changes in the prevailing circulation driven by major tectonic events (e.g. the Messinian Salinity Crisis and the Neogene northward drift of Africa, the onset of the NHG, and the progressive closure of the Panama gateway).

Outlook

Besides the findings presented in this thesis, studies concerning the Fe-Mn deposits in the NE Atlantic are still in their infancy and there are still significant gaps in our knowledge remaining. A part of these remaining questions I will try to answer in future work.

Despite the fact that Fe-Mn crusts in the Portuguese EEZ show promise as an economic resource, many questions remain unanswered. The definition of permissive areas for crust coverage presented in Chapter V was limited to theoretical considerations and thus permissive surface area reductions are poorly constrained. Detailed mapping and systematic sampling, ROV profiles, geochemical and mineralogical studies are needed to determine variations in composition, distribution and thickness, and to better constrain the grade and tonnage of this potential resource. This will contribute important new knowledge to the evaluation of resources of the Portuguese EEZ.

Radiogenic isotope time series obtained from the studied Fe-Mn crusts show that the reconstruction of water mass mixing and evolution, as well as of the long-term changes of the detrital inputs into the eastern Atlantic Ocean are viable. These records provide a long-term evolution and can complement other high resolution paleoceanographic studies.

Most difficulties found in paleoceanographic studies are related to resolution issues. Despite the fact that Fe-Mn crusts cannot be used for high-resolution studies, fact is that the major long-term changes in oceanic and climatic history have been reconstructed based on the study of radiogenic isotopes in crusts. Nonetheless, the assumptions made in the thesis, especially concerning Chapter IV, would benefit from increased resolution, for example by laser ablation profiling and an improved age control of the records. Moreover, inclusion of more records from the study area would help to constrain the results. Also, better defining the end-member compositions, especially concerning North African sources, would be of great advantage for provenance studies.

Complementary studies of isotope geochemistry work with detailed studies of the oceanography of the seamounts would contribute to the knowledge of the sediment dynamics and therefore to interpreting the results.

Other isotope geochemical studies, such as the study of stable metal isotopes, are also important for the factors that have controlled the records from the study area. In fact,

during the course of the thesis work, a first study of stable Fe isotopes was also performed. The goal was to obtain a comparative time-series study to gain the first data on Fe isotope-related geochemical changes over the past ~12 million years. These preliminary data are not included in the thesis and will be subject of future work.

The stable Fe isotopic work was done in collaboration with Prof. Dr. Michael Staubwasser now at the *Institute of Geology and Mineralogy, University of Cologne, Germany* (and formerly at the *Institut fur Mineralogie, Universität Hannover, Germany*). For this purpose, sub-samples of surface scrapings and from older parts of the dated crusts were prepared and measured at the *Institut fur Mineralogie, Universität Hannover* and at the *Institute of Geology and Mineralogy, University of Cologne*. The study of stable metal isotope fractionation will provide information on the range and nature of fractionation among elements during incorporation of metals into the crusts (e.g. chemical speciation, redox-processes, equilibrium fractionation).